COMP[illegible]
18 7

AFOSR
NE

MOLECULAR DYNAMICS
&
SURFACE CHEMISTRY
CONTRACTORS
CONFERENCE

AF OFFICE OF SCIENTIFIC RESEARCH

1984

1984

Molecular Dynamics and Surface Chemistry

Contractors' Meeting

ABSTRACTS

INDEX

I. "Star Wars" by Donald Stedman.......... page 3

II. Speakers

1. S.H. Bauer.......... 5
2. A. Kuppermann and J.F. Garvey.......... 7
3. R. Zare, R.J.S. Morrison and W.E. Conaway.......... 11
4. R.D. Levine.......... 15
5. M.C. Heaven.......... 17
6. P.L. Houston.......... 20
7. S.J. Davis and M.H. Van Benthem.......... 23
8. G.P. Perram, P.J. Wolf and S.J. Davis.......... 24
9. J. Wiesenfeld.......... 25
10. J. Cooper.......... 27
11. M.T. Bowers.......... 30
12. T.J. Dyke and J.W. Nibler.......... 33
13. M. Henchman, J.F. Paulson and A.A. Viggiano.......... 36
14. A. Rahbee.......... 38
15. J. Ross.......... 41
16. J. Erskine.......... 45
17. P.C. Stair.......... 48
18. T. Engel.......... 51
19. P.T. Murray.......... 55
20. T.W. Haas, B.C. Lamartine, K.G. Eyink and J.v. Czarnecki.......... 58
21. P.R. Davis.......... 59
22. L.P. Davis.......... 62
23. P.D. Whitefield and M.R. Berman.......... 66

III. Non-Speakers, Molecular Dynamics

1. G. Burns.......... 70
2. R.D. Coombe.......... 73
3. F.F. Crim.......... 76
4. J. Dyke.......... 77
5. J.B. Fenn, S.B. Ryali and S. Shen.......... 78
6. R.W. Field and J.L. Kinsey.......... 81
7. M.F. Golde.......... 85
8. D.M. Golden, N. Selamoglu and M.J. Rossi.......... 88
9. S.L. Guberman.......... 90
10. F. Kaufman.......... 93
11. S.R. Leone, V.M. Bierbaum and G.B. Ellison.......... 97
12. R.C. Oldenborg and S.L. Baughcum.......... 100
13. J.C. Polanyi.......... 104
14. H. Rabitz.......... 106
15. S.A. Rice.......... 109
16. J.I. Steinfeld.......... 112
17. J. Tellinghuisen.......... 116
18. H.-t. Wang and D.J. Bogan.......... 119
19. R.G. Weiss, S. Chattopadhyay, B.B. Craig and W.L. Faust.......... 123
20. C. Wittig and H. Reisler.......... 128

IV. Non-Speakers, Surface Chemistry

1. F. Abeles, M.L. Theye and V.N. Van....133
2. J. Benziger....135
3. R.R. Cavanagh and J.C. Stephenson....137
4. T.F. George....141
5. L.M. Raff and D.L. Thompson....145
6. S.J. Sibener....148
7. T.G. Slanger....151
8. B.J. Tatarchuk....153
9. N. Winograd....156
10. F.J. Wodarczyk....159
11. J.T. Yates....164

STAR WARS

by Dr. Donald Stedman

"Star Wars"

Myers says the weather here is absolutely AFWL
Register now or else the lunch you eat will not be lawful
Bauer's babies jump across low barriers from both sides
While Kupperman's clever crew create exciting trihydrides.
Here today and gone tomorrow, Zare's playing golf with NH_3^+.
Algebraic bilinear Hamiltonian dynamics thus
Leave me behind, Levine's long walk is just
In time for lunch to which we will be bussed.

"Return of the Jiodide"

Heavenly Clyne studied Iodine, bromine and chlorine too
MPI from Houston's new... Davis is a disciple true
Perram pumps with delta g. Excimers lase from bound to free!
Weisenfeld then did his bit; his iodine system is full of something!

"The Empire Struck Back"

Bowers clusters ions, deconvolutes his peaks.
Oregon's famous for water clusters which Tom Dyke carefully seeks.
Structure in amazing spectra, tricky tunneling and swift
Multi-media Henchman's hydroxide rates, hydrated in his SIFT
He lost the switch, Oh Dear oh me! The empire strikes again!
Rahbee's FTMS needs a blonde, it will not sell till then.
Nerve conduction, dimer switches, triple points and chaos
Delivery most elegant by no one else but John Ross.
Here tomorrow, gone today, Pimentel pushing peroxide, true!
Berkeley ideas for powders white and lasers infra-blue.

"Superficial Lightsabers"

ESDIAD Yates SPIES NH_2, a high resolution snoop
EELS Erskine's view graphs flapping fast, what a remarkable troupe.
The Brouillion Zone they ought to know is a local ethnic soup
Stair is a LEEDer whose mosaics form a rotated infinite group.
Then up spake Big Bucks Engel swinging acronyms with all his might. I'll
Bet he spends in megabucks as many words are in his title!
TES is son of EELS, thus tells us P.T. Murray.
"The Air Force," Haas said, "has these needs, and needs them in a hurry."
Haas spoke up for Lambertine, his work's functioning overtime,
Sees photons which he should not see. Quite surprising. I'm
Amazed at all these Davises, Welsh influence applied
To thermionic convertors of Llanthanum Boride.
MINDO Davis calculates, computer codes collide.
IF quenching rates at least as fast as Phillip Whitefield wide!
Myers moves megabucks with molecular dynamics
Thank you for your welcome here. Again many thanks.

Speakers

REACTIONS WITH LOW ACTIVATION ENERGIES

S. H. Bauer, Cornell University (9/15/84) F49620-84-C-0031

To ascertain the conditions under which the rates of chemical reactions, in collisionally dominant systems, are limited by propensities for intra vs inter energy transfers, and by the partition of energy between vibration and rotation/translation during molecular encounters, one must measure system rate constants, in contrast to state-to-state transition probabilities, for very fast reactions. The pre-exponential terms, rather than the activation energy terms, would reflect these factors. A direct approach is to measure the rates of isomerizations and of dissociations over low barriers, in the second order regime. To bring such rates into the range of available diagnostics the experiments must be conducted at low temperatures (200-400°K), with molecular species which have sparse densities of states at excitation levels in the vicinity of the potential barrier. During the past several years our experiments were limited to line-shape analyses of gas phase NMR spectra. Recently we designed an experimental configuration (not yet constructed) for measuring the enhanced rates of photoconversion of a reacting species by collision with diluent species in which overtones of bond-stretching vibrations were excited. The temperature dependence of the augmented rate will have to be measured precisely. This should provide information on the partition of energy during collisions.

We have investigated the following systems: (i) rotation (π) kinetics about the O-NO bonds in alkyl nitrites; (ii) association-dissociation kinetics in HCl + Me_2O and in formic acid; (iii) rotation about the C-SH bond in thioformic acid. Reports on these have been published or are in process of publication. We also have incomplete data on interconversions in aziridine, the acetylacetones, and substituted acidic acids. We anticipate making more extensive NMR spectral measurements when our new 400 MHz Varian instrument is delivered (in about 4 months) on the dissociation relaxation in N_2F_4 and of $(FSO_3)_2$. The novel aspects of our experiments are briefly listed below:

A. In the alkyl nitrites, where the density of vibrational states at the potential maximum (≈10 kcal/mole) is less than 50/cm^{-1}, for pressures below the onset of the second order regime, the directly calculated bimolecular rate constant increases with decreasing pressure. This effect was confirmed by other investigators for methyl nitrite, and it was also observed in SF_4. We propose a limited phase space model to account for these observations.

B. The dissociation-association relaxation time in Me_2O:HCl and in formic acid are faster than we could measure. Our results place an upper limit of 8.5 kcal/mole for the activation energy in Me_2O:HCl; thermochemical dissociation enthalpy for this model hydrogen bonded system is 6.9 kcal/mole. The association reaction requires de-excitation by a third body to take place in less than 10^{-10} sec.

C. Our data indicate that the activation energy for rotation in

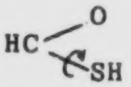

$HC\overset{O}{\underset{SH}{<}}$ is significantly lower in the gas phase than in solution. This suggests that the tunneling contribution is greater in the gas phase.

In one of our publications we called attention to the fact that the generally quoted equations for unimolecular reactions, and all the available computer codes apply strictly to nonreversible processes. We developed corrections which are valid both at the low and the high pressure limits for reversible reactions. Additionally we proposed use of a relaxation-kinetics model which requires fewer arbitrary assumptions than does the conventional RRKM model, and is simple to apply.

THE GENERATION AND PROPERTIES OF A BEAM OF METASTABLE H_3 MOLECULES

James F. Garvey and Aron Kuppermann
A. A. Noyes Laboratory of Chemical Physics
California Institute of Technology

The object of our research program is to perform experimental and theoretical studies of elementary chemical reactions. The experimental approach consists in part of studying the reactions of monoenergetic H or D atoms with other simple molecules, as a function of collision energy, in a crossed molecular beam geometry. The theoretical approach consists of performing both accurate and approximate quantum mechanical calculations on these same or closely related reactions, in order to gain insight into the relation between the potential energy surfaces governing such reactions and the ensuing state-to-state dynamics.

An important component of the experiments is a beam of high intensity, high energy H atoms, generated in an arc heated discharge through H_2 molecules, similar to the one used previously by Young et al. [1] and by Way et al. [2]. This beam is depicted in Figure 1, together with a simple test set-up designed to detect and characterize the beam with the help of an electron bombardment ionizer and quadupole mass spectrometer.

When operating this beam we were surprised to find a significant $m/e = 3$ signal using H_2 in the arc source, and an $m/e = 6$ signal using D_2, as shown in Figure 2. Prior to entering the mass spectrometer the ions generated in the arc discharge are removed from the beam with the help of a 1 kV/cm electrostatic deflection field. Furthermore, the observed signal virtually vanishes when the electron beam in the mass spectrometer ionizer is turned off. A careful analysis of the experimental conditions excluded in the possibility of attributing the observed signal to secondary processes in the mass spectrometer ionizer, leaving neutral H_3 or D_3, molecules in the beam as the only possible explanation of the observations. A crude energy analysis with the help of retardation fields after electron bombardment ionization indicates a lifetime of these species in excess of 40 μsec. An absolute intensity measurement furnished a value in excess of 10^{20} molecules/sterad/sec.

These results are consistent with the H_3 or D_3 species in question being in a metastable $2p\ ^2A''_2$ state previously observed by Herzberg [3] and calculated by King and Morokuma [4]. Further confirmation of our interpretation came from analysis of the light emitted by the plasma plume which appears directly in front of the nozzle of the beam source [5]. We were further able to surface ionize the H_3 using a hot tungsten wire, which produced H_3^+ and H^+ ions, but no H_3^+ ones.

This intense beam of metastable H_3 will, in subsequent experiments, be energy-selected with a Stern-Gerlach magnet, and its spectroscopic and dynamic properties investigated in detail. Because of its high internal energy content and its metastability, it is expected to have interesting reactivity properties. Furthermore, being an electronically excited state of the transition state of the $H + p\text{-}H_2 \rightarrow o\text{-}H_2 + H$ reaction, its spectroscopy may give experimental information closely related to the shape of the potential energy surface of this important reaction.

James F. Garvey and Aron Kuppermann (Cont'd)
A. A. Noyes Laboratory of Chemical Physics
California Institute of Technology

References

1. Young, W.S., Rodgers, W.E., and Knuth, E.L., Rev. Sci. Instrum. 40, 1346 (1969).
2. Way, K.R., Yan, S.C., and Stwalley, W.C., Rev. Sci. Instrum. 9, 1049 (1976).
3. King, H.R., and Morokuma, K., J. Chem. Phys. 71, 3213 (1979).
4. Herzberg, G., J. Chem. Phys. 70, 4806 (1979).
5. Garvey, J. F. and Kuppermann, A., Chem. Phys. Lett. 107, 491 (1984).

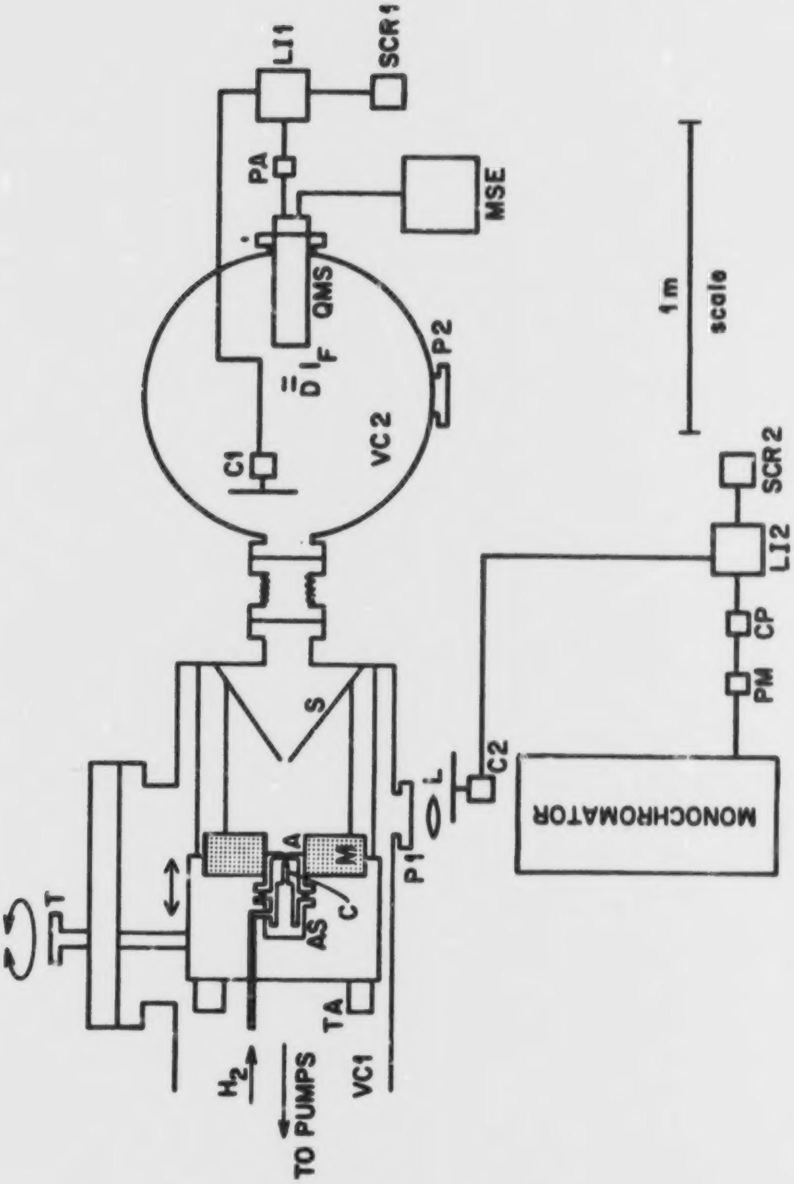
LI1
SCR1
PA
MSE
QMS
D
F
P2
C1
VC2
1 m
scale
SCR2
LI2
CP
PM
S
L
C2
MONOCHROMATOR
A
M
P1
C
AS
T
TA
H2
TO PUMPS
VC1

Figure 1. A schematic view of the top of the machine: VC1 - vacuum chamber one, AS - anode assembly, A - anode, C - cathode, M - magnet, S - water-cooled copper skimmer, TA - translation assembly, T - translator, P1 - viewport, L - optical lens, C2 - 150 Hz chopper, Mono - 0.5 m Jarrel-Ash monochromator, PM - photomultiplier, CP - current preamp, L12 - lock-in amplifier, SCR2 - strip chart recorder, VC2 - vacuum chamber 2, C1 - 10 Hz chopper, D - electric field deflectors, F - mechanical flag, QMS - quadrupole mass spectrometer, P2 - port, PA - preamp, LI1 - lock-in amplifier, MSE - mass spectrometer electronics, SCR1 - strip chart recorder.

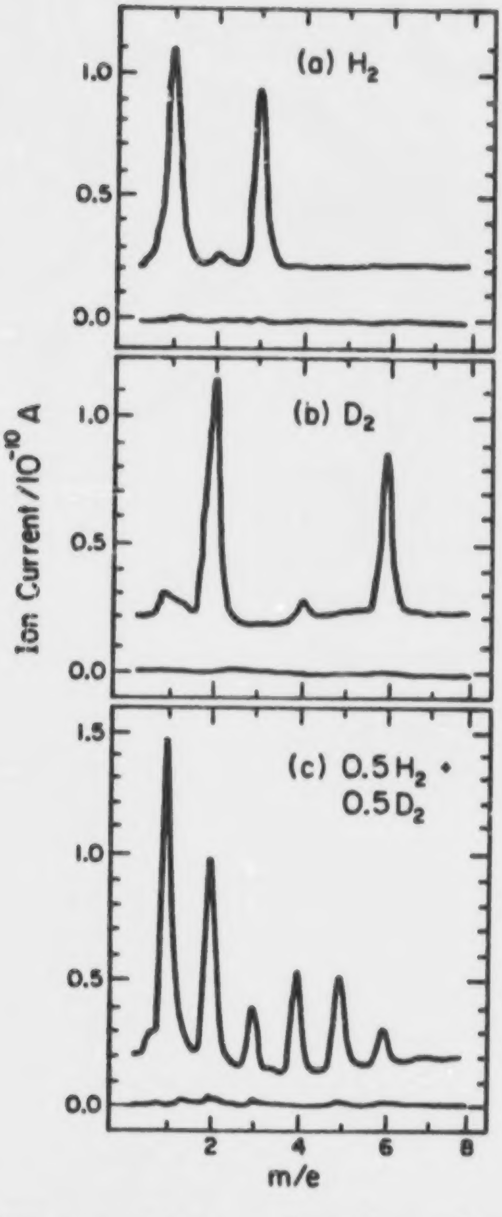

Figure 2. AC ion current as a function of m/e. In each panel the lower curve is the AC background obtained with the electron beam turned off, and the upper curve is the AC ion current signal shifted upwards by 0.2×10^{-10} A for convenience of display. Electron impact current: 100 μA. Electron accelerating voltage: 60V. Ion source pressure: 2.1×10^{-5} torr measured by an uncalibrated ion gauge. (a) H_2 in the molecular beam source; (b) D_2 in that source; (c) and equimolar mixture of H_2 and D_2 in that source. For all the panels, the stagnation pressure in the molecular beam source was 60 torr. (Nozzle conditions changed slightly.)

STATE-SELECTED ION-MOLECULE REACTION DYNAMICS

RICHARD J.S. MORRISON, WILLIAM E. CONAWAY, AND RICHARD N. ZARE
Department of Chemistry, Stanford University
Stanford, California 94305

By analyzing the photoelectron energies in several systems, it can be demonstrated that multiphoton ionization (MPI) will selectively produce molecular ions predominantly in a single vibrational level selectable by the proper choice of the laser frequency. Thus, MPI provides a powerful new technique for producing high densities of internally state-selected reagent ions for chemical reaction dynamics studies. This approach is being taken for studying the ion-molecule reactions of $NH_3^+(v)$ which has been prepared with $v = 0 - 9$ vibrational quanta in the umbrella-bending (ν_2) mode.

The experimental arrangement consists of a 2+1 laser multiphoton ion source and an ion optics system for controlling the energetics of the reactant ion beam (Figure 1). A constant pressure of the target neutral species is maintained in a field-free collision cell. Forward-scattered products and unreacted primary ions are collected and analyzed by a quadrupole mass spectrometer and detection electronics. The mass signal as a function of the reaction cell potential (primary ion translational energy) and of the laser wavelength (primary ion vibrational energy) is then recorded by a computer system.

Two reaction products have been observed from the reaction of NH_3^+ + D_2. The D atom abstraction channel to form NH_3D^+ is slightly exothermic while the D atom exchange channel to form NH_2D^+ is thermoneutral (Figure 1). We observe the former channel to dominate over the NH_3^+ translational energy range examined (0 - 10 ev in the center of mass frame). A sharp

BEST COPY AVAILABLE

decrease in the NH_3D^+ yield is found above an energy corresponding closely to the HD bond strength. For all vibrational levels investigated, this decrease is correlated with an increase in the NH_2D^+ product signal (Figure 2). These results can be attributed to the onset of a third reaction channel

$$NH_3^+ + D_2 \dashrightarrow NH_2D^+ + H + D \qquad (I)$$

in which the likely precursor to the NH_2D^+ product is NH_3D^+ initially formed with excess internal energy.

A pronounced vibrational effect on the exchange channel is seen at energies deficient to permit process (I). Plotted in Figure 2 is the branching ratio, defined by NH_2D^+/NH_3D^+, versus the NH_3^+ reagent ion collision energy for several NH_3^+ reagent ion vibrational states. Below 4 eV, vibrational energy appears to be effective in promoting the NH_2D^+ channel, which is totally absent for vibrationless reagent ions. In marked contrast, translational energy has little effect on this reaction in this energy region.

It may be expected that the thermoneutral exchange channel be accompanied by a small barrier to reaction, as was suggested in the earlier work on this reaction by Henglein. Owing to the implicit lack of control over the ion internal states in these experiments, no evidence for such a barrier was actually observed. Our results would suggest that a barrier is indeed present and that it can be effectively surmounted by vibrational energization of the NH_3^+ reagent ion to levels above v = 4.

G. Eisele, A. Henglein, P. Botschwina, and W. Meyer, Ber. Bunserges. physik. Chem. 78,1090 (1974).

SCHEMATIC OF EXPERIMENTAL APPARATUS

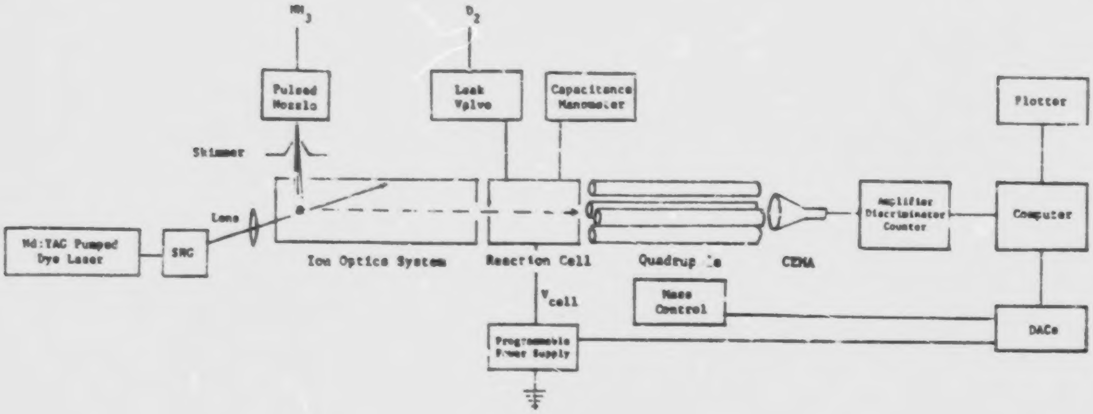
NH_3
D_2
Pulsed Nozzle
Leak Valve
Capacitance Manometer
Plotter
Skimmer
Lens
Nd:YAG Pumped Dye Laser
SHG
Ion Optics System
Reaction Cell
Quadrupole
CEMA
Amplifier Discriminator Counter
Computer
V_{cell}
Mass Control
DACs
Programmable Power Supply

ENERGY SCHEMATIC: $NH_3^+ + D_2$

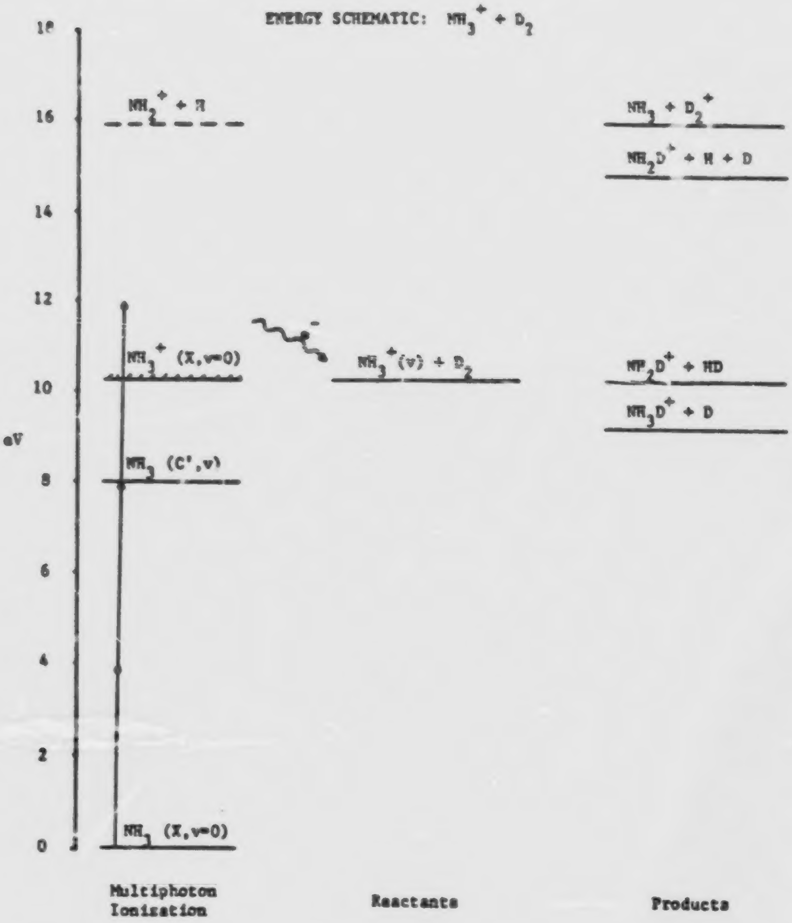
18
16
14
12
10
8
6
4
2
0
eV
$NH_2^+ + H$
NH_3^+ (X,v=0)
NH_3 (C',v)
NH_3 (X,v=0)
$NH_3^+(v) + D_2$
$NH_3 + D_2^+$
$NH_2D^+ + H + D$
$NH_2D^+ + HD$
$NH_3D^+ + D$
Multiphoton Ionization
Reactants
Products

Figure 1. Schematic representation of ion-molecule reaction apparatus and energy levels for the reaction $NH_3^+ + D_2$.

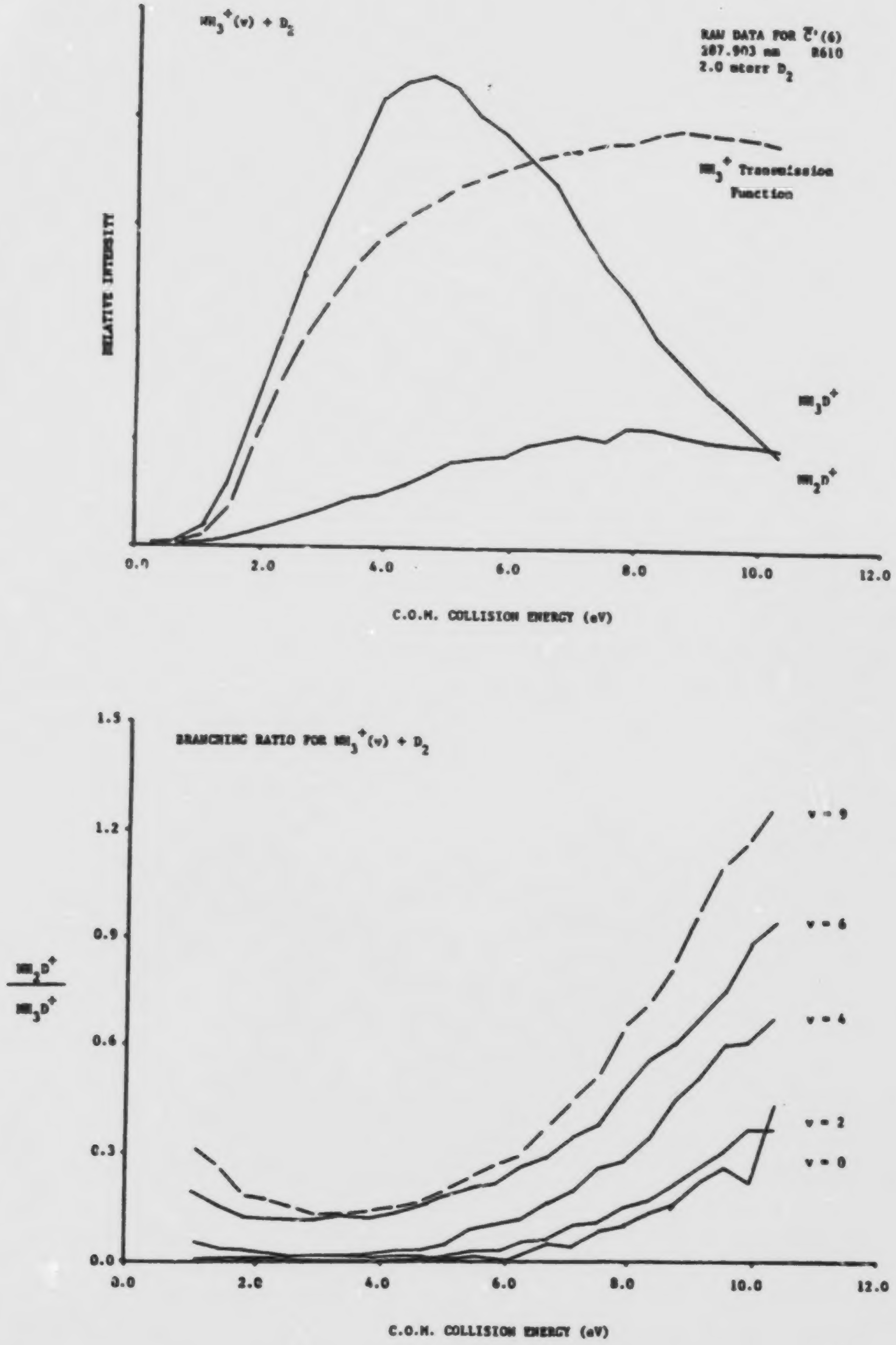

Figure 2. Data showing how the two product channels depend on the ion translational energy and how their ratio depends on the ion vibrational quanta.

DYNAMICAL SYMMETRIES

R.D. Levine

Energy and anharmonicity are closely tied up in molecular dynamics. Spectroscopic probing of energy rich states and their intramolecular relaxation and dissociation require explicit account of anharmonicities. The same is true for intermolecular processes. The algebraic approach is a systematic dynamic theory of the structure and time evolution of mechanical systems. It has the advantage that even in zero order the anharmonicity can be incorporated. The major current shortcoming is that it lacks a complete geometrical interpretation.

During the past year the approach was developed mainly along two lines. The first is the construction of generic Hamiltonians suitable for a class of chemical phenomena. An example of a completed project is a simple Hamiltonian for the vibrational (including bending) motion of triatomics. With a very small number (4 to 6) of parameters such a Hamiltonian provides a near quantitative (few wave numbers) account of the vibrational overtones and includes all the familiar coupling mechanisms (e.g. Fermi, Darling-Dennison) of molecular spectroscopy. Figure 1 is an example of overtones of stretching modes predicted by such a Hamiltonian. Better accuracy is possible by using somewhat more complicated Hamiltonians and this has been explored for O_3 and H_2O. Work is in progress on shape transitions in triatomic molecules at higher vibrational excitation, on propensity rules in optical excitation and on vibrational-rotational coupling.

The second development is the practical formulation of the approach for time evolving states. This is based on a variational principle. By solving a classical like equation of motion (i.e. single trajectory) one obtains the quantal state of the system throughout the collision. Computational studies are in progress for simple model problems for the purpose of demonstrating the method for systems where other quantal methods are feasible so that comparisons can be carried out.

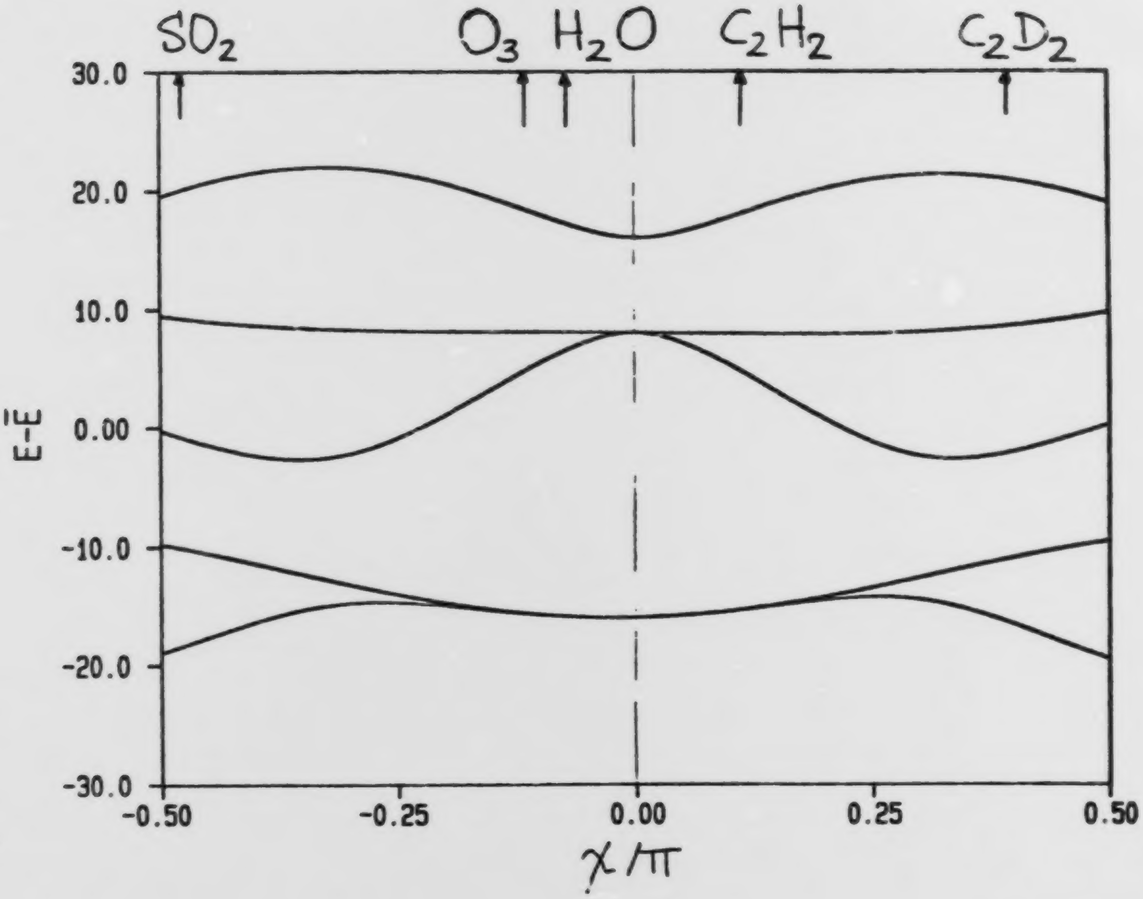

Figure 1. The energy levels of the overtones of stretching vibrations of triatomics for the multiplet where the sum of the two vibrational quantum numbers is 5. χ, the 'mixing parameter' , tnχ is the ratio of the coupling strength of the local modes to their anharmonicity. χ → 0 is the local mode limit and χ → ±π/2 is the normal mode limit. On such a reduced plot each specific molecule corresponds to a particular value of χ and some values are indicated.

BEST COPY AVAILABLE

Laser Induced Fluorescence Study of the $HeBr_2$ van der Waals Complex

Michael C. Heaven
Department of Chemistry
Illinois Institute of Technology
Chicago, Illinois 60616

The triatomic van der Waals complexes which are produced when a rare gas atom is bound to a diatomic halogen form a particularly interesting group of molecules for spectroscopic study. They provide prototype systems for investigation of the nature of the van der Waals bond, and for the study of photodissociation dynamics on a single adiabatic potential energy surface.

The $HeBr_2$ complex has been observed for the first time using laser induced fluorescence techniques. The apparatus used for this work is shown in Fig. 1. It consisted of a small vacuum chamber which was pumped by a Roots blower system. A supersonic free jet was formed by seeding Br_2 in He, and expanding the mixture through a 0.1mm orifice. The free jet was intersected by the beam from a tunable dye laser (0.05 cm^{-1} linewidth) at a point 3mm downstream from the nozzle. Laser excited fluorescence was detected by a PMT and recorded by a transient digitizer.

Fig. 2a shows a low resolution spectrum for Br_2 seeded in He. The intense bands are easily identified as the Br_2 (B-X) system. Accompanying each of these bands is a weaker feature which belongs to the $HeBr_2$ complex. Rotationally resolved spectra have been recorded for the 11-0 to 38-0 bands of the complex. As an example, Fig. 2b shows the rotational structure of the 12-0 bands of $HeBr_2$ and Br_2. On average the band origins of the complex were blue shifted by ~4.2 cm^{-1} from the uncomplexed Br_2 bands. Analysis of the rotational structure provided geometric parameters for the complex. The molecule is 'T' shaped in both the ground and excited states, and there is a significant barrier to internal rotation.

Vibrational predissociation of the Br_2-He band was observed via homogeneous broadening of the rotational lines. Predissociation rates, derived from the lineshape data, showed a strong dependence on Br_2 vibrational excitation. Rates varied from $10^{10}s^{-1}$ for v'=11 up to $5x10^{11}s^{-1}$ for v=38. The data can be adequately described by simple 'energy gap' model for the predissociation probability.

BEST COPY AVAILABLE

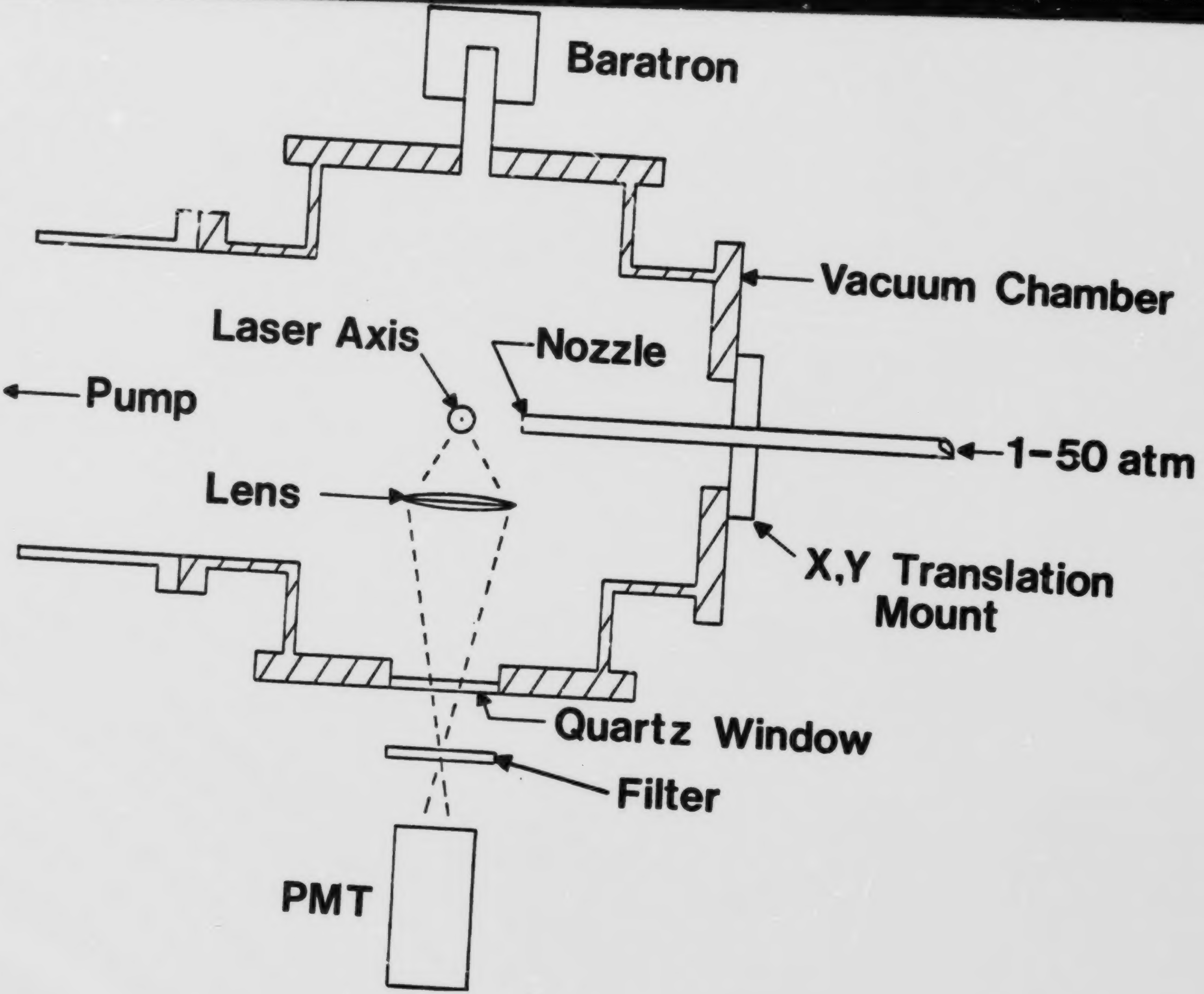
Baratron
Vacuum Chamber
Laser Axis
Nozzle
Pump
1–50 atm
Lens
X,Y Translation Mount
Quartz Window
Filter
PMT

Figure 1.

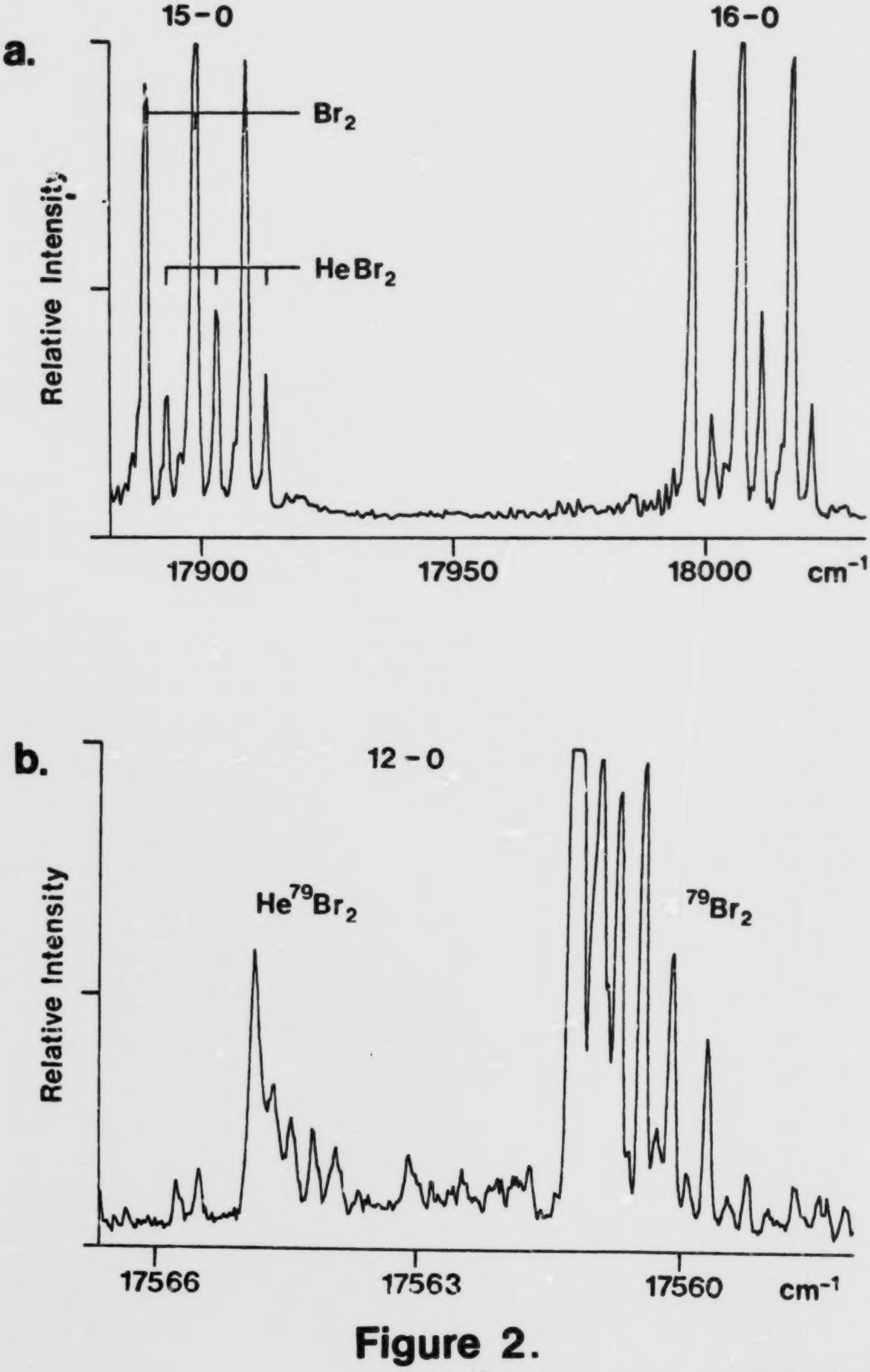

Figure 2.

BEST COPY AVAILABLE

LASER STUDIES OF HALOGENS AND OXYGEN

Paul L. Houston
Department of Chemistry
Cornell University
Ithaca, NY 14853

Electronically excited oxygen, $O_2(^1\Delta)$, is an energy source which can be chemically generated and used to pump electronic transition lasers. Despite its importance in, for example, the chemical oxogen/iodine laser system, sensitive detection methods for $O_2(^1\Delta)$ have not yet been developed. The most widely used technique, infrared detection of the 1.27 μm fluorescence, suffers both from the long radiative lifetime of $O_2(^1\Delta)$ and from the low sensitivity of photodetectors at this wavelength. This technique has not generally been able to provide information about vibrational and rotational distributions within th $O_2(^1\Delta)$ state.

We have used multiphoton ionization to detect sensitively $O_2(^1\Delta)$ both in a microwave discharge and from the 266-nm photodissociation of O_3. A tunable ultraviolet source (Quanta-Ray DCR-2A, PDL-1, WEX) was focused between two parallel plates, and current produced by two-photon absorption followed by one-photon ionization was amplified and recorded by a boxcar integrator. The resulting spectra consisted of 4-5 vibrational bands for each of several Rydberg transitions in the 260-245 nm region as well as for one valence band near 340 nm. Figure 1 displays, for example, the spectrum of the 2-0 band for one of the series. As can be seen from the spectral detail, it is possible to use the MPI technique not only to detect $O_2(^1\Delta)$, but to determine its vibrational and rotational distribution as well.

Although the assigment of the Rydberg transitions is still in progress, it appears that all components of the $3d\pi_g$ Rydberg transition have been observed. Because the spin-orbit interaction is larger than or comparable to the separation between the six sub-levels ($^1\Sigma^-{}_g$, $^3\Delta_g$, $^3\Sigma^+{}_g$, $^3\Sigma^-{}_g$, $^1\Delta_g$, and $^1\Sigma^+{}_g$), the spectra are highly perturbed. The $^1\Delta_g$ sub-level has been unambiguously identified by the absence of two-photon absorption when the linear polarization of the laser light is replaced by circular polarization, as shown in Fig. 2.

Determination of detection limits and application of the MPI technique to studies of the dynamics of $O_2(^1\Delta)$ are in progress.

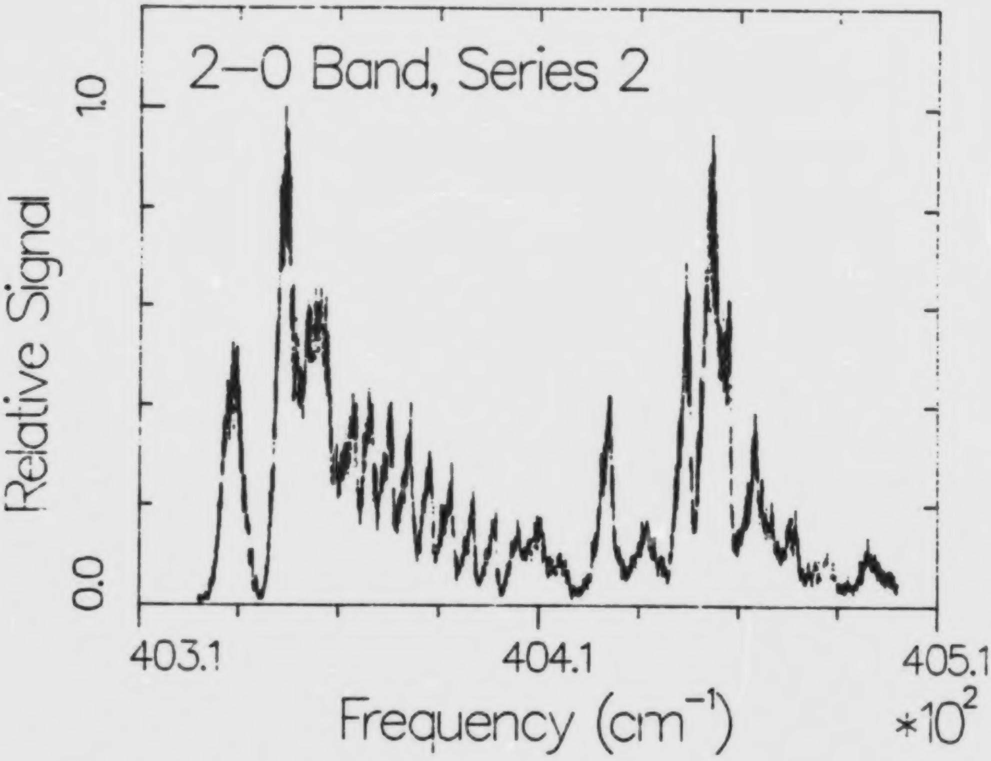

Figure 1. One Vibrational Band of the $O_2(^1\Delta)$ $3d\pi_g$ Rydberg Series.

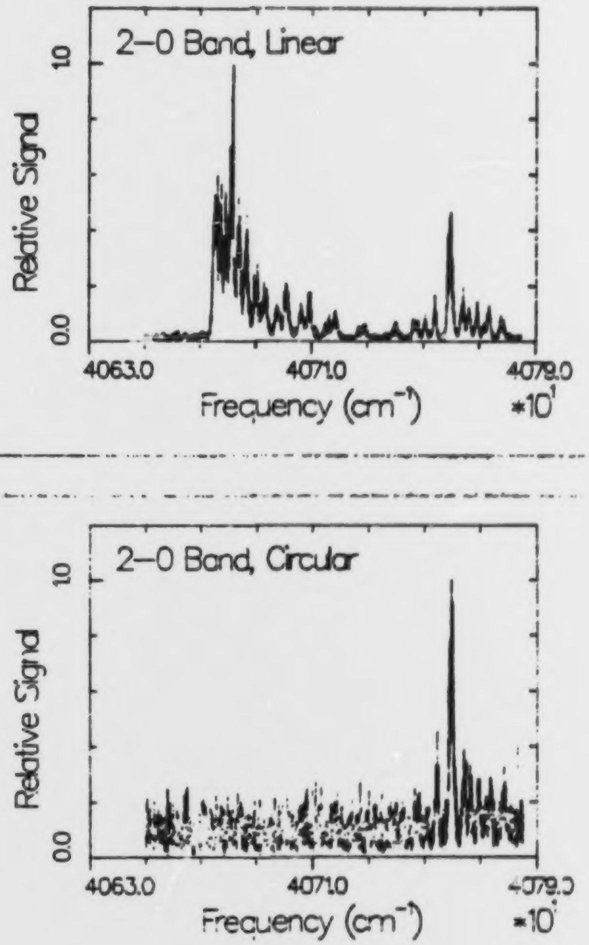

Figure 2. Multiphoton Ionization Spectrum of a $^1\Delta - {}^1\Delta$ Transition. The two-photon absorption strength vanishes for circular polarization.

DETECTION OF VIBRATIONALLY EXCITED I_2 IN THE DISSOCIATION REGION OF CHEMICAL OXYGEN-IODINE LASERS

M. H. Van Benthem and S. J. Davis
Air Force Weapons Laboratory
Kirtland AFB, New Mexico 87117

ABSTRACT

Direct evidence of vibrationally excited $I_2X(v = 33 - 44)$ has been observed in the reaction region of $I_2(X(v' = 0)) + O_2(^1\Delta)$. Using a flow tube reactor and an LIF technique, a laser excitation spectrum of the vibrationally excited species was obtained. In the region of maximum LIF intensity, the population density in the vibrationally excited state maximizes at $v'' = 35$, with approximately 0.04 percent of all $I_2(X)$ in the levels $(v'' = 33 - 44)$. $I_2(v'' = 33 - 44)$ appears to be a precursor of I^* according to flow tube temporal profile studies. Inferences concerning the operation of oxygen-iodine lasers will be discussed.

Collisional Dynamics of Excited Halogens and Interhalogens

G. P. Perram, P. J. Wolf and S. J. Davis

Air Force Weapons Laboratory
Kirtland AFB NM 87117

Pulsed and C-W laser fluorescence techniques are being utilized to investigate collisional quenching and energy transfer in the $B^3\Pi$ states of IF, BrCL and Br_2. Studies of V-T, R-T and V-V transfer with a variety of collision partners will be presented. These results will be related to the operation of B → X halogen laser systems. The scaling dependence of V-T rates as a function of vibrational quantum number will be discussed for the IF molecule.

STUDIES OF ELECTRONICALLY EXCITED STATES

JOHN WIESENFELD
Department of Chemistry, Cornell University
Baker Laboratory, Ithaca, NY 14853

The continuing study of halogen atom kinetics is motivated by interest in the development of the chemical oxygen iodine laser. Because Cl_2 is involved in the chemical generation of $O_2(^1\Delta)$, special attention has been paid to the deactivation of electronically excited iodine atoms, $I^*(5^2P_{1/2})$, by this molecule.

$$I^* + Cl_2 \longrightarrow I(5^2P_{3/2}) + Cl_2 \qquad [1a]$$
$$\longrightarrow ICl + Cl \text{ (or } Cl^*) \qquad [1b]$$

Two previous studies yielded $k_1 = 2.1 \times 10^{-13}$ and 1.7×10^{-12} cm^3 $molec^{-1}$ sec^{-1} using kinetic absorption spectroscopy[1] and infrared emission,[2] respectively. Were the rate constant for deactivation so large, significant quenching of I^* in the COIL would be expected, yet apparently this has not been observed.

In order to resolve the apparent discrepancy between the kinetic measurements and to better understand the kinetics of the COIL system, the rate of [1] was measured once again by monitoring the time-resolved infrared emission, $I^* \longrightarrow I + h\nu$ ($\lambda = 1.315\ \mu$) following the photolysis of $CF_3I/Cl_2/Ar$ mixtures at 266 nm. Excellent sensitivity was achieved through the use of a liquid N_2 cooled intrinsic germanium detector and extensive signal averaging of the emission transient. In initial experiments carried out with a static mixture, the rate of I^* deactivation was found to increase dramatically following repeated photolysis, e. g., from 300 to 4000 sec^{-1} following 64 laser shots of 5 mJ energy. Further experiments carried out using continuously replenished flowing mixtures revealed a dependence of the observed rate coefficient upon the photolysis energy and laser pulse repetition rate (Figure 1). Data obtained at minimum energies (0.03 mJ) and repetition rate (0.1 Hz) yield $k_1 = 8 \times 10^{-15}$ cm^3 $molec^{-1}$ sec^{-1}, a value which must be regarded as an upper limit to the true rate coefficient. This result is lower still than a recent flow system measurement of 1.7×10^{-14}.[3]

Careful examination of the emission data obtained at relatively high laser power density (~1 mJ cm^{-2}) reveals a characteristic departure from first-order kinetics (Figure 2). The removal of I^* accelerates immediately following photolysis but then at long time slows down noticeably. Extensive numerical simulation of possible mechanisms suggests that a chain mechanism leading to a steady state concentration of Cl atoms and subsequent deactivation of I^* by Cl play a significant role in establishing the observed kinetics.

---

[1] R. J. Donovan, F. G. M. Hathorn, and D. Husain, Trans. Farad. Soc. 64, 1228 (1968).

[2] H. Hofmann and S. R. Leone, J. Chem. Phys. 69, 641 (1978).

[3] H. V. Lilenfeld, P. D. Whitefield, and G. R. Bradburn, private communication.

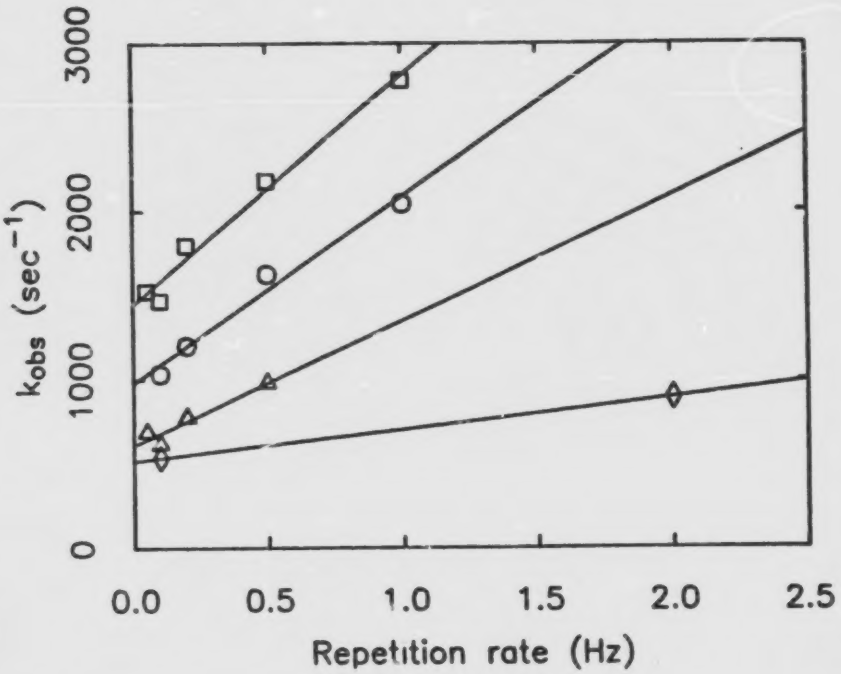

Figure 1. Observed decay rates vary with both photolysis energy and laser repetition rate. Squares: 1.0 mJ; circles: 0.3 mJ; triangles: 0.1 mJ; diamonds: 0.03 mJ.

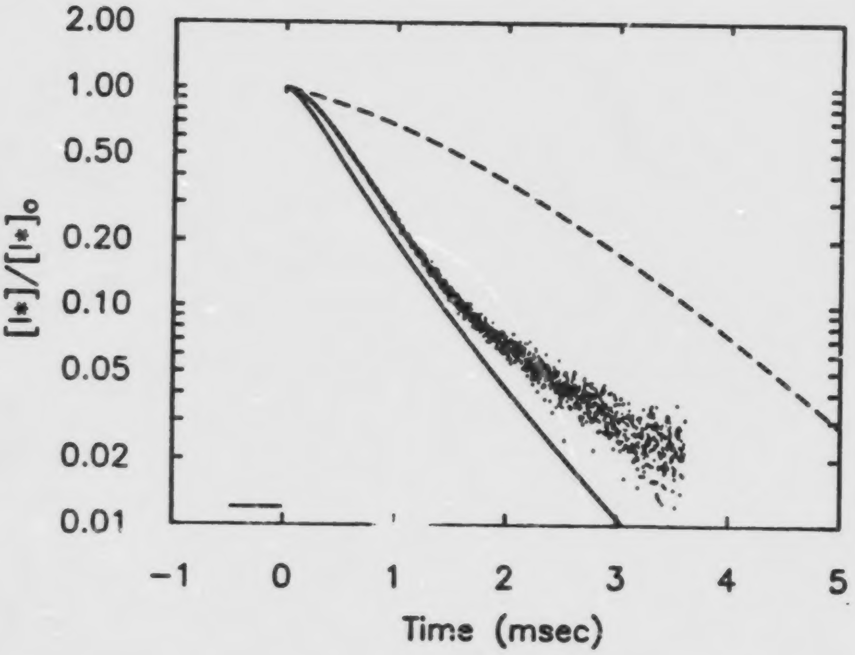

Figure 2. Time-resolved I* emission following photolysis (E = 1 mJ cm^{-2}, 0.1 Hz) of test mixture (P[CF_3I] = 1.0 torr, P[Cl_2] = 1.2 torr, P[Ar] = 4.0 torr). A total of 20 shots were averaged. The model results are shown for k(I* + Cl) = 0 (----) and 3 x 10^{-10} (——).

BEST COPY AVAILABLE

AFOSR/AFWAL Molecular Dynamics and Surface Chemistry Conference (24-26 Oct. 1984)

INTRA-COLLISIONAL STUDIES FROM LIGHT SCATTERING

J. Cooper
Joint Institute for Laboratory Astrophysics/Department of Physics
University of Colorado, Boulder, CO 80309

The objective of this work is to use scattering of near-resonant laser light to obtain information concerning intra-collisional dynamics and inter-atomic potentials of collision complexes, with the ultimate aim to elucidate collisional mechanisms (such as quenching and energy transfer) associated with metastable states in the alkaline earths (Ca, Mg, Sr, etc.). With this information it may prove possible that such states may be optimally "switched" by intense laser fields.

The techniques being used in this study have already been successfully applied to the study of collision complexes associated with allowed transitions in Sr and Ba.[1] As indicated schematically in Fig. 1 for the barium system, off-resonant laser light (green), incident upon barium vapor in a rare gas environment in a heated oven, excites the Ba during a collision and the details of the resulting population are probed by a second (red) on-resonance laser (with fluorescence (blue) being observed). The response to polarized probe light depends on the populations of the Zeeman- sub-levels of the $6p\,^1P$ state, which, in turn, depend on the evolution of the collision from the point of absorption of the "green" light to the end of the collision. Polarization properties, combined with line wing data (see Fig. 2), provide a unique interpretation of the interatomic potentials involved and is quite sensitive to the mixing of states at large internuclear separation (where molecular states no longer give an adequate description). Far wing satellites are apparent in Fig. 2, and the zero circular polarization is a consequence of a Σ-Σ^* transition. Alignment and orientation cross-sections are also simply obtained from these data.

Essentially we are measuring "half collisions" in the transient alkaline earth atom/rare gas system, so that in many ways these studies are complementary to molecular photodissociation studies.[2] Theoretically one must keep track of the effect of a series of collisions in the cell, so that the statistical-mechanical description is quite complicated.[3] We[4] are completing a detailed study of the three-level system, which includes two-photon absorption within a single collision, absorptions in different (subsequent) collisions, and all possible Raman processes in its description. Extension of theory to systems in which the initial excitation is asymptotically forbidden, but has a transient dipole during collisions (such as to the $Ca\,^3P$) is underway.

Preliminary experiments are in progress on the Ca/rare gas system. The initial step (compare Fig. 1) $4s^2\,^1S$-$4s4p\,^3P$ ($\sim$657 nm) is forbidden, but the second step $4s4p\,^3P_1$-$4s5s\,^3S_1$ (at 614 nm) is allowed. Although the transition probability of the first step is small (corresponding to a life time of order $\sim$340 μs, (which gives $\sim$1 ms when collisional fine structure mixing is taken into account)), adequate ($\sim 10^{11}$ cm^{-3}) densities of $Ca\,^3P$ can be obtained using either pulsed or ring lasers ($\sim$100 mW). Off-resonant excitation of the second step then gives information on the ^3P potentials. It is apparent that the collisional quenching cross-section for the ^3P is very sensitive to impurities[5] and energy-pooling reactions, such as $Ca(4p\,^3P) + Ca(4p\,^3P) \rightarrow Ca(5s\,^3S) + Ca(4s\,^1S) + 1000\ cm^{-1}$, must be taken into account. Our preliminary quenching cross-section for $Ca\,^3P$ by Ar, obtained from a pulsed experiment, is at least two orders of magnitude smaller than previously reported.[5b]

This combination of experimental reaction rate, line-wing, and polarization behavior with theoretical interpretation will present a unique and detailed characterization of the collision-complexes associated alkaline earth ^3P metastables.

1(a). Alford, J., Burnett, K., and Cooper, J., Phys. Rev. A27, 1310 (1983).
(b). Alford, J., Andersen, N., Burnett, K., and Cooper, J. Phys. Rev. A, (in press).
2. Greene, C.H. and Zare, R.N., Ann. Rev. Chem. 33, 119 (1982).
3. Burnett, K., and Cooper, J., Phys. Rev. A22, 2005, 2027, and 2044, (1980).
4. Alber, G., and Cooper, J. (to be published).
5(a). Hussain, D. and Schifino, J., J. Chem. Soc. Faraday Trans.2, 79, 1677 (1983).
(b). Malins, R.J. and Benard, D.J., Chem. Phys. Lett. 74, 321 (1980).

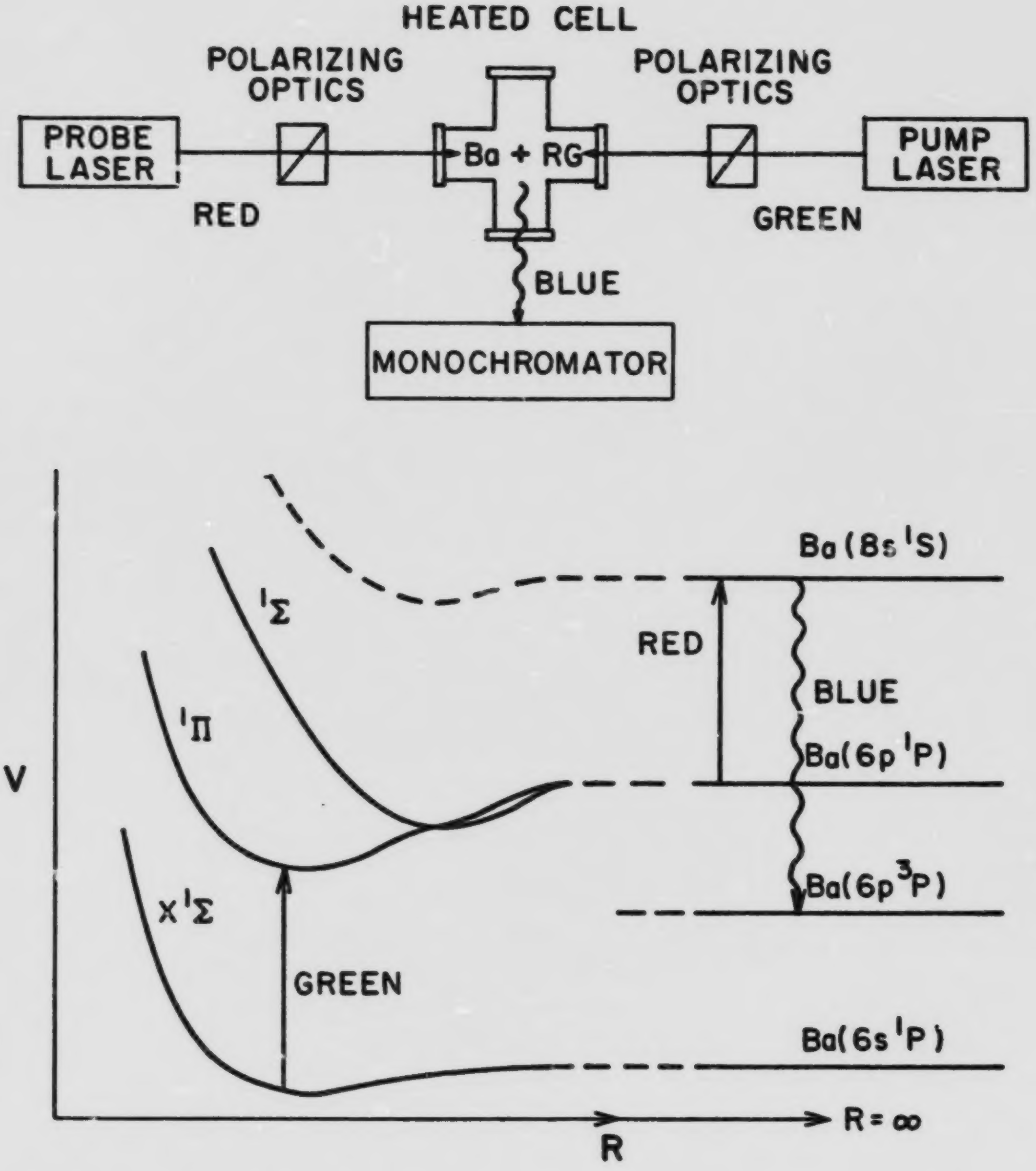
HEATED CELL
POLARIZING OPTICS
POLARIZING OPTICS
PROBE LASER
Ba + RG
PUMP LASER
RED
GREEN
BLUE
MONOCHROMATOR
$^1\Sigma$
$^1\Pi$
$X\,^1\Sigma$
V
Ba(8s ^{1}S)
RED
BLUE
Ba(6p ^{1}P)
Ba(6p ^{3}P)
GREEN
Ba(6s ^{1}P)
R
R = ∞

Figure 1(a). Schematic of experimental arrangement.
(b). Energy levels and absorption sequence in barium/rare gas system.

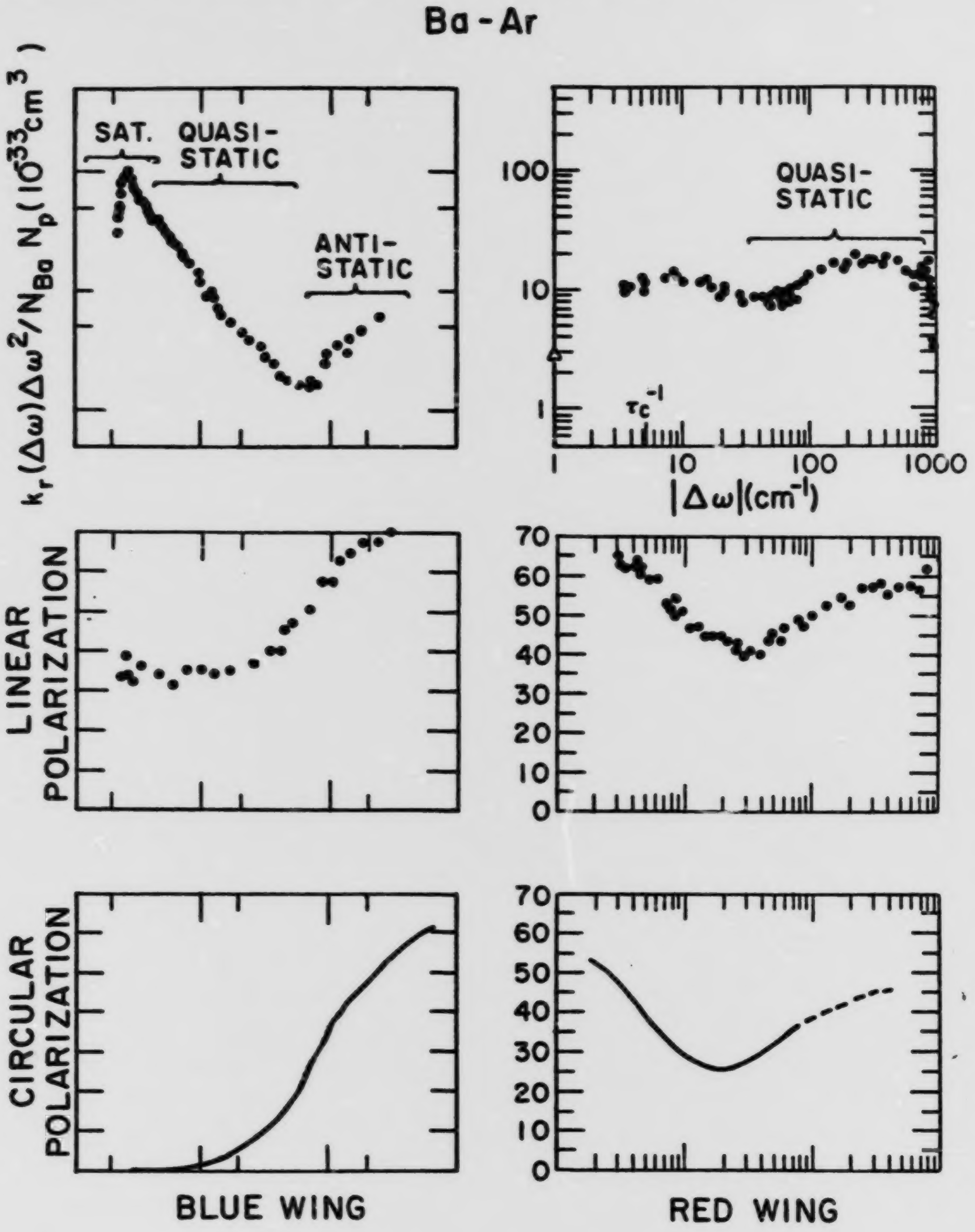

Figure 2. Representative data for barium/argon system as a function of detuning $\Delta\omega$.

(a). Collisional redistribution coefficient $k_r(\Delta\omega)$ multiplied by $(\Delta\omega)^2$ and normalized to Ba and Ar densities.
[Note: (i) Blue wing satellite, (ii) A Lorentzian would be a horizontal line.]

(b). Linear polarization $P_L = (I_\parallel - I_\perp)/(I_\parallel + I_\perp)$.

(c). Circular polarization $P_C = (I_+ - I_-)/(I_+ + I_-)$.
[I_+ corresponds to positive helicity, etc.]

BEST COPY AVAILABLE

PHOTODISSOCIATION DYNAMICS AND ENERGETICS OF SMALL CLUSTER IONS

Michael T. Bowers
Department of Chemistry, University of California
Santa Barbara, California 93106

Small cluster ions are of importance in a number of complex chemical systems including the earth's ionosphere. Very little work has been reported on the photochemistry of these species. The early work concentrated on the measurement of total photodestruction cross sections in the visible wavelength region without product analysis [1]. This abstract describes work recently accomplished in our laboratory of measurements of the detailed dynamics of the photodissociation process including information on energy disposal, product branching ratios, limits on excited state lifetimes and information on the nature of the photorecessed excited state surface and its symmetry.

The experimental set up used is shown schematically in Figure 1. Cluster ions are made in a cooled high pressure ion source by 3 body ion-molecule association reactions. They drift from the ion source, are accelerated and mass selected by the magnet. The mass selected ion beam is brought to a spatial focus where it is crossed by a focused laser beam. The photodissociation products are mass and energy analysed by a high resolution electrostatic analyser (ESA) and detected by pulse counting techniques. Variation of the plane of polarization of the laser allows determination of the product ion kinetic energy distribution and detailed dynamics of the photodissociation in the center of mass system.

Systems studied to date include $(N_2)_2^+$[2], $(NO)_2^+$[3] $(NO)_3^+$[4] $(CO_2)_2^+$, $(SO_2)_2^+$, $(Mn)_2^+$, $(N_2O)_2^+$, KrO_2^+ and $ArCO_2^+$. In the $(N_2)_2^+$ $(NO)_2^+$, and $(N_2O)_2^+$ symmetric dimer systems the photodissociation transition accesses a short lived repulsive state that results in products that are both translationally and rotationally excited. In $(CO_2)_2^+$ the predominant mechanism is via a repulsive excited state but a minor fraction accesses a bound excited state that interconverts to the ground state before vibrationally predissociating. The $(SO_2)_2^+$ dimer photodissociates via a bound excited state that either directly vibrationally predissociates to yield electronically excited SO_2^+ product or interconverts to the ground state and then dissociates. The branching ratio is a strong function of wavelength. Both the $Kr \cdot O_2^+$ and $Ar \cdot CO_2^+$ systems undergo an intramolecular charge exchange upon photon absorption to yield $Kr^+ \cdot O_2$ and $Ar^+ \cdot CO_2$ which subsequently dissociate to Kr^+/O_2 (exclusively) and Ar^+/CO_2 (predominantly). The neutral product (O_2 or CO_2) is formed vibrationally excited. The experiment allows determination of vibrational state distribution, average rotational energies and translational state distributions in these systems. Finally, $(Mn)_2^+$ photodissociates to form both electronically excited Mn^+ and ground state Mn^+. Analysis of the data yield a bond strength for $(Mn)_2^+$ of ≥ 1.35 eV the ionization energy of Mn_2 of 6.41 eV(Mn = 7.45 eV and bulk Mn = 4.1 eV) Several of the kinetic energy distributions are given in Figure 2 as examples.

1. For an example see G.P. Smith and L.C. Lee, J. Chem. Phys. 69, 5393 (1978).
2. M.F. Jarrold, A.J. Illies and M.T. Bowers, ibid 81, 214(1984).
3. ibid, 79, 6086 (1983).
4. ibid, 81, 222 (1984).

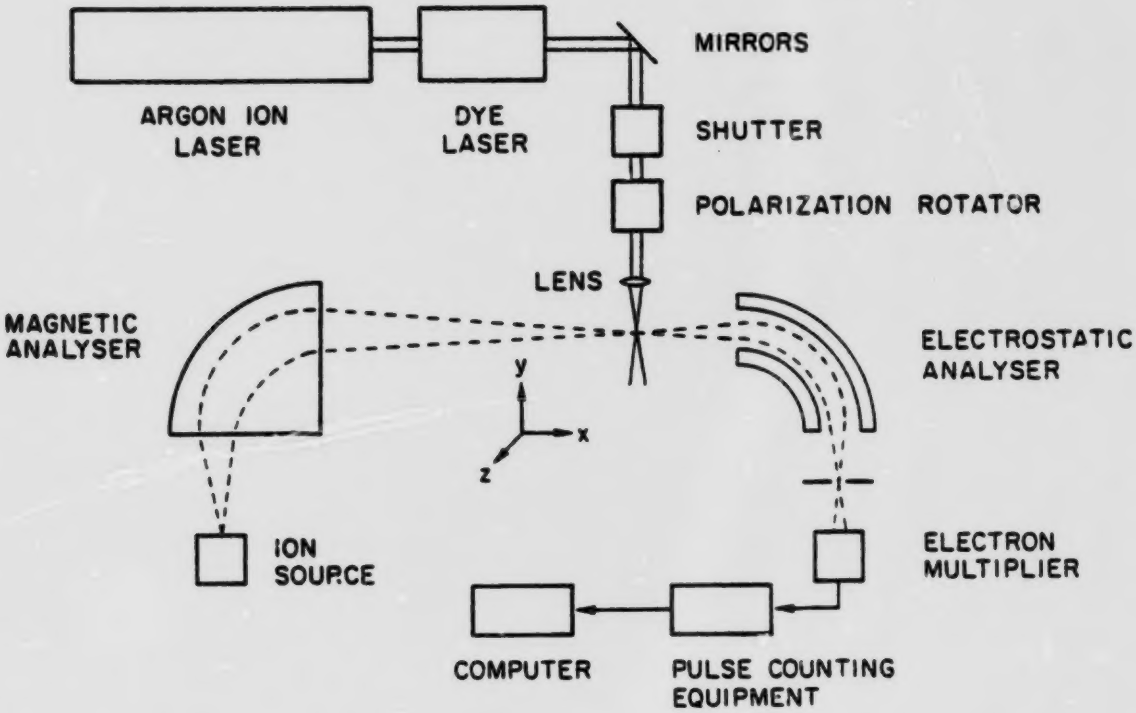
MIRRORS
ARGON ION LASER
DYE LASER
SHUTTER
POLARIZATION ROTATOR
LENS
MAGNETIC ANALYSER
ELECTROSTATIC ANALYSER
y
x
z
ION SOURCE
ELECTRON MULTIPLIER
COMPUTER
PULSE COUNTING EQUIPMENT

Fig. 1. Schematic representation of the photodissociation instrument.

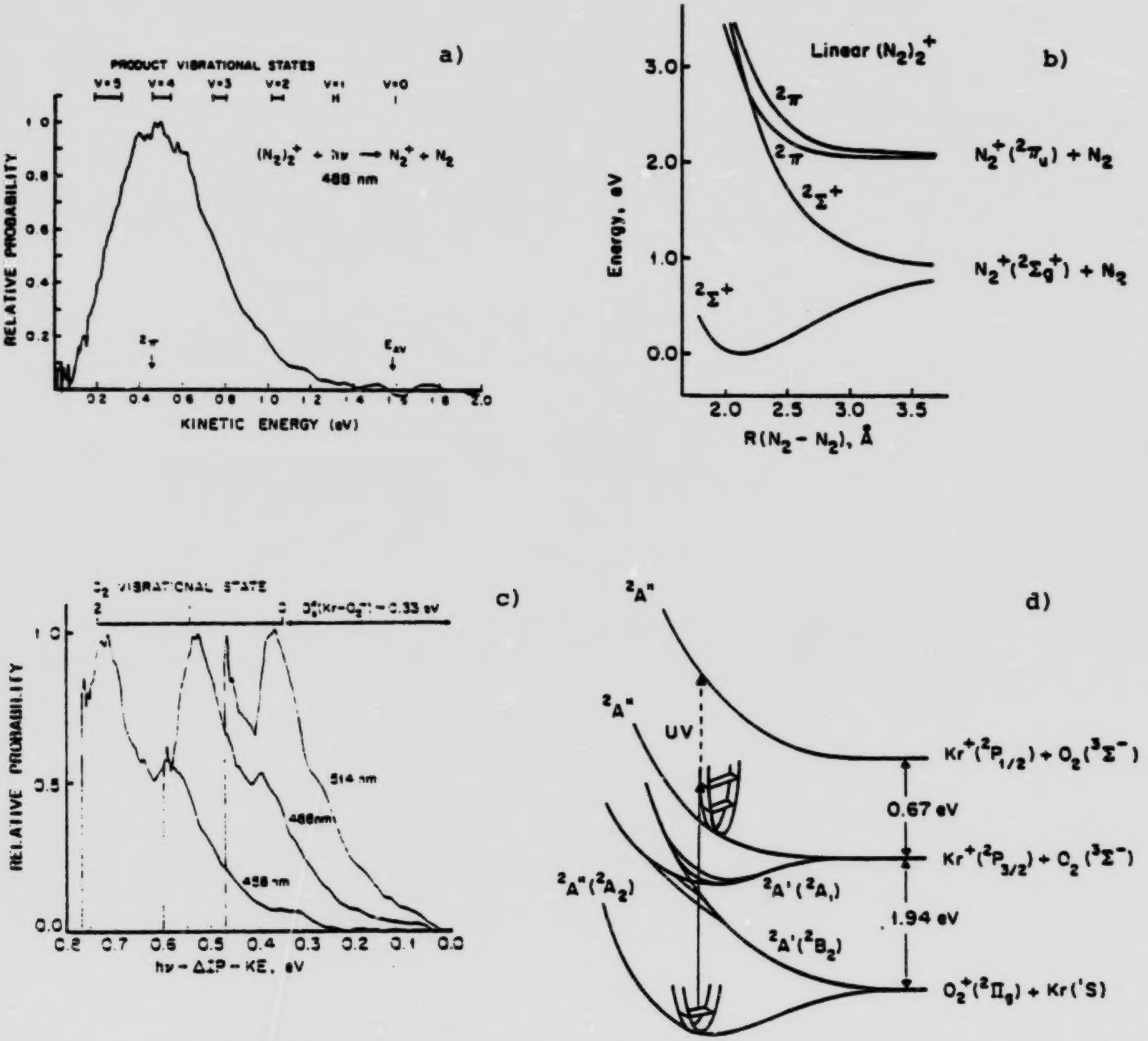

Figure 2. a) Kinetic energy distribution of N_2^+ from photodissociation of $(N_2)_2^+$ at 488 nm. Vibrational states of the N_2^+/N_2 products are indicated and are not resolved.

b) Semiqualitative reaction coordinate diagram for the $(N_2)_2^+$ dimer system.

c) Kinetic energy distributions for photodissociation of $Kr \cdot O_2^+$ at the indicated wavelengths plotted on a constant energy scale. The O_2 fragment is vibrationally excited.

d) Schematic potential energy diagram for the KrO_2^+ photodissociation process.

Rotational and Vibrational Spectra of Molecular Clusters

Thomas R. Dyke, Department of Chemistry, University of Oregon, Eugene, OR 97405

Joseph W. Nibler, Department of Chemistry, Oregon State University, Corvallis, Oregon 97331

The goal of this project is to determine rotational and vibrational spectra of cluster molecules. The long range purpose of this work is to provide basic information for modelling the effects of these molecules in atmospheric phenomena and for understanding hydrogen bonds. Molecular beam techniques are used to obtain high number densities of cluster molecules under isolated molecule conditions. Electric resonance spectroscopy provides microwave and radiofrequency rotational spectra with linewidths as narrow as 2 kHz, resulting in precise rotational constant, electric dipole moment and nuclear hyperfine determinations. To obtain vibrational frequencies, we have decided to try the CARS technique, (Figure 1) which can be made quite sensitive by employing high power lasers and can be readily extended to low frequencies to study the important intermolecular modes of clusters. The two methods provide complementary information concerning the spectra and structural properties for the molecular complexes of interest. We are particularly pleased to report the first observation, that we are aware of, of a vibrational spectrum of a hydrogen bonded complex using the molecular beam/CARS technique (Figure 2).

Our recent work using the molecular beam electric resonance technique to obtain microwave and radiofrequency spectra has included $(H_2O)_2$, $NH_3 \cdot H_2O$, $NH_3 \cdot H_2S$, $H_2S \cdot Ar$ and SO_2 complexes with NH_3, H_2O and HF. We have finished one series of measurements on K=0 tunneling-rotational spectra for $(H_2O)_2$ and $(D_2O)_2$. The large observed tunneling doubling for $(H_2O)_2$, 19,530 MHZ, helps to explain the complexity of the $(H_2O)_2$ rotational spectrum. The microwave spectrum of various deuterated forms of $NH_3 \cdot H_2O$ has been obtained and its structure determined. These results will be compared with work on the $NH_3 \cdot H_2S$ complex, which has begun. We are also interested in looking at weak complexes such as H_2O with N_2, O_2, inert gases, etc. Along these lines, we have recently analyzed some $H_2S \cdot Ar$ spectra which were obtained earlier and should help in initiating this effort. The $H_2S \cdot Ar$ structure is of some interest as it is apparently not hydrogen-bonded.

One of the major goals of our project is to obtain vibrational spectra of clusters in molecular beams. We are interested in using a Raman technique, specifically the CARS method, (Figure 1) in order to provide different sensitivities than in an infrared experiment, and in order to eventually extend the work to the low frequency "intermolecular" modes of the complex. For the initial work, we have chosen the HCN polymer system, which has been extensively studied in matrix isolation infrared experiments and to a lesser extent in the gas phase. In Figure 2, CARS spectra of HCN in a free jet expansion are shown in the ν_1 Q-branch region. Depending on the conditions, dimer, trimer and higher polymer spectra are seen. Similar experiments have been done with DCN and for the ν_3 mode of HCN. This work illustrates that the CARS technique combined with molecular beam methods is a useful way of obtaining vibrational spectra for molecular clusters.

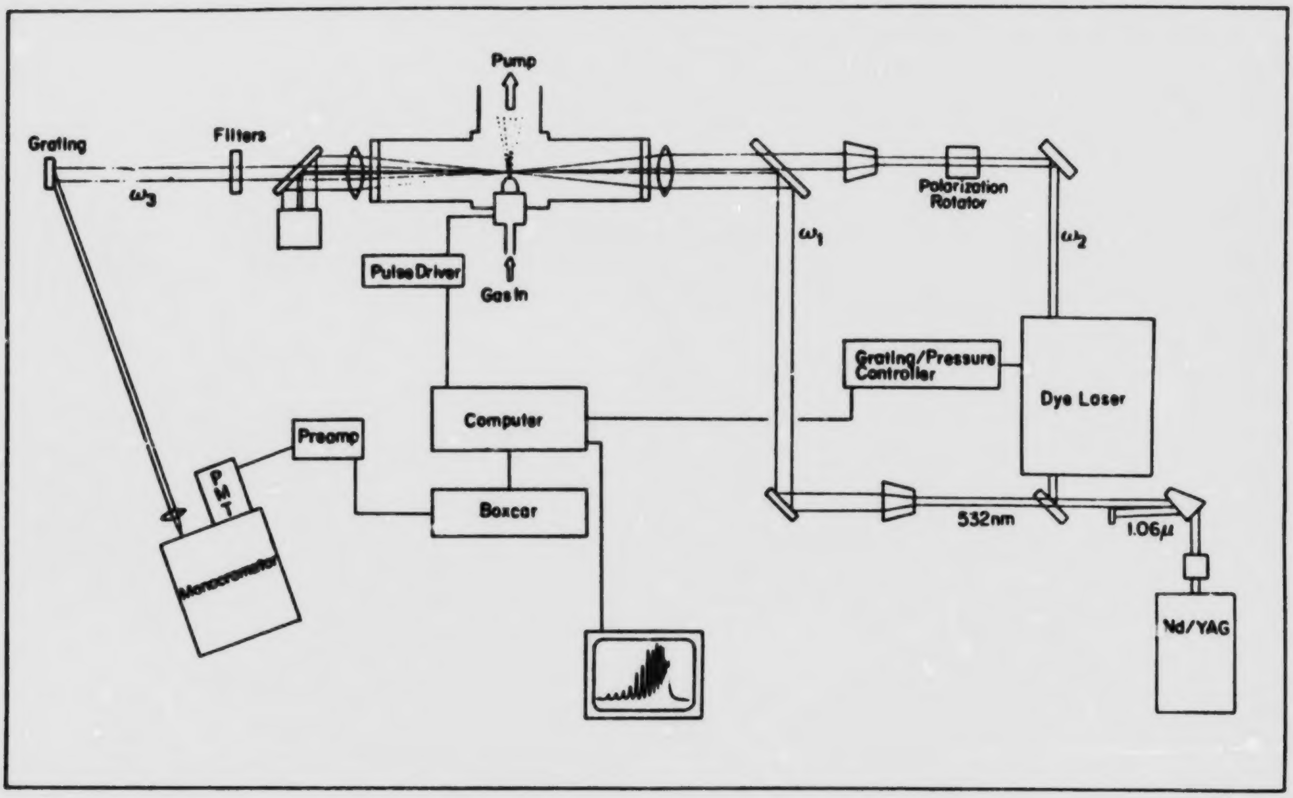
Pump
Grating
Filters
ω_3
Polarization Rotator
ω_1
ω_2
Pulse Driver
Gas In
Grating/Pressure Controller
Dye Laser
Computer
Preamp
PMT
Boxcar
532nm
1.06μ
Monocromator
Nd/YAG

Figure 1. Schematic diagram of CARS apparatus.

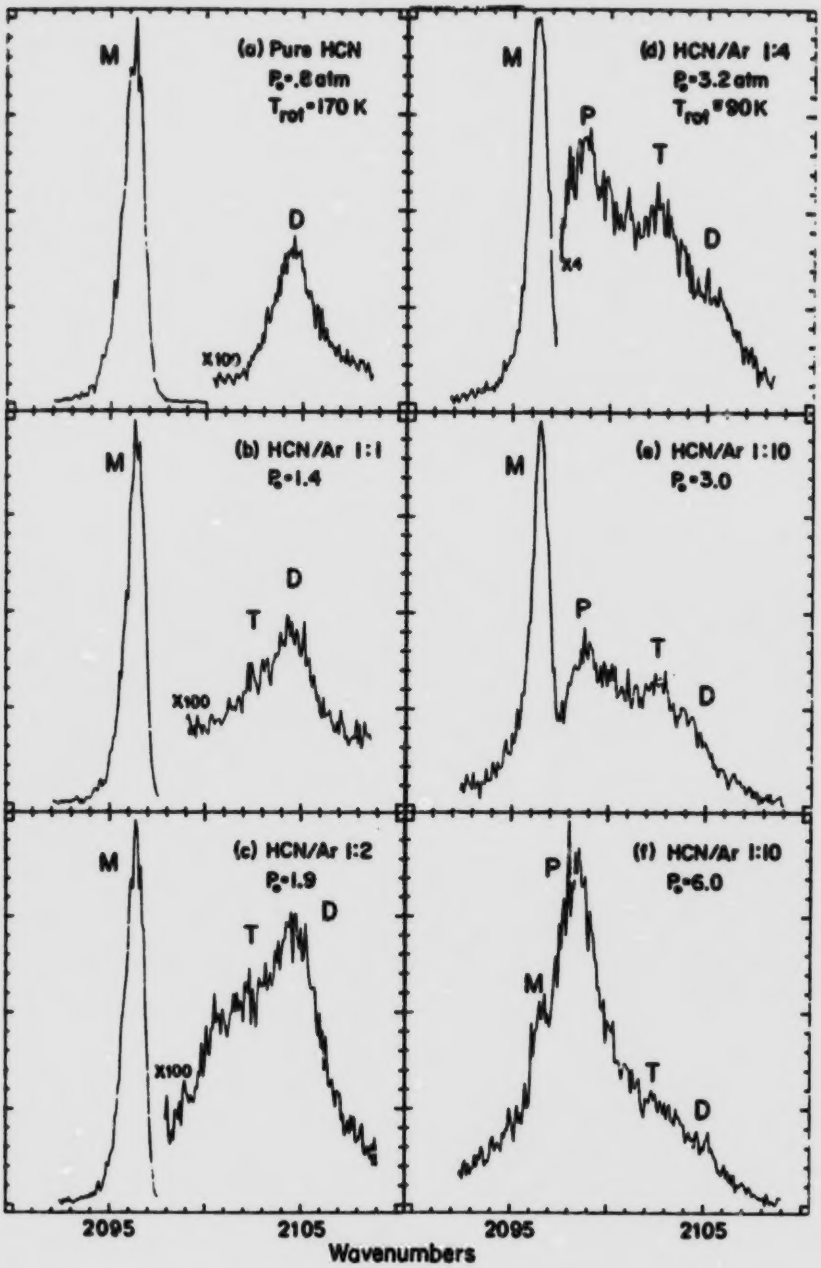

Figure 2. CARS spectra of HCN monomer (M), dimer (D), timer (T) and higher polymers (P) in the ν_1 Q-branch region.

RATE MEASUREMENTS OF THE REACTIONS OF SELECTIVELY SOLVATED IONS IN THE TEMPERATURE RANGE 85 - 500 K

JOHN F. PAULSON, ALBERT A. VIGGIANO AND MICHAEL HENCHMAN*
Air Force Geophysics Laboratory (AFSC), Hanscom AFB, MA 01731

The rates of chemical reactions between ions (positive or negative) and neutral molecules are studied in a flow tube in the temperature range 85 - 500K. Reactant ions include solvated or cluster ions $X^{\pm}\cdot Y_n$, where both the number and type of the cluster molecules or solvates may be selected ($Y = H_2O$, CH_3OH, CH_3CN, HNO_3, H_2SO_4 etc.; $n < 4$). Of particular interest is the dependence of reaction rate and branching ratios on temperature, pressure, solvate identity and solvation number. The formation of clusters by collisional and radiative stabilization is studied, and this yields insight into the structure of clusters. Interest in the stability of negative ions leads to the identification of molecules with large electron affinities and to the measurement of these electron affinities.

The principal apparatus is a temperature-variable selected-ion flow tube (Figure 1). The solvated ions are prepared in a high-pressure ion source, developed for the purpose. This has been the first facility capable of studying negative-ion clusters injected into a flow tube, and, to date, it remains so. It has proved possible to use corrosive reagents (HF, H_2SO_4, HNO_3 etc.) which are of particular interest in stratospheric ion chemistry.

Three-body attachment rates have been measured as a function of temperature, cluster size and buffer gas (He or H_2 or N_2) for systems of stratospheric interest - HCl with $NO_3^-(HNO_3)_{0,1,2}$ and $HSO_4^-(H_2SO_4)_{0,1,2,3}$ - to show a T^{-n} dependence with n increasing with cluster size (Figure 2).[1]

The temperature dependence of associative detachment reactions has been determined for the first time, e.g., a T^{-n} dependence for $O^- + NO$, $S^- + CO$ and $S^- + O_2$ where $n = 0.7 \pm 0.1$.[2] Temperature studies of the reactions $N^+ + CO$ and $C^+ + NO$ have been compared with the suprathermal results of Schlier *et al* using the guided beam technique.[3] Charge transfer and fluoride ion transfer reactions to WF_6 have estimated its electron affinity as ~ 3.4 eV.

Using a beam machine, the reaction of $OH^-(H_2O)_{0,1,2,3}$ with CO_2, SO_2[4] and CH_3Br[5] has been studied as a function of translational energy and hydration. The new ion H_3O^- has been prepared and its binding energy estimated.[6] A review of negative ion reactions has been published including unpublished data on the negative ion chemistry of acetonitrile.[7] Spectroscopic measurements on SO_2^+ have been performed in a triple-quadrupole photodissociation mass spectrometer.[8]

*AFSC/URRP Visiting Professor 1984-1985. Permanent address: Department of Chemistry, Brandeis University, Waltham, MA 02254.

1. Viggiano, A.A., J., Chem. Phys. *81*, Sept 14 (1984).
2. Viggiano, A.A., Paulson, J.F. *Ibid*. *79*, 2241 (1983).
3. Miller, T.M., Wetterskog, R.E., Paulson, J.F. *Ibid*. *80*, 4922 (1984).
4. Hierl, P.M., Paulson, J.F. *Ibid*. *80*, 4890 (1984).
5. Henchman, M., Paulson, J.F., Hierl, P.M., J. Amer. Chem. Soc. *105*, 5509 (1983).
6. Paulson, J.F., Henchman, M. in *Ionic Processes in the Gas Phase* (M.A. Almoster Ferreira, ed.), Reidel, Dordrecht 1984.
7. Viggiano, A.A., Paulson, J.F. in *Swarms of Ions and Electrons in Gases* (W. Lindinger, T.D. Mark, F. Howorka, eds.) Springer Verlag, Wien 1984.
8. Thomas, T.F., Dale, F., Paulson, J.F., J. Chem. Phys. *79*, 4078 (1983).

SELECTED ION FLOW TUBE (SIFT) FOR ION CHEMISTRY

FIGURE 1

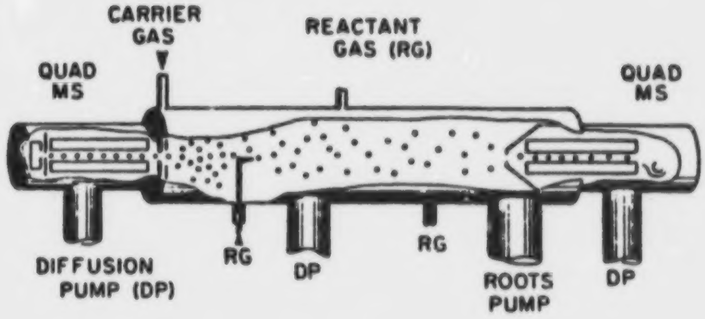
CARRIER GAS
REACTANT GAS (RG)
QUAD MS
QUAD MS
DIFFUSION PUMP (DP)
RG
DP
RG
ROOTS PUMP
DP

ASSOCIATION RATE COEFFICIENTS AS A FUNCTION OF TEMPERATURE, CLUSTER MOLECULE AND CLUSTER SIZE

FIGURE 2

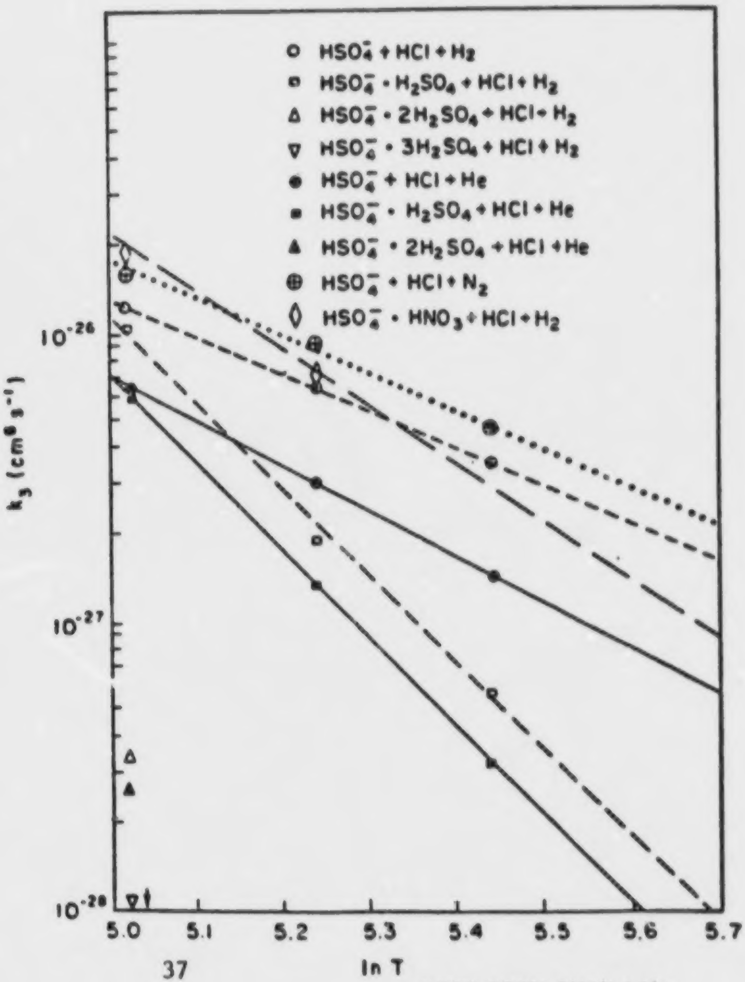

APPLICATION OF MAXIMUM ENTRPY METHOD
TO FOURIER TRANSFORM MASS SPECTROMETRY

A. Rahbee

Air Force, Geophysics Laboratory

Hanscom AFB, Ma.

A Fourier transform mass spectrometer, acquired recently at AFGL has been employed to study chemical reactions of both positive and negative ions with neutral species. The interesting features of the instrument itself, such as simultaneous detection of all the ions, capability to provide time histories of parent and product ions, multiple ion ejection for study of the behavior of a particular ionic species will be discussed. The heart of the apparatus, the spectrometer cell, is shown schematically in Fig. 1. Ions produced by electron bombardment, are all excited to cyclotron orbits by application of a frequency chirp, applied to two of the electrodes. Image current produced in the other two electrode, is measured and analyzed by fast fourier transformation. The results of some measurements of the $N^{+}+O_2$ reaction as well as some negative ion reactions will be presented and compared to the rates reported in the literature.

In addition to the chemical rate measurements, a new analytical method for analysis of the time domain signal to obtain mass spectra will be discussed. The method which is named maximum entropy method (MEM) was first devised by J.P. Burg for application to geomagnetic phenomena. In contrast to fast fourier transformation (FFT) which requires acquisition of several thousant data points, zero-filling and apodization of the measured time domain signal, the MEM uses only a few hundred points of the data to calculate the elements of a filter called prediction error filter. The filter in turn is used to calculate the MEM spectrum. Mass spectra obtained by both FFT and MEM will be shown and compared. The MEM results are by far superior to FFT results both in terms of absence of the famous sidelobes and resolution enhancement. A sample result is shown in Fig. 2 where a 4000 point FFT is compared to 125 point MEM spectrum. Not only there are no sidelobes, the resolution is enhanced by a factor of four. Applications of the new method as wells its implication in ion chemistry measurements will also be presented.

BLANK PAGE

BLANK PAGE

BLANK PAGE

SCHEMATICS OF THE CELL

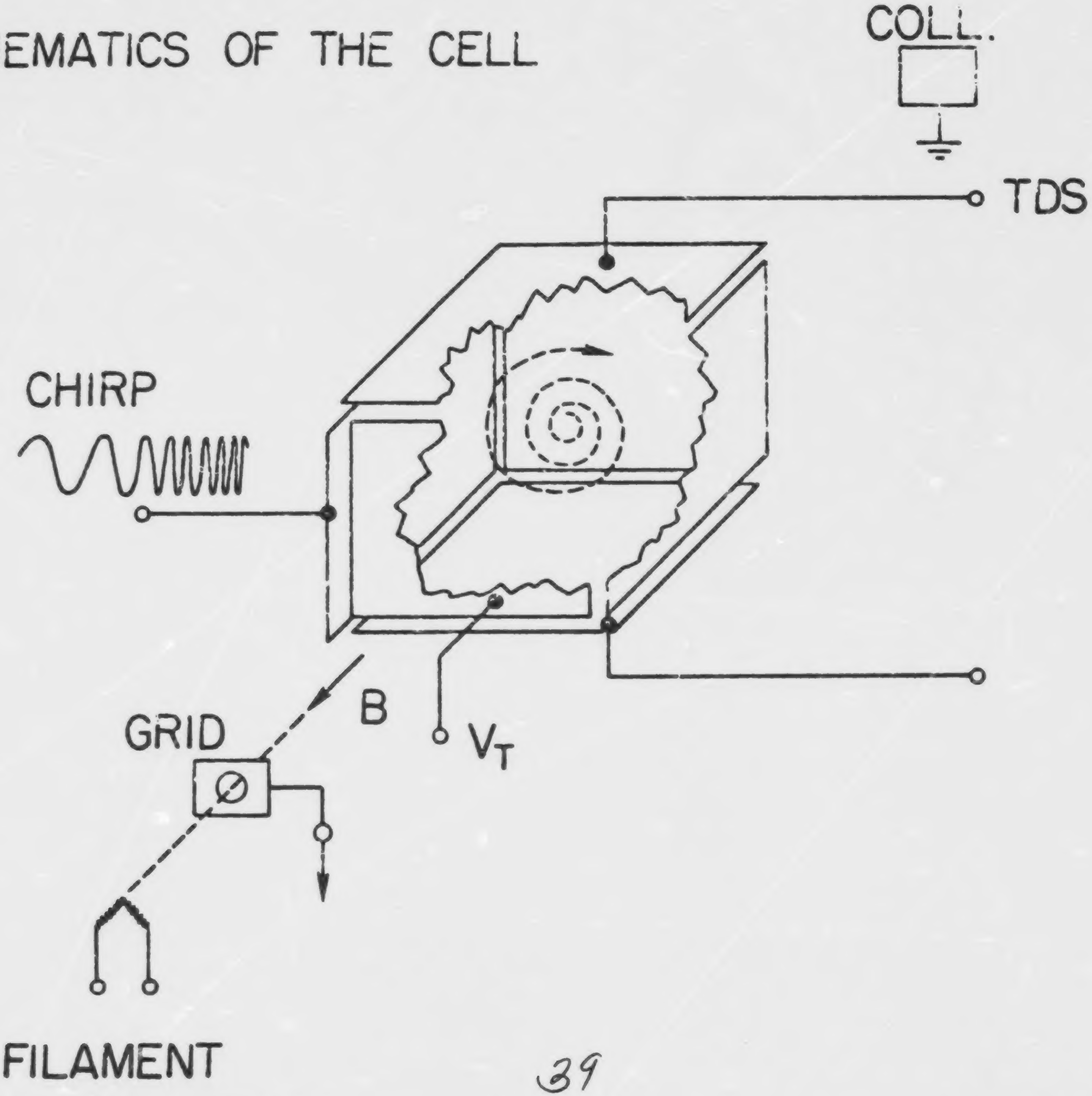
COLL.
TDS
CHIRP
B
GRID
V_T
FILAMENT

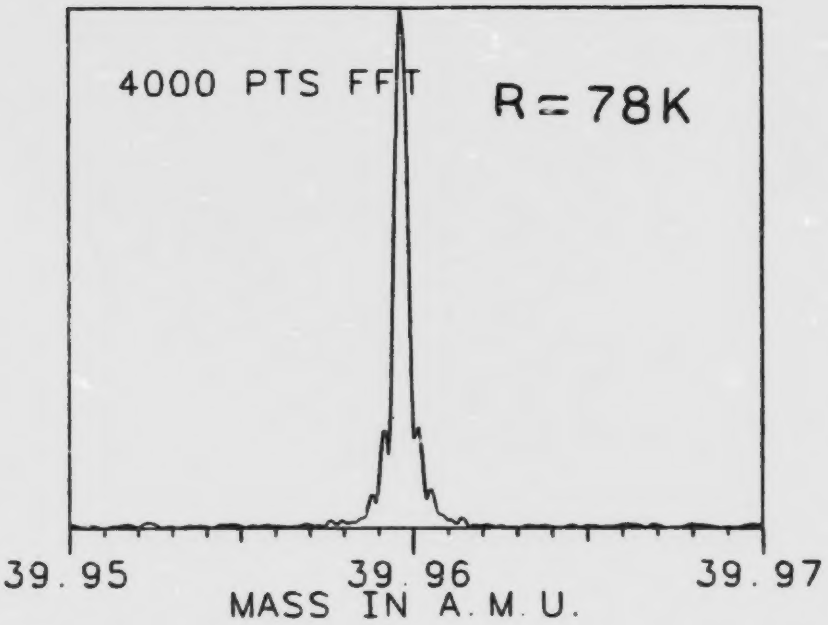
4000 PTS FFT
R=78K
39.95
39.96
39.97
MASS IN A.M.U.

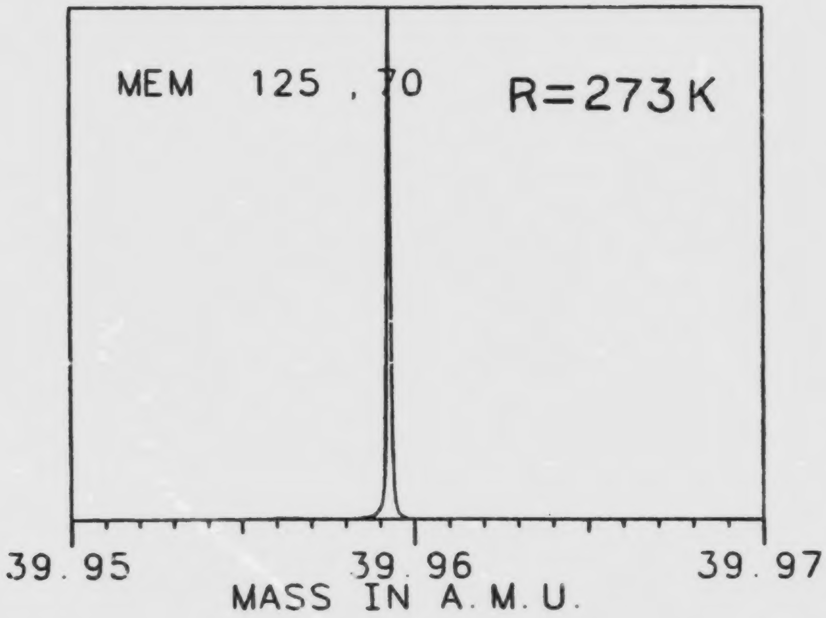
MEM 125 , 70
R=273K
39.95
39.96
39.97
MASS IN A.M.U.

TEMPORAL AND SPATIAL STRUCTURES IN CHEMICAL REACTIONS

Dr. John Ross
Department of Chemistry, Stanford University

Systems far from equilibrium may develop interesting temporal and spatial structures. We present some new experiments, both technqiues and results, on the formation of such structures in chemical systems including multiple stationary states (bi- and tri-stability), stabilization of unstable stationary states, limit cycles, chemical fronts (waves) and time-independent spatial structures.

The photo-illuminated gas phase reaction, $S_2O_6F_2 \rightleftarrows 2\ SO_3F$ shows bistability and hysteresis due to a positive feedback loop involving the absorption of light by SO_3. We have observed bistability in this sytem as predicted and find mean first passage times from one branch of stable stationary states to the other to be very long except in the immediate vicinity of marginal stability points. A simple modification allows a number of other interesting experiments, Fig. 1A. Light transmitted by the sample can be detected and amplified, and the signal after delay can activate a modulator which controls the light input into the system. Thus it is possible to stabilize unstable stationary states of the system without external feedback, Fig. 2A. The system with external feedback also shows limit cycle oscillations, inverted Hopf bifurcations, and is predicted to have chaotic behavior.

We have developed an experimental method for the quantitative measurement of propagating chemical profiles in reactions far from equilibrium. The measurements are made on circular waves in a thin layer of Belousov-Zhabotinsky reaction by means of light absorption of ferroin, Fig. 1B. The transmission profile of the wave is measured with a linear photo-diode array to a resolution of 50 microns. The chemical front is about 400 microns in width and we confirm experimentally the remarkable property of the constancy of the profile in space and time, Fig. 2B. The relaxation of the wave profile behind the front is characterized by two distinct time constants. We have measured front velocities at various initial reactant concentrations, temperatures and depth of solution. We have also measured annihilation of front profiles and have observed the transition from a homogeneous to an inhomogeneous spatial structure after the passage of the wave (a mosaic pattern).

We are continuing our studies of periodic precipitation processes which are a time-independent chemical spatial structure. In the case of PbI_2 precipitate we measure the total lead concentration as a function of time and position in a one-dimensional band formation experiment, and total iodide concentration and the free iodide ion concentration; at the same time we take photographs of microscope observations of particle formation and distribution. There is no evidence of flocculation in the lead iodide system. Nucleation is continuous in space contrary to the Ostwald theory and its many variants; band formation occurs within the region of continuously nucleated material by a self-focussing instability mechanism.

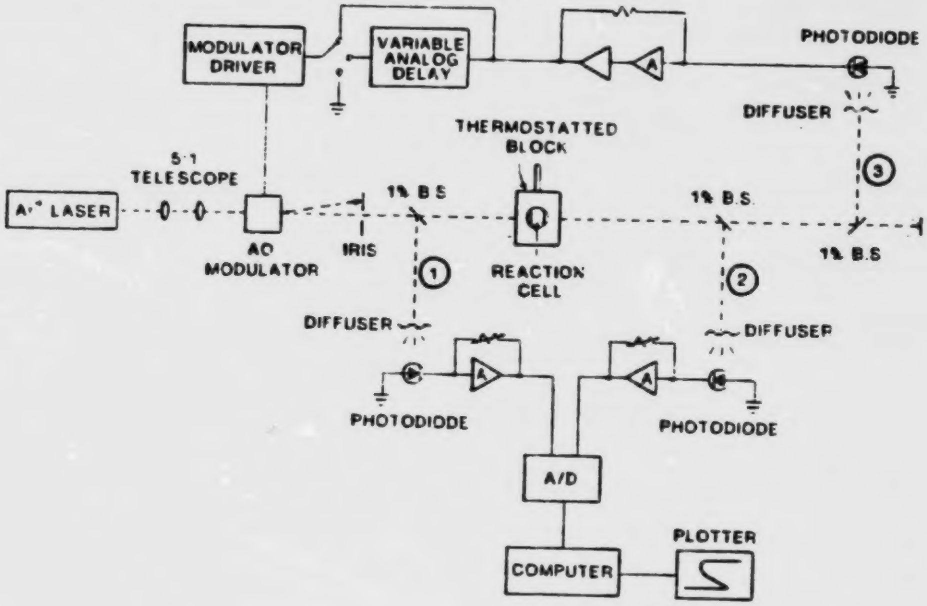
MODULATOR DRIVER
VARIABLE ANALOG DELAY
A
PHOTODIODE
DIFFUSER
THERMOSTATTED BLOCK
5:1 TELESCOPE
Ar+ LASER
AO MODULATOR
IRIS
1% B.S
REACTION CELL
1% B.S.
③
1% B.S
①
②
DIFFUSER
DIFFUSER
PHOTODIODE
PHOTODIODE
A/D
COMPUTER
PLOTTER

Fig. 1A. Schematic of the experimental apparatus

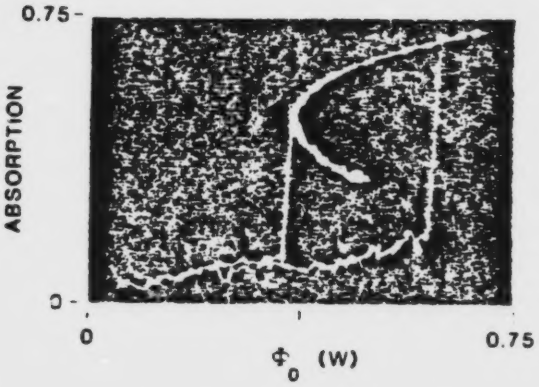

Fig. 2A. Storage oscilloscope trace showing stabilization of a portion of the intermediate absorption branch of the illuminated $S_2O_6F_2/SO_3F$ system by application of external feedback. Superimposed (with no change in scale, or shift in origin) is the hysteresis loop of the system in the absence of feedback.

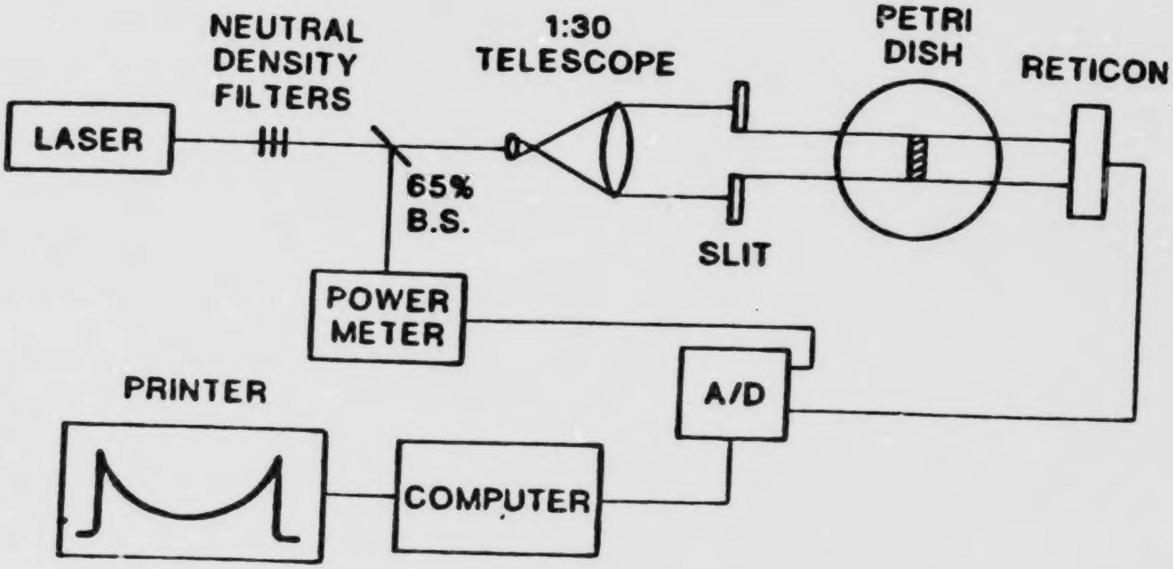
NEUTRAL DENSITY FILTERS
1:30 TELESCOPE
PETRI DISH
RETICON
LASER
65% B.S.
SLIT
POWER METER
A/D
PRINTER
COMPUTER

Fig. 1B. Schematic of the experimental arrangement.

Fig. 2B. See page 5.

a) Transmission wave profile in space taken 253.9 sec after wave initiation. $[NaBrO_3]_0$ = 0.250 M.

b) Transmission wave profile as a function of time at a given position in space (5.9 mm in part (a)). The time axis has been inverted and linearly displaced. The measurement furthest to the right in the graph corresponds to a time 8.0 sec after wave initiation.

c) Overlap of profile in space of graph (a), indicated by dots, with profile in time of graph (b), represented by open circles.

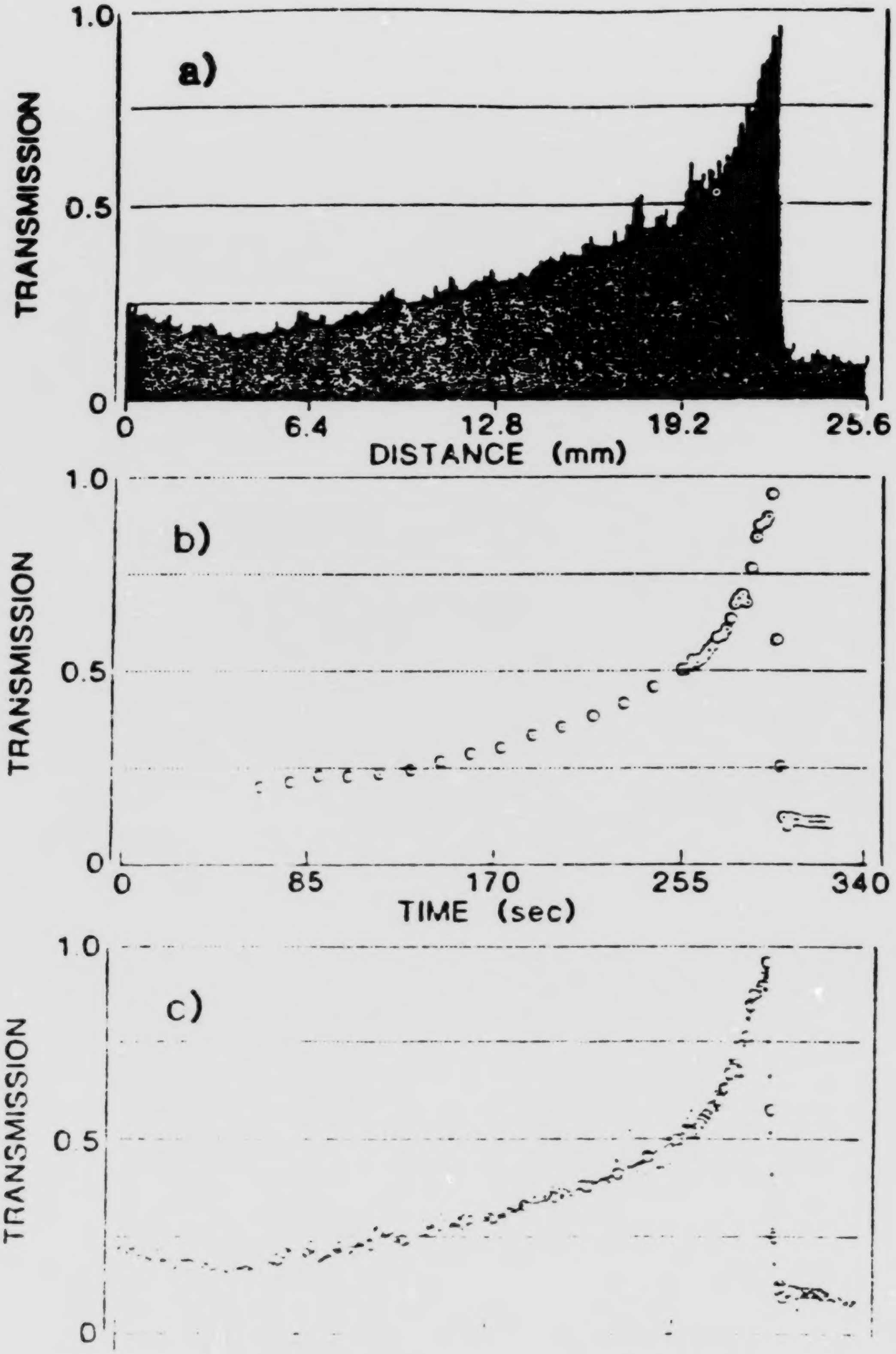
a)
TRANSMISSION
1.0
0.5
0
0
6.4
12.8
19.2
25.6
DISTANCE (mm)
b)
TRANSMISSION
1.0
0.5
0
0
85
170
255
340
TIME (sec)
c)
TRANSMISSION
1.0
0.5
0

Fig. 3B.

INELASTIC ELECTRON SCATTERING FROM SURFACES:

EXPLORED REGIONS AND FRONTIERS

J. L. Erskine
Department of Physics
University of Texas
Austin, Texas 78712

High resolution electron energy loss spectroscopy (EELS) is currently being developed into an extremely useful probe of the properties of surfaces. EELS is a true "molecular" spectroscopy because it measures vibrational properties of surfaces and adsorbed complexes at surfaces. In addition, it can be used as a structural probe when combined with lattice dynamical calculations. This paper describes recent advances in the use of EELS as a structural probe by combining the results of experimental studies (the measurement of surface phonons throughout the two-dimensional Brillouin zone) with lattice dynamical calculations.

The experimental apparatus[1] and the two primary kinematic conditions for scattering are described in Figure 1. Figure 2 displays a typical EELS spectra and phonon bands for C(2x2) O/Ni(100) along a specific direction of the two-dimensional Brillouin zone obtained from many spectra.

We have used the EELS technique to study the O/Al(111)[2,3] system, the O/Ni(100)[4,5] system and the O/Ti(0001)[6] system. All three of these systems represent cases where low-energy-electron diffraction has failed to yield an accurate structural model, and in which other experiments have met with difficulty in explaining some of the observations (for example, characterizing the underlayer formation which accompanies O chemisorption on Al(111) and O and N chemisorption on Ti(0001)).

Our EELS studies of O and N chemisorption on Al(111) and Ti(0001) illustrate the sensitivity of vibrational spectroscopies to various structural configurations associated with chemisorption on surfaces, and our EELS studies of the O/Ni(100) system combined with lattice dynamical calculations have shown that vibrational spectroscopy can be regarded as a direct structural probe.

New applications of EELS which require accurate experimental measurements of the absolute scattering cross section are currently being investigated. These studies (and routine studies of impact scattering needed to map surface phonon bands) will require new generation EELS spectrometers. This new instrumentation and theoretical studies of the scattering cross sections represent the frontier of the field.

1. R. L. Strong and J. L. Erskine, Rev. Sci. Inst. 55, 1304 (1984).
2. J. L. Erskine and R. L. Strong, Phys. Rev. B25, 5547 (1982).
3. R. L. Strong, B. Firey, F. W. de Wette, and J. L. Erskine, Phys. Rev. B25, 5547 (1982).
4. R. L. Strong and J. L. Erskine, (submitted to Phys. Rev. Lett.).
5. R. L. Strong and J. L. Erskine, (submitted to Phys. Rev. B).
6. R. L. Strong and J. L. Erskine, J. Vac. Sci. Technol (submitted).

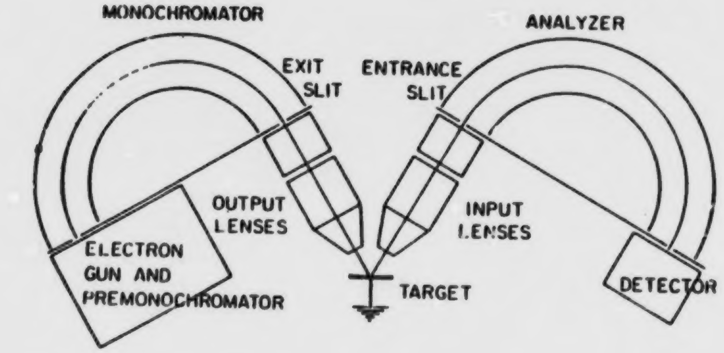
MONOCHROMATOR
ANALYZER
EXIT SLIT
ENTRANCE SLIT
OUTPUT LENSES
INPUT LENSES
ELECTRON GUN AND PREMONOCHROMATOR
TARGET
DETECTOR

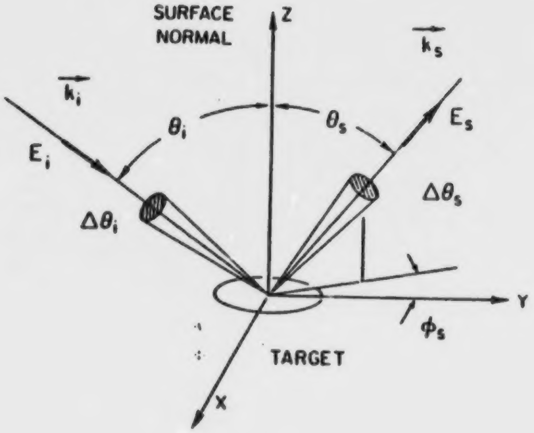
SURFACE NORMAL
Z
$\vec{k}_s$
$\vec{k}_i$
θ_i
θ_s
E_s
E_i
$\Delta\theta_i$
$\Delta\theta_s$
Y
ϕ_s
TARGET
X

$$E_i = E_s + \hbar\omega$$

$$\vec{k}_i \sin\theta_i = \vec{k}_s \sin\theta_s + \vec{q}_\parallel + \vec{G}$$

$$|\vec{q}_\parallel| = \frac{2m_e}{\hbar} \left| \sqrt{E_i} \sin\theta_i - \sqrt{E_i - \hbar\omega} \sin\theta_s \right|$$

Figure 1: Upper half, schematic diagram of experimental apparatus. Electrons having energy E_i (± 2meV energy spread) are generated by the monochromator. Scattered electrons are analyzed (E_s) by the analyzer with similar energy resolution. Lower half, scattering geometry with appropriate parameters required to characterize the inelastic scattering event. E_i, Θ_i and k_i describe the incident electron energy, direction and momentum, E_s, Θ_s and k_s are the corresponding scattered electron parameters. The two upper equations describe the kinematical scattering conditions, the lower equation describes momentum transfer to a surface vibration.

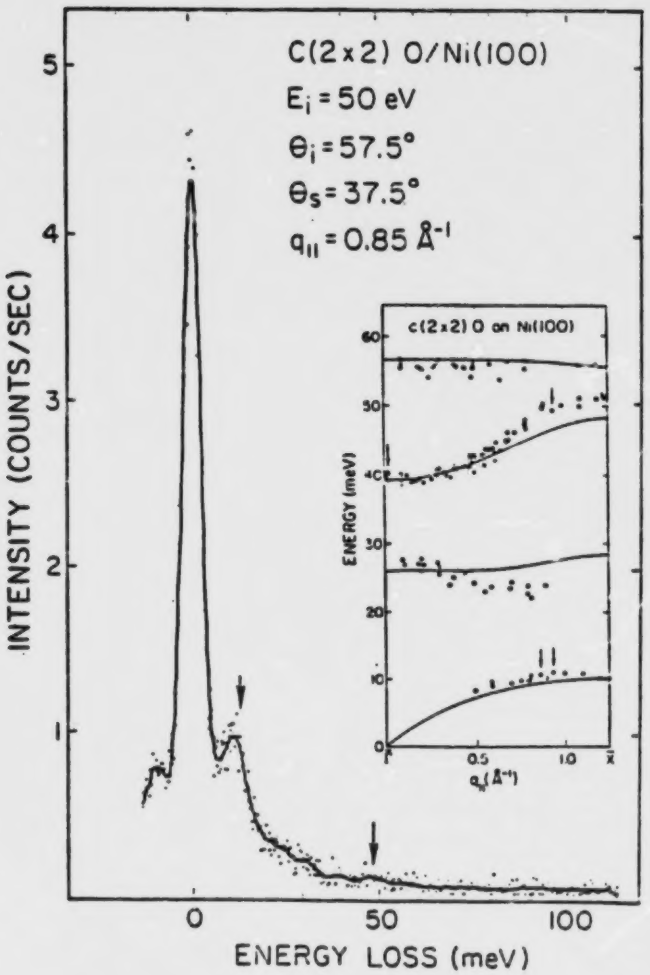

Figure 2: Typical EELS spectrum for C(2x2) O/Ni(100) showing the peaks corresponding to the elastic peak ($\Delta E = 0$), the S_4 surface phonon (arrow at 10 meV) and the oxygen parallel mode (arrow at 48 meV). Inset: experimentally determined surface phonon bands for C(2x2) O/Ni(100), dots, and calculated surface phonon bands (solid lines) assuming an oxygen height of 0.92Å above the surface. These experimental results and lattice dynamical calculations established the chemisorbed oxygen bond distance.

SURFACE DEFECTS AND SURFACE OXIDATION

PETER C. STAIR
Department of Chemistry, Northwestern University
Evanston, IL 60201

Studies of the oxidation of single crystal metal surfaces have largely ignored the role of surface structural defects on the kinetics and mechanism of oxide film growth. However, since structural defects can produce sites of low coordination number or provide efficient transport to the crystal bulk, their presence on the surface will influence oxide film growth. This paper describes our current research efforts to characterize extended structural defects on aluminum single crystal surfaces and to correlate their production, nature and number with the kinetics of aluminum surface oxidation.

Low energy electron diffraction (LEED) is used to study extended structural defects. Each type of defect will change the shape of the diffracted beams in a characteristic manner; in general, any imperfection will broaden the beams from the shapes they would have if the crystal were perfect. The extent of broadening as a function of electron energy depends upon the nature and concentrations of defects in the probed area. Two-dimensional contour plots of the LEED beam intensities, such as shown in Figure 1, enable shapes to be discerned and defect concentrations calculated. Subsequently the oxidation kinetics can be determined by exposing the crystal to oxygen while monitoring surface atom chemical states with either Auger electron spectroscopy (AES) or x-ray photoelectron spectroscopy (XPS), as depicted in Figure 1. Metallic and oxidized aluminum have different Auger electron spectral line shapes and different photoelectron peak positions, making detection of the transition from chemisorbed oxygen to metal oxide straightforward.

The construction of an apparatus capable of performing the necessary LEED measurements together with the oxidation experiments has been recently completed, and is depicted in figure 2. A single pass cylindrical mirror analyzer is used for the AES experiments. LEED measurements are made with a special digital detector developed in our laboratory. The phosphor screen in a display-type optics is replaced by a position sensitive, pulse counting detector, consisting of a Chevron Channel Electron Multiplier Array backed by a resistive film anode (see Figure 2). Positions of diffracted electrons are analyzed by special electronics and then collected by a NOVA 840 computer for display and calculation. Preliminary oxidation experiments have been performed on well-annealed or "perfect" and highly facetted Al(111) surfaces. The results are shown in Figure 2. The facetted surface is oxidized much more rapidly than the well annealed surface, with oxide forming at exposures < 10 Langmuirs. However, the perfect surface shows no noticeable oxide formation until > 80 Langmuirs of oxygen exposure. These results confirm the premise that structural defects alter the kinetics of surface oxidation.

LEED CONTOUR PLOTS
(Contain quantitative information on the nature and concentration of extended surface structural defects such as steps, kinks, mosaic domains and surface strain.)

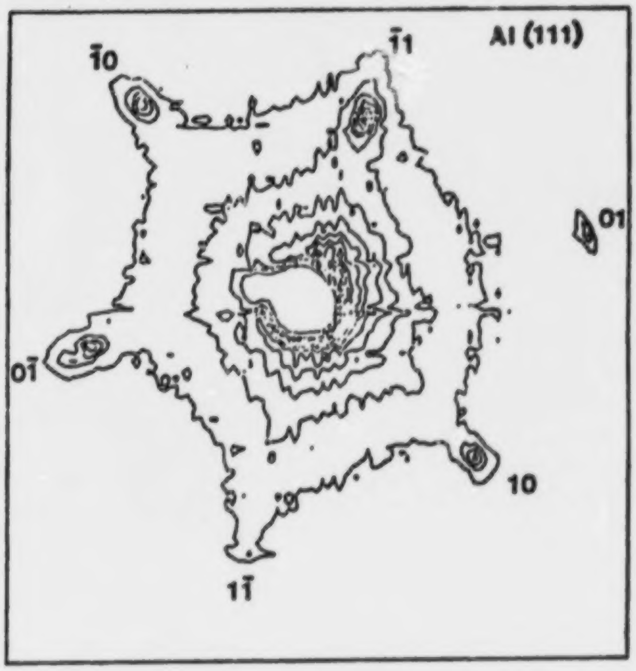

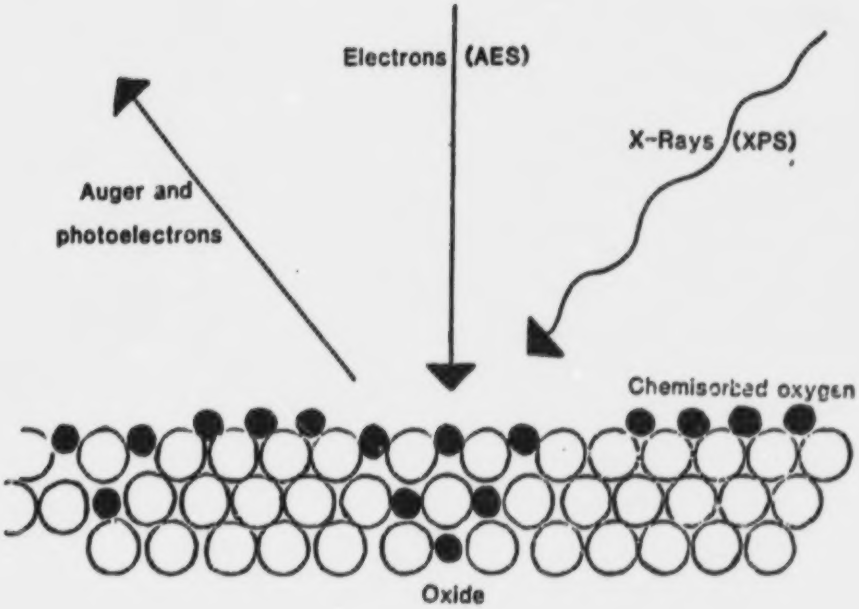
Electrons (AES)
X-Rays (XPS)
Auger and photoelectrons
Chemisorbed oxygen
Oxide

FIGURE 1: Pictoral representation of the oxidation experiments. Auger electron spectral line shape changes and x-ray photoelectron peak positions differentiate aluminum with chemisorbed oxygen from aluminum oxide. The rate of oxide formation can be correlated with the initial surface structure as determined by quantitative LEED beam profile measurements.

BEST COPY AVAILABLE

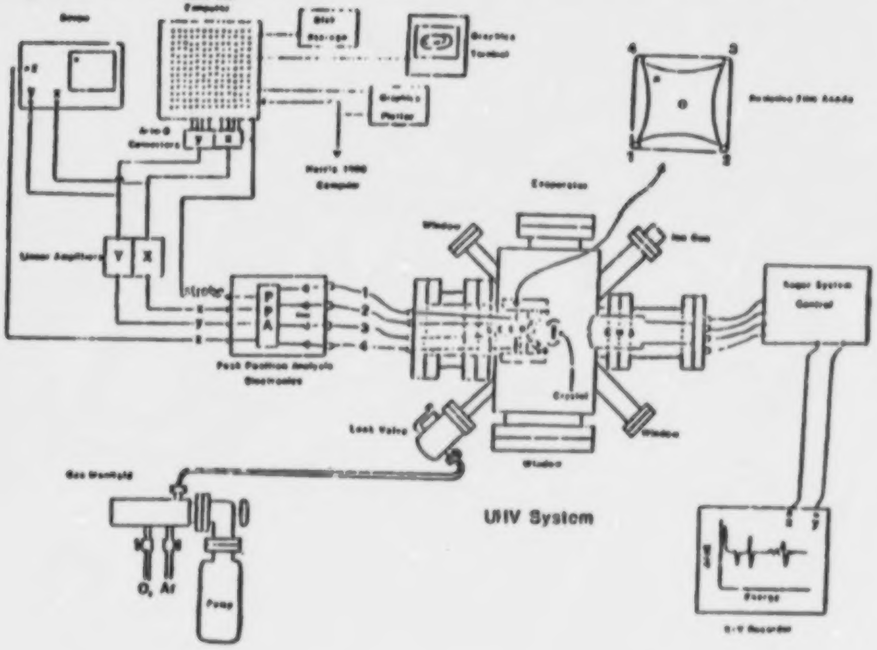
Evaporator
Window
Ion Gun
Crystal
Lock Valve
Window
Window
Gas Manifold
O, Ar
Pump
UHV System
Auger System Control
X-Y Recorder
Peak Position Analysis Electronics
PPA
1
2
3
4
X
Y

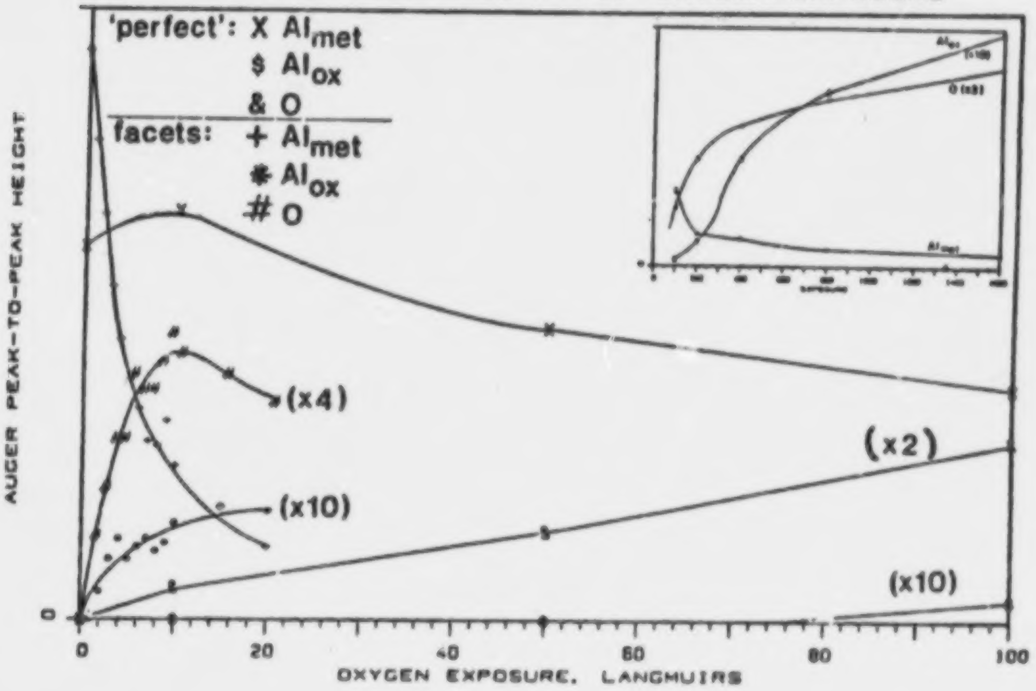
PEAK-TO-PEAK HEIGHT VS. OXYGEN EXPOSURE

FIGURE 2: The completed digital LEED and surface chemistry apparatus is shown above. Preliminary results obtained from "perfect" and facetted Al(111) surfaces are also shown. Notice that oxide forms at exposures < 10 Langmuirs (1 Langmuir = 1 x 10(-6) torr sec) on the facetted surface, but not until > 80 Langmuirs for the "perfect" surface.

SILICON CORROSION KINETICS

Thomas Engel
University of Washington, Department of Chemistry
Seattle, WA 98195

The study of reaction kinetics on surface has lagged considerably behind gas phase studies due both to the complexity of the N-body surface configuration and to the technological difficulties of surface studies. The use of relaxation studies, in which the response of the reaction system to an intensity modulation of the beam is examined, has proved to be very useful in studying surface reactions in which 1-3 intermediates occur between reactants and products. More complex reactions cannot in general be interpreted in a unique fashion since the information on the surface intermediates is gained only indirectly through the gas phase products formed and the reaction waveform.

To investigate the kinetics of semiconductor corrosion on an atomic level, relaxation techniques must be complemented with additional techniques which can identify the relevant surface intermediates. Only in this way can the reaction mechanism and the rate constants be determined uniquely. We are presently constructing a UHV molecular beam surface scattering system in which we will study the reactions of O_2, O, F_2 and F with single crystal silicon surfaces. This system will be capable of modulated molecular beam measurements using a doubly differentially pumped rotatable quadrupole mass spectrometer detector at one position in the chamber and LEED, XPS, AES, ISS and SIMS experiments in a second position.

The apparatus in its present state of construction is shown in figure 1. It consists of a UHV scattering chamber and a 3 stage molecular beam generating chamber. The nozzle-skimmer chamber is pumped by a 20,000 ℓsec^{-1} pump to allow an adequately low pressure for r-f discharge sources needed to produce atomic beams, whereas the remaining 2 stages are pumped by 700 ℓ/sec pumps with UHV flanges to assure vacuum compatibility with the scattering chamber. The large diameter flange at the top of the scattering chamber holds the hemispherical energy analyzer and the sources necessary to carry out XPS, ISS, AES, and SIMS. The rotatable differentially pumped mass spectrometer which will be used for relaxation studies, angular distribution measurements and time of flight experiments will be added on to the large flange at the bottom of the scattering chamber at a later date.

The principle of the measurements planned is shown in figure 2. The square wave modulated reactant beam will lead to a product waveform of the types shown here which were calculated for a simple first order process. The sensitivity of the technique to the activiation energy and pre-exponential factor is very high as can be seen from the curves. A systematic study of the waveforms at different temperatures and values of incident flux allows many details of the reaction mechanism to be learned.

If a number of reaction intermediates are present, direct information on their identity and relative concentrations is needed to uniquely interpret the product waveforms. We will obtain this information with time resolved XPS and SIMS. As indicated in figure 2, the hemispherical energy analyzer will be gated open for a time period Δt occuring at a time t_o after the beam is pulsed on so that an instantaneous picture of the surface concentrations are obtained. Since with the beam technique a new experiment is carried out with each pulse, good signal-to-noise ratios can be obtained by signal averaging. Since the reactions of interest will be carried out at elevated temperatures and silicon atoms are removed, the surface is continuously regenerated and contamination problems which occur in static studies are not of concern here. By repeating this measurement $T/\Delta t$ times where T is the period of the beam modulation, the time evolution of the surface concentrations can be directly measured. The data taken will be accelerated by installation of a multichannel detector in 1985.

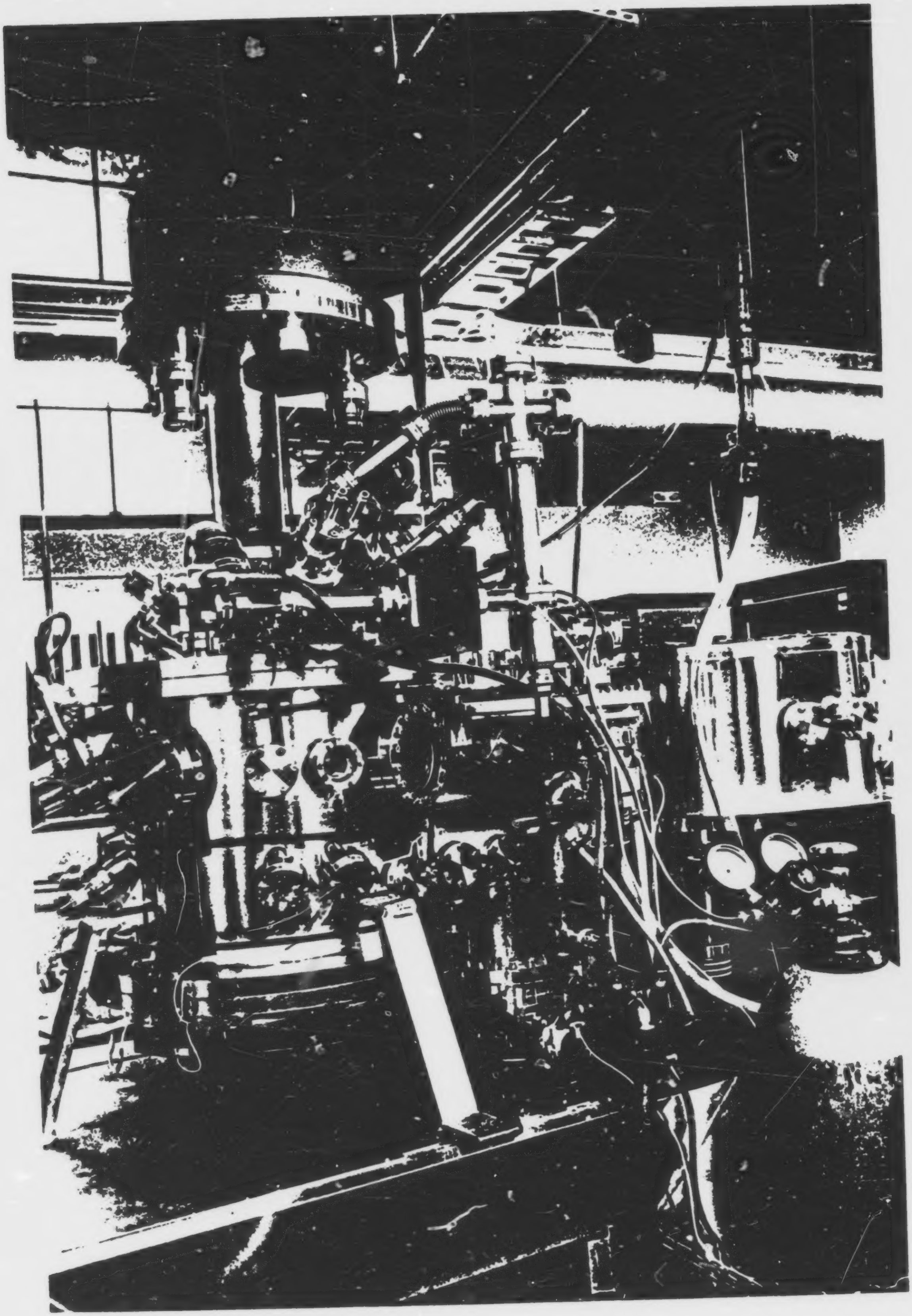

Figure 1

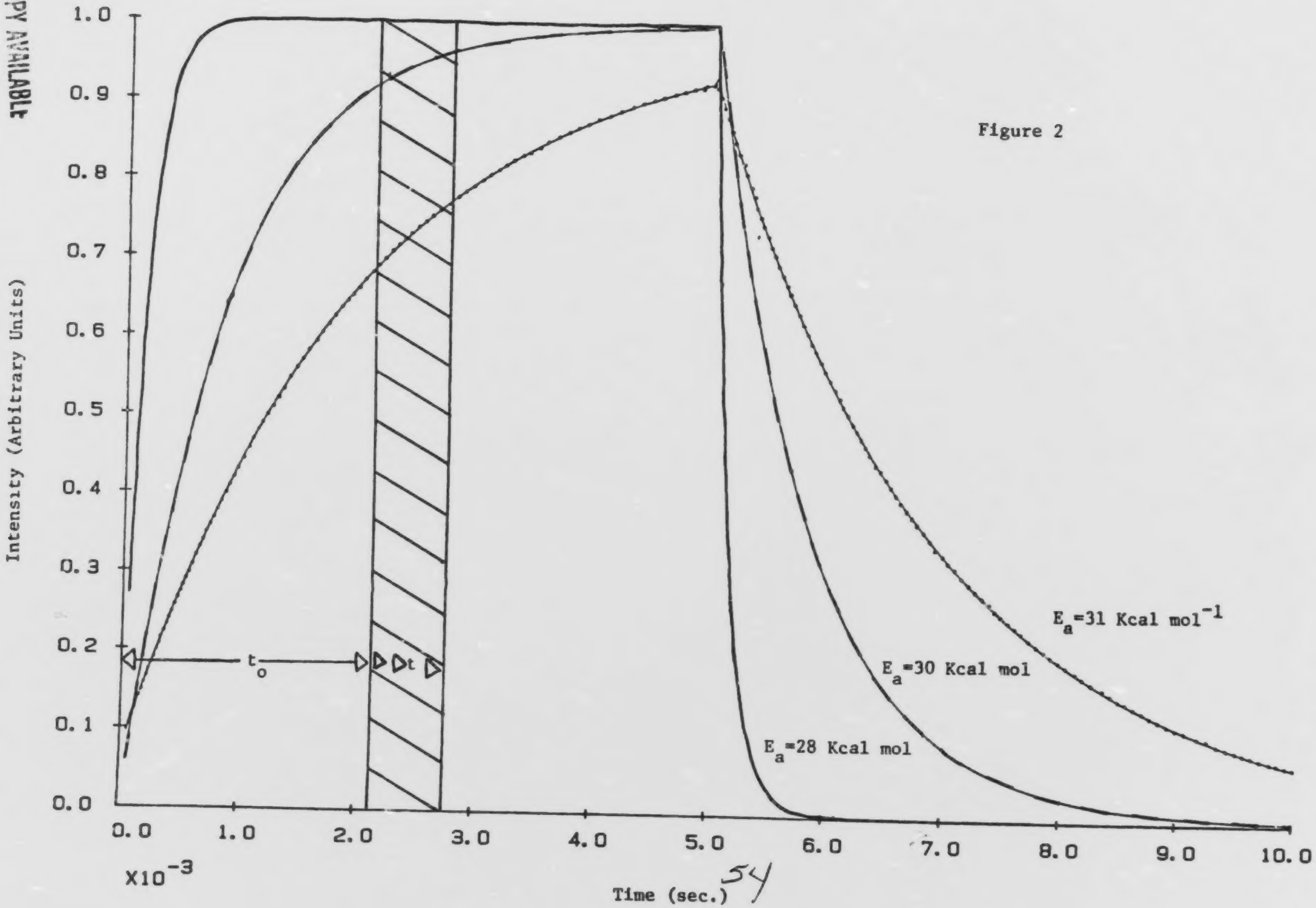
1.0
0.9
0.8
0.7
0.6
0.5
0.4
0.3
0.2
0.1
0.0
Intensity (Arbitrary Units)
t_o
Δt
E_a=31 Kcal mol^{-1}
E_a=30 Kcal mol
E_a=28 Kcal mol
0.0
1.0
2.0
3.0
4.0
5.0
6.0
7.0
8.0
9.0
10.0
X10^{-3}
Time (sec.)

Figure 2

THRESHOLD EXCITATION SPECTROSCOPY OF SOLID SURFACES

P. Terrence Murray
Research Institute
University of Dayton
Dayton, Ohio 45469

Electron energy loss spectroscopy (EELS) is a powerful technique for studying the electronic structure of solid surfaces. Such experiments entail bombarding the specimen of interest with a beam of nearly monoenergetic electrons and performing kinetic energy analysis on those electrons scattered from the surface. On characteristic of the conventional EELS method is the low efficiency with which the scattered electrons are collected (this is primarily a result of the small solid angle through which most dispersive energy analyzers operate). One consequence is that a considerable electron dose may be required to achieve acceptable signal levels; such doses may result in significant beam-induced damage to the surface under investigation. The purpose of the experiments described in this paper is to determine the feasibility of using Threshold Excitation Spectroscopy (TES) as a new method of performing surface analysis. TES experiments involve detecting only those electrons which undergo near total energy loss upon colliding with the target. Such a loss mechanism occurs when the primary electron matches an electronic transition of the solid surface. The result of such a collision is a scattered electron with near zero kinetic energy; the advantage of detecting such low energy electrons is the fact that such species can be collected very efficiently. Thus, TES has the potential of providing similar information as the conventional EELS experiment with substantially less electron-induced damage.

The experimental approach is depicted in Figure 1. The basic procedure entails measuring the (scattered) low energy electron signal as a function of primary electron energy; this is accomplished by using a steradiancy filter (1). Our initial experiments have focused on examining thin films (~200 Å) of LiF, the results of which are presented in Figure 2. The threshold excitation spectrum exhibits peaks at 3.5, 4.6, and 6.1 eV. This is in excellent agreement with previous electron transmission studies of Huang and Hamill (2) who attributed the peaks to optically forbidden excitonic transitions occurring at or near the LiF surface. The fact that we observe similar structure (with better resolution) demonstrates that the TES approach is indeed a feasible method of performing surface analysis. Our present efforts are directed at determining the extent to which TES is surface-sensitive and establishing the collection efficiencty of our instrument.

(1) T. Baer, W.B. Peatman, and E.W. Schlag, Chem. Phys. Lett. 4, 243 (1969).

(2) T. Huang and W.H. Hamill, J. Phys. Chem. Solids 36, 661 (1975).

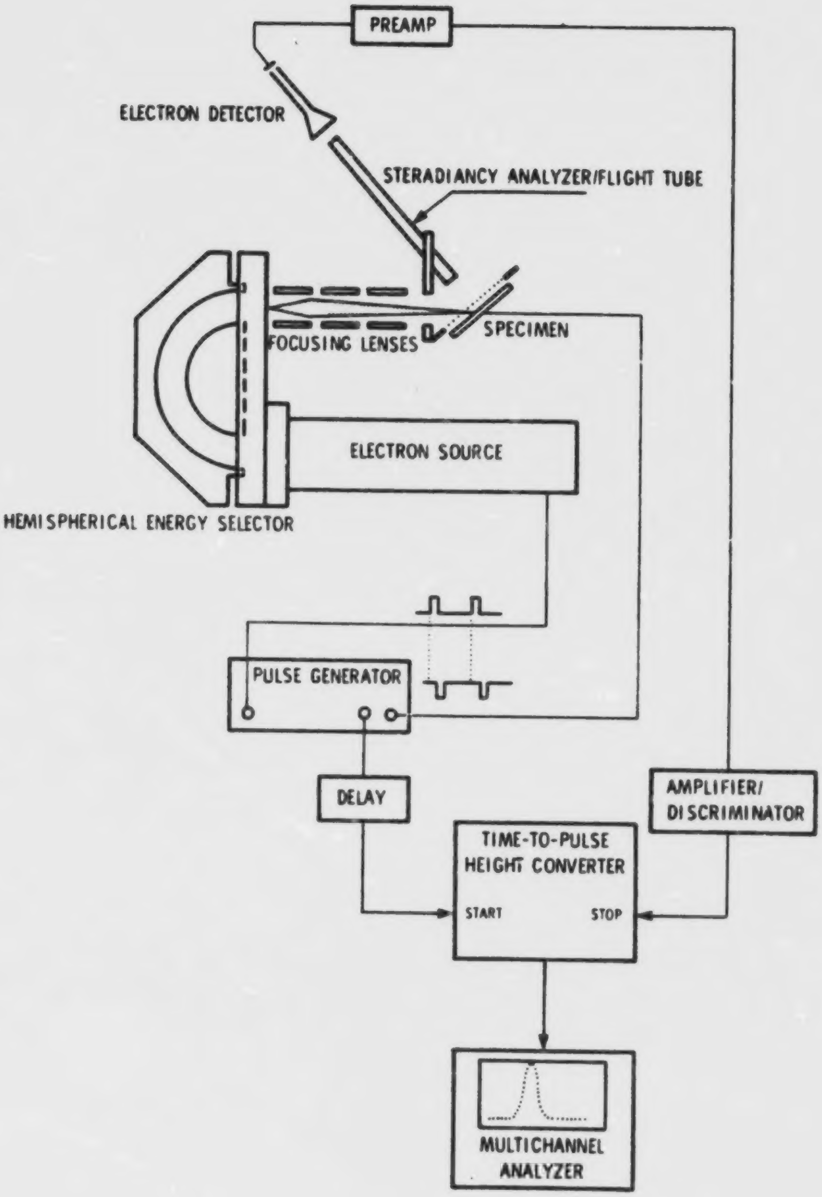
PREAMP
ELECTRON DETECTOR
STERADIANCY ANALYZER/FLIGHT TUBE
FOCUSING LENSES
SPECIMEN
ELECTRON SOURCE
HEMISPHERICAL ENERGY SELECTOR
PULSE GENERATOR
DELAY
AMPLIFIER/
DISCRIMINATOR
TIME-TO-PULSE
HEIGHT CONVERTER
START
STOP
MULTICHANNEL
ANALYZER

Figure 1. Schematic Representation of the Threshold Excitation Spectrometer.

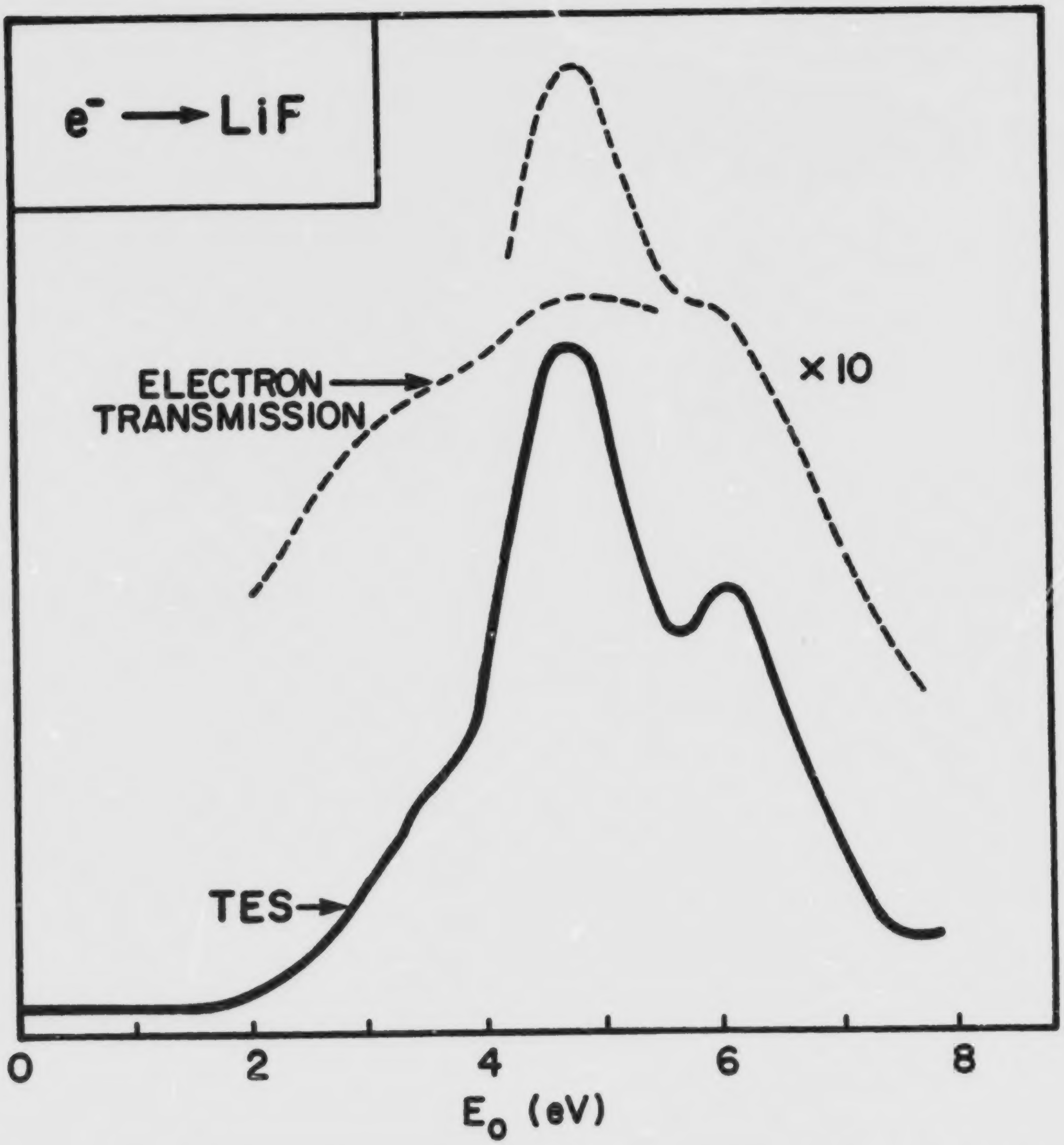

Figure 2. Threshold Excitation Spectrum and Electron Transmission Spectrum (from reference 2) of LiF.

ABSTRACT

Surface State Spectroscopy: A New Characterization Technique

by

B. C. Lamartine, K. G. Eyink, J. v. Czarnecki, and T. W. Haas
Aeronautical Systems Division, Materials Laboratory
Wright Patterson AFB OH 45433

It has been found that filled surface states of certain materials are more abundant than previously thought. Comparison of previous literature with current experiments reveals that surface states have often been misidentified as instrument artifacts. The discovery of an unambiguous technique for measurement of the energy levels and widths of surface states is discussed. The energy of the surface state relative to the Fermi and vacuum levels can be obtained, and the appropriate peak shapes can be decomposed into separate components of importance. Several physical variables were found to influence the shapes of surface state features measured by electron spectroscopy. In particular, incident photon energy and polarization, residual gas composition, and chemical adsorption were found to influence the magnitude and energies of surface state peaks. Further experiments and applications to related research endeavor is also discussed.

AFOSR/AFWAL Molecular Dynamics and Surface Chemistry Conference
24-26 October 1984.

PROPERTIES OF LaB_6 SINGLE CRYSTAL SURFACES

PAUL R. DAVIS
Oregon Graduate Center
19600 N.W. Walker Road, Beaverton, OR 97006

Thermionic energy conversion is a means of directly converting heat into electrical energy, using a plasma diode arrangement. Efficient thermionic devices provide high power densities and exhibit characteristics desirable for space power applications. A typical thermionic energy converter (TEC) consists of a cesium vapor diode with a heated emitter of work function ϕ_e and a cooled collector of work function ϕ_c (where $\phi_e > \phi_c$) in a closely spaced, parallel geometry. The efficiency of such a device is dependent upon both electrode properties and low voltage plasma arc parameters. The goal of this project is to investigate both clean and cesium-covered low work function surfaces for converter applications.

Figure 1 is a schematic diagram of the experimental setup. The arrangement shown in Fig. 1(a) allows us to characterize clean or adsorbate-covered sample electrode surfaces, transport them to a test converter for operational testing and then perform postoperational surface studies, all without exposing the specimen to atmosphere. The surface analysis capabilities available in this system are shown in Fig. 1(b). The facility shown in Fig. 1 represents the first attempt at careful surface study of TEC electrodes under controlled environmental conditions.

We have investigated surface properties of single crystal faces of the emitter candidate material LaB_6 which exhibits a work function as low as 2.4 eV (for the (310) crystal face), and low volatility at elevated temperature in ultra-high vacuum. Figure 2 summarizes long-term evaporation rate measurements made in our laboratory and illustrates the effect of O_2 upon these rates. Evaporation of oxide species, observed directly by line-of-sight mass spectrometry, is the mechanism responsible for the enhancement of material loss at O_2 pressures greater than about 1×10^{-7} torr. Evaporation in good vacuum is isotropic, but this enhanced evaporation is anisotropic, and we have observed faceting of certain crystal faces after long-term heating in O_2. These results have stimulated more detailed investigations, currently in progress, of active gas interactions with different crystal faces of LaB_6.

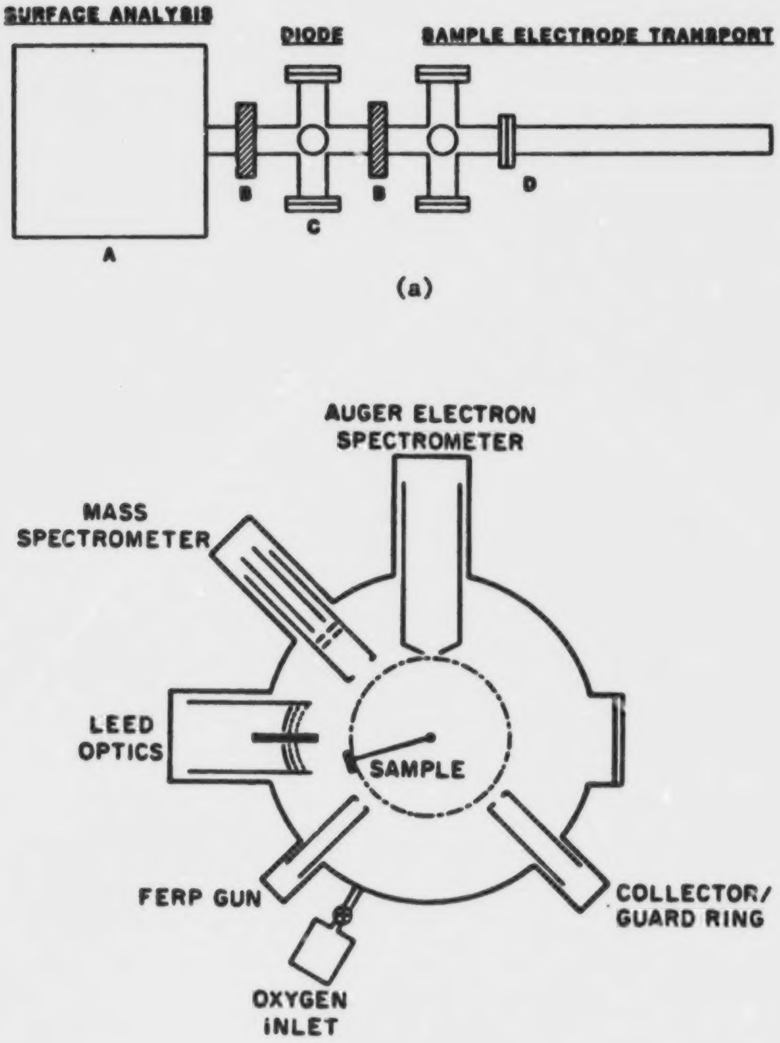
SURFACE ANALYSIS
DIODE
SAMPLE ELECTRODE TRANSPORT
B
B
C
D
A
(a)
AUGER ELECTRON SPECTROMETER
MASS SPECTROMETER
LEED OPTICS
SAMPLE
FERP GUN
COLLECTOR/ GUARD RING
OXYGEN INLET

(b)

Figure 1 (a). Block diagram of analysis/test system. A: Surface analysis system; B: Ultra-high vacuum gate valve; C: Test diode chamber with variable spacing; D: Sample transport assembly. Sections C and D are separately pumped. (b). Detail of surface analysis system (A above), showing instruments available: Auger electron spectrometer for surface composition studies; Field emission retarding potential (FERP) gun and thermionic emission collector/guard ring for work function measurements; Low energy electron diffraction (LEED) optics for surface geometrical studies; Line-of-sight mass spectrometer for determination of evaporation products.

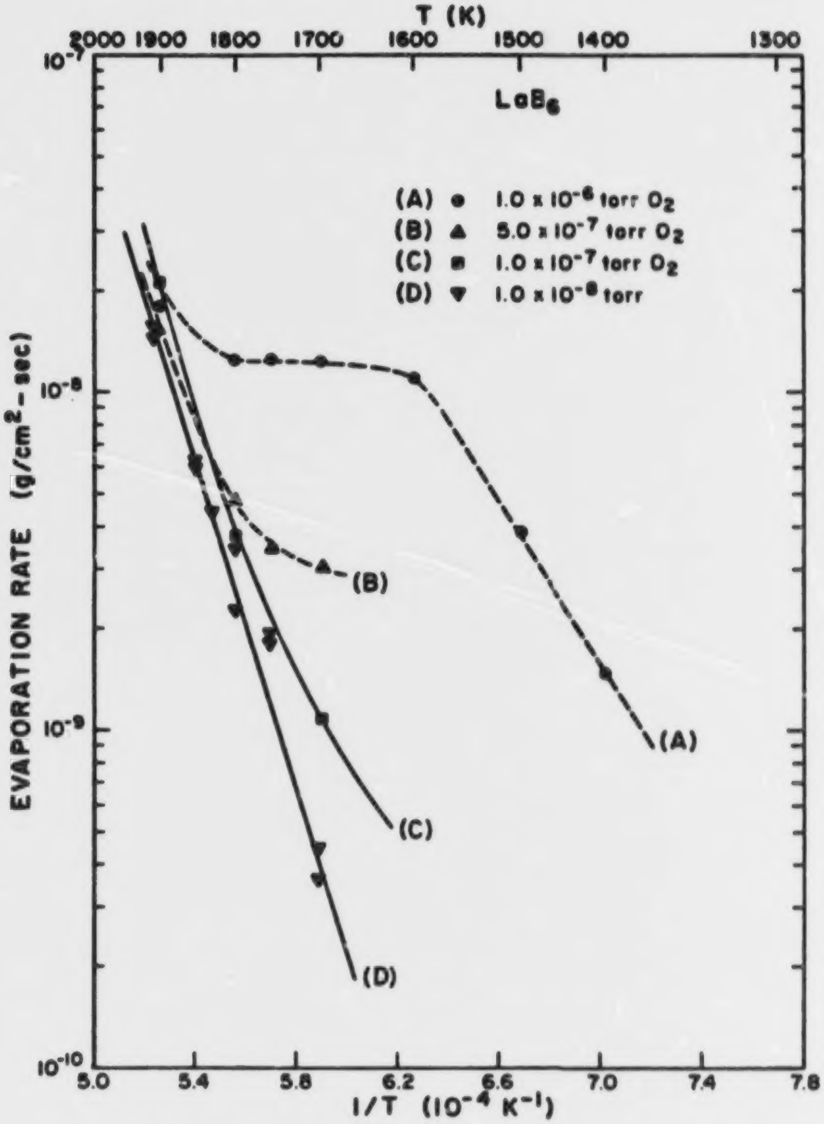

Figure 2. Summary of evaporation rate studies on LaB$_6$ single crystals in good vacuum (D) and in various O$_2$ pressures (A) - (C). Rates are determined experimentally by measurement of dimensional changes of individual crystals held at the indicated temperatures for times of 100-1000 hrs.

THEORETICAL CHEMICAL CALCULATIONS AT THE UNITED STATES AIR FORCE ACADEMY

Larry P. Davis
Department of Chemistry, United States Air Force Academy

Theoretical chemical calculations on large molecules are of interest to the Air Force in the areas of explosives and propellants, biological systems, electrochemistry, and ceramic and catalytic materials. Theoretical predictions of molecular geometries, energies, and reaction mechanisms can be used to explain and correlate experimental observations, as well as make predictions in areas either unsuitable for experiment or to assist experimental planners. Figure 1 shows the general approach to these theoretical efforts. We have chosed Dewar's MNDO semi-emperical molecular orbital method[1] as the procedure most likely to give us reasonable accuracies for the size of molecules that we are dealing with. We have established a theoretical chemistry group a the United States Air Force Academy composed of members from the Frank J. Seiler Research Laboratory and the Department of Chemistry to study these areas.

For several years, we have investigated the thermochemical decomposition of explosives, most notably TNT. We have used 1-nitropropene as a theoretical model to study TNT thermochemical decomposition, and the results of our study of possible first steps in the decomposition mechanism will appear shortly.[2,3] The results indicated the strong possibility that an intermolecular hydrogen atom transfer between the methyl group of one TNT molecule to a nitro group on a second TNT molecule gives rise to experimental observations early in the decomposition. Figure 2 shows the energy profile for this step plus some possible follow-on steps in the overall mechanism. Work is also progressing along similar lines on decomposition of nitramines and nitroenamines.

We have recently begun a program to study the mechanism of enzyme catalysis on some simple ester and amide cleavage reactions. The overall goal is to determine mechanisms as well as apply this knowledge to reaction of nerve agents with enzymes. We have chosen α-chymotrypsin as a model enzyme to study because of the availability of experimental data for it. As a preliminary, we have recently completed a study of the peptide bond in some simple dipeptides. Results indicate the general applicability of MNDO to this type of biological system.

Researchers at the Frank J. Seiler Research Laboratory have been developing low temperature molten salts for the application to batteries for a number of years. These systems are composed of mixtures of aluminum chloride and either pyridinium or imidazolium chlorides. We recently began a theoretical study of the structure of these melts and possible reactions in these melts. Our initial goal is to explain an NMR line-broadening of $AlCl_4^-$ and $Al_2Cl_7^-$ species in the melt. We have calculated activation energies for exchange reactions of the type $Al^*Cl_4^- + Al_2Cl_7^- \geq Al^*AlCl_7^- + AlCl_4^-$, and there is general agreement with the experimentally-observed activation energy. We are continuing to determine the structure of these melts and other equilibria which may be present.

Finally, we have begun a theoretical study of silica polymerization reactions. Since there is some question of the accuracy of MNDO for silicon-containing compounds, we started with a comparison of MNDO-calculated results vs. available experimental data on gas-phase silicon compound reactions, in particular fluorine affinities of silanes, pseudorotations of 5-coordinate silica compounds, and gas-phase acidities of silanes. Results are promising, although it appears that for hydrogen transfer reactions the predicted activation barriers are probably too high.

References

1. Dewar, M. J. S. and Thiel, W., J. Am. Chem. Soc., 1977, 99, 4899-4917.

2. Turner, A. G. and Davis, L. P., J. Am. Chem. Soc., accepted for publication.

3. Turner, A. G. and Davis, L. P., J. Energ. Mat., accepted for publication.

BLANK PAGE

BLANK PAGE

BLANK PAGE

PREDICT DECOMPOSITION MECHANISM

GOAL: PROVIDE THEORETICAL BASIS FOR
EXPERIMENTAL INTERPRETATIONS

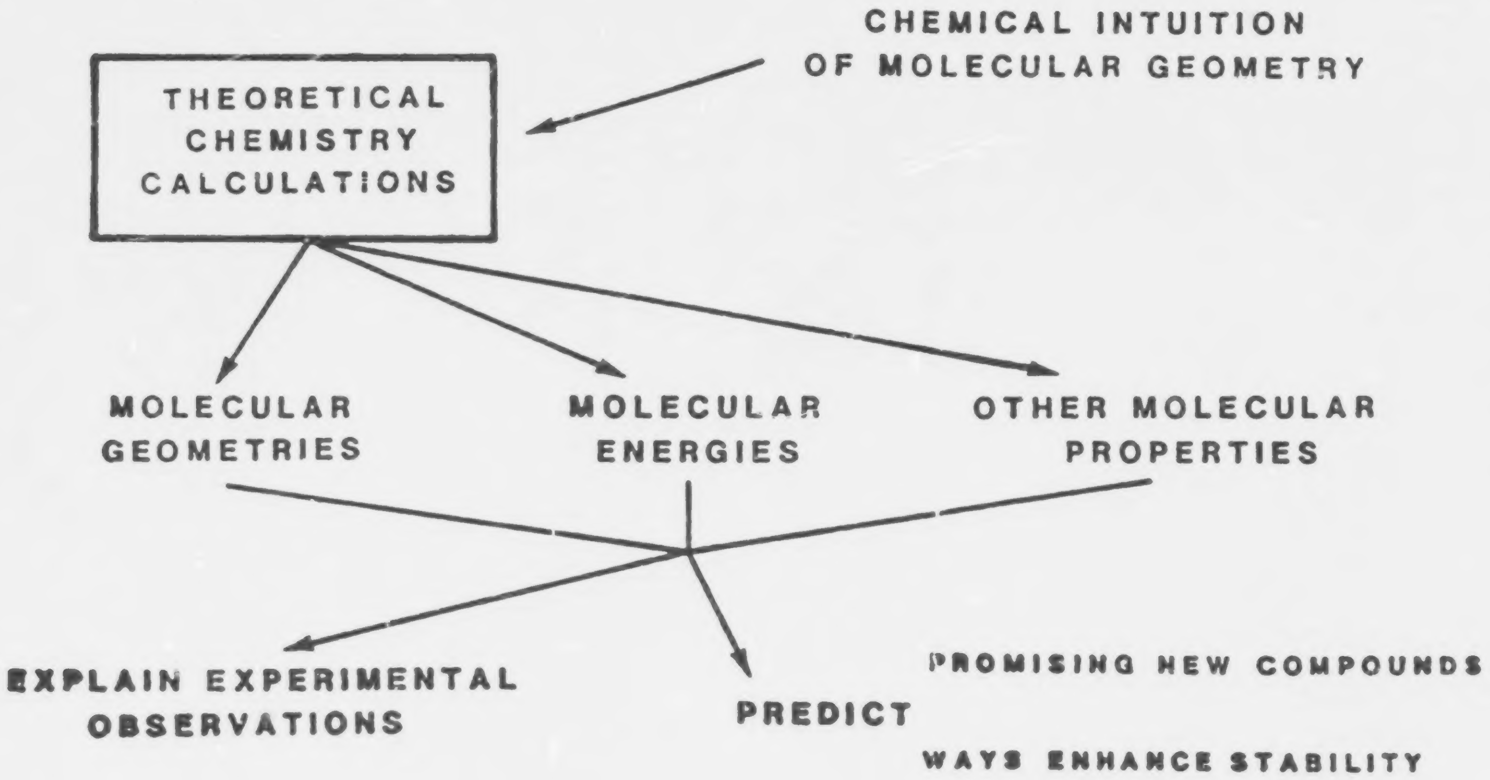

CHEMICAL INTUITION
OF MOLECULAR GEOMETRY

THEORETICAL
CHEMISTRY
CALCULATIONS

MOLECULAR
GEOMETRIES

MOLECULAR
ENERGIES

OTHER MOLECULAR
PROPERTIES

EXPLAIN EXPERIMENTAL
OBSERVATIONS

PREDICT

PROMISING NEW COMPOUNDS

WAYS ENHANCE STABILITY

Figure 1. General approach to theoretical chemistry.

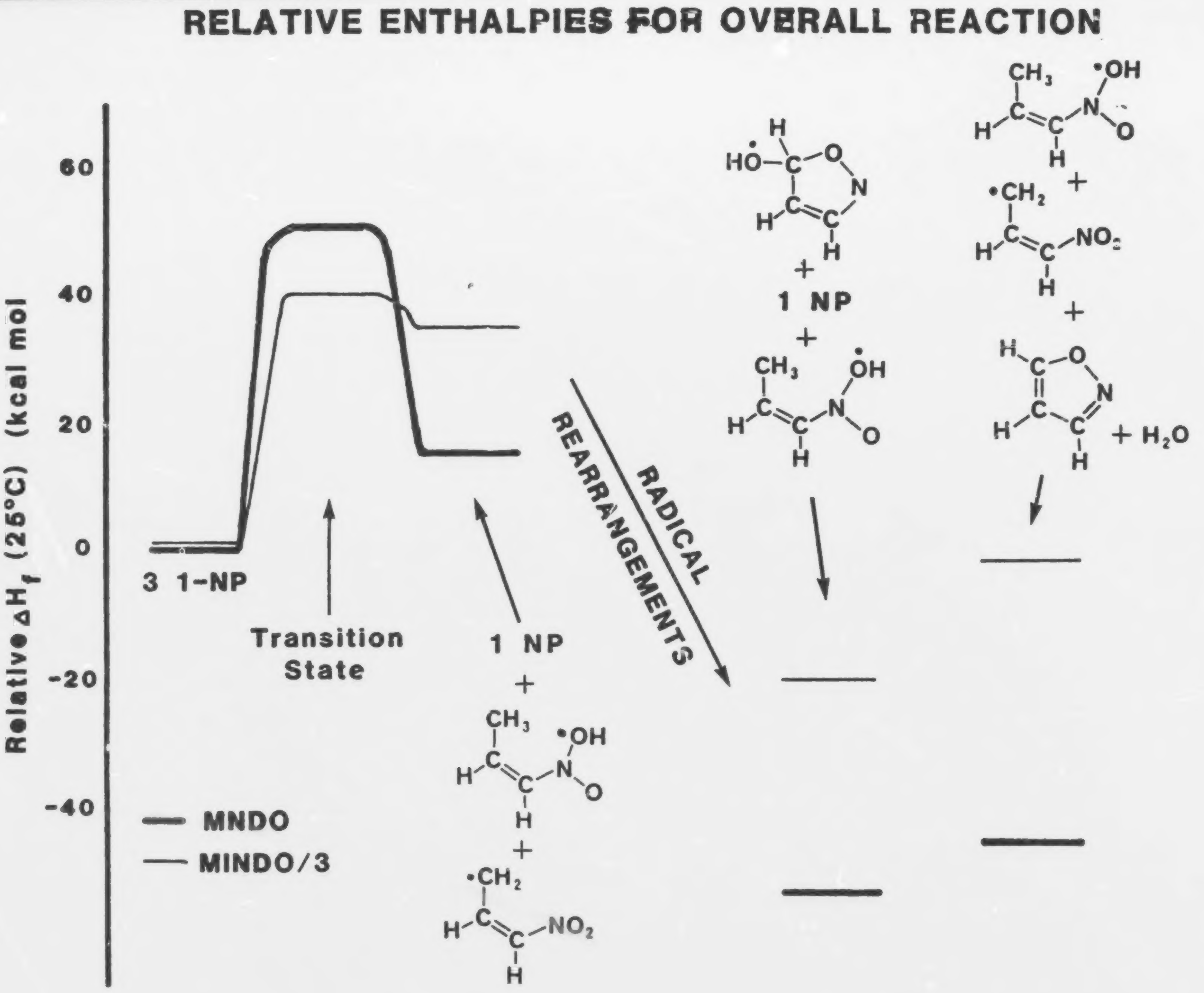

RELATIVE ENTHALPIES FOR OVERALL REACTION

Figure 2. Reaction profile for 1-nitropropene as a model for TNT thermochemical decomposition.

OXYGEN-IF KINETICS CONTRACT NO. F29601-83-C-0049.

PRINCIPAL INVESTIGATORS: Philip D. Whitefield and Michael R. Berman
McDonnell Douglas Research Laboratories
P. O. Box 516, St. Louis MO 63166

The objective of this program has been to provide kinetic data on potentially important elementary processes proposed in mechanisms for an $O_2(^1\Delta)$ pumped IF(B-X) electronic transition chemical laser. The following reactions were studied:

$$I(^2P_{1/2}) + F_2 \rightarrow \text{Products, } T = 300K \quad (1)$$

$$I(^2P_{3/2}) + F_2 \rightarrow \text{Products, } T = 300K \quad (2)$$

$$IF(B)v' + I_2(X) \rightarrow IF(X) + I_2(X), \ T = 300K \quad (3)$$

Reactions (1) and (2) were studied under pseudo-first order kinetic conditions ($[I] << [F_2]$). I atoms were generated by laser photolysis of alkyl halides at 266 nm. Excited I atoms were monitored by observing time resolved infra-red emission at 1315 nm and also by atomic resonance absorption on the $[I(6s\,^2P_{3/2} \leftarrow 5p^5\,^2P_{1/2})]$ transition at 206.2 nm. Ground state I atoms were monitored by observing time resolved atomic resonance absorption on the $[I(6s\,^2P_{3/2} \leftarrow 5p^5\,^2P_{1/2})]$ transition at 183.0 nm. The rate constant for the reaction of $I(^2P_{1/2}) + F_2$ has been measured to be:

$$k_1 = (1.7 \pm 0.2) \times 10^{-13} \text{ cm}^3 \text{ s}^{-1} \text{ at } 300K$$

The rate constant for the $I(^2P_{3/2}) + F_2$ reaction has been found to lie within the range:

$$(1 \times 10^{-14} < k_2 < 3 \times 10^{-14}) \text{ cm}^3 \text{ s}^{-1}$$

The quenching of $IF(B)v'$ by $I_2(X)$ was studied in a static cell. Time resolved laser induced fluorescence measurements were made of the decay of the IF(B) fluorescence produced when IF(X) was pumped to $IF(B)v'$ with a YAG pumped dye laser. The IF(X) was generated by adding F_2 into a cell of I_2 at a known total pressure ($[F_2] << [I_2]$). In situ absolute I_2 concentrations were monitored with a laser absorption technique employing a krypton ion laser at 482.5 nm.

A gas kinetic rate was measured for all vibrational levels investigated.

Presentations on parts of this work have been made at the VIIIth International Symposium on Gas Kinetics, Nottingham, England (July 1983) and XVI Informal Conference on PhotoChemistry, Cambridge, Massachusetts, August 1984.

POTENTIAL IF(B) EXCITATION MECHANISM - PUMPING BY $O_2(^1\Delta)$

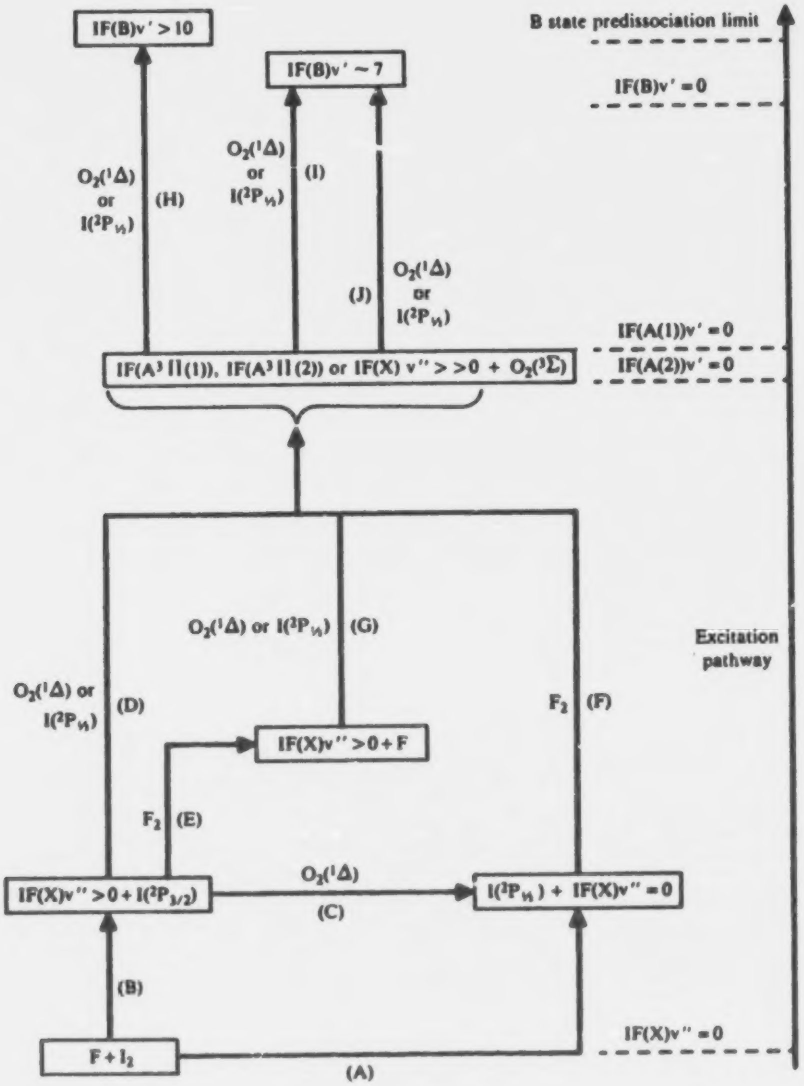
IF(B)v' > 10
IF(B)v' ~ 7
B state predissociation limit
IF(B)v' = 0
O2(1Δ) or I(2P½) (H)
O2(1Δ) or I(2P½) (I)
(J) O2(1Δ) or I(2P½)
IF(A(1))v' = 0
IF(A(2))v' = 0
IF(A3Π(1)), IF(A3Π(2)) or IF(X) v" >>0 + O2(3Σ)
O2(1Δ) or I(2P½) (G)
Excitation pathway
O2(1Δ) or I(2P½) (D)
F2 (F)
IF(X)v" >0+F
F2 (E)
IF(X)v" >0+I(2P3/2)
O2(1Δ)
(C)
I(2P½) + IF(X)v" = 0
(B)
IF(X)v" = 0
F + I2
(A)

Laser-Photolysis/Optical-Emission-
Spectroscopy Apparatus

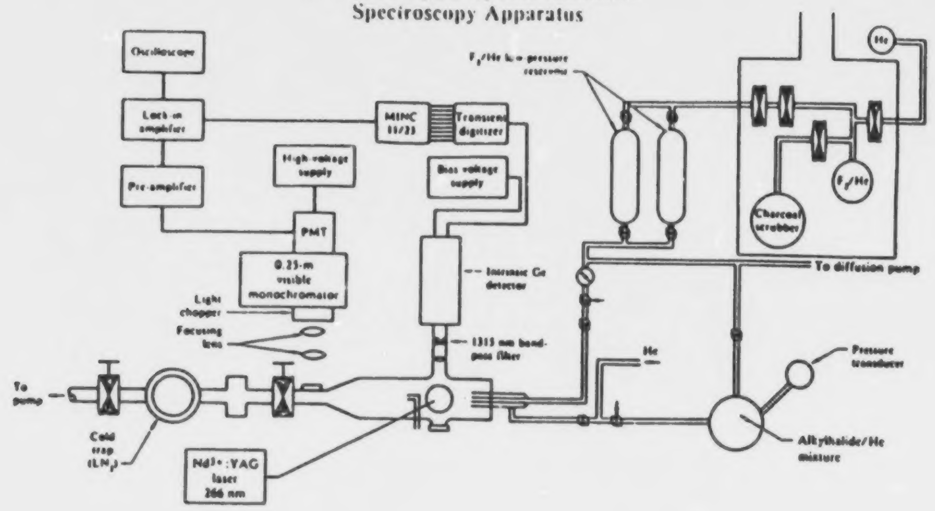
Oscilloscope
Lock-in amplifier
Pre-amplifier
High-voltage supply
PMT
0.25-m visible monochromator
Light chopper
Focusing lens
MINC 11/23
Transient digitizer
Bias voltage supply
Intrinsic Ge detector
1315 nm band-pass filter
F_2/He low-pressure reservoirs
He
F_2/He
Charcoal scrubber
To diffusion pump
He
Pressure transducer
Alkylhalide/He mixture
To pump
Cold trap (LN_2)
Nd^{3+}:YAG laser 266 nm

Experimental Conditions for $I(^2P_{1/2}) + F_2$ Study

High Flow Velocity, Low Pressure

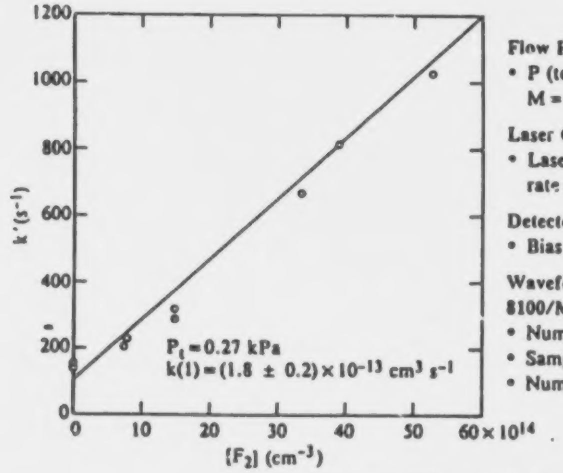

Flow Reactor Conditions

- P (total) = 0.27 kPa; u = 2.7 m/s; CF_3I: M = 1:50; F_2: M = 1:10

Laser Conditions (Quadrupled YAG)

- Laser power = 20 mJ/pulse at 266 nm; rep. rate = 10 Hz

Detector Conditions (Intrinsic Germanium)

- Bias voltage = −200 V; temperature = 77 K

Waveform Digitizer/Averager (Biomation 8100/Minc 11-23)

- Number of shots averaged = 100-4000
- Sample interval = 5-10-20 microseconds/channel
- Number of channels = 1000

Low Flow Velocity, High Pressure

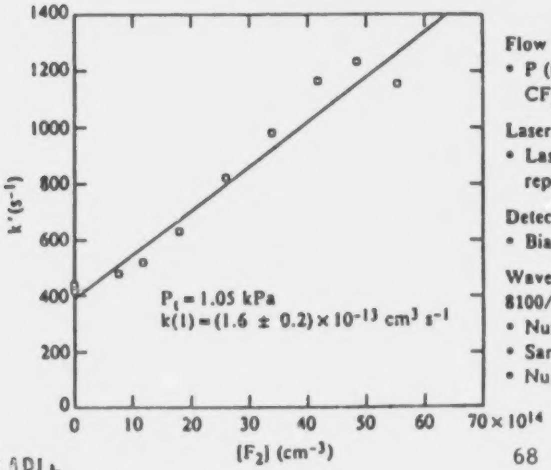

Flow Reactor Conditions

- P (total) = 1.05 kPa; u = 0.5 m/s; CF_3: M = 1:50; F_2: M = 1:10.

Laser Conditions (Quadrupled Nd^{3+}: YAG)

- Laser power = 20 mJ/pulse at 266 nm; rep. rate = 10 Hz

Detector Conditions (Intrinsic Germanium)

- Bias voltage = −200 V; temperature = 77 K

Waveform Digitizer/Averager (Biomation 8100/Minc 11-23)

- Number of shots averaged = 100-4000
- Sample interval = 5-10-20 microseconds/channel
- Number of channels = 1000.

BEST COPY AVAILABLE

Nonspeakers

Molecular Dynamics

STUDY IN MOLECULAR LASERS

George Burns
Chemistry Department, University of Toronto,
Toronto, Canada M5S 1A1

The experimental approach to the study of chemical reactions in molecular lasers was centered around a sensitive LIF apparatus in which reactions were generated by a Quanta Ray Nd:YAG plus a dye laser (Fig.1), which was tuned using a photoacoustic detector. Reactivity of HF(v=5) with unsaturated hydrocarbons was studied.[1] Using the same equipment, it was possible to observe a time-delayed multielectron photoemission (TDMP) from a trialkali antimonide photocathode.[2] The initiation of this photoemission is correlated to irradiation of photocathode with a weak (less than 1 femptojoule/cm^2) light pulse but otherwise it appears to be statistical. However generation of multielectron pulses from the surface of the photocathode is not statistical with up to 30 electrons leaving the photosensitive surface within the time resolution of the equipment. Such pulses are separated in time during which there are no electrons emitted (Fig.2). The phenomenon is now being studied as a function of light intensity, temperature, and the wavelength of the incident radiation.

Diatom dissociation and atomic recombinations, occurring in molecular lasers, were studied using the 3-D trajectory calculations technique, in which over 10^5 trajectories were generated. It was possible to define a new computational reaction kinetic "observable", $d^{ss}(E)$, the relative nonequilibrium energy distribution (RNED) function at the steady state. The $d^{ss}(E)$ is a plot of relative molecular densities of diatoms vs. their internal energies. The RNED, obtained as a histogram, proved to be significant for several reasons, one of which was that it can be described with a remarkably high degree of precision by a simple algebraic function. The latter is calculated from known constants and physically meaningful constraints. It required only one adjustable parameter, a. For the case of Br_2 dissociating in Ar at 3500K, $a = 12.0 \pm 0.3$, which is intriguing because the transition state theory prescribes $a = +\infty$ for all reactions. The study of d(E) and of a might provide a novel method for testing the transition state and other quasi-equilibrium theories. Preliminary results indicate that the much used strong collision assumption of unimolecular reaction theories is inadequate in describing reactions occurring on strongly attractive surfaces.[3] Much work on this project is now being prepared for publication.

1. Billard, T.C., Burns, G., Nature, 306, 247-248 (1983).
2. Beck, W.H., Burns, G., Can. J. Chem., Nov. 1 issue(in press).
3. Burns, G., Cohen, L.K., J. Chem. Phys., Dec. 1 issue (in press).

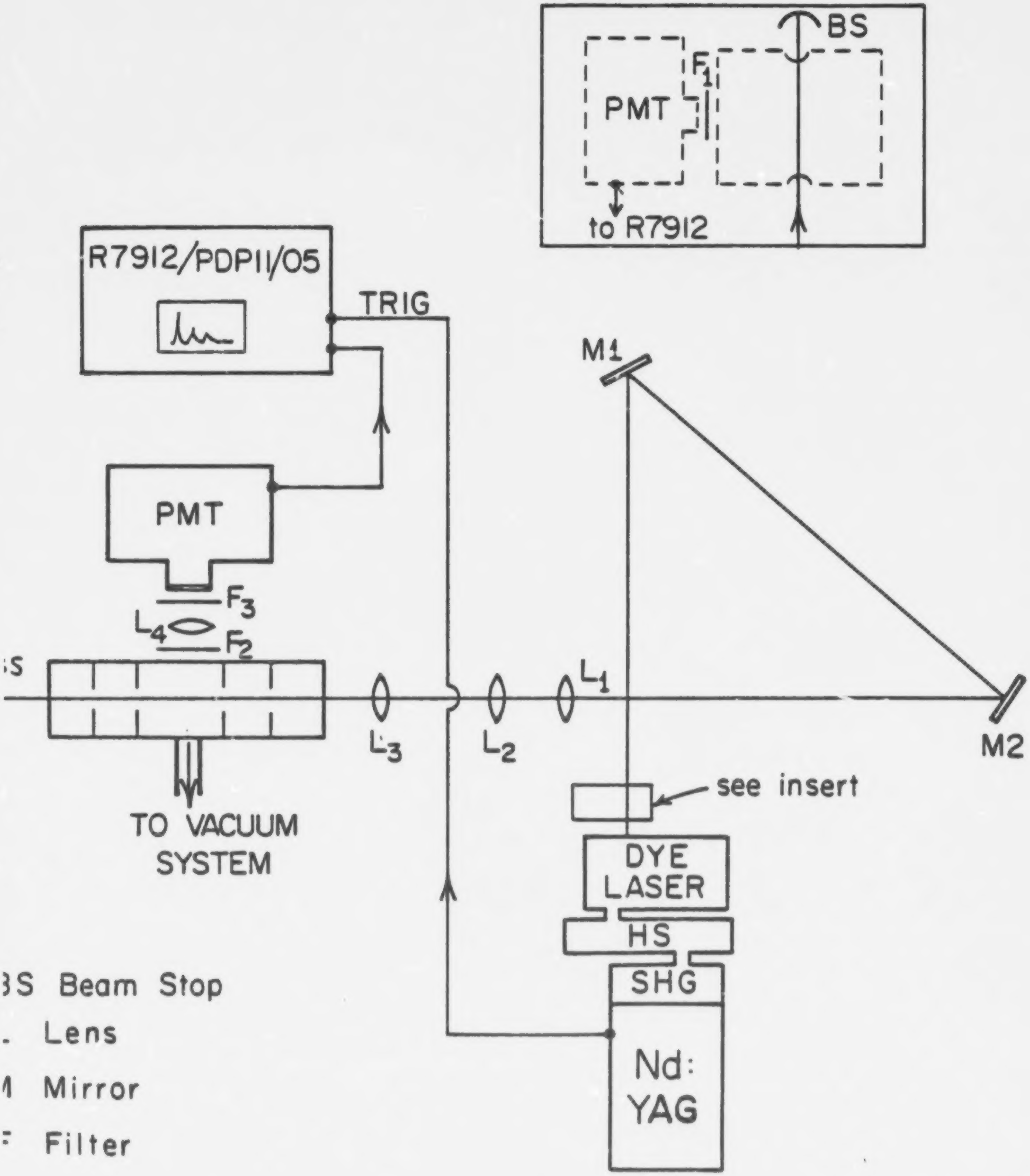
BS
F1
PMT
to R7912
R7912/PDP11/05
TRIG
M1
PMT
F3
L4
F2
S
L1
L3
L2
M2
TO VACUUM SYSTEM
see insert
DYE LASER
HS
SHG
Nd: YAG
S Beam Stop
Lens
Mirror
Filter

Figure 1 Schematic of the Experimental Apparatus.

Figure 2 Representative Time-Delayed Multielectron Photoemission

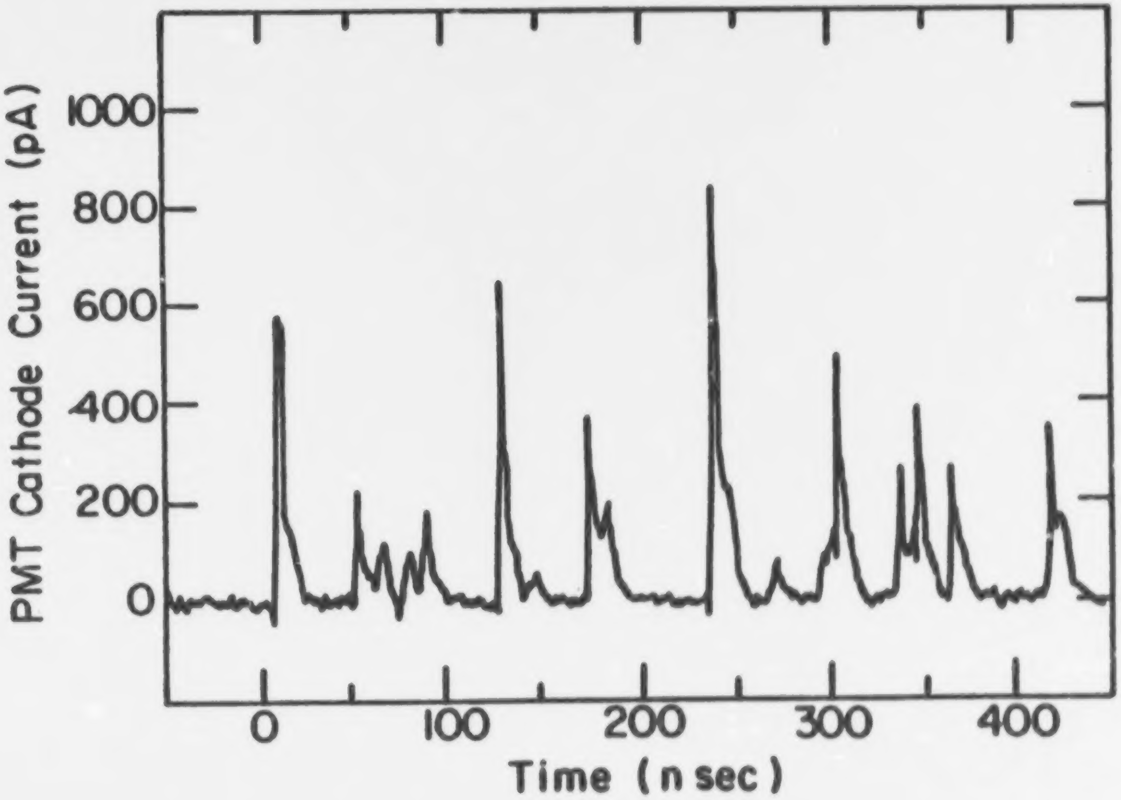

PHYSICAL CHEMISTRY OF ENERGETIC NITRIDES

R.D. Coombe
Department of Chemistry, University of Denver
Denver, CO 80208

The halogen azides (XN_3, X=halogen) and halogen isocyanates (XNCO) are a group of molecules capable of unique chemical reactivity and photochemical behavior. The strong perturbation exerted by the halogen atom on the electrons of the N_3 or NCO chain tends to destabilize these compounds, such that they are metastable with respect to the ground states of the nitrenes and N_2 or CO. Hence, an additional amount of energy is made available to the fragments of photodissociation processes or to the products of chemical reactions involving these molecules. The objective of our recent work on these systems has been to specify the energetics of such processes, and to search for new or unique photochemical mechanisms or reaction paths which may result.

To date, we have studied the molecules ClN_3, BrN_3, and ClNCO.[1-3] The UV absorption spectra of these species exhibit features which are convenient for photodissociation by the output of pulsed rare gas halide lasers. Spin-allowed dissociation of excited singlet states of these compounds can produce two singlet fragments, two doublets, or two triplets. In the singlet manifold of fragments, the $a^1\Delta$ and $b^1\Sigma^+$ excited states of the nitrogen halide diatomics are found.[1] Pulsed production of these excited species by the photolysis allows their decay kinetics to be measured in real time. Recently, rate constants for radiative and collisional decay of the $a^1\Delta$ states of NCl and NBr were determined. These data represent near completion of a data set comprised of the a→X and b→X radiative rates in NF, NCl, and NBr. This information should offer a valuable comparison for theoretical treatments of these radiative processes. In the halogen azides, dissociation to doublet fragments (halogen atoms and N_3) does not appear to be a major route, although some evidence of its occurrence has been found. The halogen atoms produced react with the parent azides to produce molecular halogens, which are subsequently excited by collisions with N_2 metastables present in the mixture. Intense $D'^3\Pi_{2g} \rightarrow A'^3\Pi_{2u}$ emission from Cl_2 and Br_2 produced in this manner has been observed.[3] Perhaps the most remarkable attribute of the halogen azides is their ability to produce excited triplet states of N_2 upon photolysis at relatively long wavelengths (up to 300 nm for BrN_3).[1-2] The accessibility of the triplet manifold of fragments at these low photon energies is a direct consequence of the metastability of the molecules. The generation of significant quantities of triplet N_2 in these systems results in the occurrence of a number of unique chemical processes, including reactions with the parent azides,[2] processes generating the excited D' states of the molecular halogens as noted above,[3] and energy pooling among the excited species present.[1] We have recently investigated the latter such processes for the ClN_3 system. Emission from states produced by energy pooling of two $N_2(A^3\Sigma_u^+)$ molecules is readily observed subsequent to photolysis of this molecule at 193 nm.[1] We have attempted to drive the ClN_3 system to the regime where such second order processes are dominant by photolysis at higher fluences corresponding to large percentage dissociation of the azide molecules. Figure 1 shows an intriguing result of this work. The spectrum of visible emissions produced at low fluence, dominated by the $b^1\Sigma^+ \rightarrow X^3\Sigma^-$ transition in NCl, is shown in Figure 1A. Figure 1B shows the emission spectrum in the same region found when the fluence is increased by a factor of three. In this case, the NCl emission has been almost completely replaced by the spectrum of first positive ($B^3\Pi_g \rightarrow A^3\Sigma_u^+$) emission in N_2.[3] From the time dependence of the first positive emission, the $B^3\Pi_g$ state is not produced by energy pooling of two $N_2(A^3\Sigma_u^+)$ molecules (as has been suggested in the literature[4]), but rather by collision of $N_2(A^3\Sigma_u^+)$ with another excited species present, likely $NCl(b^1\Sigma^+)$.

Isocyanates are in general much more stable than their azide counterparts, owing principally to the greater strength of the RN-CO bond. At issue in the case of the halogen isocyanates is whether the perturbation by the halogen atom is strong enough to significantly affect the chemistry of these species. Our recent work on ClNCO has shown that this is in fact the case. The emission observed subsequent to photolysis of this compound at 249 nm is dominated by the $A^2\Sigma^+ \rightarrow X^2\Pi$ transition in NCO. From the time dependence of the emission, the excited NCO is produced by a reaction subsequent to the photolysis, rather than as a direct photofragment. This process appears to involve the reaction of excited $N(^2D)$ atoms, generated by the photolysis, with the parent ClNCO.

1. R.D. Coombe, A.T. Pritt, Jr., D. Patel, and F.J. Wodarczyk, J. Chem. Phys., 75, 2177 (1981).

2. R.D. Coombe, J. Chem. Phys., 79, 254 (1983).

3. R.D. Coombe and C.H.-T. Lam, J. Chem. Phys., 80, 3106 (1984).

4. G. H. Hays and H.J. Oskam, J. Chem. Phys., 59, 1507 (1973).

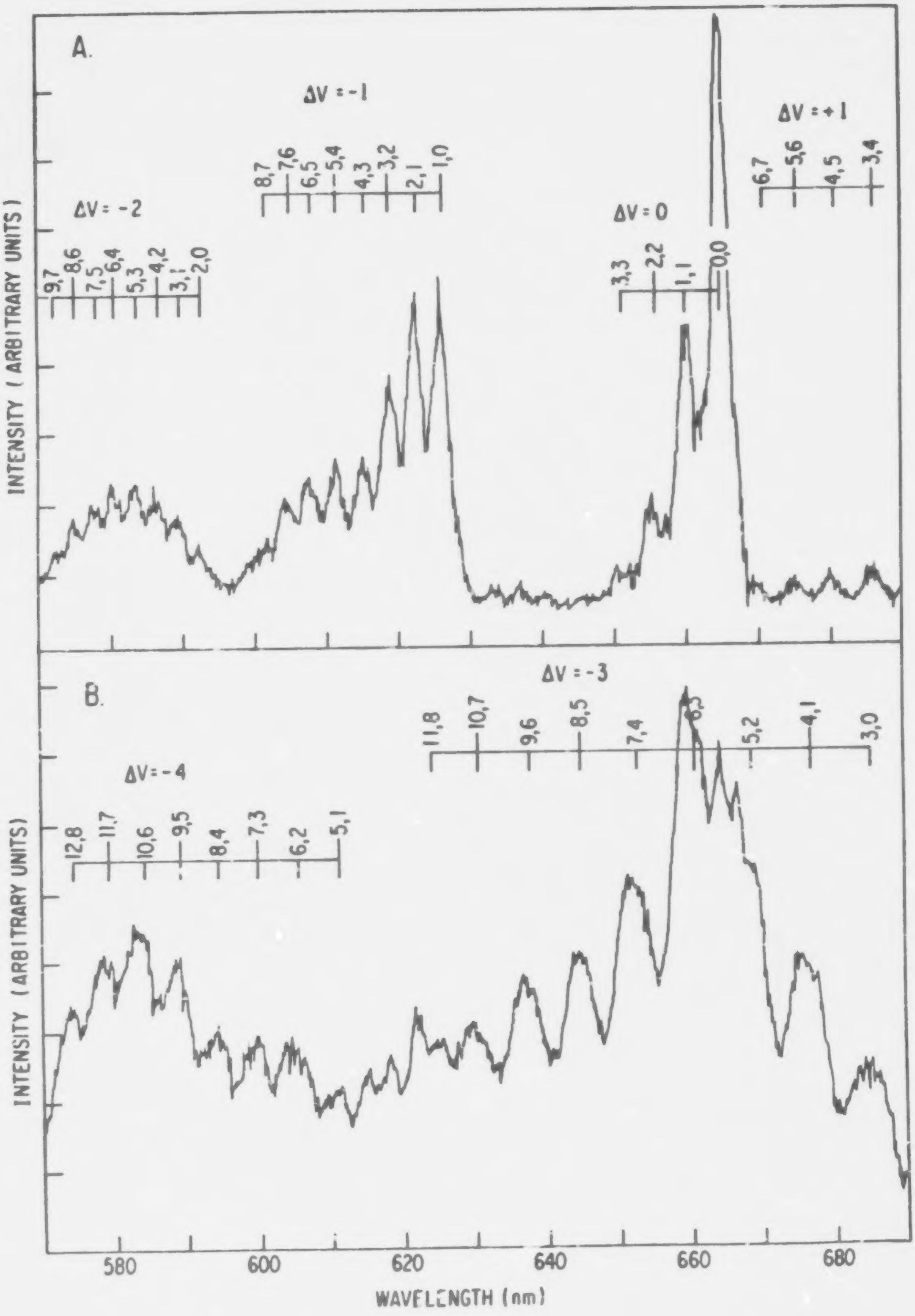
A.
ΔV = -1
8,7 7,6 6,5 5,4 4,3 3,2 2,1 1,0
ΔV = +1
6,7 5,6 4,5 3,4
ΔV = -2
9,7 8,6 7,5 6,4 5,3 4,2 3,1 2,0
ΔV = 0
3,3 2,2 1,1 0,0
INTENSITY (ARBITRARY UNITS)
B.
ΔV = -3
11,8 10,7 9,6 8,5 7,4 6,3 5,2 4,1 3,0
ΔV = -4
12,8 11,7 10,6 9,5 8,4 7,3 6,2 5,1
INTENSITY (ARBITRARY UNITS)
580
600
620
640
660
680
WAVELENGTH (nm)

Vibrational Energy Transfer Pathways in Hydrogen Fluoride

F. F. Crim
Department of Chemistry
University of Wisconsin
Madison, Wisconsin 53706

Vibrational overtone laser double resonance measurements, in which a pulsed dye laser excites an overtone vibration and a continuous hydrogen fluoride chemical laser probes the evolution of the excited population, provides new data on vibrational relaxation of HF($v = 1$ and 2). The double resonance technique is particularly well suited to measuring the temperature dependence of molecular energy transfer in HF. In recent experiments, this technique has determined the self-relaxation rate constant for HF($v = 1$ and 2) between 300 and 700 K. Rate constants for both levels show the inverse variation with temperature that is characteristic of systems dominated by long range forces. The decrease is weaker for HF($v = 2$) than for HF($v = 1$), and, in fact, the HF($v = 2$) self-relaxation rate constant shows the smallest variation with temperature of all the levels we have studied ($v = 1$ to 5). A detailed analysis of the double resonance data shows that the amount of the relaxation of HF($v = 2$) proceeding by a vibration-to-vibration energy transfer route varies only slightly with temperature over the range studied and shows a slight increase with temperature. This analysis implies a somewhat weaker variation of the vibration-vibration energy transfer pathway with temperature compared to the vibration-translation, rotation pathway. These results are consistent with the different energetics of the two pathways being the dominant factors in determining their relative importance. Another recent application of the laser double resonance technique has provided the first data on relaxation of HF($v = 1$) by hydrogen fluoride dimers. The energy transfer is extremely efficient, requiring only about two collisions compared to 100 typically needed for relaxation by the monomer.

GAS PHASE PHOTOELECTRON SPECTROSCOPY OF METALS AND METAL OXIDES OF IMPORTANCE IN THE UPPER ATMOSPHERE

Dr. John Dyke
Department of Chemistry, University of Southampton

The objective of this research is to use vacuum ultraviolet photoelectron spectroscopy to study in the gas phase the electronic structure of a number of metals and metal oxides which are of importance in the upper atmosphere. Most of the first year has been spent on the construction of a high sensitivity, multidetector spectrometer for this purpose although some results have been obtained.

The HeI photoelectron spectra of atomic scandium and vanadium have been recorded in the gas-phase. For scandium two bands associated with a $(4s)^{-1}$ ionization and one band associated with a $(3d)^{-1}$ ionization of the neutral atom have been observed. Measurement of their relative intensities allows the $\sigma_{3d}:\sigma_{4s}$ photoionization cross-section ratio in atomic scandium to be estimated. In the atomic vanadium spectrum, six bands were seen. Four of these correspond to $(3d)^{-1}$ and $(4s)^{-1}$ ionizations of the ground state of the neutral atom, the V a^4F state, whereas two bands correspond to $(3d)^{-1}$ ionizations of an excited state, the V a^6D state, which is approximately 2100 cm^{-1} above the ground state. Measurement of the intensities of bands arising from the V a^4F state allows $\sigma_{3d}:\sigma_{4d}$ to be estimated for vanadium. Comparison of the data acquisition rates obtained with both single and multidetector spectrometers demonstrates the advantage of using a multidetector instrument in high temperature photoelectron spectroscopy.

As a first step towards recording the photoelectron spectra of a number of lanthanide monoxides work has been initiated on a number of rare earth elements. Preliminary results have also been obtained on the metal oxides, BaO and SrO.

FOURIER TRANSFORM INFRARED SPECTROMETRY WITH FREE JETS AND SURFACES

Subbarao B. Ryali, Shi-da Shen and John B. Fenn
Department of Chemical Engineering, Yale University

Our research pivots on the use of Fourier Transform Infrared Spectrometry (FTIS) to determine the distribution of rotational and vibrational energy in gas phase molecules whose state is consequent to various kinds of collision processes. In particular, we have been interested in gas-gas and gas-surface encounters that are inelastic and/or reactive. While the probing of molecular internal energy states is generally more precise and sensitive with tunable lasers than with FTIS, there are many interesting and important species for which lasers of appropriate wavelength are not yet available but which do absorb and emit in the infrared region of the spectrum accessible to FTIS.

Figure 1 is a schematic representation of the essential features of the apparatus configuration used to examine the terminal state of molecules after free jet expansion. For gas-gas collision studies another nozzle is disposed so that the intersection region of the two free jets is at the focal point of the collection optics. For gas-surface studies a target surface intercepts the jet flux and the spectrometer is focussed on the flow field of reflected molecules. In all the jet-jet and jet-surface experiments in the interaction region is in the free molecule regime so that we can examine the consequences of single collisions.

With this approach we have: (1) Investigated the terminal distributions of rotational energy in free jets of CO_2 and CO and learned something about the role of rotation-rotation transfers; (2) Obtained information on the rotational energy distribution in CO_2 molecules vibrationally excited by translational energy in collisions with N_2 molecules; (3) Investigated the accommodation of rotational and vibrational energy during collisions between metal surfaces and CO, CO_2 and NO; and (4) Determined the disposition of reaction energy in the nascent products from the surface catalyzed oxidation of C and CO.

Recently we have been obtaining emission spectra of the molecules excited in the source by a corona discharge instead of simple heating. In this way we hoped to achieve high degrees of vibrational excitation for emission studies without appreciably raising the initial temperature of the source gas so that rotational band spreading would be minimized. Figure 2 shows a spectrum of a CO_2 jet taken during such discharge excitation. There are two noteworthy features that we are pursuing. One is that the terminal rotational temperature is low enough so that the combination bands emerge much more clearly. Thus we can hope to determine relaxation rates for the bending and/or stretching modes of CO_2 during expansion. The other feature is the appearance of a new band with R and P rotational branches some 70 wavenumbers to the red side of the normal CO_2 band. The rotational spacing suggests that the radiating molecule is similar to CO_2. If it is an isotope there is some remarkable enrichment mechanism at work. Another intriguing possibility is that it is due to CO_2 in an electronically excited state.

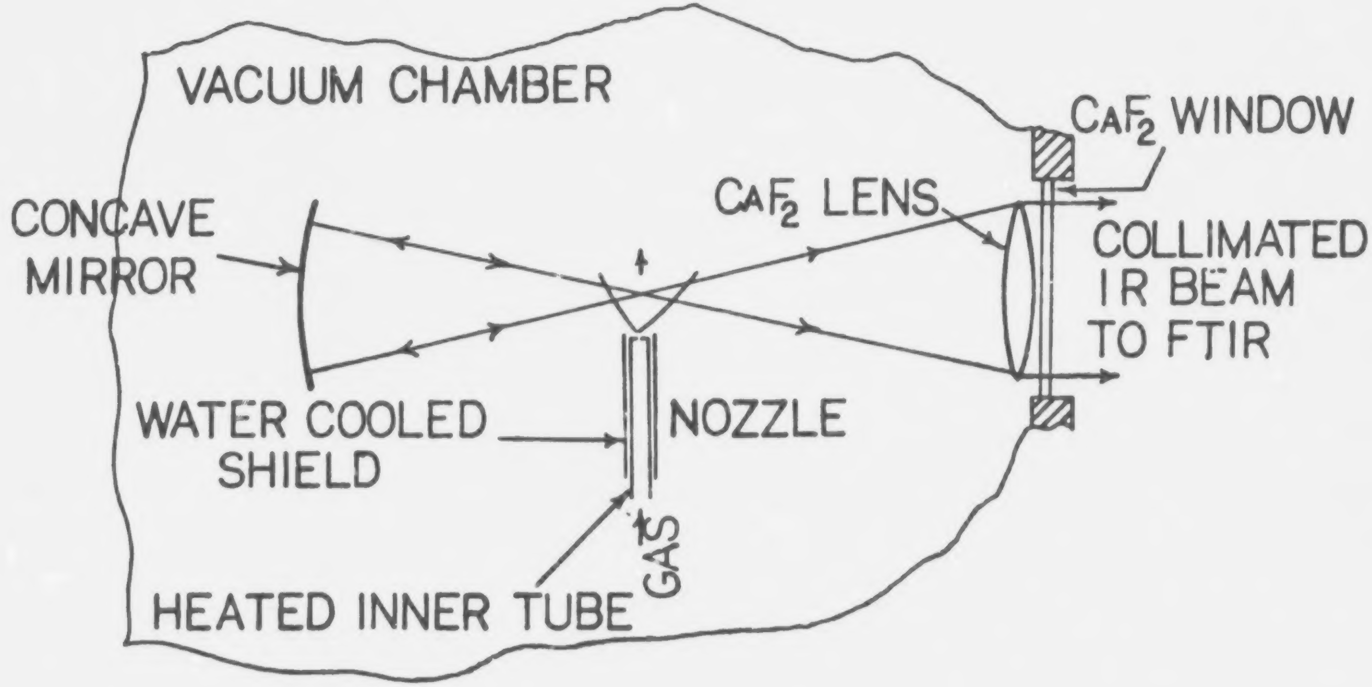
VACUUM CHAMBER
CaF_2 WINDOW
CONCAVE MIRROR
CaF_2 LENS
COLLIMATED IR BEAM TO FTIR
WATER COOLED SHIELD
NOZZLE
GAS
HEATED INNER TUBE

06/04/84 12:18:16
2569.04 SEC. MEAS. TIME
NDP = 131072
NTP = 524288
NSD = 400

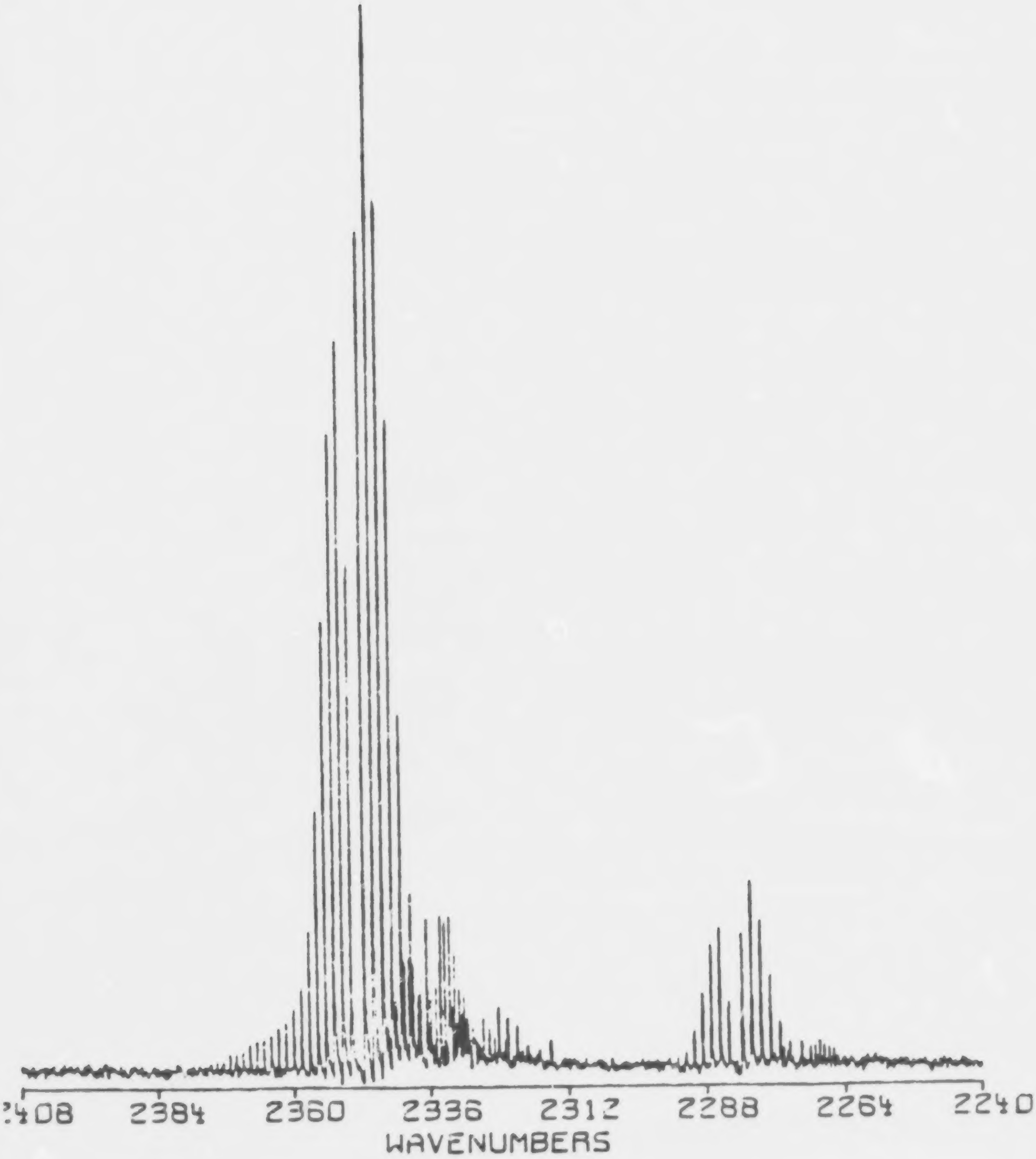

Structure and Dynamics of H_2CO S_0 and S_1

Robert W. Field and James L. Kinsey
Department of Chemistry
Massachusetts Institute of Technology
Cambridge, MA 02139

Stimulated Emission Pumping (SEP), Stark Quantum Beat (SQB), see Figure 1, Stark Anticrossing (SAC), and Transient Gain Spectroscopy (TGS), see Figure 2, are being used to characterize the electronic and vibrational structures of the $\tilde{X}^1A_1(S_0)$ and $\tilde{A}^1A_2(S_1)$ states of formaldehyde and to obtain a fundamental understanding of unimolecular (isomerization, intramolecular vibrational redistribution, quantum chaos) and bimolecular (rotational energy transfer, quenching, level specific chemistry) dynamical processes in a small polyatomic molecule.

Several of the results obtained are unique and of fundamental significance: (i) the vibrational structure of S_0 formaldehyde is "well organized" for $J=0$ up to 9500 cm^{-1} but "disorganized" for $J>10$, $K>2$[1-3]. This implies that organized and disorganized eigenstates coexist in rotationally thermalized H_2CO for $5000<E_v<9500$ cm^{-1}, that the observation of level-specific behavior in vibrationally hot polyatomic molecules may require preparation of $J=0$ samples and the kinetic process that samples the level-specificity must proceed at a rate faster than that of rotational equilibration. (ii) the tunnelling lifetime of two $J=2$ rotation-vibration levels of S_0 H_2CO near the top of the barrier to $H_2CO(S_0) \rightarrow H_2+CO$ unimolecular dissociation have been measured by SAC and SQB spectroscopy. Conventional RRKM reaction rate theory would allow a barrier height to be determined from these lifetimes, but the observation that the higher level has a lifetime 2.5 times longer than the 50 cm^{-1} lower energy level is inconsistent with the basic energy-monotonic assumption of RRKM theory. (iii) high precision (1 part in 10^4) dipole moments have been measured by SQB spectroscopy for all 5 $J=2$ levels (2_{20}, 2_{21}, 2_{11}, 2_{12}, 2_{02}) of several vibrational levels of S_1 H_2CO and D_2CO. These are being used to test a vibronic coupling model proposed by Innes and to complement the detailed information about $S_0 \sim S_1$ mixing obtained from SAC spectroscopy (see ii above). This is the first time dipole moments of electronically excited states could be measured with sufficient precision to sample nonadiabatic effects. (iv) TGS is a pulsed-cw version of SEP, which has been devised in order to measure total removal and state-to-state rotational energy transfer (RET) rates in S_1 H_2CO under "single-collision" conditions. The observed rates follow dipole propensity rules with total removal rates ~10 times faster than gas kinetic. Even more important than the rate measurements is demonstration of the feasibility of a pulsed-SEP, cw-probe scheme (transient absorption polarization spectroscopy, TAPS) which we plan to use to measure rotationally state-specific depopulation rates for vibrationally highly excited S_0 molecules.

The unique feature of this research program is that high resolution spectroscopy is being used to obtain an unusually complete picture of molecular structure at high levels of vibrational excitation in order to pose, at the single eigenstate level, precise and fundamental questions about dynamical processes that occur at chemically interesting levels of internal excitation.

1. D. E. Reisner, R. W. Field, J. L. Kinsey and H.-L. Dai, J. Chem. Phys. 80, 5968 (1984).
2. H.-L. Dai, C. L. Korpa, J. L. Kinsey and R. W. Field, J. Chem. Phys. (in press).
3. H.-L. Dai, R. W. Field and J. L. Kinsey, J. Chem. Phys. (in press).

Figure Captions:

Figure 1. Stark Quantum Beat Spectroscopy on H_2CO and D_2CO. The SQB experiment utilizes one Nd:YAG pumped dye laser to produce the decay curves (each recorded at a different electric field strength) shown on the top segment. The laser is polarized perpendicular to the E-field direction, resulting in beats between the $M_J=0$ and 2 components of the $J_{K_aK_c}=2_{1,1}$ level. The QB frequency is plotted vs. field strength in the lower left segment, which illustrates that each frequency is fit to better than $10kH_z$ out of ~40MHz.

Figure 2. Rotational Energy Transfer in the H_2CO S_1 State by Transient Gain Spectroscopy. The level diagrams for total depopulation of $13_{2,12}$ and state-to-state $12_{2,11}\rightarrow 13_{2,12}$ rate measurements are respectively at the top and bottom left. A Nd:YAG pumped dye laser populates the initial level and a cw, single mode Ar^+ laser monitors the target level population in real time for ~1μs. Upon transmission through the 1 meter sample cell, the probe beam is amplified by the optically or collisionally produced population inversion. Typical decay curves for the TGS signal are shown at the top and bottom right. The middle segment is a Stern-Vollmer plot of the more than 10 times gas kinetic total removal rate ($107MH_z$/Torr) from $13_{2,12}$ vs. pressure.

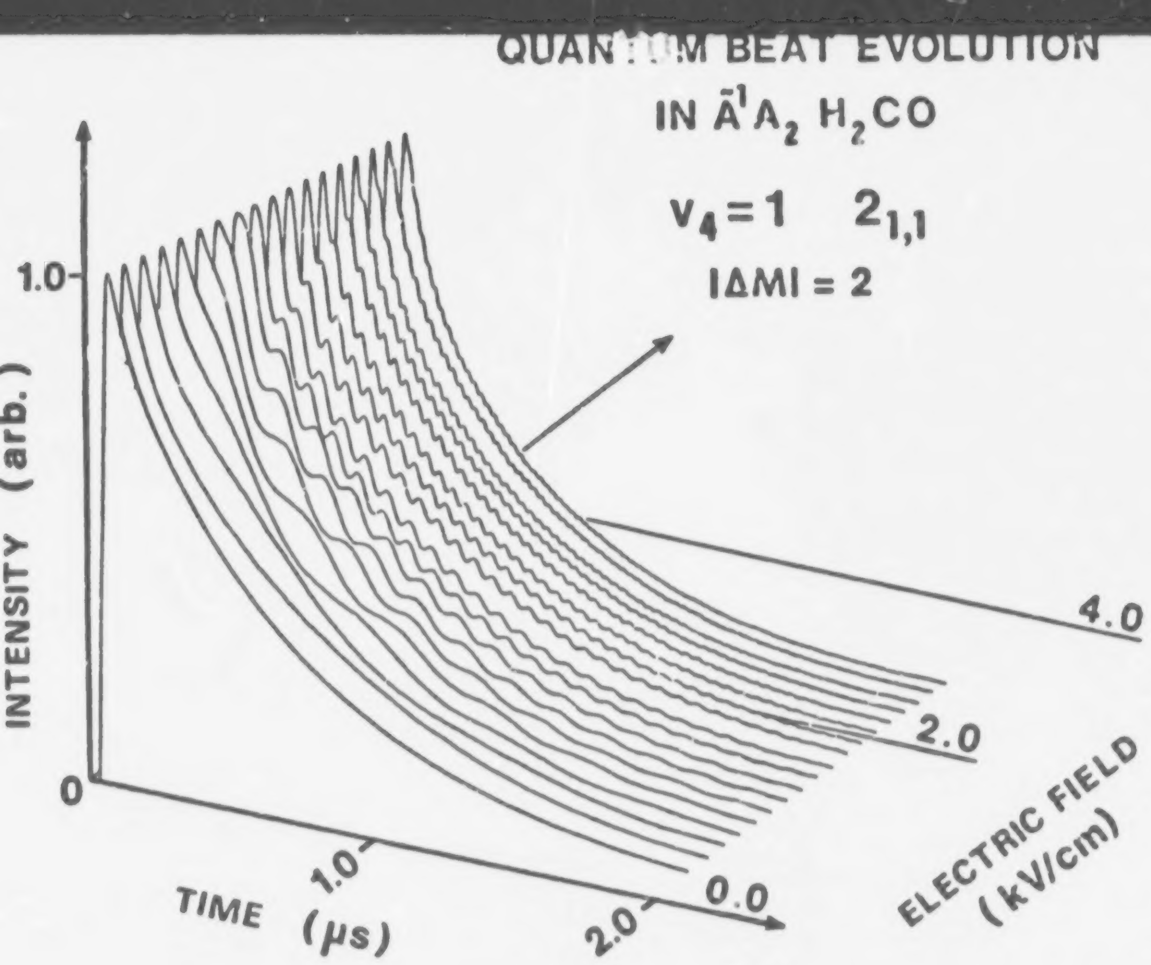
QUANTUM BEAT EVOLUTION
IN $\tilde{A}^1A_2$ H_2CO
$v_4 = 1$ $2_{1,1}$
$|\Delta M| = 2$
INTENSITY (arb.)
1.0
0
TIME (µs)
1.0
2.0
0.0
2.0
4.0
ELECTRIC FIELD (kV/cm)

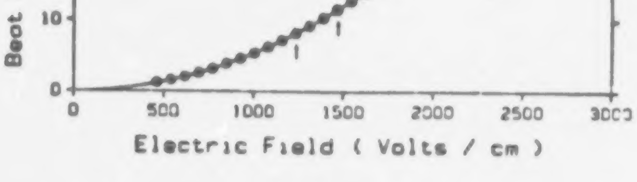
H_2CO $\tilde{A}^1A_2$ $v_4=1$ $2_{1,1}$
(|M|=2) - (|M|=0)
Beat Frequency (MHz)
Electric Field (Volts / cm)
0
10
20
30
40
50
500
1000
1500
2000
2500
3000

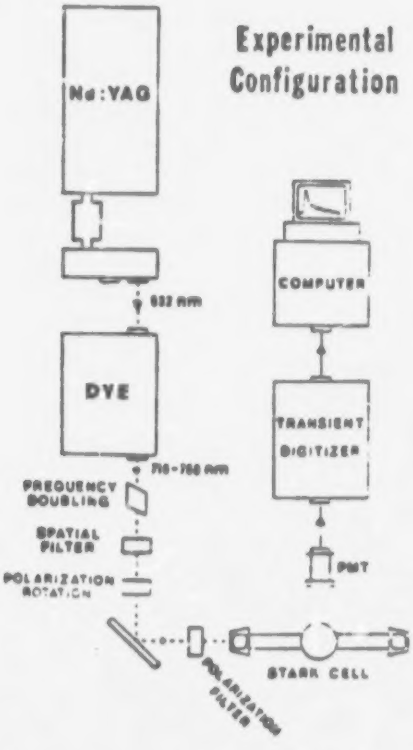
Experimental Configuration
Nd:YAG
532 nm
DYE
710-750 nm
FREQUENCY DOUBLING
SPATIAL FILTER
POLARIZATION ROTATION
POLARIZATION FILTER
STARK CELL
COMPUTER
TRANSIENT DIGITIZER
PMT

FIGURE 1.

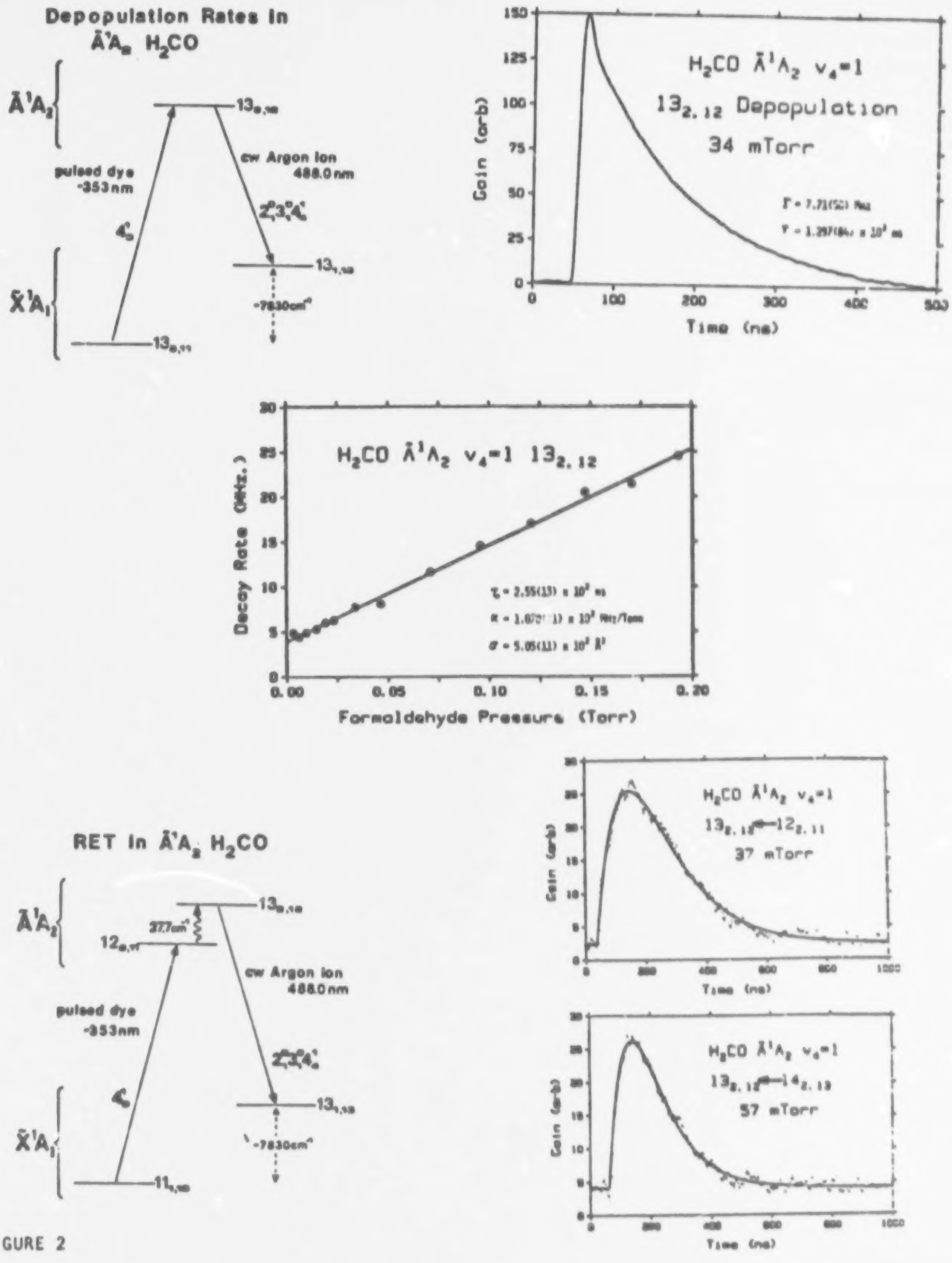
Depopulation Rates in Ã¹A₂ H₂CO
Ã¹A₂
13₂,₁₂
pulsed dye ~353nm
4⁰₀
cw Argon Ion 488.0 nm
2⁰₁3⁰₁4¹₀
13₁,₁₃
~7830cm⁻¹
X̃¹A₁
13₂,₁₁
H₂CO Ã¹A₂ v₄=1
13₂,₁₂ Depopulation
34 mTorr
Γ = 7.71(52) MHz
τ = 1.297(84) x 10² ns
Gain (arb)
0
25
50
75
100
125
150
Time (ns)
0
100
200
300
400
500
H₂CO Ã¹A₂ v₄=1 13₂,₁₂
τ₀ = 2.55(13) x 10² ns
k = 1.07?(?1) x 10² MHz/Torr
σ = 5.05(11) x 10¹ Å²
Decay Rate (MHz.)
0
5
10
15
20
25
30
Formaldehyde Pressure (Torr)
0.00
0.05
0.10
0.15
0.20
RET in Ã¹A₂ H₂CO
Ã¹A₂
13₂,₁₂
27.7cm⁻¹
12₂,₁₁
cw Argon Ion 488.0 nm
pulsed dye ~353nm
4⁰₀
2⁰₁3⁰₁4¹₀
13₁,₁₃
~7830cm⁻¹
X̃¹A₁
11₁,₁₀
H₂CO Ã¹A₂ v₄=1
13₂,₁₂←12₂,₁₁
37 mTorr
Gain (arb)
0
5
10
15
20
25
30
Time (ns)
0
200
400
600
800
1000
H₂CO Ã¹A₂ v₄=1
13₂,₁₂←14₂,₁₃
57 mTorr
Gain (arb)
0
5
10
15
20
25
30
Time (ns)
0
200
400
600
800
1000

FIGURE 2

Spectroscopic Studies of the Products of the Reactions of Electronically Excited Atoms and Small Molecules

Michael F. Golde
Department of Chemistry
University of Pittsburgh

Although many rate constants have been measured for the reactions of electronically-excited atoms and diatomic molecules with small molecules, much less is known concerning the products of these reactions. Such information is relevant to atmospheric chemistry and to laser systems, and is of fundamental importance to a full understanding of the mechanisms of energy transfer processes.

In our program, products of the reactions of excited metastable states of Ar, Kr, Xe, $N_2(A^3\Sigma_u^+)$ and $CO(a^3\Pi)$ in discharge-flow systems are detected by emission spectroscopy, saturation ion-current measurements (for ionization channels) and atomic resonance and laser-induced fluorescence (for dissociation channels). The specific aim of the project is the measurement of absolute branching fractions for the major reaction pathways of a given reaction.

Figure 1 shows the apparatus used, most recently in the studies of $N_2(A)$, for emission and resonance fluorescence measurements. The products of the weak dc discharge through N_2/Ar mixtures have been characterized; small concentrations of $N(^2D)$ and $N_2(a^1\Pi_g, a'^1\Sigma_u^-)$, approximately 5% of that of $N_2(A)$, can be readily removed by addition of D_2 directly downstream of the discharge. The same port is used for addition of CF_3H, which has been found to induce complete relaxation of the nascent vibrational distribution in $N_2(A, v = 0 \text{ to } > 3)$, without causing detectable electronic quenching.

Using these techniques, we have shown that, for several reagents, quenching rate constants and/or reaction pathways vary significantly with vibrational quantum number, v, in $N_2(A)$. Figure 2 shows the effect of CF_3H addition on H-atom and O-atom resonance fluorescence intensities in the reactions of $N_2(A)$ with respectively CH_3OH and O_2. In both cases, the large depletion of the signal in the presence of CF_3H at very low reagent concentrations shows that the rate constant for the observed channel increases with v. For O_2, but not for CH_3OH, a significant effect remains at high reagent concentration, indicating an increase in branching fraction for O-atom production with v in the O_2 reaction. It is concluded that an appreciable fraction of the reaction of $N_2(A, v=0)$ results in non-dissociative energy transfer to O_2, this fraction decreasing with increasing v. Comparable results have been obtained for the much-studied reaction of $N_2(A)$ with NO, showing for the first time that excitation of the $NO(A^2\Sigma^+)$ state is not the sole reaction pathway for vibrationally excited $N_2(A)$.

These results are crucial for the determination of reliable absolute branching fractions in the reactions of $N_2(A)$. The rapid reaction with NH_3 shows promise as a primary reference; dissociation to $NH_2 + H$ appears to be the dominant channel. Experiments employing emission and resonance fluorescence spectroscopy are being extended to other fast or medium-fast quenchers, such as N_2O, SO_2, C_2H_4 and HCl, as well as to species which quench $N_2(A, v = 0)$ very slowly ($k \sim 10^{-14}$ cm^3 s^{-1}), such as CH_4, H_2, H_2O, CO_2 and C_2H_6.

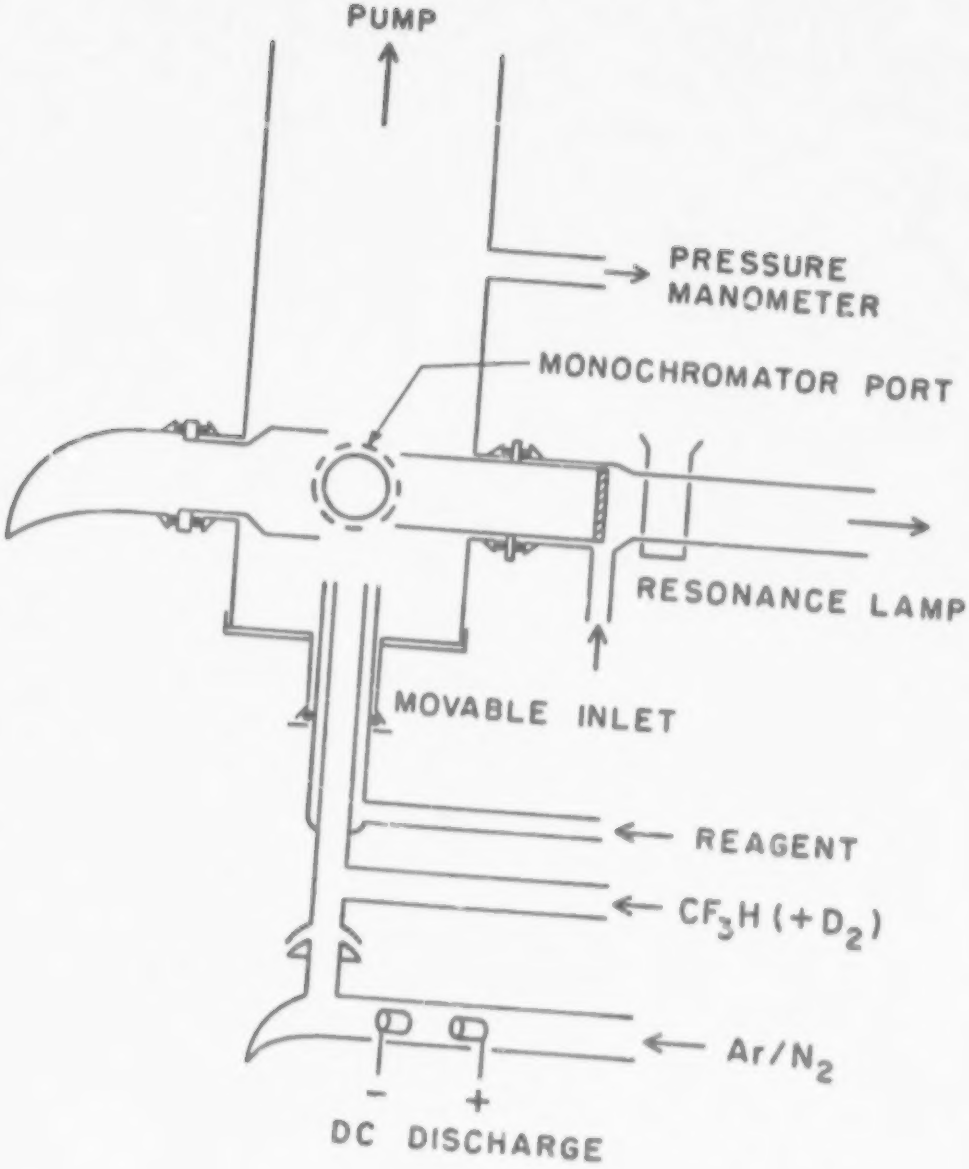
PUMP
PRESSURE MANOMETER
MONOCHROMATOR PORT
RESONANCE LAMP
MOVABLE INLET
REAGENT
$CF_3H\ (+D_2)$
Ar/N_2
−
+
DC DISCHARGE

Figure 1. Experimental apparatus used for emission and resonance fluorescence measurements.

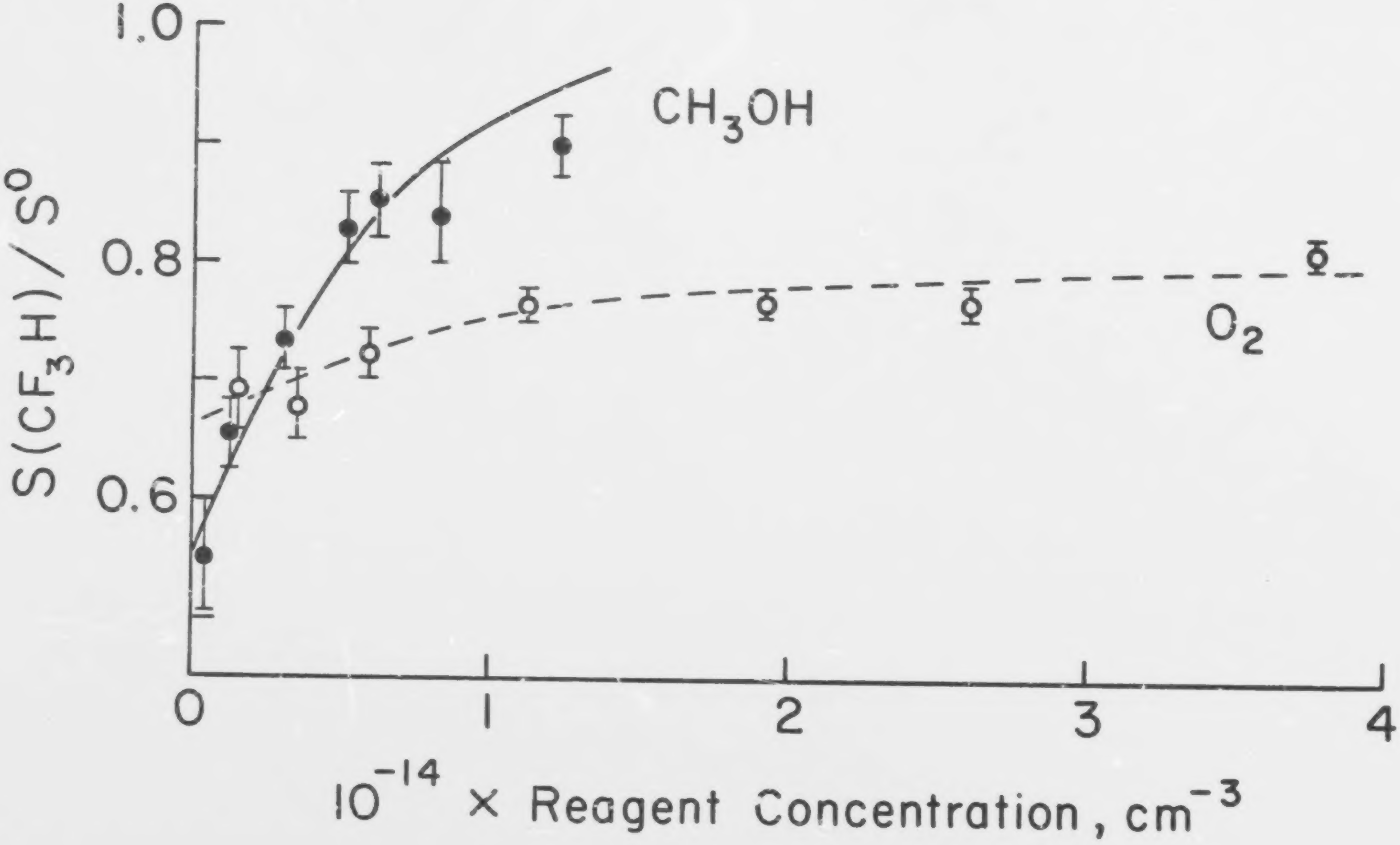

Figure 2. The effect of CF_3H addition on H- and O-atom yields in the reactions of $N_2(A)$ with respectively CH_3OH and O_2.

LASER-INDUCED KINETICS: ABSOLUTE RATE CONSTANTS FOR RADICAL METATHESIS AND RECOMBINATION REACTIONS

N. Selamoglu, M. J. Rossi, and D. M. Golden
Department of Chemical Kinetics
SRI International, Menlo Park, CA 94025

Abstract

The reaction system (1) was reinvestigated as the temperature of the

$$\dot{C}F_3 + Br_2 \xrightarrow{k_1} CF_3Br + \dot{B}r \qquad (1)$$

$$\dot{C}F_3 + \dot{C}F_3 \xrightarrow{k_2} C_2F_6 \qquad (2)$$

the VLPΦ reactor was varied. It turned out that under our present reaction conditions, the recombination reaction (2) was competitive with reaction (1). k_2 was measured to be 5×10^{-12} cm^3 $molecule^{-1}$ s^{-1} under our experimental conditions. We noted a strong influence of the reaction vessel wall conditions on the CF_3Br product yields. The latter may arise from k_1 being dependent on surface conditions, or surface absorption of the product. The interplay between homogeneous and heterogeneous processes was a strong function of the wall temperature.

The absolute rate constant for the metathesis reaction of $\dot{C}H_3$ with Cl_2 and Br_2 (reactions 3 and 4) will be reported:

$$\dot{C}H_3 + Cl_2 \xrightarrow{k_3} CH_3Cl + \dot{C}l \qquad (3)$$

$$\dot{C}H_3 + Br_2 \xrightarrow{k_4} CH_3Br + \dot{B}r \qquad (4)$$

Analogous to reaction (1), it was found that $\dot{C}H_3$ recombination competed effectively with reaction (3) and reaction (4), even at the highest halogen concentrations used, so that the rates of reactions (3) and (4) had to be studied relative to methyl recombination, reaction (5), whose absolute rate

$$\dot{C}H_3 + \dot{C}H_3 \xrightarrow{k_5} C_2H_6 \qquad (5)$$

constant was measured in our VLPΦ system. Reactions (3) and (4) were recently studied by Kovalenko and Leone by a different technique. Their rate constant for (3) agreed very well with our result, whereas we obtained a rate constant

lower by a factor of five for reaction (4). We also will report on results for reactions (3) and (4) at higher and lower temperature than ambient.

Finally, we will report on the absolute rate constant for a benzyl radical (reaction 6), whose recombination kinetics is not well known in the gas phase. Benzyl radical recombination is a proto-typical radical-radical reaction whose absolute rate constant in the gas phase is missing from a catalog of reactions of stabilized polyatomic radicals. By the same token, the metathesis reaction rate constants of reactions (7) and (8),

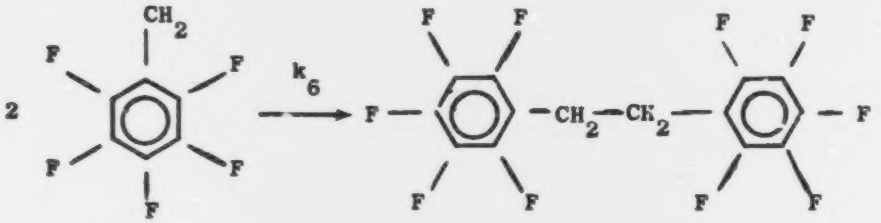
2
CH2
F
F
F
F
F
k6
F
F
F
F
F
CH2
CH2
F
F
F
F
F

(6)

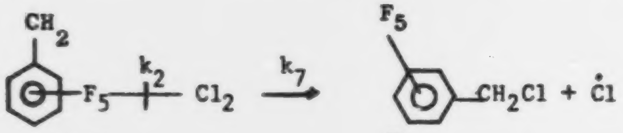
CH2
F5
k2
Cl2
k7
F5
CH2Cl + Ċl

(7)

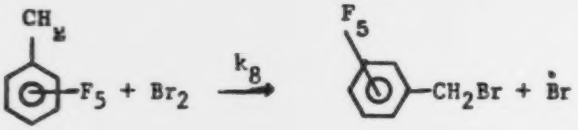
CH2
F5 + Br2
k8
F5
CH2Br + Ḃr

(8)

as well as their temperature dependence will be discussed and compared to the analogous reactions involving $\dot{C}H_3$ (reactions 3 and 4).

THEORETICAL STUDIES OF DISSOCIATIVE RECOMBINATION

STEVEN L. GUBERMAN
Smithsonian Astrophysical Observatory
Cambridge, MA 02138

The dissociative recombination (DR) of the molecular ion, O_2^+, with an electron is described by

$$O_2^+ + e^- \rightarrow O + O .$$

In this work, ab initio methods are being developed and applied to the study of the DR of important atmospheric ions. In particular, the dependence of the total DR cross sections, rate constants, and product atomic state quantum yields upon electron temperature and ion vibrational temperature are being determined. Since it is often difficult to determine experimentally the precise molecular ion vibrational distribution and the electronic states of the product atoms or molecules, a theoretical approach offers unique advantages for understanding the mechanism of DR.

The DR cross sections are directly proportional to an electronic width given by Fermi's golden rule. In this study, a technique has been developed which allows for the calculation of free electron capture widths by using Rydberg orbitals with high principal quantum numbers. It can be shown that the Rydberg widths converge rapidly with increasing principal quantum number to the free electron capture width. The configuration interaction (CI) wave functions for the reactants and products are determined by using matrix partitioning techniques to develop a matrix optical potential for the reactants. The incoming channel wave functions are allowed to distort in a potential that includes the dissociative channels. Calculations on the repulsive $^2\Pi$ states, important in the DR of NO^+, give matrix elements that are within about 10% of the experimentally derived values.[1]

Results for the application of these techniques to the DR of O_2^+ leading to the aeronomically important $O(^1S)$, the upper state of the green line at 5577A, are shown in Fig.s 1 and 2. The results have been determined by using first order CI wave functions generated from a large set of reference configurations.[2] The electronic widths are determined from scaled first order CI calculations in which the 2σ orbitals of O_2 are unexcited. The calculated width for the $^1\Sigma_u^+$ state of O_2, the major route for generation of $O(^1S)$ from the low vibrational levels of O_2^+ is .17eV. The cross sections and rate constants[3,4] are determined using vibrational harmonic oscillator wave functions and the delta function approximation for the nuclear part of the golden rule matrix element. The cross section rises near 0.2eV due to the large Franck-Condon factor which overwhelms the inverse electron energy dependence. The structure in the cross section above 0.2eV is due to autoionization via excited vibrational levels of the ion. At higher energies, the Franck-Condon factor leads to a rapid decrease in the cross section. The rate constant shown in Fig. 2 for a vibrational temperature of 300K increases with increasing electron temperature between about 700K and 17000K.

1. R. Gallusser and K. Dressler, J. Chem. Phys. 76, 4311(1982).
2. S. L. Guberman, Potential Energy Curves for Dissociative Recombination, in Physics of Ion-Ion and Electron-Ion Collisions, ed. by F. Bouillard and J. W. McGowan (Plenum, New York, 1983), p.167.
3. J. N. Bardsley, J. Phys. B 1, 349(1968).
4. A. Giusti, J. Phys. B 13, 3867(1980).

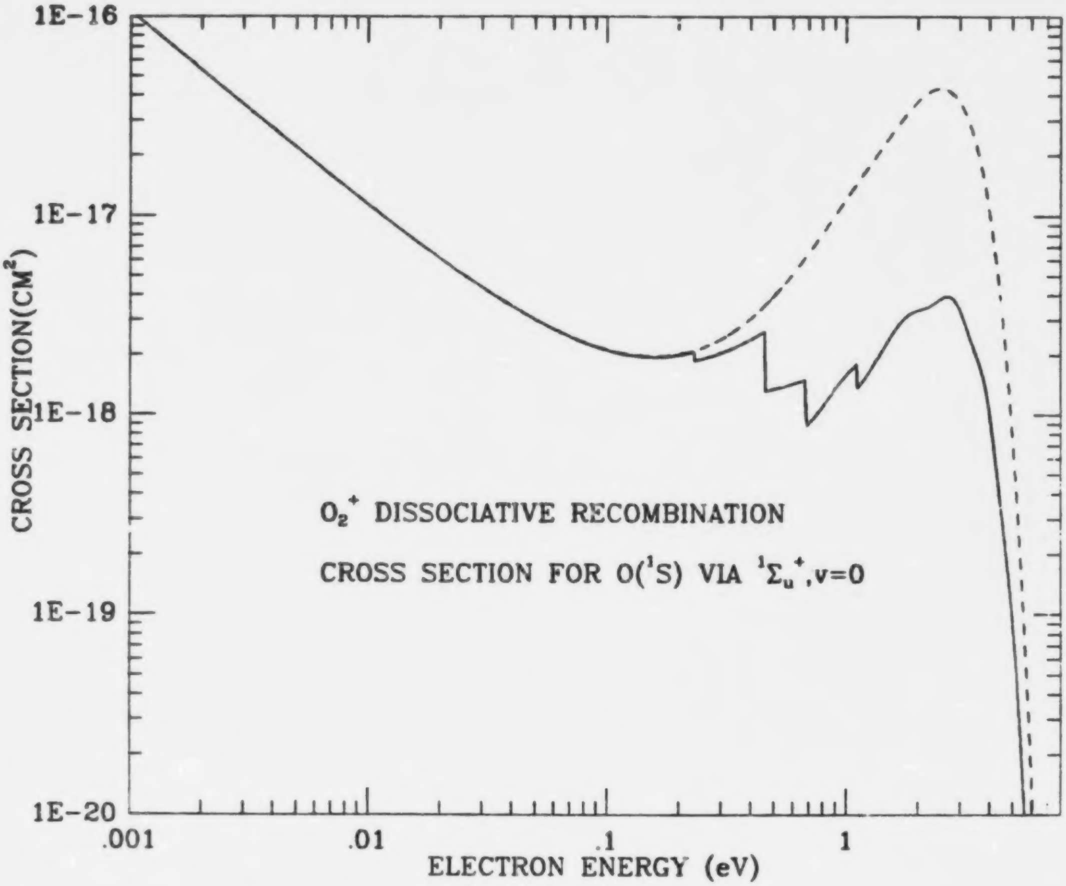

Figure 1. Cross section for dissociative recombination. The dotted line is the capture cross section, i.e. the cross section that results if autoionization is ignored. The solid line includes the effects of autoionization and shows structure due to autoionization back to excited ion vibrational levels. The lowest six vibrational levels of O_2^+ are included in the calculation. The neutral Rydberg resonances responsible for indirect recombination have not been included in the Figure.

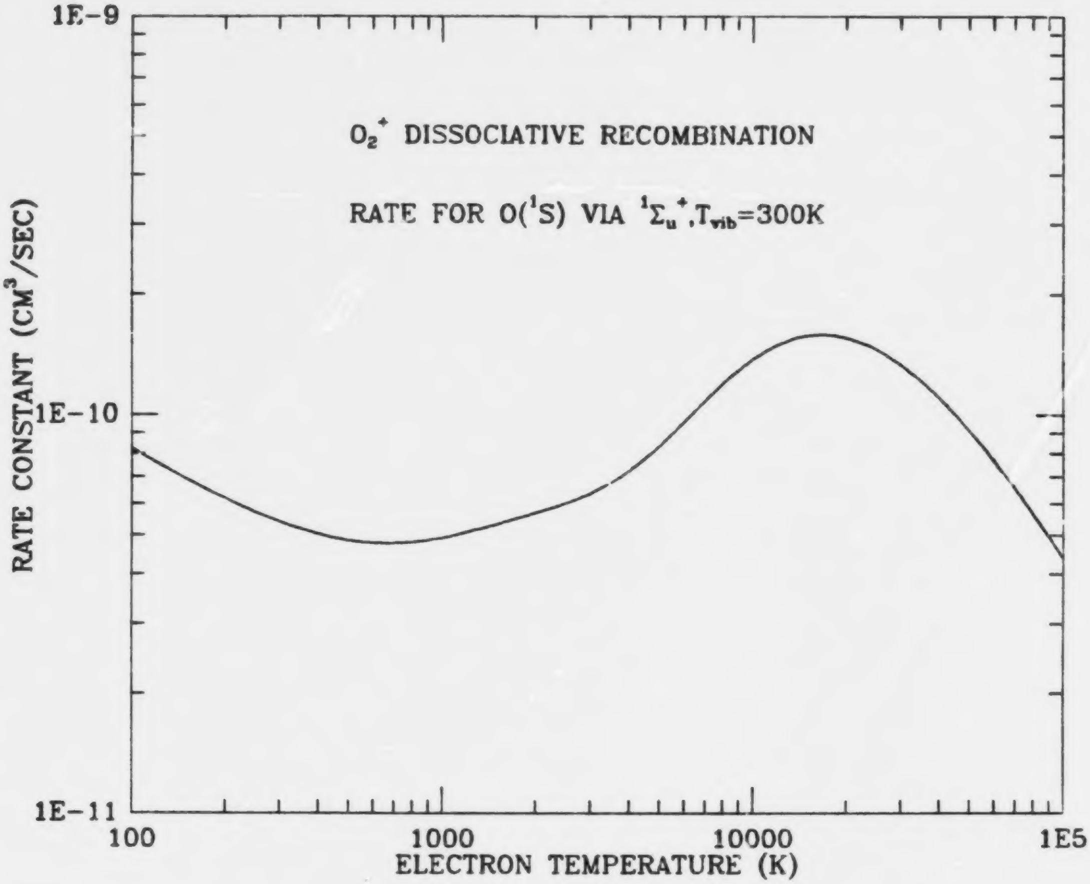

Figure 2. Rate constant for dissociative recombination at an ion vibrational temperature of 300K. The solid curve of Figure 1 was used for determining the rate.

MEASUREMENT OF RATE CONSTANTS OF ELEMENTARY GAS REACTIONS

F. Kaufman, Department of Chemistry, University of Pittsburgh
Pittsburgh, PA 15260

The direct measurement of single step, elementary rate processes of energy transfer and of radical-molecule or radical-radical reactions (a) is of crucial importance to our understanding of the nature of inelastic and reactive molecular interactions, to guidance of theoretical work, and to extension to other, as yet uninvestigated, processes; and (b) finds immediate application in the modeling of high power chemical lasers, of atmospheric processes at all altitudes, and of combustion phenomena of all types. These elementary steps are the building blocks of all gas phase reactions and their characterization ought to carry the highest research priority.

The experimental approach is shown in Figures 1a and 1b, the former for vibrational energy transfer studies in hydrogen halides by infrared chemiluminescence and the latter for radical reaction studies in a highly instrumented flow reactor (discharge flow, DF) apparatus. Vibrational energy transfer rate constants are obtained (Figure 1a) by recording the IR emission spectra of, say, HCl, HF, or DF due to a fast generating reaction, e.g. $H + F_2 \rightarrow HF(v) + F$, in the absence and presence of various concentrations of added (unreactive) quencher gases, inverting the spectra to yield HF(v) concentrations, and analyzing the data in terms of a $\Delta v = -1$ stepladder model. In this manner, about 200 relaxation rate constants have been measured[1-7] for HCl, HF, and DF.

The versatile flow reactor apparatus (Figure 1b) uses laser IR multiphoton dissociation (LIRMPD) to generate radicals at the upstream end of the flow tube and makes use of three methods, viz. laser-induced fluorescence (LIF), vacuum u.v. resonance fluorescence (VUVRF), and molecular beam inlet mass spectrometry (MS) for their detection following their reaction with other species added through a movable injector tube.[8] The reaction region is temperature controlled from about 200 to 500 K. Both systems are uniquely versatile and highly productive.

During the last year, we have studied the $CH_3O + NO_2$ reaction from 220 to 473 K using LIF and MS detection. CH_3 radicals were produced by LIRMPD and converted to CH_3O by their fast reaction with excess NO_2. Figures 2a and 2b show typical pseudo-first-order decays of CH_3O, k^I, due to $CH_3O + NO_2$ and k^I vs. $[NO_2]$ plots whose slopes are the second-order rate constants.

The overall reaction has two exothermic product channels: $CH_3O + NO_2 + M \xrightarrow{1a} CH_3ONO_2 + M$, $\Delta H^o_{298} = -40$ kcal mol^{-1} and $CH_3O + NO_2 \xrightarrow{1b} H_2CO + HNO_2$, $\Delta H^o_{298} = -56$ kcal mol^{-1}. k_{1a} and k_{1b} are expected to exhibit different P- and T-dependences, especially near the low pressure limit of 1a. This is shown in Figure 2b where the P-dependence becomes weaker with increasing T showing the rising importance of the disproportionation channel, 1b. Fitting the data to $k_{1a} = C(T/300)^n$ at low pressure, $k_{1b} = A \exp(-E/RT)$, and allowing for a Lindemann P-dependence of k_{1a} over the small experimental P-range, the following expressions were obtained, albeit with large uncertainty limits:

$$k_{1a}^{0} = 2.6 \times 10^{-29}\ (T/300)^{-4.5}\ \mathrm{cm^6\ s^{-1}}$$

$$k_{1b} = 9.6 \times 10^{-12}\ \exp(-2.3\ \mathrm{kcal\ mol^{-1}}/RT)\ \mathrm{cm^3\ s^{-1}}$$

These rate parameters are reasonable for the two types of reactions and predict branching ratios in poor to excellent agreement with several indirect, published results.

1. B. M. Berquist, J. W. Bozzelli, L. S. Dzelzkalns, L. G. Piper, and F. Kaufman, J. Chem. Phys. 76, 2972 (1982)
2. B. M. Berquist, L. S. Dzelzkalns, and F. Kaufman, J. Chem. Phys. 76, 2984 (1982).
3. L. S. Dzelzkalns and F. Kaufman, J. Chem. Phys. 77, 3508.
4. L. S. Dzelzkalns and F. Kaufman, J. Chem. Phys. 79, 3836 (1983).
5. L. S. Dzelzkalns and F. Kaufman, J. Chem. Phys. 79, 3363 (1983).
6. L. S. Dzelzkalns and F. Kaufman, J. Chem. Phys. 80, 6114 (1984).
7. L. S. Dzelzkalns and F. Kaufman, J. Chem. Phys., in press.
8. J. B. Jeffries, J. A. McCaulley, and F. Kaufman, Chem. Phys. Lett. 106, 111 (1984).

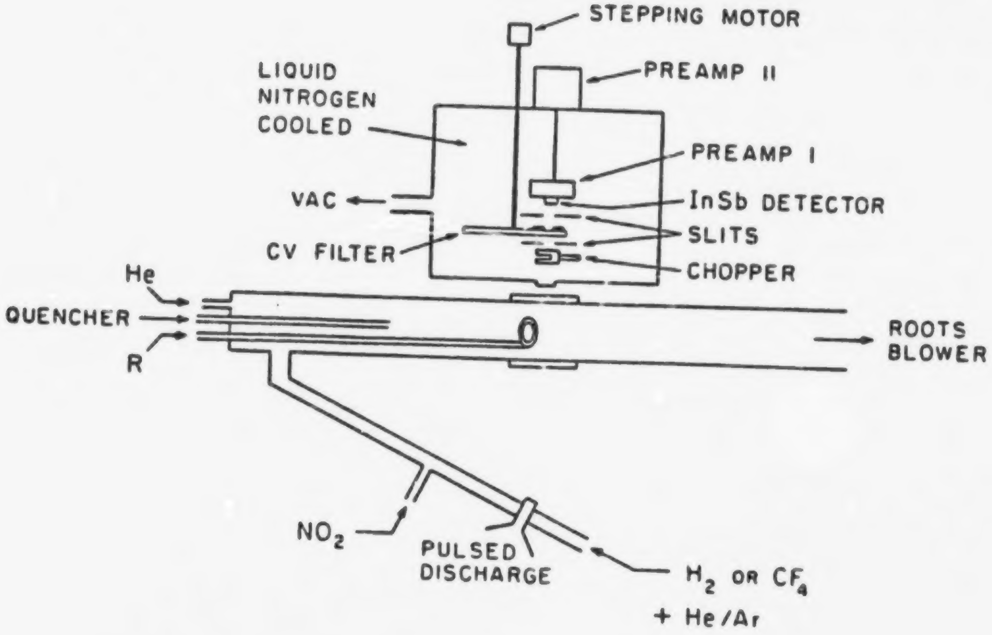

STEPPING MOTOR
LIQUID NITROGEN COOLED
PREAMP II
PREAMP I
VAC
InSb DETECTOR
SLITS
CV FILTER
CHOPPER
He
QUENCHER
R
ROOTS BLOWER
NO2
PULSED DISCHARGE
H2 OR CF4 + He/Ar

FIGURE 1a. Infrared Chemiluminescence Apparatus.

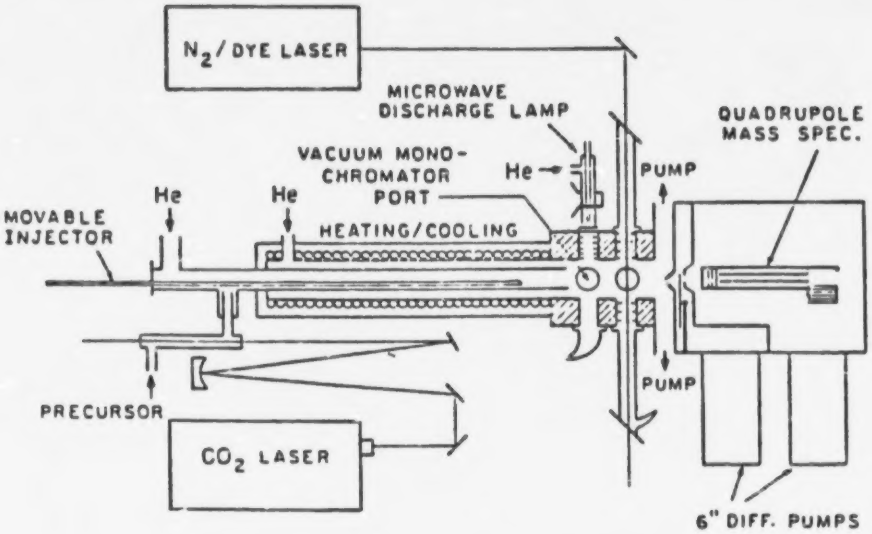

N_2/DYE LASER
MICROWAVE DISCHARGE LAMP
QUADRUPOLE MASS SPEC.
VACUUM MONO-CHROMATOR PORT
He
He
He
PUMP
MOVABLE INJECTOR
HEATING/COOLING
PUMP
PRECURSOR
CO_2 LASER
6" DIFF. PUMPS

FIGURE 1b. Flow Reactor Apparatus

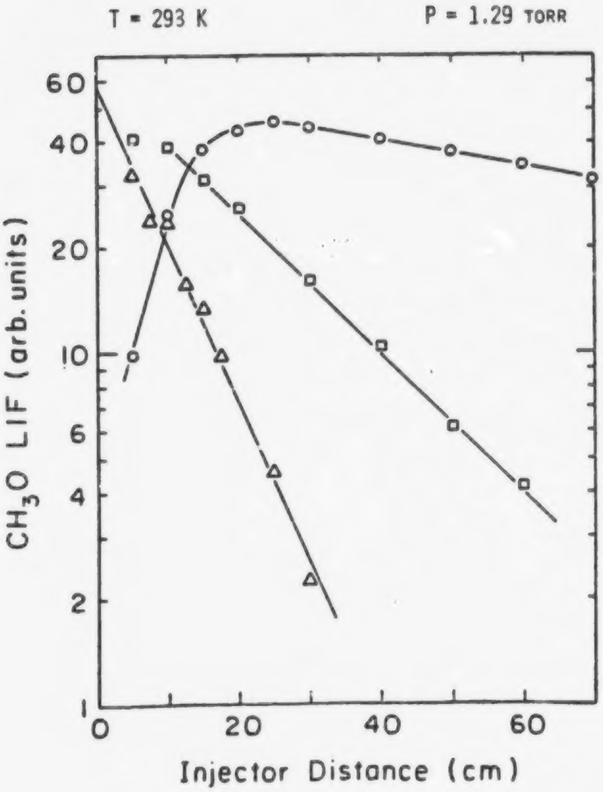

FIGURE 2a. Semilog Decay Plots of [CH_3O] vs. Injector Distance.
○-[NO_2] = 4.8×10^{12} cm^{-3}; □-[NO_2] = 4.8×10^{13} cm^{-3}; Δ-[NO_2] = 1.14×10^{14} cm^{-3}.

BEST COPY AVAILABLE

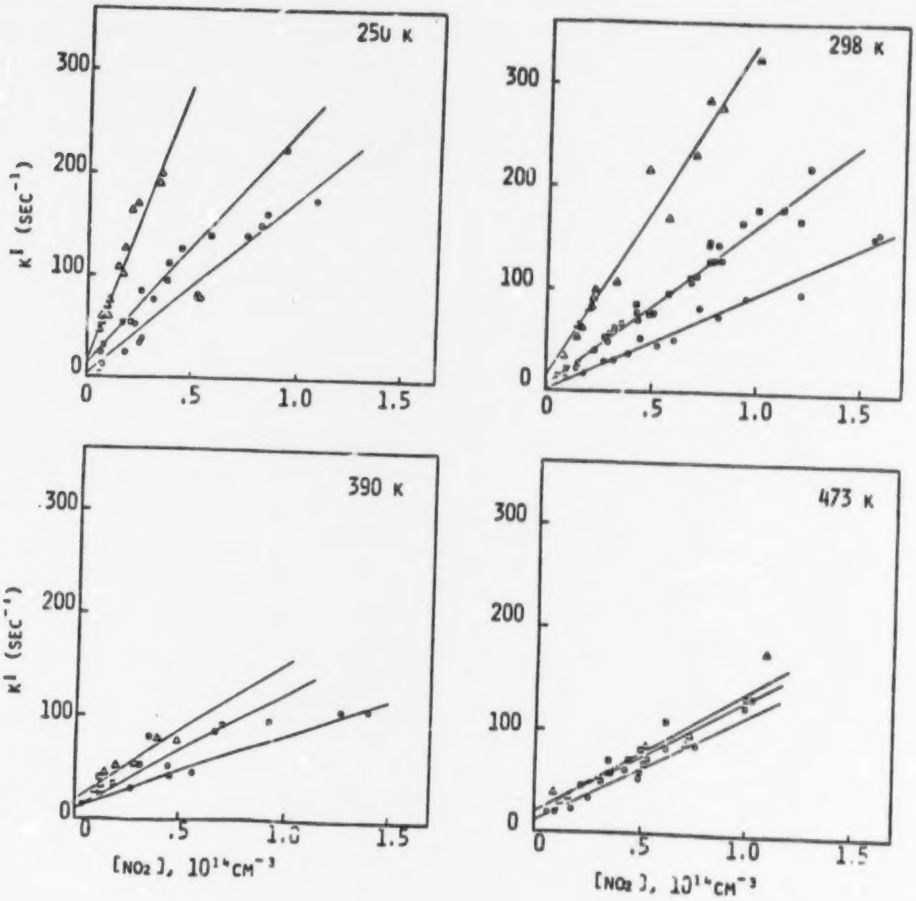

FIGURE 2b. Plots of Pseudo-First-Order Rate Constants, k^I, vs. $[NO_2]$ as Function of p and T. o-p = 0.74 Torr; □-p = 1.29 Torr; Δ-p = 4.04 Torr.

INFRARED AND LASER STUDIES OF ION-MOLECULE REACTION DYNAMICS

Stephen R. Leone, Veronica M. Bierbaum, and G. Barney Ellison
Joint Institute for Laboratory Astrophysics
National Bureau of Standards and University of Colorado
and Department of Chemistry, University of Colorado
Boulder, Colorado 80309

The dynamics of thermal energy ion-molecule reactions are investigated by measuring vibrational and rotational state distributions in the products. The method involves optical detection by infrared chemiluminescence and laser-induced fluorescence in a flowing afterglow and in a single collision beam-type apparatus. The results are of interest with regard to the mechanisms for emitting species in normal and disturbed atmospheres, such as the Aurora Borealis.

Significant improvements have been made in the detection of the products of ion reactions by laser-induced fluorescence (Fig. 1). By generating the initial ions in a higher pressure region and expanding them through a 1 cm diameter orifice into the flow tube, a tremendous reduction in background light has been achieved. Thus the elementary charge transfer reaction $N^+ + CO$, which eluded precise measurements before, has now been studied in great detail. The population ratios produced in the CO^+ product v=0, 1, and 2 states is 77%, 21%, and 2%, respectively (Fig. 2). Even the very minor channel has been obtained accurately. The mechanism appears to be similar to a long range (Franck-Condon) electron transfer. The rate of deactivation of $CO^+(v=1)$ with N_2 has been obtained for the first time ($1.5 \pm 0.5 \times 10^{-10}$ cm^3 $molecule^{-1}$ sec^{-1}) in the course of this work.

The first measurements on $Ar^+ + CO$, which can produce CO^+ up to v=6, show predominant excitation in the v=5 and 6 levels, with a ratio for v=5/6 of 1.0/0.6. In the single collision beam apparatus, the rotational excitation in both v=5 and 6 is found to be ~800 K, indicative of an intimate collision mechanism for the charge transfer.

Recent interest in the $N^+ + O_2$ reaction as a possible source of $O(^1S)$ in the Aurora has prompted us to make further investigations of this reaction. By replacing the infrared detector with a photon counting system, a measurement of the yield of $O(^1S)$ is possible. Repeated determinations show that the $O(^1S)$ yield in the $N^+ + O_2$ reaction is less than 2% of the total product formation. This suggests that $N^+ + O_2$ is not a major contributor to $O(^1S)$ in the Aurora.

Wavelength-resolved infrared emission has been used to carry out a more exacting study of the $F^- + HBr$ reaction and new studies on the $F^- + DBr$ reaction. Both produce highly vibrationally excited HF(DF) products. It is found that earlier $F^- + HBr$ results were slightly relaxed; both ion reactions actually populate vibrational states with as much excitation as the coresponding neutral F + HBr (DBr) reactions. The results will be important because of the availability of new potential energy surfaces for these reactions (P. Rosmus), which should allow more refined calculations on the differences between the ion and neutral reactions. A preliminary investigation of the $SF_6^- + HBr$ reaction has shown evidence for infrared emission from the $FHBr^-$ bihalide species at ~2850 cm^{-1}. Further work is in progress to study this interesting species.

BEST COPY AVAILABLE

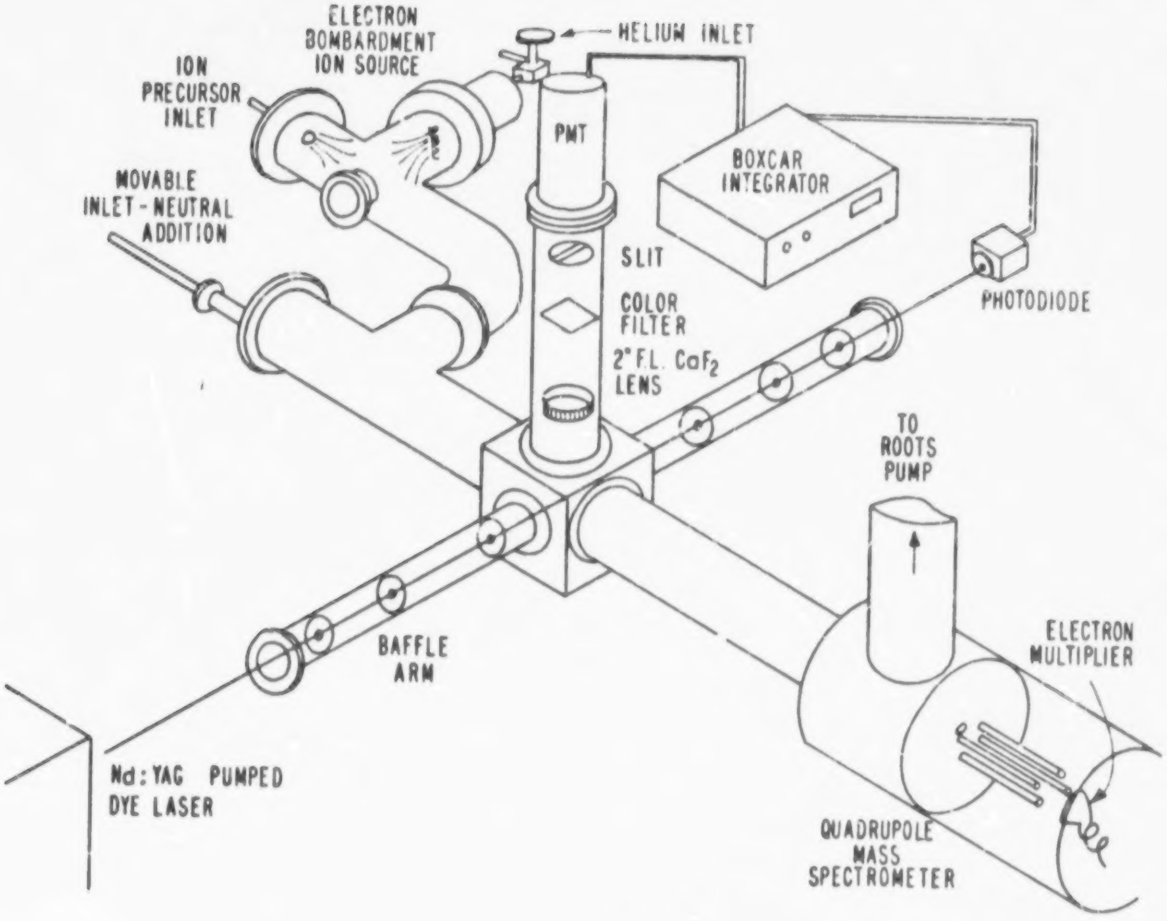
ELECTRON BOMBARDMENT ION SOURCE
HELIUM INLET
ION PRECURSOR INLET
PMT
BOXCAR INTEGRATOR
MOVABLE INLET-NEUTRAL ADDITION
SLIT
COLOR FILTER
2" F.L. CaF$_2$ LENS
PHOTODIODE
TO ROOTS PUMP
BAFFLE ARM
ELECTRON MULTIPLIER
Nd:YAG PUMPED DYE LASER
QUADRUPOLE MASS SPECTROMETER

Fig. 1. Experimental apparatus for high sensitivity detection of product states of ion reactions by laser-induced fluorescence.

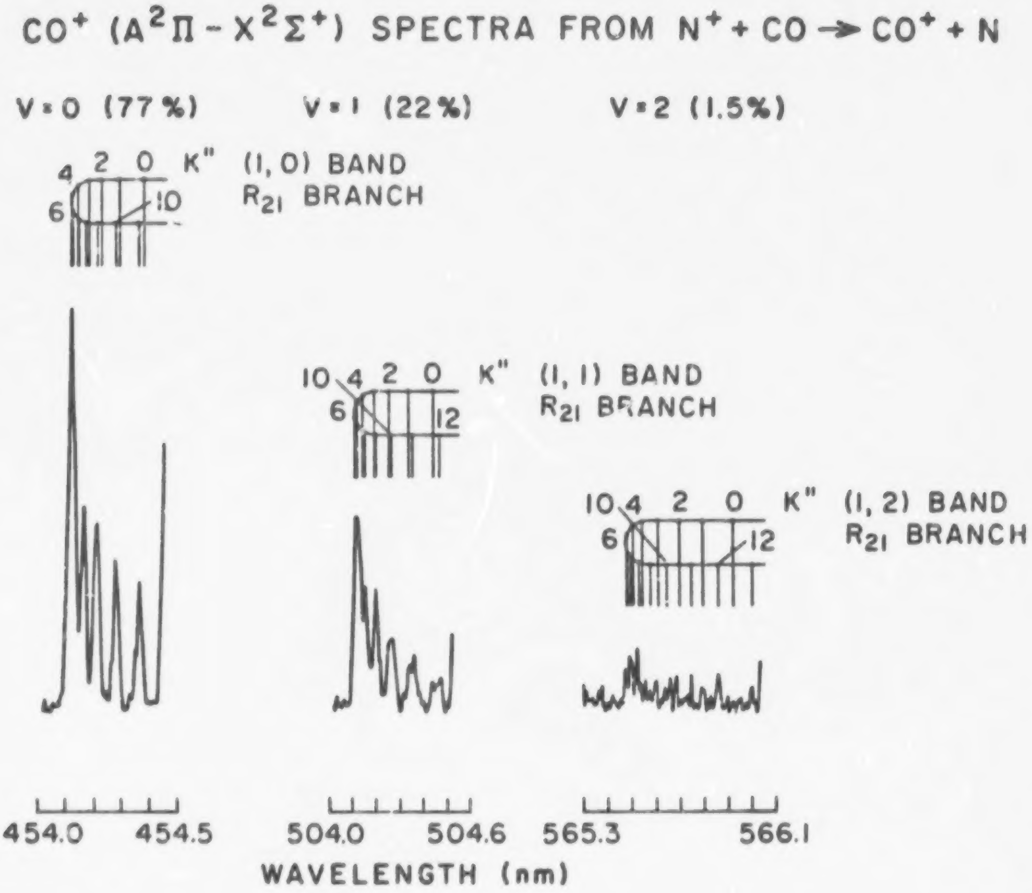

Fig. 2. Laser-induced fluorescence signals from CO^+ (v=0,1, and 2) produced by the thermal energy charge transfer reaction of N^+ with CO. Note the excellent signal-to-noise even on the minor (2%) v=2 channel.

A CHEMICALLY-DRIVEN VISIBLE TRANSITION ENERGY-TRANSFER LASER

AFOSR ISSA 84-11

R. C. Oldenborg and S. L. Baughcum
Chemistry Division
Los Alamos National Laboratory
Los Alamos, New Mexico 87545

The first electronic transition chemical laser to be driven solely by chemical energy was the oxygen-iodine chemical transfer laser. In this device, metastable $O_2(^1\Delta)$ is produced by purely chemical means and its energy is transferred to atomic iodine which then lases. We have identified a fully analogous scheme to produce a chemically-driven visible transition energy-transfer laser. Atoms of Group III metals Ga, In, and Tl react with selected fluorinating agents to produce long-lived excited $(a^3\Pi)$ diatomic metal fluorides,

$$M + RF \longrightarrow MF(a^3\Pi) + R$$

where M = Ga, In, Tl, and RF = F_2, NF_3, ClF_3, etc. These then can quickly transfer their energy to additional metal atoms by a nearly resonant process to produce excited (^2S) metal atoms.

$$MF(a^3\Pi) + M(^2P) \longrightarrow MF(X^1\Sigma^+) + M(^2S)$$

As amply demonstrated in previous photodissociation laser experiments, these metals can readily lase with only a partial population inversion (like iodine atoms) because the ^2P ground state is widely split, with the $^2P_{3/2}$ state having essentially no population even at moderate temperatures.

The objective of this project is to measure the rate parameters for the relevant reaction and energy transfer processes so that the potential for using this system as a visible transition chemical transfer laser can be critically evaluated. Our approach is to use excimer laser photolysis to dissociate organometallic compounds of the Group III metals in the presence of selected fluorinating agents. The time history of the metal atoms and the reaction and energy transfer products is followed using laser-induced fluorescence (LIF) and emission spectroscopy. The optical set-up for these experiments is shown in Fig. 1a. By varying the reactant and diluent pressures, the rate constants for the excitation reaction and subsequent energy transfer can be deduced.

Much of our initial effort has been devoted to the construction of the laser photolysis cell in which to conduct these experiments as shown in Fig. 1b. A new fluorine-compatible stainless-steel cell is now complete that allows various organometallic compounds to be injected through a variable length inlet and subsequently photolysed. All gas flows (organometallic, buffer, and reactant) into the cell are regulated by mass flow controllers. The cell has purged windows through which the photolysis and probe lasers can enter and exit, as well as fluorescence observation windows.

Several key experiments have been completed involving the photodissociation of trimethylgallium (TMGa). When mtorr quantities of TMGa in 25 torr argon are irradiated at 193 nm with fluences up to 100 mJ/cm^2, prompt emission is observed from the atomic Ga(5^2S) excited state. Two excimer laser photons are energetically required to produce the excited Ga atoms directly in the TMGa dissociation, and the intensity of this emission is found to have a quadratic dependence on the laser fluence. This experiment clearly shows that atomic Ga is quickly liberated in the TMGa photolysis.

The prompt emission decays under these conditions with a 50-ns lifetime after which the LIF technique is employed to assess the production of the ground-state Ga($4^2P_{1/2}$) atoms. The Ga(5^2S) state is excited at 403.3 nm using a Quanta-Ray Nd:YAG laser-pumped dye laser with wavelength extender and the resulting (5^2S-$4^2P_{3/2}$) fluorescence is monitored near 417.2 nm. The LIF intensity is directly proportional to the ground-state Ga($4^2P_{1/2}$) density present during the 10-ns duration of the dye laser pulse. By scanning the delay between the excimer laser photolysis and the dye laser probe, the time evolution of the atomic Ga can be monitored. A typical time scan is shown in Fig. 2a. A rapid rise from zero in the LIF intensity is seen when the photolysis laser fires, which is indicative of the instantaneous production of the Ga atoms. The small spike at this time is from the excited Ga(5^2S) produced directly in the photolysis. The LIF intensity and the corresponding Ga($4^2P_{1/2}$) density continue to rise for nearly a 100 µs, presumably due to cascading from excited Ga states (predominantly $4^2P_{3/2}$) produced in the photolysis. After that the Ga density remains fairly constant, limited only by diffusion out of the probe volume.

When some of the argon diluent is replaced by reactant gases, this time history changes and various reaction rates can be evaluated. Although the reaction rate of Ga atoms with F_2 is of particular interest, it can not yet be measured because the TMGa prereacts with the F_2. This will be studied in the future using a different precursor (e.g., $GaCl_3$). Other fluorides have been investigated and Fig. 2b shows the effect of CF_4 on the Ga atom time history. The CF_4 quickly deactivates the Ga($^2P_{3/2}$) to the ground-state $^2P_{1/2}$, and so the gradual rise has disappeared. A preliminary measurement of the rate constant for this deactivation process by CF_4 is 3×10^{-12} cc/molecule-s. At long times (>200 µs), the ground-state Ga atoms are removed, presumably by reaction with CF_4, with a rate constant of roughly 5×10^{-15} cc/molecule-s. It is obvious from these rates that CF_4 would make an excellent buffer gas in a chemical laser, since it readily deactivates the lower laser level without significantly perturbing the total Ga atom density. Future experiments will address the kinetics of other important processes.

LASER PHOTOLYSIS/LASER PHOTOLYSIS PROBE APPARATUS

(a) OPTICAL SCHEMATIC

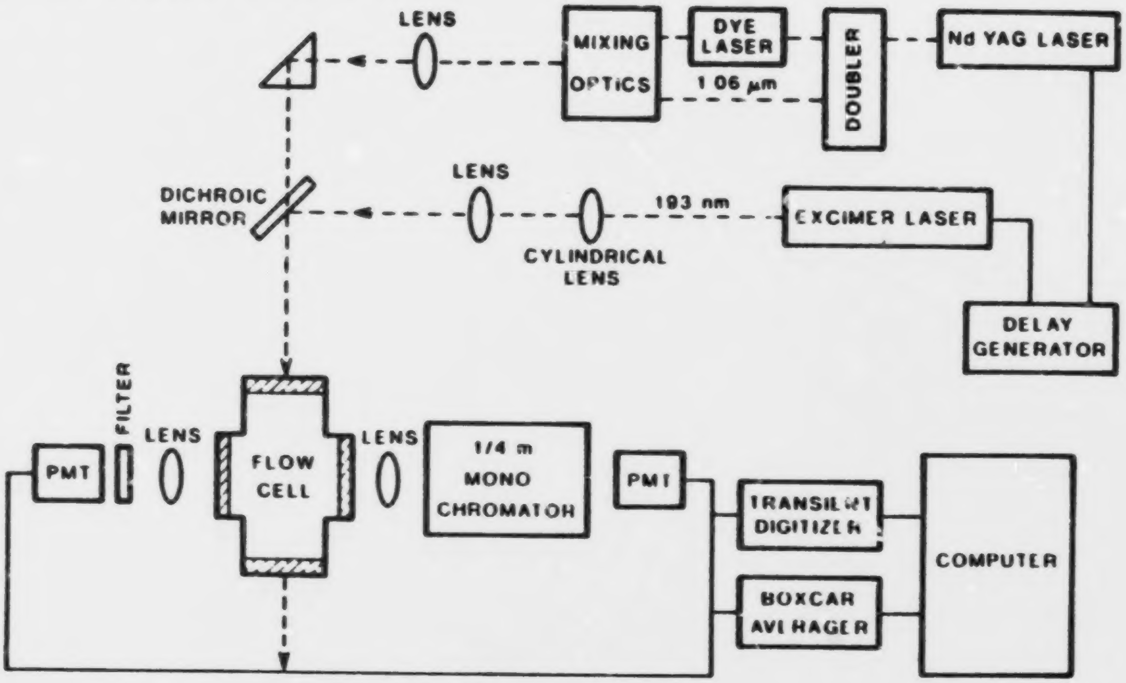
LENS
MIXING OPTICS
DYE LASER
1.06 µm
DOUBLER
Nd YAG LASER
DICHROIC MIRROR
LENS
193 nm
CYLINDRICAL LENS
EXCIMER LASER
DELAY GENERATOR
FILTER
PMT
LENS
FLOW CELL
LENS
1/4 m MONO CHROMATOR
PMT
TRANSIENT DIGITIZER
BOXCAR AVERAGER
COMPUTER

(b) FLOW SCHEMATIC

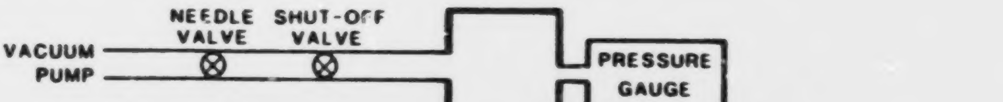
VACUUM PUMP
NEEDLE VALVE
SHUT-OFF VALVE
PRESSURE GAUGE
WINDOW PURGE
VARIABLE LENGTH INLET
MASS FLOW CONTROLLER
BUFFER
MASS FLOW CONTROLLER
REACTANT
PRECURSOR MIXTURE
MASS FLOW CONTROLLER

CHM - VG - 6322
Figure 1

TIME BEHAVIOR OF GROUND STATE GALLIUM (4 $^2P_{1/2}$) DENSITY AFTER 193 nm PHOTOLYSIS OF $Ga(CH_3)_3$

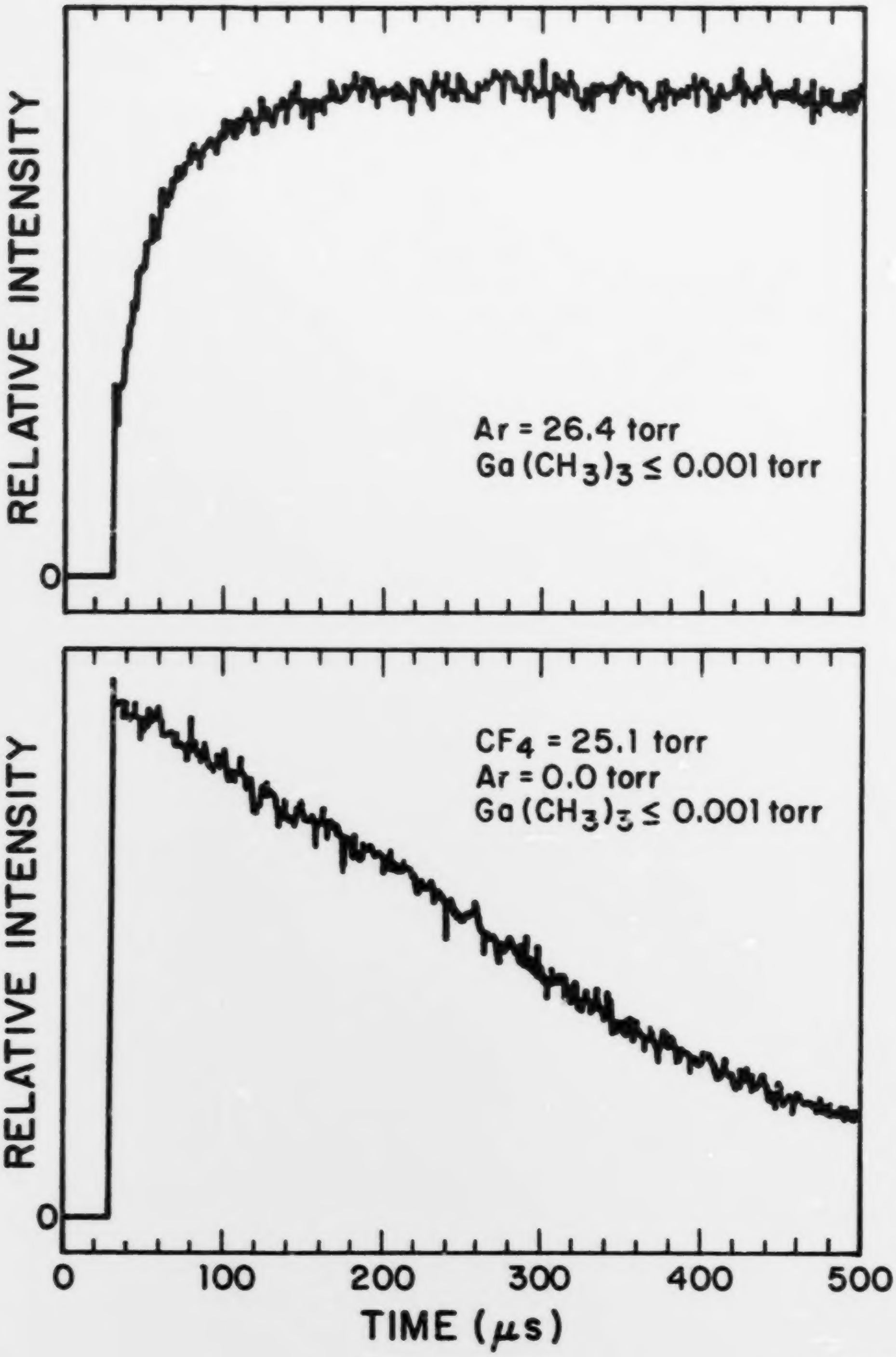

BEST COPY AVAILABLE

CHM-VG-6319
Figure 2

MOLECULAR DYNAMICS OF REACTIONS FORMING ELECTRONICALLY EXCITED PRODUCTS

J. C. Polanyi
Department of Chemistry, University of Toronto

The objective of this research is to improve our understanding, at a fundamental level, of chemical processes that lead to the formation of electronically excited atomic products. The work undertaken stresses simple systems for which reagent energies can be controlled and varied, and for which theory and experiment can be pursued concurrently and interactively.

(1) Experiments on the thermal reaction $F + Na_2 \rightarrow NaF + Na^*, Na^{**}, ...$, where Na^*, Na^{**}, .. symbolizes six electronically excited states, have been completed. Excited Na^*, Na^{**}, ..., formed at the crossing point of two partially-collimated beams, have been shown to be distributed in a non-statistical fashion over the observed energy-states. A report is in manuscript.

(a) Work is complete on a molecular beam apparatus for the study of the effect of increased collision energy on the product energy-distribution over electronically-excited states in the reaction $\overline{F} + Na_2 \rightarrow NaF + Na^*, Na^{**}, ..$ The atomic $\overline{F}$ comes from a heated seeded supersonic jet. Early experiments performed on this new apparatus show an orders-of-magnitude increase in the probability of forming the high electronic states of Na^* by way of the $F + Na_2$ reaction at ~ 0.5 eV collision energy.

(3) A third apparatus has now been completed, for the study of the effect of enhanced reagent vibrational excitation on the product energy distribution over electronically excited states in the reaction $F + Na_2^{\ddagger} \rightarrow NaF + Na^*$, Na^{**}, .. The source of our molecular beam of Na_2 (vibrationally excited, ground electronic-state Na_2) will be Na_2 excited by a CW laser from its ground electronic state, X, to its excited state, A, from which it fluoresces into high vibrational levels of X.

(4) This same apparatus is at present being used for a study of emission from a beam of NaI irradiated by 222 nm ultraviolet from an excimer laser. The objective of the experiment is to record 'free-to-bound emission' as the NaI^* is in the process of falling apart to give $Na^*(3^2P) + I$. This type of investigation falls under the heading of "transition state spectroscopy", a topic which is referred to once more under item (6) below.

(5) In a 'pulse' and 'probe' two-laser experiment performed in a cell, we have excited pure Br_2 gas at 0.01 - 1.0 Torr from its $X^1\Sigma_g^+$ ground state to its $B^3\Pi(0_u^+)$ excited state, Br_2^*, using 532 nm radiation. We have then probed the $Br^*(^2P_{1/2})$ and $Br(^2P_{3/2})$ photo-products, employing a tunable vacuum uv probe laser, as a function of Br_2 pressure. With increasing Br_2 pressure the ratio $[Br^*]/[Br]$ increases from 0.1 to > 10. We are now studying the kinetics of this change principally by varying the time delay between the pulse and the probe. The ratio $[Br^*]/[Br]$ is substantially enhanced by increased Br_2 pressure even for the time interval ($\Delta t \lesssim 20$ ns) during which no $Br_2 + Br_2$ collisions occur. This suggests that the concentration of $Br_2 -- Br_2$ dimers may be contributing to the formation of Br^* (e.g., $(Br_2)_2 + h\nu \rightarrow Br^* + Br_3$).

(6) We have completed a theoretical study of transition-state spectroscopy using the Monte Carlo trajectory method in 1D and also in 3D; the intermediate whose spectrum was computed was $H_3^\ddagger$ in the fundamental exchange reaction, $H + H_2 \rightarrow H_3^\ddagger \rightarrow H_2 + H$. During reaction $H_3^\ddagger \xrightarrow{h\nu} (H_3^\ddagger)^*$. The absorption spectrum is revealing of the reaction dynamics and points the way to a field which shows promise for the future.

(7) Theoretical studies of non-adiabatic reaction have been completed. Potential-energy surfaces have been varied systematically in Monte Carlo 'trajectory surface hopping' (TSH) studies, in order to illuminate various categories of reaction dynamics in reactions forming electronically-excited products. Two papers on this topic are in press.

1. Emission from Molecules and Reaction Intermediates in the Process of Falling Apart, H.-J. Foth, J.C. Polanyi and H.H. Telle, J. Phys. Chem. Vol. 86, 5027 (1982).

2. Collisional and Radiational Energy Transfer in the System $Na^*(3^2P) + Na_2(X^1\Sigma^+) \rightarrow Na(3^2S) + Na_2^*(A^1\Sigma^+)$, P. Arrowsmith, S.H.P. Bly, P.E. Charters, P. Chevrier, J.C. Polanyi and H.H. Telle, Chem. Phys. 79, 31 (1983).

3. Line Broadening in a Half-Collision, H.-J. Foth, J.C. Polanyi and H.H. Telle, Spectral Line Shapes, Vol. 2, 813 (1983).

4. Spectroscopy of Transition States in $H = H_2$ Reaction and NaI Photodissociation, H.-J. Foth, H.R. Mayne, R.A. Poirier, J.C. Polanyi and H.H. Telle, Laser Chem. 2, 229 (1983).

5 Spectroscopy of the Transition State (Theory). II. Absorption by $H_3^\ddagger$ in $H + H_2 \rightarrow H_3^\ddagger \rightarrow H_2 + H$, H.R. Mayne, R.A. Poirier and J.C. Polanyi, J. Chem. Phys. 80, 4025 (1984).

6. Spectroscopy of the Transition State (Theory). III. Absorption by $H_3^\ddagger$ in 3D Reactions, $H + H_2$, H.R. Mayne, J.C. Polanyi and N. Sathyamurthy, J. Phys. Chem. 88, 4064 (1984).

7 Dynamics of Non-Adiabatic Reactions (Theory). I. Branching Ratios for Early and Late Seams, H.R. Mayne, J.C. Polanyi and J.C. Tully, in press, J. Chem. Phys. (1984).

8. Dynamics of Non-Adiabatic Reactions (Theory). II. Product Vibrational Excitation, H.R. Mayne and J.C. Polanyi, in press, J. Chem. Phys. (1984).

9. Dynamics of Non-Adiabatic Reactions. II. $F + Na_2 \rightarrow NaF + Na^*$. P. Arrowsmith, S.H.P. Bly, P.E. Charters, P. Chevrier and J.C. Polanyi. To be published.

THEORETICAL METHODS FOR CHEMICAL PHYSICS

Herschel Rabitz
Department of Chemistry
Princeton, N.J. 08544

The research in this program aims to develop and apply new theoretical techniques for the analysis and understanding of chemical dynamics phenomena. The research is concerned with both macroscopic kinetic processes as well as microscopic atomic scale events. In keeping with this dual effort two particular avenues of research presently are being pursued with a summary given below.

I. The functional relationship between potential surfaces and scattering cross sections. The purpose of this work is to probe the interrelationship between the structure of potential surfaces and resultant laboratory-observable cross sections or kinetic processes. We have considered functional gradient techniques to elucidate this relationship. In particular, our initial work has focused on elastic scattering as a means for testing the concepts and establishing an understanding on how to interpret functional gradients. For example, the formal theory allows for the numerical calculation of the gradients $\delta\sigma(E)/\delta V(r)$ which gives a direct measure of how a variation in a potential surface at r will influence the total cross section at energy E. Even for the case of elastic scattering some intriguing results have been found. In particular for a system having a nominal repulsive potential, the functional gradient surface shows clear quantum oscillations and a surprising negative region. This is illustrated in the accompanying figure 1. This negative region implies that a positive incremental addition to the potential in that region would have the effect of reducing the total cross section. Work is continuing to extend this research to treat inelastic processes and also calculate inverse gradient $\delta V(r)/\delta\sigma(E)$. The latter gradients have a direct bearing on inverse scattering and provide information on how given cross sections map onto a potential surface.

II. Steady state reactive kinetics on surfaces exhibiting defect structures. This work has focused on the steady state situation of an active surface exposed to two species which may absorb, defuse on the surface, desorb and also react. The surface is assumed to contain defect structures corresponding to either inherent lattice faults or foreign material on the surface. In addition, a simple model taking into account the local temperature and heat transfer into the bulk was also considered. A number of case studies were examined corresponding to different assumptions about the desorption and kinetic characteristics of the defect sites. These species profiles, their fluxes and curvatures are examined to gain physical insight into the competing surface processes. The net effect of surface defects on chemical production rates was examined by integrating the local production rate over a test region on the surface. The reaction-diffusion equations of these models were solved by the multi-grid technique which shows promise for providing an efficient numerical procedure capable of handling practical large scale problems. Figure 2 gives an illustration of the calculations corresponding to a model bimolecular process on a faulted surface.

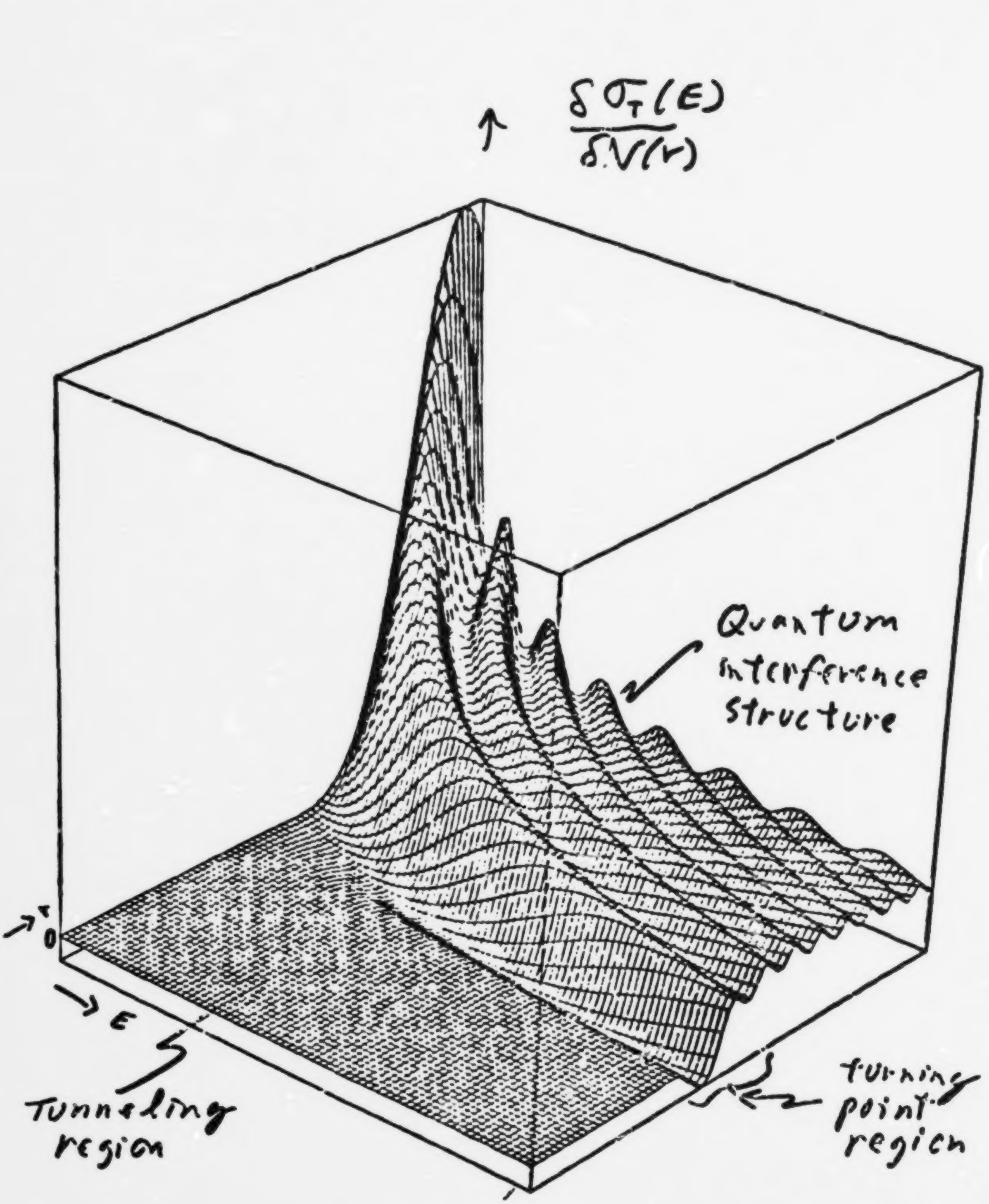

Figure 1. The functional derivative of the elastic total cross section with respect to the potential surface for a system having a nominal repulsive potential. Some features of particular interest are indicated on the plot. In general a surface provides a map of how a variation in the potential at point r is related to the cross section and energy E.

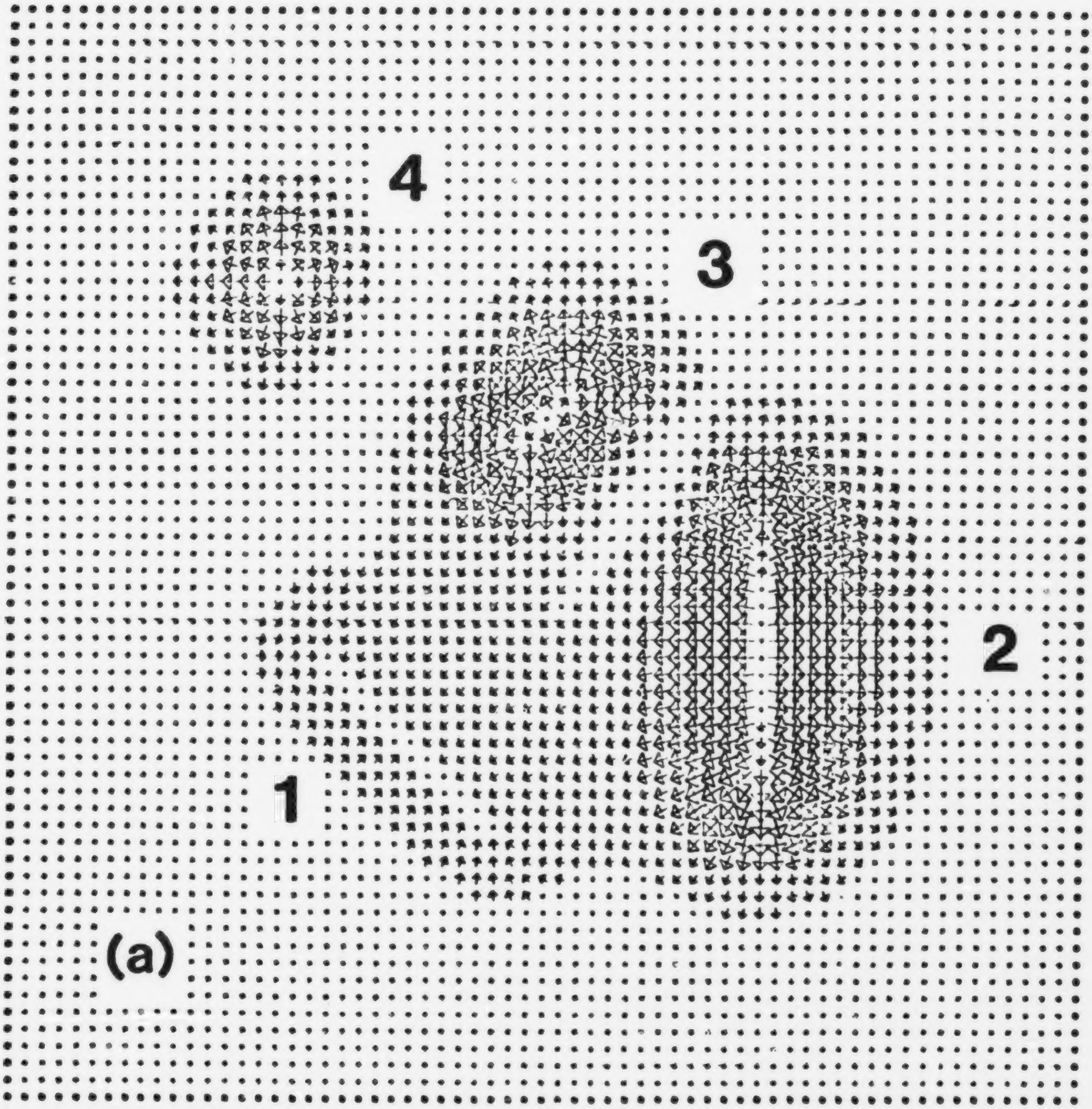

Figure 2. A flux diagram for one chemical species in the vicinity of four absorptive sites. The site labelled 1 is also capable of reactive enhancement of the two chemical species on the surface. It is apparent that sites 1, 2 and 3 are acting in a cooperative fashion with material flowing from the latter two sites to the reactive fault. The size and direction of the arrows is proportional to the species flux vector.

THEORETICAL AND EXPERIMENTAL STUDIES OF MOLECULAR DYNAMICS

Stuart A. Rice

The University of Chicago, Chicago, Illinois 60637

Research supported under AFOSR F49620 is devoted to understanding the elementary dynamics of photochemical processes. The research involves both theoretical and experimental studies intended to provide information which, for example, permit improvements in laser performance, enable the synthesis of new or rare compounds, provide techniques for analysis in situ of trace impurities, and the like. The achievements of the research are the following. First, the discovery of very low energy collision-induced energy transfer has been experimentally exploited and a theory proposed to explain the observations. This theory is in good agreement with the available experimental data. Second, the phenomenon of dissociation of van der Waals molecules has been studied as a function of the amount of excitation energy in the molecule and the pattern of product formation compared with the pattern of energy transfer in analogous collision-induced relaxation processes. The results of these experiments provide a data base from which will be drawn the concepts necessary to formulate a unified theory of the dissociation and collision induced energy transfer processes. Third, experimental and theoretical studies of the coherent evolution of an excited state of an isolated cold molecule, have been carried out and a method devised for measuring the properties of ultrafast light pulses. Finally, joint experimental and theoretical studies have identified key features of the molecular dynamics which lead to selectivity of excitation and deexcitation of vibrations in ordinary collisions.

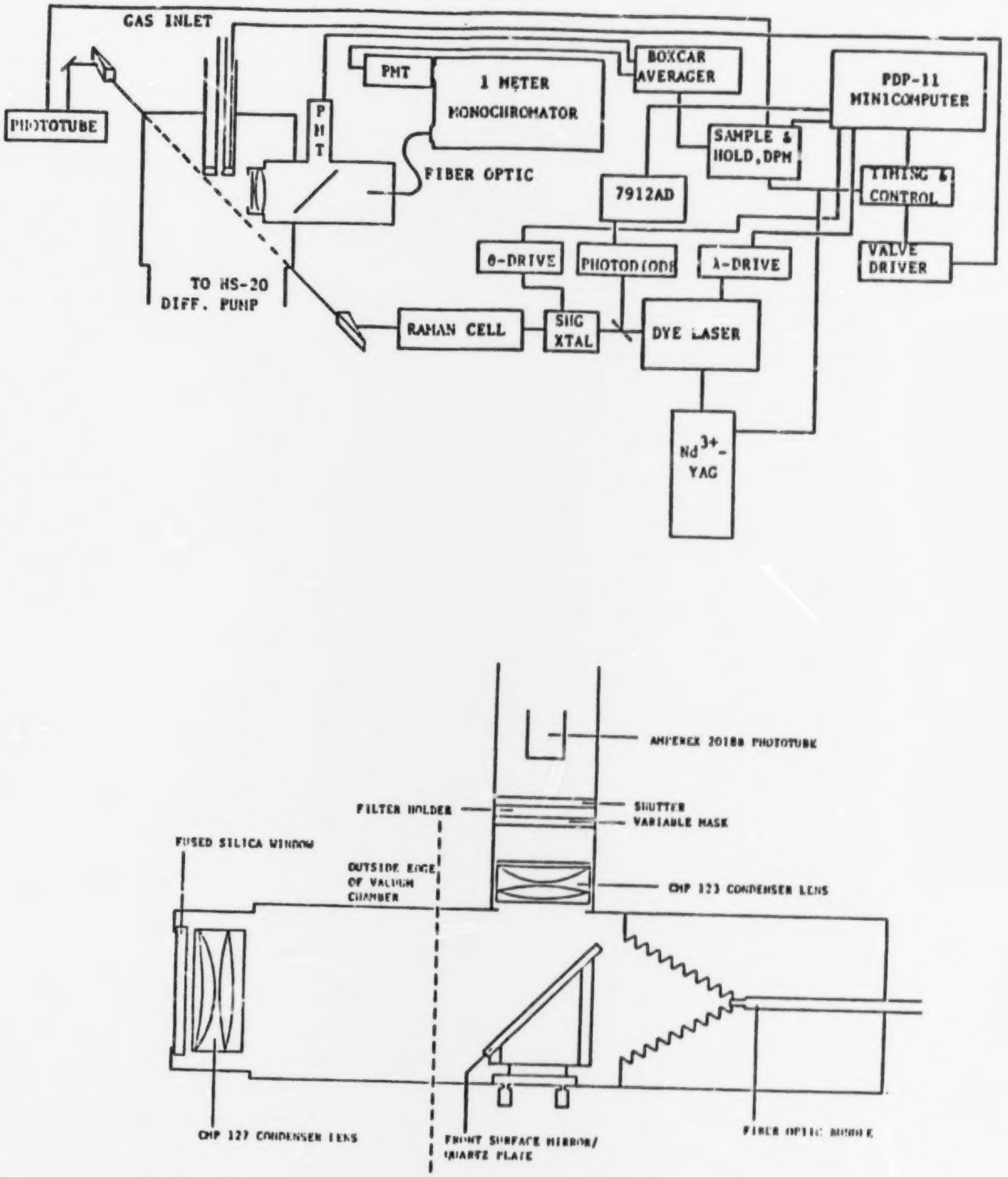
GAS INLET
PHOTOTUBE
PMT
1 METER MONOCHROMATOR
BOXCAR AVERAGER
PDP-11 MINICOMPUTER
P M T
SAMPLE & HOLD, DPM
FIBER OPTIC
TIMING & CONTROL
7912AD
θ-DRIVE
PHOTODIODE
λ-DRIVE
VALVE DRIVER
TO HS-20 DIFF. PUMP
RAMAN CELL
SHG XTAL
DYE LASER
Nd^{3+}-YAG
AMPEREX 20188 PHOTOTUBE
FILTER HOLDER
SHUTTER
VARIABLE MASK
FUSED SILICA WINDOW
OUTSIDE EDGE OF VACUUM CHAMBER
CHP 123 CONDENSER LENS
CHP 127 CONDENSER LENS
FRONT SURFACE MIRROR/ QUARTZ PLATE
FIBER OPTIC BUNDLE

Block diagram of experimental apparatus (above) and of the collection optics assembly (below).

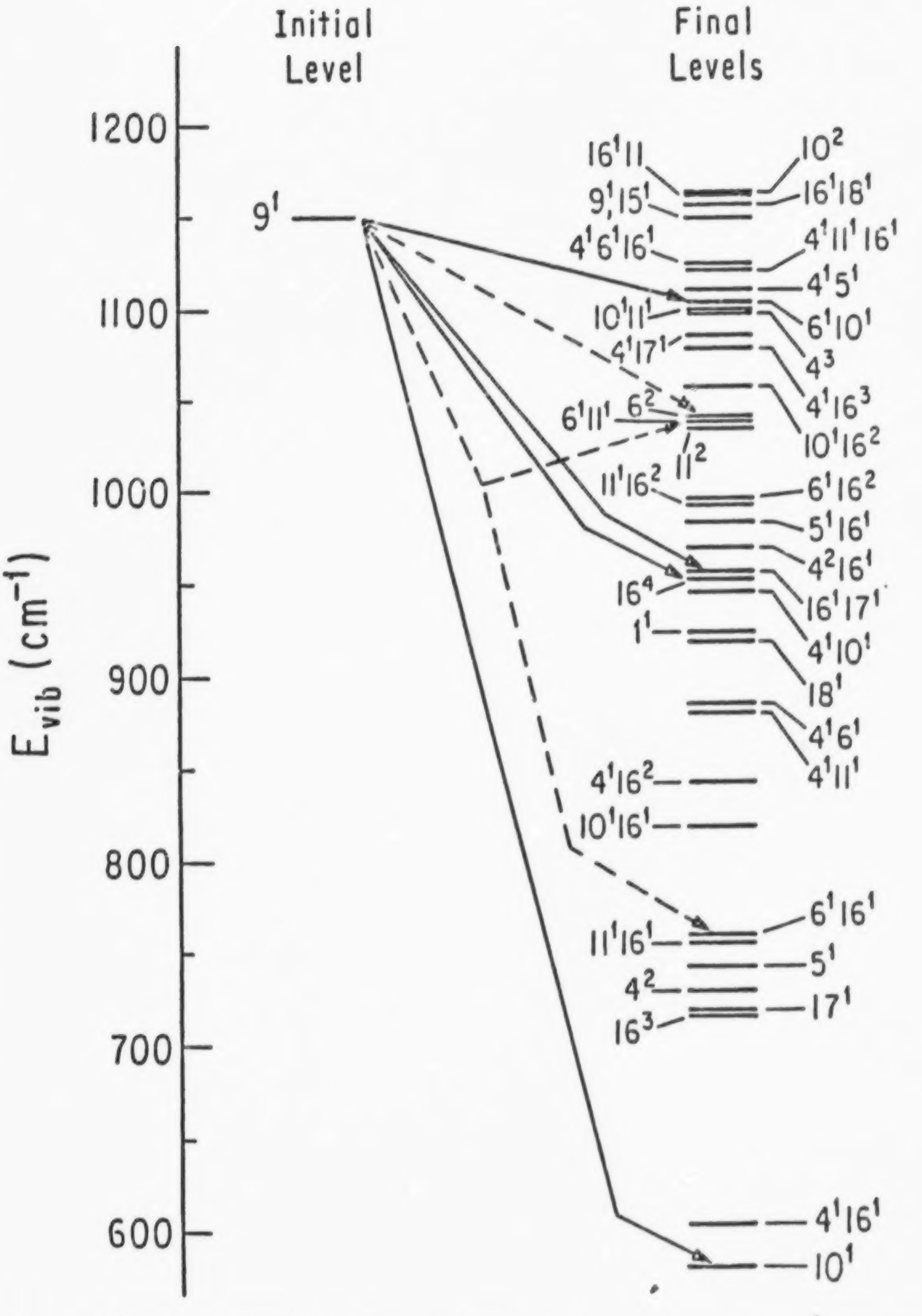

Initial Level
Final Levels
1200
1100
1000
900
800
700
600
E_{vib} (cm^{-1})
9^1
$16^1 11$
10^2
$9^1_, 15^1$
$16^1 18^1$
$4^1 6^1 16^1$
$4^1 11^1 16^1$
$4^1 5^1$
$10^1 11^1$
$6^1 10^1$
$4^1 17^1$
4^3
$4^1 16^3$
$6^1 11^1$
6^2
$10^1 16^2$
11^2
$11^1 16^2$
$6^1 16^2$
$5^1 16^1$
$4^2 16^1$
16^4
$16^1 17^1$
1^1
$4^1 10^1$
18^1
$4^1 6^1$
$4^1 11^1$
$4^1 16^2$
$10^1 16^1$
$6^1 16^1$
$11^1 16^1$
5^1
4^2
17^1
16^3
$4^1 16^1$
10^1

Vibrational relaxation pathways following excitation of the 9_0^1 transition in He$_1$-benzene (——) and He$_2$-benzene (- - -) complexes.

1984 AFOSR/AFWL MOLECULAR DYNAMICS AND SURFACE CHEMISTRY CONFERENCE
24-26 October 1984, KIRTLAND AFB
Abstract Pg 1

REACTIONS OF LASER-GENERATED FREE RADICALS AT SEMICONDUCTOR SURFACES[1]

J. I. STEINFELD
Department of Chemistry, Massachusetts
Institute of Technology, Cambridge, Mass. 02139

There is considerable interest in gaining an understanding of the chemical mechanisms involving reactive gas-phase species at semiconductor surfaces. These reactions may lead to either etching (transport of material from the surface as volatile products) or deposition of thin films on the surface. Both of these processes are essential steps in the fabrication of microelectronic devices.

The current state-of-the-art in etching and deposition is the RF plasma technique. Our approach is to generate the active species by laser dissociation of the parent molecules. Unlike a plasma, this method can produce selected neutral species in the gas phase, whose reactivity toward specific surfaces can be studied in detail. Figure 1 describes the apparatus assembled for this work, in which reactive species (CF_2, SiF_2, SiH_2, CF_3, etc.) may be produced by either infrared multiple-photon dissociation or u.v. photolysis, or generated in a d.c. discharge. Laser-induced fluorescence is used for quantitative detection of these species in the gas phase and following interaction with surfaces. This technique has recently been applied to the study of reactive plasmas[2,3], and to a much more limited extent thus far, to characterization of laser-induced surface reactions.

Initial measurements using this technique have concentrated on the reactions of CF_2, detected *via* its $\tilde{A}$-$\tilde{X}$ transition at 261 nm, with Si and SiO_2. Figure 2A shows the excitation and single vibronic level fluorescence spectra of CF_2 produced in a CF_4 discharge. Figure 2B shows preliminary results for accommodation of CF_2 at Si and SiO_2 surfaces. A simple reaction-diffusion model permits us to estimate the surface reaction probabilities α_r from these data.

We have also been carrying out extensive measurements[4] on Si(111)7x7 surfaces dosed with XeF_2, in order to identify the reaction intermediates which exist on that surface. X-ray photoelectron spectroscopy results for the F(1s) level have shown that only one type of fluorine is observed on a stable overlayer in this system. Thermal desorption measurements indicate that SiF_3 and SiF_2 are the principal desorption products of the stable overlayer. At very high dosage levels, additional features appear in the F(1s) and Si(2p) XPS line, and SiF_4 is observed as a desorption product. These and related results can be explained by migration of F atoms in the lattice, either vertically from bulk to surface sites or laterally from one binding site to another. Additional experiments are in progress to clarify the details of this mechanism.

1. Grant AFOSR-83-0007.
2. R. A. Gottscho, R. H. Burton, D. L. Flamm, V. M. Donnelly, and G. P. Davis, J. Appl. Phys., **55**, 2707 (1984).
3. P. J. Hargis, Jr., "Laser Diagnostic Studies of Plasma Etching and Deposition," Proc. Int. Conf. on Laser Processing and Diagnostics: Applications in Electronic Materials (Linz, Austria, July 1984).
4. B. Roop, S. Joyce, J. C. Shultz, N. D. Shinn, and J. I. Steinfeld, "A TDS Study of Fluorinated Si(111)7x7" (to be published).

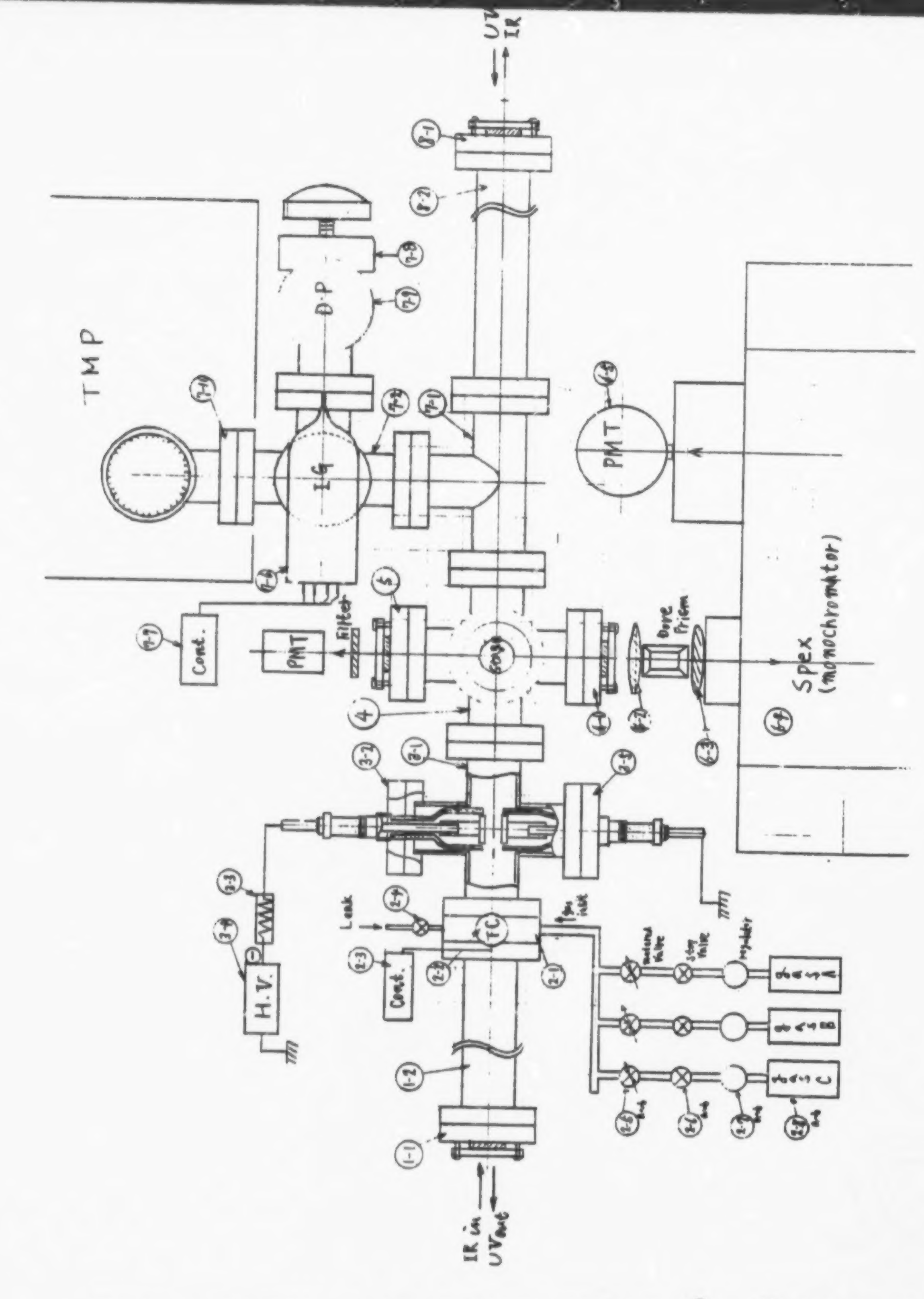
UV
IR
TMP
D.P
I.G
PMT
Cont.
Filter
PMT
Dove Prism
Spex (monochromator)
H.V.
Leak
TC
Cont.
Gas A
Gas B
Gas C
IR in
UV out
1-1
1-2
2-1
2-2
2-3
2-4
3-1
3-2
3-3
3-4
3-5
4
5
6-1
6-2
6-3
6-4
6-5
7-1
7-2
7-4
7-7
7-8
7-9
7-10
8-1
8-2

Figure 1. Schematic of flow-photolysis apparatus. ① and ⑧ windows and baffles. ② gas manifold. ③ d.c. discharge. ④ reaction and detection region (six-way cross chamber). ⑤ filter and PMT for total luminescence. ⑥ dispersed fluorescence detection assembly. ⑦ pumping and vacuum control components (TMP = turbomolecular pump).

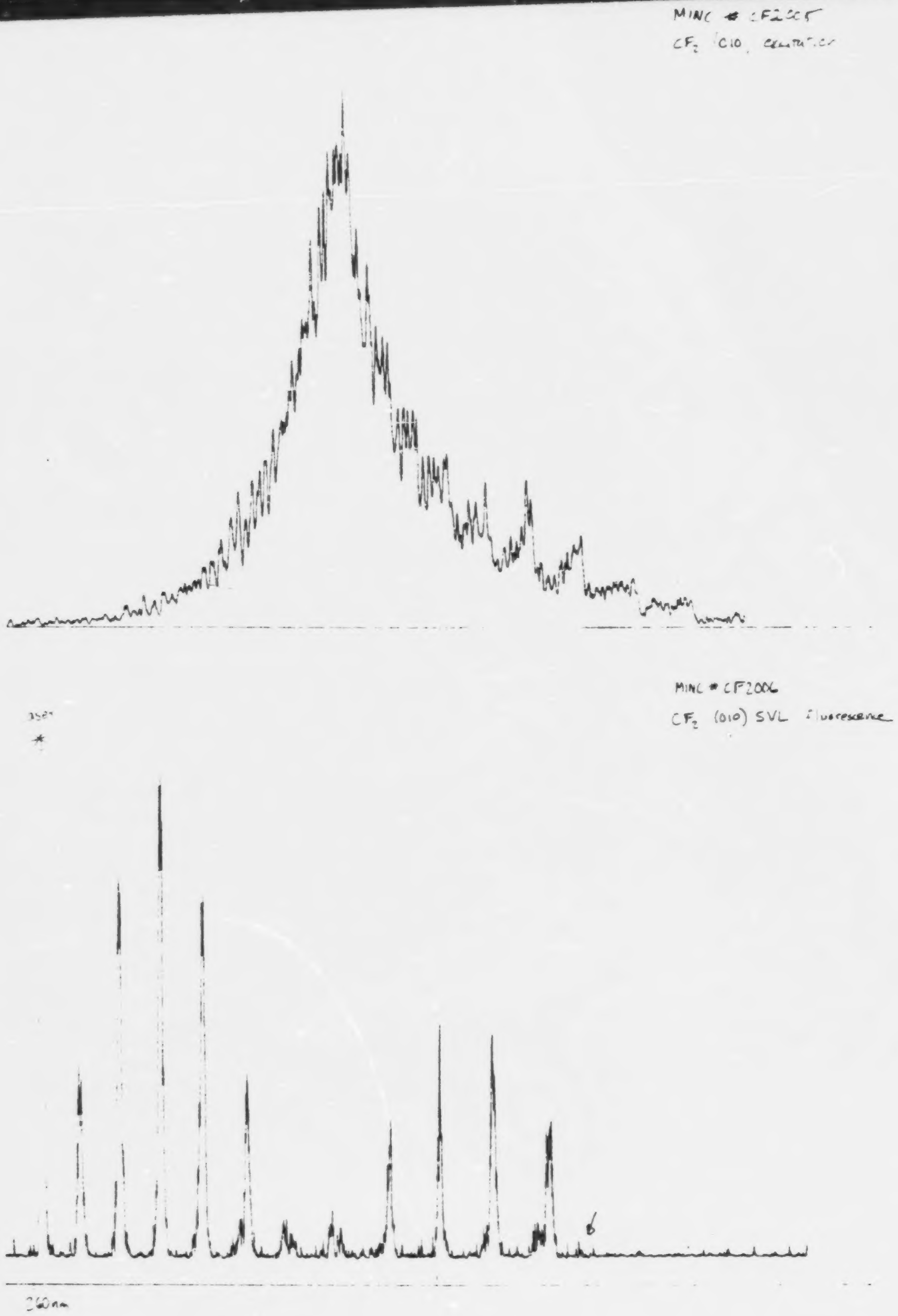

Figure 2A. LIF excitation spectrum and SVL fluorescence spectrum for CF$_2$ $\tilde{A}$-$\tilde{X}$ transition.

BEST COPY AVAILABLE

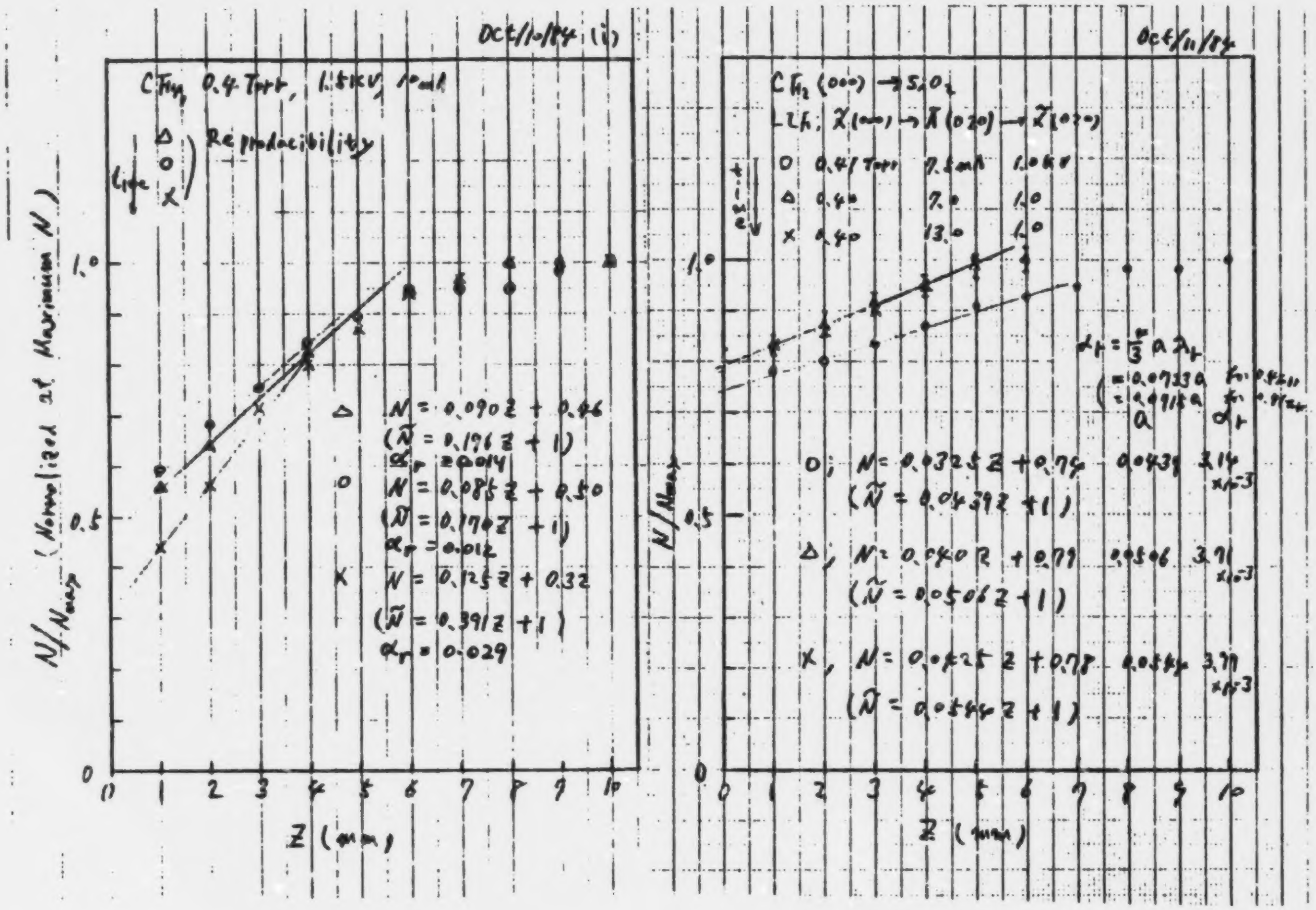

Figure 2B. Normalized CF_2 densities as a function of distance from Si or SiO_2 surface; CF_2 is detected via $\tilde{X}(000) \rightarrow \tilde{A}(020)$ at 261.75 nm, $\tilde{A}(020) \rightarrow \tilde{X}(020)$ at 270.30 nm.

HALOGEN SPECTROSCOPY

Joel Tellinghuisen
Department of Chemistry, Vanderbilt University

I. Introduction

In the past decade a number of new lasers have been developed which operate on electronic transitions in the atomic and diatomic halogens. The lasers in question include both physically pumped (e.g. optical- or discharge-pumped) and chemically pumped systems. The understanding and optimization of these new lasers demands a more complete and detailed description of the spectroscopy and dynamics of the excited states of the diatomic halogens than has existed heretofore. The present work concerns mainly the spectroscopy of these molecules, knowledge of which is fundamental to a proper understanding of their dynamics. By way of illustration of the latter point, in the early development of the $O_2(^1\Delta)$-pumped I-atom laser, it was speculated that the process, $O_2(^1\Delta) + I_2(X) \rightarrow O_2(X) + I_2(A')$, was of essential importance in the dissociation of I_2 in the laser. However, spectroscopic data showed that the A' state of I_2 lay 2000 cm^{-1} too high to be accessed by "cold" $O_2(^1\Delta)$.[1] Consequently it was suggested [1,2] that vibrationally hot $I_2(X)$ might play a role, and that it could be produced via the quenching of $I^*(^2P_{1/2})$ by $I_2(X)$, which has long been known to be very efficient. Although the I_2 dissociation mechanism in this laser remains unclear today, the production of vibrationally hot $I_2(X)$ has been shown to be a significant channel in the quenching of I^* by I_2.[3]

II. Emission Spectroscopy

The present studies employ more-or-less conventianal methods of emission spectroscopy, with a few unconventional twists. The emphasis is on the UV-visible spectra produced by mild discharges of the homo- and heteronuclear halogens in the presence of a large pressure of inert buffer gas (e.g. 1 atm Ar). Under these conditions the emission orginiates mainly from low v' levels of the low-lying ion-pair excited states and terminates on one or more of the excited valence states. In many cases the resulting spectra have been known for decades but never properly interpreted. There are several reasons for confusion: (1) Many of these molecules are "heavy," meaning the spectra are rotationally and vibrationally congested, a problem which is exacerbated by the high temperatures produced in typical discharge sources. (2) In most cases there is further complication from multiple isotopomers and overlapping electronic transitions. We have overcome these difficulties using moderate-to-high resolution to photograph the emission from tesla discharge sources containing isotopically pure halogens. These tesla sources typically operate cool (~360 K);[4] and at ~1 atm of inert buffer gas, the emitting ion-pair states appear to be near-Boltzmann with respect to their rotational, vibrational, and local electronic energies.[5]

In the past, such methods have been used in my laboratory to record and analyze a number of emission transitions in I_2 and Br_2.[1,5-7] Under the present grant we have extended our work to the interhalogens and have so far analyzed emission spectra of ICl,[8] BrF,[9] and BrCl.[10] In each case the emission is dominated by a transition which we designate D' → A', in which the initial state is very likely the $\Omega = 2$ or 2_g state which arises from the ion pair, $X^- = Y(X)^+(^3P_2)$; and the terminus is the $\Omega = 2$ or 2 component of the lowest $^3\Pi$ manifold. The A' state is then also the lowest excited state in the halogens.

III. Computational Methods

The development of computational methods for treating diatomic problems has always been a strong component of the work done in my laboratory. In the past year I have investigated a very simple sum rule for total radiative decay rates,[11] whereby the customary sum over final states is reduced to a simple expectation value,

$$\sum_{v''} \nu^3_{v'v''} |> v''|\mu_e(R)|v'>|^2 = < v'|V^3(R)\mu_e^2(R)|v'> ,$$

in which $V(R)$ is the difference potential, $V(R) = U'(R) - U''(R)$. Numerical tests show this approximation to be typically valid to better than 1%. Moreover, the expectation value on the right can usually be evaluated classically by means of a ratio of two 4-point sums, with comparable reliability.[12]

IV. Quenching of $I_2(A')$

In a spin-off of my spectroscopic work on I_2, I have recently studied the quenching of the A' state of I_2.[13] The experiments were performed in the laboratory of Professor Leon F. Phillips at the University of Canterbury in Christchurch, New Zealand. The technique involved excitation of I_2/Ar and I_2/N_2 mixtures with an ArF excimer laser at 1930 Å, followed by a delayed absorption probe at 2950 Å (doubled N_2-pumped dye laser). The excitation/detection scheme is summarized in Fig. 1. It is worth noting that the production of thermally equilibrated A' molecules occurs on roughly the time scale of the ArF laser pulse, since the internal conversion, D→D' radiative decay, D' → A', and vibrational relaxation in A' are all very fast under the conditions of these experiments ($P_{buf} > 100$ torr). The quenching of $I_2(A')$ was found to be first order in all components, with the following rate constants (units cm^3/s, T = 296±2 K): $k_{Ar} = 2.8(2)\times10^{-14}$, and $k_{N2} = 7.2(7)\times10^{-14}$, and $k_{I2} = 8.3(1.0)\times10^{-11}$. The Ar and N_2 rates

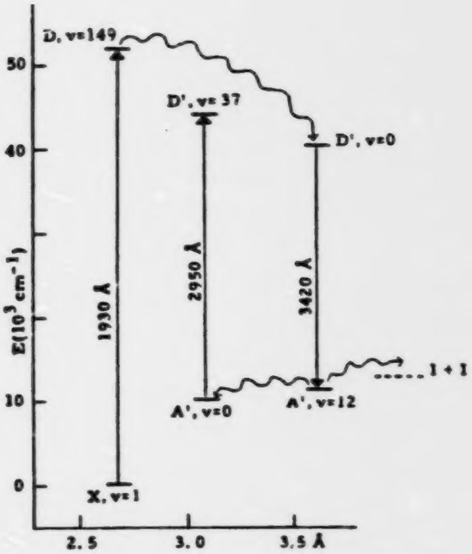

Figure 1. Simplified potential diagram of I_2 illustrating processes initiated by ArF laser photolysis in inert buffer gases. Also shown is the absorption probe transition for low v levels of A'. Note that the absorption spectrum is Franck-Condon shifted and broadened relative to the emission spectrum.

probably are dominated by thermal dissociation, but by a process of elimination the I_2 rate is attributed to $I_2(A') + I_2 \rightarrow I_3 + I$, in which the I_3 must be energetically more stable than $I_2(A')$. Temperature dependence studies, now underway, should help to clarify the picture.

The results of these studies have important implications for the age-old question of the mechanism of atomic recombination in the halogens. They also have a possible bearing on the mechanism of the chemical I^* laser. Furthermore, they may point the way toward the development of solar-pumped lasers which operate via atomic recombination.[14]

1. J. Tellinghuisen, J. Mol. Spectrosc. 94, 231, (1982).
2. J. Tellinghuisen, informal meeting of Air Force contractors, Kirtland AFB, September, 1981.
3. G.E. Hall, W.J. Marinelli, and P.L. Houston, J. Phys. Chem. 87, 2153 (1983).
4 M.R. McKeever, et al., Rev. Sci. Instrum. 50, 1136 (1979).
5 A.L. Guy, et al., Chem. Phys. Lett. 73, 582 (1980).
6. J. Tellinghuisen, et al., Chem. Phys. Lett. 84, 528 (1981).
7 K.S. Viswanathan and J. Tellinghuisen, J. Mol. Spectrosc. 101, 285 (1983).
8 J.D. Spivey, J.G. Ashmore, and J. Tellinghuisen, Chem. Phys. Lett. 109, 456 (1984).
9 S.D. Henderson and J. Tellinghuisen, Chem. Phys. Lett. (to be submitted).
10 D.K. Chakrobertty, J.G. Ashmore, and J. Tellinghuisen, (in preparation).
11 J. Tellinghuisen, Chem. Phys. Lett. 105, 241 (1984).
12 J. Tellinghuisen, and P.S Julienne, J. Chem. Phys. (in press).
13 J. Tellinghuisen, A.R. Whyte, and L.F. Phillips, J. Phys. Chem. (submitted).
14 J. Tellinghuisen, to be published

The H^+ + F^- Ion-Ion Reaction Kinetics

H.-t. Wang and D. J. Bogan
Naval Research Laboratory
Code 6180
Washington, D. C. 20375-5000

Ion-ion neutralization / recombination reactions (IINR / IIRR) have the largest rate constants among chemical reactions due to the long range Coulomb potential force between the positive and negative charges. Their reaction products are mostly electronically excited states and the emissions to the corresponding ground states are in the uv and vuv regions. These characteristics make ion-ion reactions (IIR) good sources of fast uv-vuv photon generation. Thus they are potentially excellent pumping mechanisms for powerful uv-vuv lasers.

However, the reaction kinetics of IIR's are currently not well understood. There have been a large number of overall rate measurements, but only one example of a product state resolved (PSR) study exists in the literature.[1] The overall reaction rates are nonetheless in dispute. For example, the rate of the pumping reaction of the ArF laser,

$$Ar^+ + F^- \longrightarrow ArF^* \qquad \text{IIRR} \qquad (1)$$

ranges from 2×10^{-6} cm^3/sec [2] to 2×10^{-9} cm^3/sec.[3] The latter value is actually smaller than the rates of negative ion - neutral molecule reactions which are typically 5×10^{-9} cm^3/sec.[4]

The reaction system of,

$$H^+ + F^- \longrightarrow H\,(n=2) + F\,(^2P_{3/2}); \qquad \text{IINR} \qquad (2)$$

$$H^+ + F^- \longrightarrow HF\,(B\,^1\Sigma\,,\ v' < \infty); \qquad \text{IIRR} \qquad (3)$$

represents a prototype of IIR's since the optical emission of,

$$H\,(n=2) \longrightarrow H\,(n=1) + h\nu \qquad (4)$$

is the Lyman-α line and the ,

$$HF\,(B^1\Sigma\,,\ v') \longrightarrow HF(X^1\Sigma\,,\ v'') + h\nu \qquad (5)$$

emission manifold has been spectroscopically well characterized.[5] Furthermore, reaction (2) is thermoneutral ($\Delta H_0^o < -0.01$ kcal/mole), so that its rate may exceed 10^{-6} cm^3/sec.[1] Since {H (n=2) + F ($^2P_{3/2}$)} is the dissociative pair of HF with the lowest excitation energy, the repulsive curve of the HF (B) state (Figure 1) does not intercept any other neutral molecular curve, and thus does not suffer any curve crossing or anti-crossing complications. In other words, HF (B) is a pure ionic state. In fact, it is the only known example of a pure ionic state, to our knowledge.

Although the emission manifold is well understood and the chemiluminescence study is expected to be straight-forward, the construction of the ion sources has been time consuming. The present designs of the ion sources are as follows; A) F^- ions will be generated from the dissociative-attachment reaction,

$$F_2 + e^- \longrightarrow F^- + F \qquad (6)$$

by injecting electrons, from an electron gun,[4] into the F_2 stream, B) H^+ ions will be produced by a colutron[6] or by mixing H_2 with metastable He.[7] In either case there will be substantial amounts of H_2^+ produced. However, for practical purposes, the reaction,

$$H_2^+ + F^- \longrightarrow HF\ (B\ ^1\Sigma,\ v' \leqslant 36) + H \qquad (7)$$

may prove to be more efficient than reaction (3) in populating the HF (B) state.

From Figure 1, it is clear that the HF (B) and (X) states have very different geometries. Reaction (5) will most likely produce HF (X) in high v" levels which will then be removed via fast vibrational relaxation. Hence, the population inversion, initiated by reactions (3) and (7), can be maintained easily.

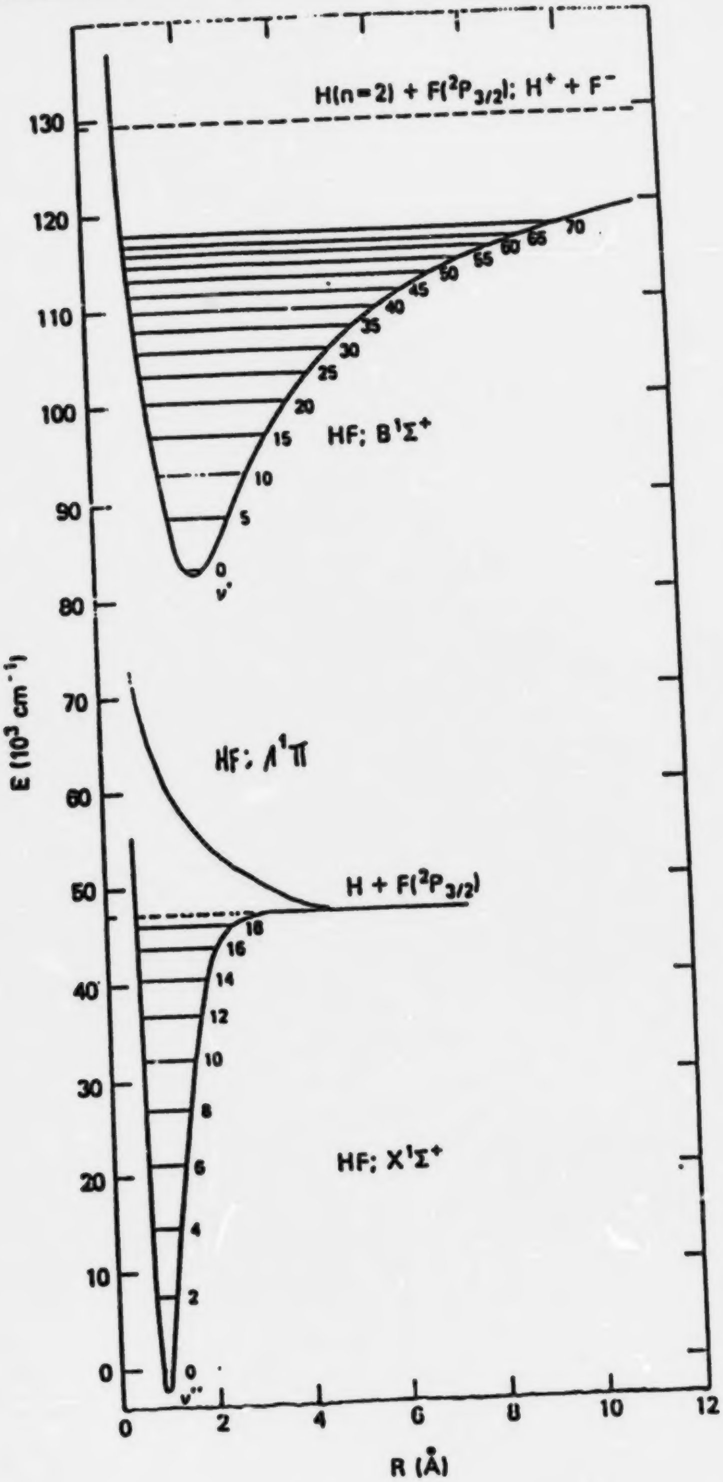

Figure 1

Potential curves of HF are shown as functions of internuclear distance R. The $X^1\Sigma$ curve and the $v' \leq 26$ part of the $B^1\Sigma$ curve are RKR potentials.[5] The $A^1\Pi$ curve is estimated from absorption spectrum. The $v'>26$ part of B is extrapolated from $v' \leq 26$. The asymptotes are for both HF B and X states.

These unique properties of the HF (B) state make it an attractive candidate for uv-vuv laser action. This detailed PSR kinetics study will establish the foundation, not only for possible laser application, but also for basic understanding of IIR kinetics in general.

REFERENCES:

1.) J. Weiner, W. B. Peatman, and R. S. Berry, Phys. Rev., 4, 1825 (1979).

2.) J. Hsia, Appl. Phys. Lett., 30, 101 (1977).

3. D. Smith and N. G. Adams, "Physics of Ion-Ion and Electron-Ion Collisions", Edited by, F. Brouillard and J. W. McGowan, Plenum, N. Y., 1983, pp. 501 - 531.

4.) J. C. Weisshaar, T. S. Zweier, S. R. Leone, J. Chem. Phys., 75, 4873 (1981).

5.) G. Di Lonardo and A. E. Douglas, Can. J. Phys., 51,434 (1973).

6.) M. Menzinger and L. Wahlin, Rev. Sci. Instr. 40, 102 (1969).

7.) J. H. Kolts and D. W. Setser, in "Reactive Intermediates in the Gas Phase", Edited by D. W. Setser, Academic Press, N. Y., 1979, pp. 152 - 231.

TEMPORAL STUDIES OF NON-LINEAR FRAGMENTATION

S. Chattopadhyay[1], R.G. Weiss[1], B.B. Craig[2] and W.L. Faust[2]
[1]Georgetown University, Department of Chemistry
[2]Naval Research Laboratory

Although energetic materials are important to commerce and defense, very few studies have been directed at understanding the microscopic processes which are responsible for energy release from these materials at the molecular level. Fundamental knowledge about the nature, identity and kinetics of fast photo-induced reactions in simple energetic molecules can provide generic models for processes important in fuels, explosives and propellants. This work describes the application of picosecond laser techniques, coupled with fast time-resolved diagnostics, to elucidate the primary processes of fragmentation subsequent to non-linear excitation. This method of initiating and interrogating fast reactions offers several methods of advantages over other methods: (i) The use of short laser pulses (30 ps) provides a very convenient method for sharp definition of initiation. (ii) The time resolution afforded by picosecond pulse excitation allows the photolysis to be carried out at relatively large pressures yielding high fragment concentration. (iii) The application of sophisticated time-resolved techniques facilitates interrogation at early times after initiation. (iv) The current literature on photofragmentation is largely devoid of temporal information. Kinetic information has usually been inferred by conventional methods such as steady-state emission studies, mass spectrometric technique, final product analysis, etc. Our techniques allow direct measurement of kinetic pathways through observation of emissive fragments. Also, the use of isotopically labeled parent compounds provides the capability to distinguish between the various fragment formation channels.[1,2]

We have studied the temporal development of emissive neutral diatomic fragments, especially CN B, C_2 d, NH A and CH A,C subsequent to non-linear UV excitation (266 nm, photon flux $\sim 10^{19}$ cm^{-2}) in the gas phase. A schematic representation of the experimental setup is displayed in Fig. 1a. The Nd:YAG laser system utilizes an active opto-acoustic loss modulator (Quantronix) and a passive saturable absorbing dye (Kodak 9860) in a flow cell. A high-spatial quality IR pulse (1064 nm, 30 ps) of 30-40 mJ is obtained through two-stage amplification, apodization and spatial filtering of 1064 nm single pulse. The photolyzing pulse (266 nm) of up to 10 mJ is produced through the efficient doubling and redoubling of the IR pulse by KD*P. The photolyzing pulse was focused into a static gas cell. The emission was collected at right angles in a 1 m Czerny-Turner spectrometer. The transient signal was detected by a Varian-154 crossed-field photomultiplier (GaAs, spectral range 200-900nm; 0.15 ns risetime) and signal-averaged by a Tektronix 7912 AD digitizing oscilloscope (system step-function risetime 0.85 ns) interfaced to a Tektronix 4052 computer. An OMA II ISIT Vidicon was used for acquisition of time-averaged spectra. Absolute pressure measurements were taken with an MKS Type 220 Baratron gauge (0-14 Torr).

We have made an extensive study of the effect of pressure on the dynamics of photofragmentation of the simple nitriles, XCN ($X=CH_3$, Cl and CN). The initial excitation is believed to proceed through simultaneous absorption of two photons ($2h\nu = 9.32$ eV). Dissociation at this level competes with further excitation to yield superexcited states (XCN**). For ClCN and C_2N_2, we observe both prompt ($2h\nu$ process) and delayed component ($3h\nu$ process) of the

S. Chattopadhyay[1], R.G. Weiss[1], B.B. Craig[2] and W.L. Faust[2]
1 Georgetown University, Department of Chemistry
2 Naval Research Laboratory (Cont'd)

CN B emission. However, CH_3CN exhibits only protracted formation of emissive diatomics (≥ 2hν process). Figure 1b displays CN $B^2\Sigma^+ \rightarrow X^2\Sigma^+$ emission (388.3 nm) waveforms from 3 Torr of CH_3CN in 10 ns and 2 ns timescales. The emission spectra of CN violet band for $\Delta\nu = 0$ and $\Delta\nu = -1$ progressions are displayed in figure 1c. The CN B fragment exhibits pressure dependent protracted formation rates (for 3hν channel). The plots of rate vs. pressure are characterized by intercepts and slopes which correspond to zero-pressure lifetimes of precursors and the bimolecular rate constant (k_Q) for the collision-induced removal of the precursors, respectively. For CH_3CN such a plot yields a metastable precursor lifetime of 20 ns and a k_Q of $13x10^{-10}$ cm^3 s^{-1}. The large values of collision-free lifetime and k_Q appear to be consistent with either Rydberg or "ion-pair" characters of a superexcited species, XCN** (3hνprocess). Our data does not support XCN^+ as the precursor. For CH_3CN, the use of isotopically labeled compound establishes two major intramolecular channels for CN B yield; the dominant channel involves the retention of the CN association of the parent (61%) and the other channel is associated with the intramolecular methyl carbon (19%). These two channels orginate from the same precursor since they share a common risetime. Also, for CH_3CN, intermolecular channel accounts for 19% of CN B production. A quantitative treatment of the emission yields and the kinetics suggests that perhaps the intermolecular channel is associated with a single collision complex (parent ** + parent). Extensive studies of pressure dependence of fragmentation kinetics of ClCN and C_2N_2 also supports the above conclusion that the dominant yield of CN B is associated with the collisional removal of XCN**. We have parameterized the CN B waveforms from ClCN and C_2N_2 with a kinetic model outlined in a previous paper.[3] This model includes rate constants k_1 and k_2 and a ratio D of delayed/prompt signals. The pressure dependence of k_1 and D yield certain pressure-independent quantities; R, the ratio of parent populations which initially enter the delayed and the promp channels; k_{10}, the rate constant for spontaneous fragmentation of precursors; k_{1G}, the bimolecular rate constant for collisions productive of CN B and k_{1Q}, the bimolecular rate constant for nonproductive removal of precursors. The efficiency of the CN B production from the metastable precursors is given by

$$\phi 1 = (k_{10} + k_{1G}P)/(k_{10} + k_{1G}P + k_{1Q}P)$$

The efficiency of the collision-induced production of CN B from the precursors is expressed as

$$\phi 1c = k_{1G}/(k_{1G} + k_{1Q})$$

Figure 2 displays the plots of k_1 and k_2 vs. P for ClCN. The intercept of k_2 vs. P plot yields a zero-pressure lifetime of 58 ns for CN B which agrees well with the literature value of 60 ns for the radiative lifetime of CN B state. The intercept of k_1 vs. P plot yields a collision-free lifetime of 105 ns and a slope ($k_{1G} + k_{1Q}$) of 14 x 10^{-10} cm^3 s^{-1}. ϕ_{1c} is obtained from the functional dependence of D on reduced pressure; $P_r = P/Po$, where $P_o = k_{10}/(k_{1G} = k_Q)$. Thus, D is expressed as

$$D(1 + P_r) = R(1 + \phi_{1c}P_r).$$

For ClCN, the pressure dependence data of D indicates that the collisional

S. Chattopadhyay[1], R.G. Weiss[1], B.B. Craig[2] and W.L. Faust[2]
1 Georgetown University, Department of Chemistry
2 Naval Research Laboratory (Cont'd)

removal of the precursors leads to CN B production with nonzero efficiency (i.e., ϕ_{1c} 0) and the spontaneous unimolecular fragmentation of XCN is very small.

Acknowledgement

This work was supported by AFOSR Molecular Dynamics and Surface Chemistry Program.

References

1. B.B. Craig, W.L. Faust, L.S. Goldberg, and R.G. Weiss, J. Chem. Phys. 76, 5014 (1982).
2. B.B. Craig, W.L. Faust and R.G. Weiss, J. Chem. Phys. 79, 1286 (1983).
3. B.B. Craig and W.L. Faust, J. Phys. Chem. 87, 4568 (1984).

Figure Captions

Figure 1(a)	Schematic of the experimental set up.
Figure 1(b)	CN B waveforms from 3 Torr of CH_3CN monitored at 388.3 nm.
Figure 1(c)	Spectra of CN violet system emission ($\Delta v = 0$ and $\Delta v = -1$) derived from CH_3CN at 3 Torr. Data are accumulated for 128 laser shots.
Figure 2	Plots of k_1 and k_2 vs. P for ClCN.

BEST COPY AVAILABLE

FIG. 1

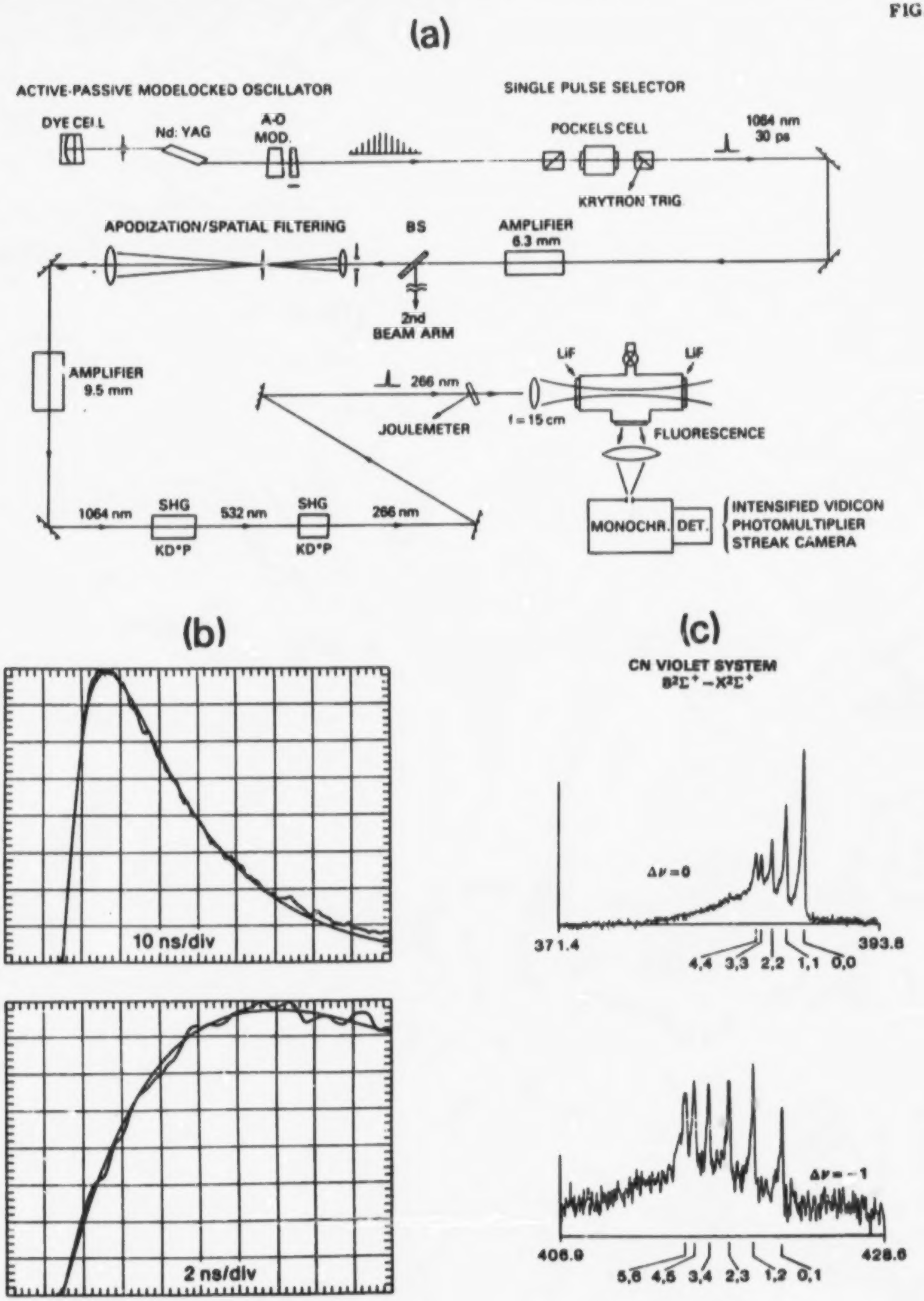
(a)
ACTIVE-PASSIVE MODELOCKED OSCILLATOR
SINGLE PULSE SELECTOR
DYE CELL
Nd: YAG
A-O MOD.
POCKELS CELL
1064 nm 30 ps
KRYTRON TRIG
APODIZATION/SPATIAL FILTERING
BS
AMPLIFIER 6.3 mm
2nd BEAM ARM
AMPLIFIER 9.5 mm
266 nm
JOULEMETER
f = 15 cm
LiF
LiF
FLUORESCENCE
MONOCHR.
DET.
INTENSIFIED VIDICON
PHOTOMULTIPLIER
STREAK CAMERA
1064 nm
SHG
KD*P
532 nm
SHG
KD*P
266 nm
(b)
10 ns/div
2 ns/div
(c)
CN VIOLET SYSTEM
B²Σ⁺ – X²Σ⁺
Δν = 0
371.4
393.8
4,4
3,3
2,2
1,1
0,0
Δν = –1
406.9
428.6
5,6
4,5
3,4
2,3
1,2
0,1

BEST COPY AVAILABLE

FIG. 2

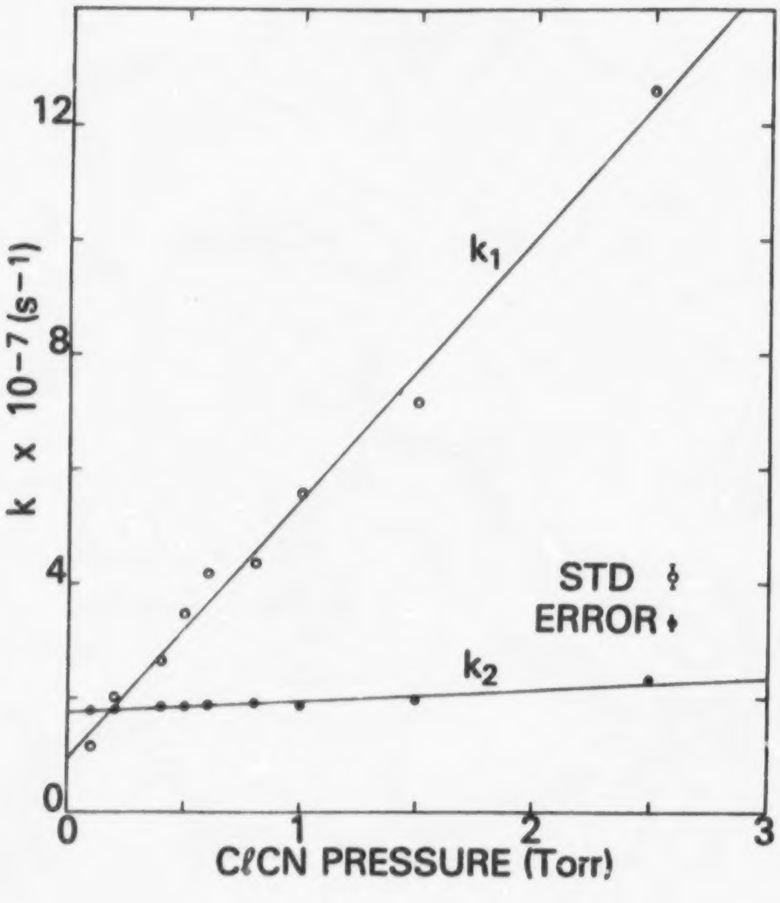

BEST COPY AVAILABLE

LASER KINETIC SPECTROSCOPY OF UNIMOLECULAR AND BIMOLECULAR PROCESSES IN THE GAS PHASE

Curt Wittig and Hanna Reisler
Department of Chemistry, University of Southern California
SSC 403, MC 0484, Los Angeles, CA 90089-0484

The photodissociation dynamics of NCNO and ICN have been studied at 300K and in a free jet expansion. Our goal is to unravel the microscopic detail of elementary processes which transpire in small molecular systems, and to compare them with theoretical models. The experimental approach relies on laser photodissociation under collision-free conditions, and LIF probing of the products. In addition to the standard LIF arrangement, we are able now to bring about the photodissociation with polarized lasers, and to detect Doppler profiles of selected rotational lines of the fragments with a probe laser with an intracavity etalon.

The relative orientations of the lasers and their electrical vectors are shown at the top of Fig. 1, which also displays the line shapes obtained for N"=0, 20 and 52 of CN($X^2\Sigma^+$,v"=0) following the 266 nm photodissociation of ICN.(1) The high resolution results show, for the first time, unequal nascent populations of the spin-rotation doublets (F_1 and F_2) of CN, which are also manifest in the photodissociation of BrCN and ClCN.(2) From the Doppler measurements and the spatial recoil anisotropies we are able to obtain separate CN(X) rotational distributions for the I($^2P_{3/2}$) and I($^2P_{1/2}$) channels, and their respective anisotropy parameters, β. The results are analyzed in terms of the potential surfaces involved in the dissociation.(1)

Fig. 2 presents results concerning V,R energy distributions for nascent CN($X^2\Sigma^+$), following the 1-photon photodissociation of expansion cooled NCNO via $\pi^* \leftarrow n$ excitation throughout the region 450-585 nm.(3,4) The spectrum in the rear is obtained by monitoring CN($X^2\Sigma^+$,v"=0,N"=0) as the photolysis wavelength is varied. The individual CN LIF spectra at specific photolysis wavelengths, are presented perpendicular to the horizontal axes.

At the observed threshold for dissociation (585.3 nm), >90% of the CN Product is in v"=0,N"=0, with the remainder in N"=1, corresponding to $\langle E_{rot} \rangle$ <0.4 cm^{-1}. CN($X^2\Sigma^+$,v"=1) and CN($X^2\Sigma^+$,v"=2) thresholds are observed at photolysis wavelengths which correspond exactly to E_p-D_0(v"=1) and E_p-D_0(v"=2) where D_0(v") is the dissociation energy to produce CN($X^2\Sigma^+$,v") and E_p is the photon energy. These observations can only be reconciled with a vibrational predissociation mechanism, and spectroscopic observations(5) suggest that this occurs following internal conversion to the ground state surface. With E_p-D_0(v") less than ~ 2000 cm^{-1}, the phase space theory of unimolecular reactions (PST) predicts the CN rotational distributions with high accuracy. However, when product vibrations are accessible, PST cannot be used, but we are able to reconcile the present experimental findings with a modified statistical model.

Results obtained at 300K are similar, but at wavelengths > 585 nm, dissociation occurs predominantly by exciting NCNO "hot bands."(6)

1. I. Nadler, D. Mahgerefteh, H. Reisler, and C. Wittig, to be published.
2. F. Shokoohi, S. Hay, and C. Wittig, Chem. Phys. Lett. (in press).
3. I. Nadler, H. Reisler, M. Noble, and C. Wittig, Chem. Phys. Lett. 108, 115 (1984).
4. I. Nadler, M. Noble, H. Reisler, and C. Wittig, submitted.
5. M. Noble, I. Nadler, H. Reisler, and C. Wittig, J. Chem. Phys. (in press).
6. I. Nadler, J. Pfab, H. Reisler, and C. Wittig, J. Chem. Phys. 81, 653 (1984).

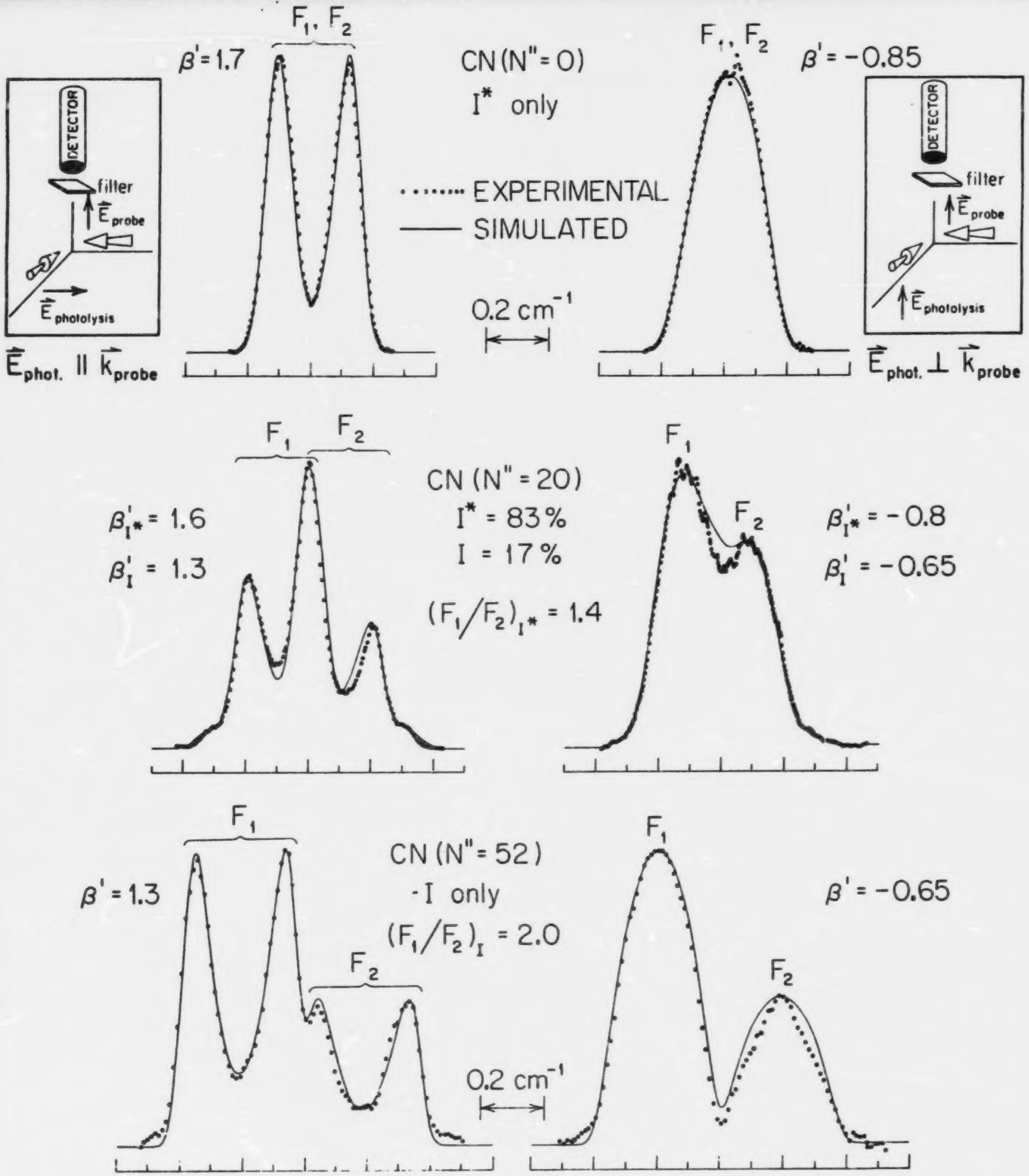

Fig. 1: Doppler profiles of CN($^2\Sigma^+$,v"=0,N") obtained in the 266 nm photolysis of ICN. (····) - experimental data. (——) - calculated data.

FIGURE 1

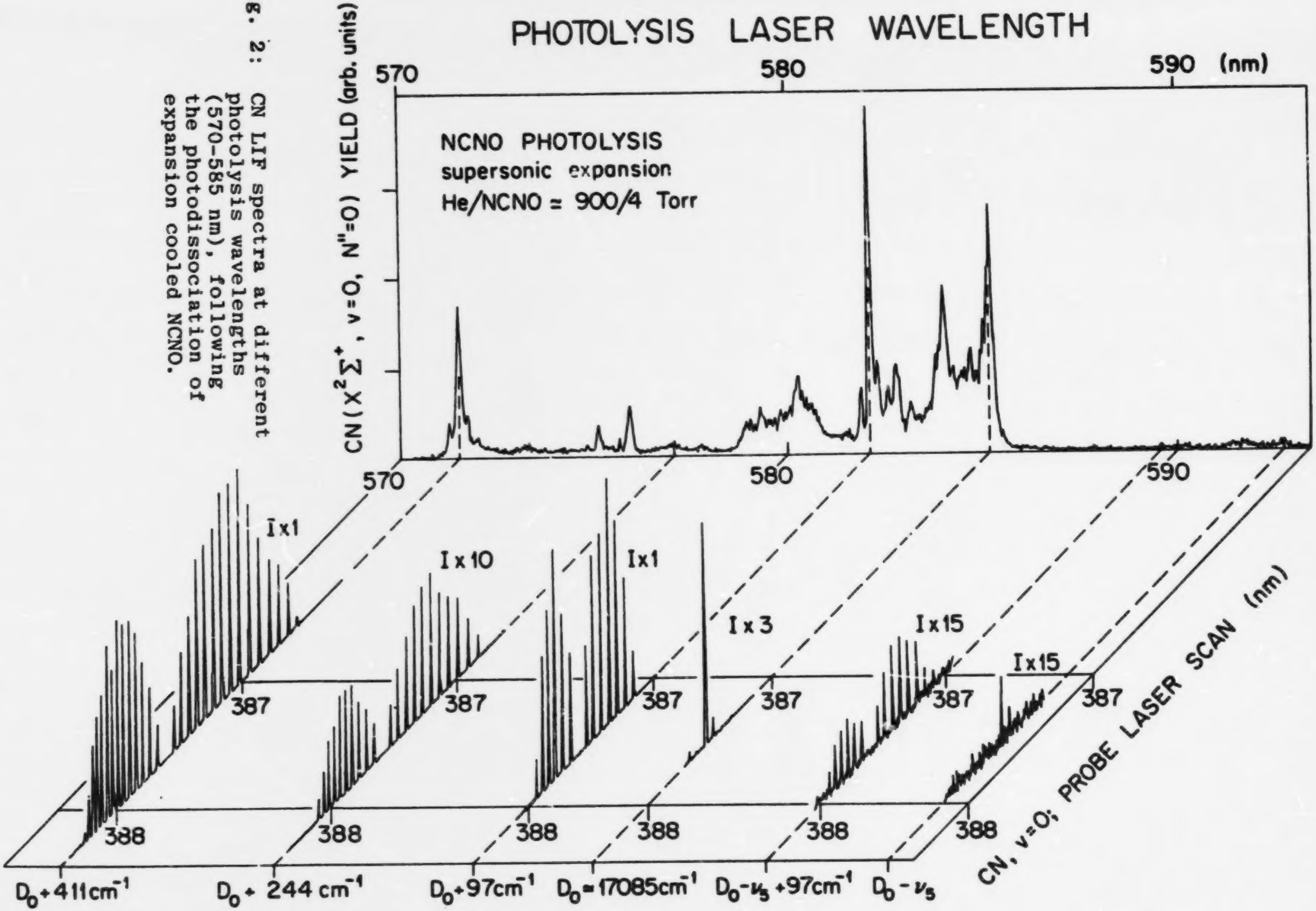

Fig. 2: CN LIF spectra at different photolysis wavelengths (570-585 nm), following the photodissociation of expansion cooled NCNO.

Nonspeakers

Surface Chemistry

RELATIONSHIPS BETWEEN ELECTRONIC STRUCTURE AND STABILITY OF METALLIC GLASSES

F. Abeles, M. L. Theye, and V. Nguyen Van
Laboratoire d'Optique des Solides
Universite P. et M. Curie

The aim of this work was to prepare amorphous metallic alloy thin films by controlled co-evaporation under ultra-high vacuum onto substrates maintained at low temperature (15-20K), and to investigate in situ, as a function of temperature, their d.c. electrical resistivity and their optical properties over a large spectral range (0.6 to 4.5 eV). It was attempted, on the one hand to determine the range of (meta) stability of these amorphous alloys with respect both to temperature and composition, on the other hand to study the influence of disorder on the electronic properties, especially on the conduction electron behavior, as a function of composition. Two alloy systems which were expected to present a free-electron-like behavior, have been considered:

a. Alloys between a noble metal and Ge for compositions close to the eutectic ($x_{Ge} \simeq 25\%$). Au-Ge and Ag-Ge amorphous alloys were obtained at low temperature for x_{Ge} comprised approximately between 20 and 40%. The temperature range where these alloys remain amorphous is however rather limited, especially in the Ag-Ge case, and all of them crystallize, at least partially, below room temperature. For $20 < X_{Ge} < 30\%$, the amorphous alloys have d.c. electrical resistivity values of the order of 120-150 $\mu\Omega$cm, with very small negative temperature coefficients (a few 10^{-5} K^{-1}), and their optical properties present a metallic behavior. Their structure, as determined by electron diffraction, closely resembles that of the corresponding liquid alloys. Their complex dielectric constant followed quite well, at least at the lowest energies (from 0.6 to 1.25 and to 1.6 eV for Au-Ge and Ag-Ge respectively), the free-electron Drude model with a constant relaxation time τ_0. Such a Drude analysis allows to determine both the relaxation time τ_0 and the ratio n/m_0, n being the average number per atom and m_0 the optical mass, of the alloy conduction electrons. The h/τ_0 values are large, of the order of 2-3 eV, but still smaller than those reported for sputtered Au-Si amorphous alloys. The n/m_0 ratio is close to the value expected from a rigid-band free-electron model where each noble metal and Ge atom gives 1 and 4 electrons respectively to the alloy conduction band, but not equal. The differences can be due, either to optical mass effects, or to hybridization effects between the noble metal d electrons and the Ge s,p electrons. In the Au-Ge case, a contribution of interband transitions involving the Au d states is still observed, but it is strongly damped, with a very smooth edge. For $x_{Ge} > 30\%$, the electron diffraction studies show the presence of Ge-Ge covalent bonds, which induce fluctuations of the short-range order. The d.c. electrical resistivity of these alloys is larger and their optical properties deviate from a Drude behavior; they could be interpreted, at least qualitatively, by an effective medium theory, applied to a random mixture of Au-Ge amorphous metallic alloy and amorphous Ge. A similar model could also account for the properties of phase-separated samples, for $x_{Ge} < 20\%$ and $x_{Ge} > 45\%$.

b. Alloys between two simple metals, which present the advantage of having valence electrons with s,p character only. Amorphous Mg-Zn alloys have been obtained at low temperature for x_{Ge} comprised between approximately 25 and 35%. These films crystallize at about 350 K, and their structure is identical to that of quenched bulk alloys. It was necessary to perform all measurements in situ, because of the rapid oxidization of the films under ambiant atmosphere. The variation with temperature between 10 and 300 K of the d.c. electrical resistivity of amorphous alloys annealed at room temperature is qualitatively similar to that reported for quenched bulk alloys, with small differences in the details. In particular, it exhibits a broad maximum around 80 K and an approximately linear behavior with a negative slope between 150-250 K. The resistivity values are however significantly larger: 70-80 μΩcm compared to 40-60 μΩcm for bulk quenched alloys, which may indicate medium-range inhomogeneities in the films. The complex dielectric constant of as-deposited amorphous alloys follows quite well the free-electron Drude model from 0.6 to 1.8 eV, which again alloys to determine the free-electron parameters separately. The h/τ_0 values are comprised between 0.5 and 0.8 eV, therefore significantly smaller than those of noble-metal-based alloys. The n/m_0 is on the other hand definitely smaller than the value expected from a free-electron model (2 conduction electrons per atom on the average, and optical mass equal to the free electron mass). So, either n is smaller than 2 ($n \simeq 1$), possibly due to hybridization effects in the conduction band, or there is a strong enhancement of the optical mass ($m_0 \simeq 2m_e$). The first assumption is however in contradiction with the results of various other experiments, giving $n=2$. It must be emphasized that the optical resistivity, obtained from the optical conduction electron parameters, is in all cases of the order of the d.c. electrical resistivity, which supports the validity of the free-electron model and the consistency of the analysis. More work is needed in order to understand the origin of the optical mass effects in such "simple" amorphous alloys.

Adsorbate Structure on Pt Electrodes

Jay Benziger
Dept. of Chemical Engineering
Princeton University

Pathways for surface reactions are frequently modified by surface modifications. Studies have shown that modification of tungsten surfaces by carbon, oxygen, and sulfur have dramatic effects on the subsequent reactions of alcohols, thiols, benzene and thiophenes. Electrochemical treatments provide an alternative method for making surface modifications, and examining the liquid-solid interface. We report here results obtained by reflection absorption infrared spectroscopy and cyclic voltammetry for adsorption on Pt electrodes.

The experimental apparatus is shown schematically in Figure 1. Central to the experiments is the electrochemical cell. The cell contains a polished polycrystalline Pt electrode which is immersed in a 1 M perchloric acid solution containing the desired adsorbate. The cleanliness of the Pt surface is verified by the its cyclic voltamagram in pure perchloric acid. The Pt electrode is then held at a desired potential and percholoric acid solution containing the adsorbate is introduced into the cell. After adsorption the solution is removed from the electrode by means of a retractable cup and an infrared spectrum of the adsorbed layer is obtained by polarization modulation techniques. After the spectrum is taken the Pt is reimmersed in the electrolyte and a cyclic voltamagram is taken to verify the nature of the adsorbed species.

Results for hydroquinone adsorption on Pt at open circuit as a function of solution concentration are shown in Figure 2. Surface coverages, as determined by cyclic voltammetry are listed in parentheses. The important result is that the CH stretching band only became apparent above a critical solution and surface concentration. Based on the surface dipole selectrion rule for adsorbed species these results indicate that a molecular orientation change of hydroquinone is induced as a function of concentration. Similar results have also been obtained for benzoquinone. In addition the spectra for benzoquinone are nearly identical to those obtained for hydroquinone indicating that benzoquinone adsorbs on the surface by an oxidative process to produce a diphenolic species. These orientation changes are important as the products from the oxidation of the adsorbed species have been shown to change as a function of solution concentration, indicating a correlation between surface structure and surface reaction.

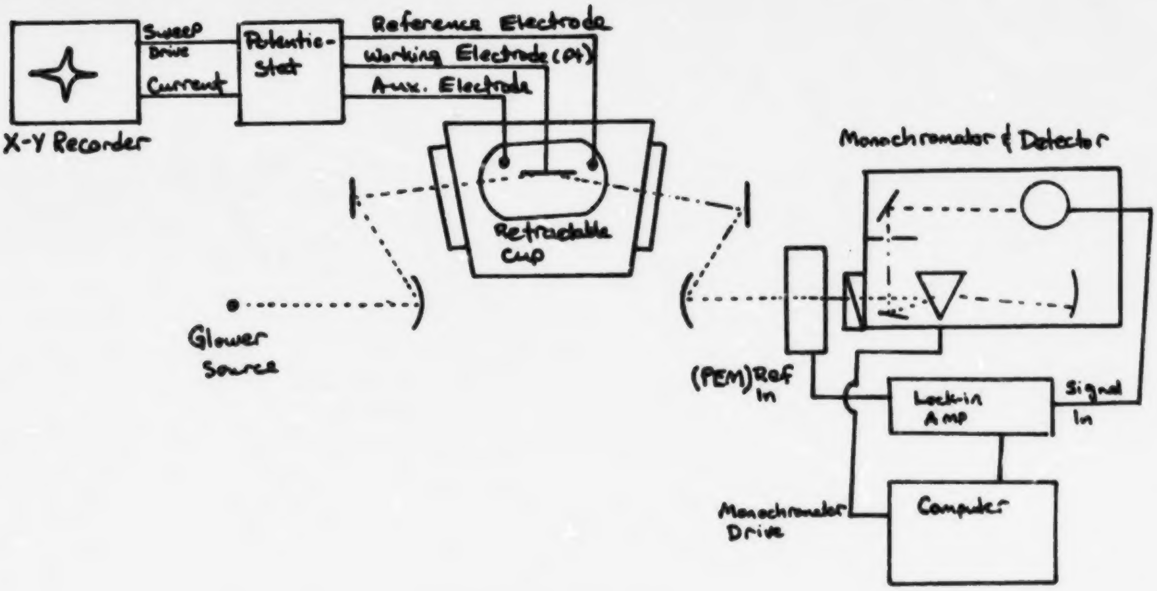
Sweep Drive
Current
Potentio-stat
Reference Electrode
Working Electrode (Pt)
Aux. Electrode
X-Y Recorder
Retractable cup
Glower Source
Monochromator & Detector
(PEM) Ref In
Lock-in Amp
Signal In
Computer
Monochromator Drive

Figure 1 Electrochemical Cell

Figure 2 Hydroquinone Adsorption

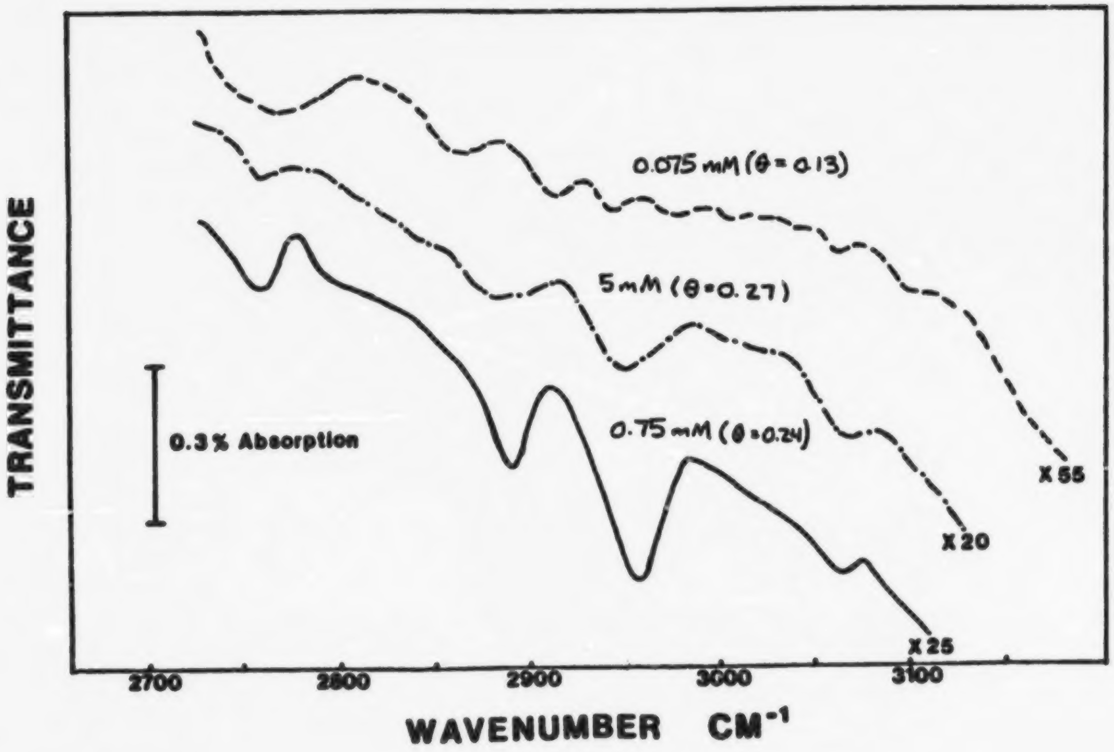

PICOSECOND LASER STUDIES OF ENERGY TRANSFER IN MOLECULES ON SURFACES

R. R. Cavanagh
J. C. Stephenson
Center for Chemical Physics
National Bureau of Standards
Gaithersburg, MD 20899

Real-time measurements of energy transfer at the gas-solid and liquid-solid interface can provide unique insight into chemical, optical, and particle induced materials modification. The focus of this program has been in elucidating the vibrational relaxation time (T_1) of small molecules bound to surfaces using infrared picosecond laser pulses. T_1 was obtained for OH ($\nu_{stretch}$=1) in the strongly bound "isolated sites" of fumed silica (SiO_2) particles in vacuum and dispersed in several liquids. We have preliminary results for several other chemisorbed surface species, including OD (deuterated OH) and NH_2 on SiO_2, and OH on B_2O_3.

The experimental method to determine T_1 was a picosecond infrared saturation and ground state recovery technique. The surface OH v=0 → 1 transition was excited with a strong picosecond IR pulse. Due to anharmonicity, the OH(v=1) species does not absorb at the pump frequency, so transfer of population to the v=1 level causes an increase in sample transmission. As v=1 population relaxes, the sample transmission returns to its equilibrium (unexcited) value, T_o. The rate of recovery of T is determined by a second weak picosecond probe pulse at the same frequency, delayed at time t_D (ps) after the pump pulse. The measurement of T (t_D) vs. t_D gives directly the vibrational relaxation rate T_1^{-1} for surface bound OH. The quantity $\ln(T/T_o)$ is proportionl to OH(v=1), and as expected decays exponentially with t_D after the pump pulse.

The apparatus is shown in Fig. 1. Tunable psec IR pulses are generated in a three-stage $LiNbO_3$ optical parametric amplifier (OPA) which is pumped by the output pulses (35 mJ, 1.064 μm, 10 Hz) of a modelocked Nd^{+3}-YAG laser. Further details about the laser system are in Refs. 1-4.

The surface sites for OH on SiO_2 are depicted in Fig. 2. Typical relaxation time data are shown in Fig. 3 for OH(v=1) on an evacuated SiO_2 pressed disk at room temperature. The average of many such decays gave T_1=204±20ps. When the SiO_2 particles are surrounded by solvents, the relaxation time of the surface OH(v=1) groups decreases: for the liquids CCl_4, CF_2Br_2, CH_2Cl_2, and C_6H_6, T_1(ps) = 159 ± 16, 140 ± 30, 102 ± 20, and 87 ± 30, respectively. T_1 does not depend on the size of the SiO_2 particles for the range 70Å ≤ diameter ≤ 150Å, or on the surface OH coverage up to an average density of 4 OH/100Å^2. Significant amounts of physisorbed water (5 H_2O/100Å^2) decreased T_1 for the isolated OH(v=1) to T_1 = 56 ± 10ps. For comparison to the surface hydroxyls, the vibrational deactivation time for OH(v=1) groups in the bulk of fused silica (OH/SiO_2 = 130 ppm by weight) was determined to be T_1 = 109 ± 11ps.

The results have been interpreted in terms of a mechanism involving multi-phonon relaxation to nearby Si-O stretching vibrations ($\nu_{Si-O} \simeq 1000\ cm^{-1}$). Energy relaxation is not caused by Förster-type energy transfer from one surface site to another, from surface to bulk OH, or among bulk OH sites. Vibrational relaxation of the surface OH is not caused by damping due to coupling to image dipoles in the SiO_2.

It has been popular to interpret the widths of spectral lines observed in surface vibrational spectroscopy (IR reflection, transmission, Raman, EELS, neutron scattering) in terms of T_1 broadening mechanisms. Our results, which are the first direct time-resolved measurements of energy transfer involving chemical bonds on surfaces, suggest that this interpretation should be used cautiously. The observed T_1 for OH on SiO_2 corresponds to an uncertainty-principle vibrational linewidth of 0.025 cm^{-1}. The observed spectral linewidths are 200-2000 times broader than this, so that the common interpretation of surface linewidth as a measure of T_1 is clearly inappropriate for these samples.

The long T_1 for these surface vibrations may be important because vibrational excitation greatly influences chemical reactivity. Vibrational excitation in molecules on surfaces, whether photon induced or caused by a chemical reaction, may last longer than times for molecular reorientation or diffusion to active surface sites. It may be possible to assess whether slow vibrational relaxation at surfaces is generally important by doing these VET measurements on many more adsorbates and substrates.

1. E. J. Heilweil, M. P. Casassa, R. R. Cavanagh, and J. C. Stephenson, J. Chem. Phys. 81, 2856 (1984).

2. J. T. Knudtson and J. C. Stephenson, Chem. Phys. Letts. 107, 385 (1984).

3. M. P. Casassa, E. J. Heilweil, J. C. Stephenson, and R. R. Cavanagh, "Time-Resolved Measurements of Vibrational Relaxation of Molecules on Surfaces: Hydroxyl Group on Silica Surfaces," J. Vac. Sci. Tech. (in press).

4. E. J. Heilweil, M. P. Casassa, R. R. Cavanagh, and J. C. Stephenson, "Vibrational Deactivation of Surface OH Chemisorbed on SiO_2: Solvent Effects," submitted to J. Chem. Phys.

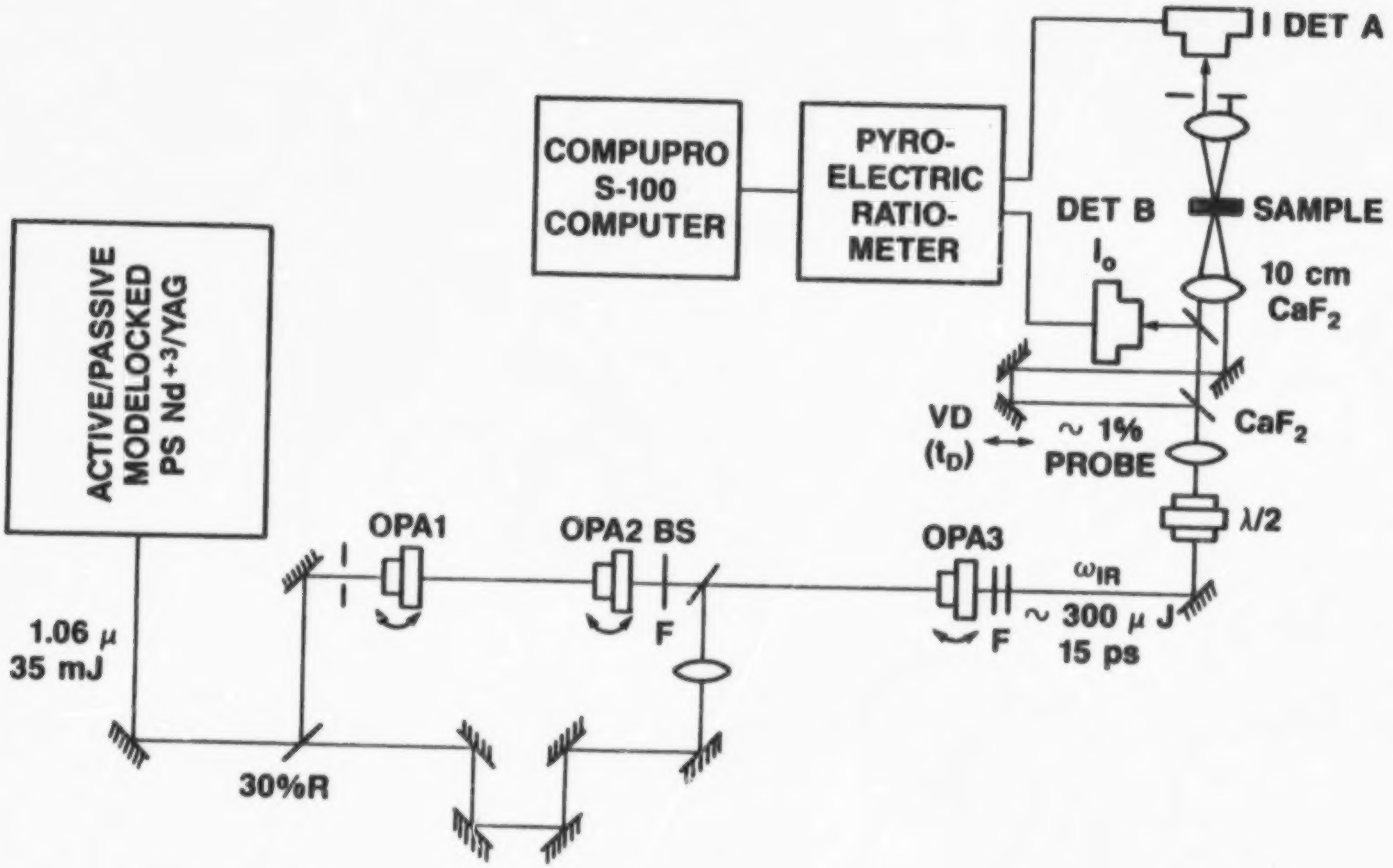
I DET A
COMPUPRO S-100 COMPUTER
PYRO-ELECTRIC RATIO-METER
DET B
SAMPLE
I_o
10 cm CaF_2
ACTIVE/PASSIVE MODELOCKED PS Nd^{+3}/YAG
VD (t_D)
~ 1% PROBE
CaF_2
$\lambda/2$
OPA1
OPA2 BS
OPA3
ω_{IR}
F
F
~ 300 μ J
15 ps
1.06 μ
35 mJ
30%R

Fig. 1

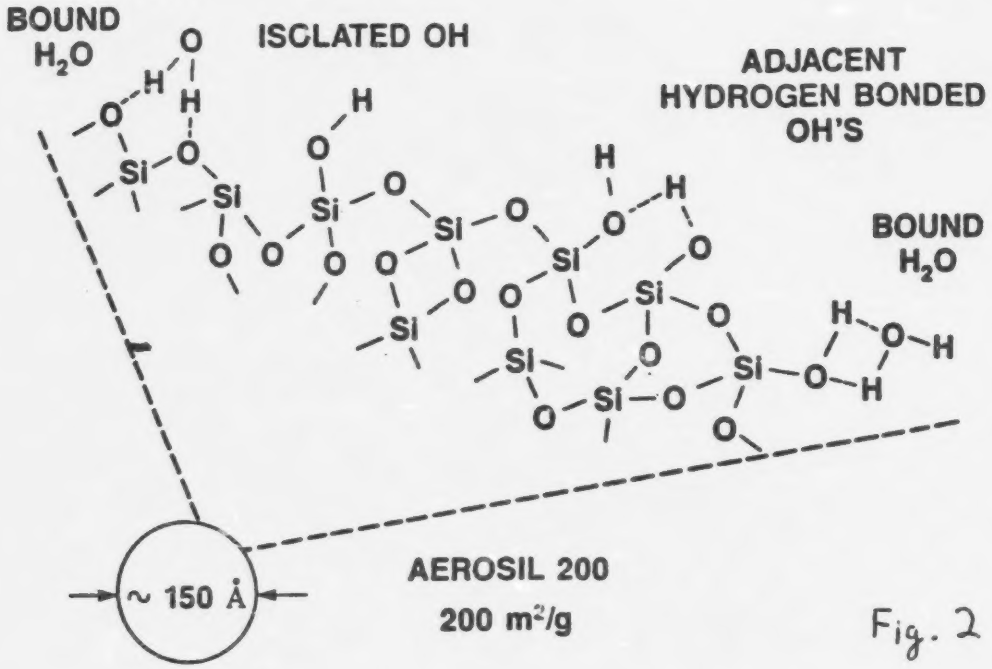
BOUND
H$_2$O
ISOLATED OH
ADJACENT
HYDROGEN BONDED
OH'S
BOUND
H$_2$O
~ 150 Å
AEROSIL 200
200 m^2/g

Fig. 2

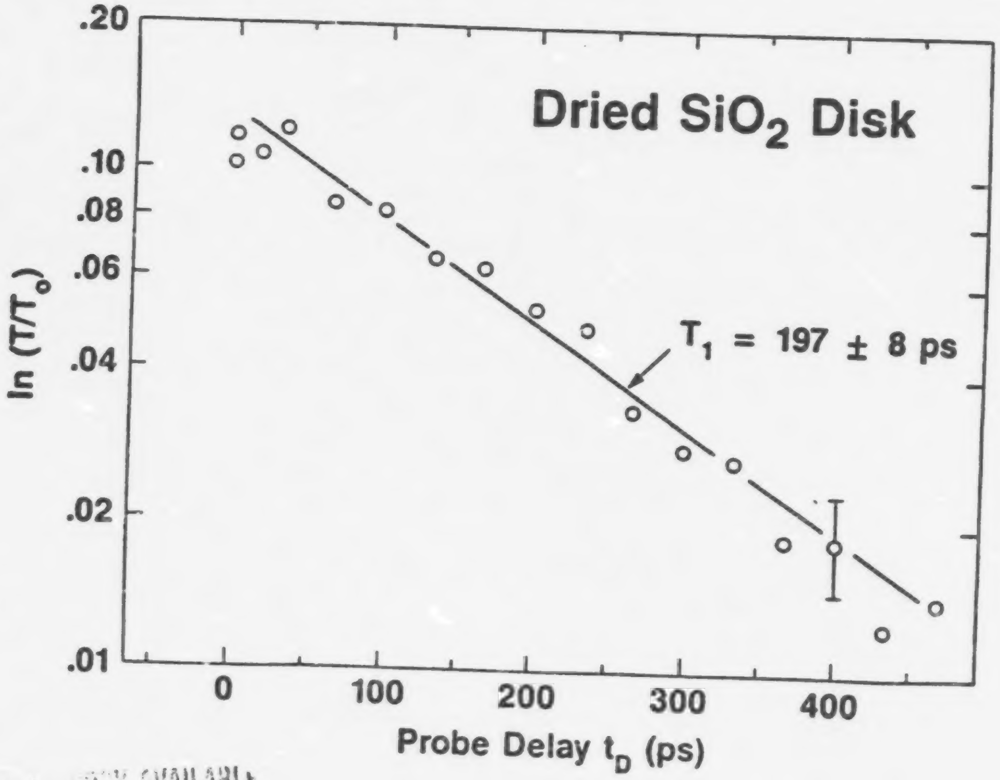
Dried SiO$_2$ Disk
T$_1$ = 197 ± 8 ps
ln (T/T$_o$)
.20
.10
.08
.06
.04
.02
.01
0
100
200
300
400
Probe Delay t$_D$ (ps)

Fig. 3

MOLECULAR DYNAMICS AND SPECTROSCOPY AT SOLID SURFACES

THOMAS F. GEORGE
Department of Chemistry, University of Rochester
Rochester, New York 14627

Theoretical studies have been carried out for molecular dynamical processes occurring at solid surfaces. These processes include electron transfer in ion-surface scattering, electron-hole pair formation in a semiconductor by vibrationally-excited molecules and relaxation of laser-excited adspecies. Spectroscopic processes have also been studied, including resonance fluorescence of atoms near a metal surface, laser-induced surface excitations on a grating and static electric field effects at the surface of a metallic cluster.

Two topics will be addressed here. The first topic is negative-ion formation from positive-ion-surface scattering at finite temperatures. In treating this two-electron transfer process, we have gone one step further than previous theories by including the effects of the correlation energy U arising from the Coulombic repulsion between the two electrons of opposite spin in the same valence level of the ion. The time-dependent probability of negative-ion formation at temperature T is given by

$$P_T(t) = \int_{\varepsilon_L-\varepsilon_d}^{\varepsilon_U-\varepsilon_d} d\varepsilon\, \rho(\varepsilon)\, f(\varepsilon) \int_{\varepsilon_L-\varepsilon_d}^{\varepsilon_U-\varepsilon_d} d\varepsilon'\rho(\varepsilon')\, f(\varepsilon')\, \left|\langle k_\uparrow k'_\downarrow|\, \tilde{T}^{(2)}(t,-\infty)\, I\rangle\right|^2 ,$$

where $\varepsilon = \varepsilon_k-\varepsilon_d$ with k and d denoting states of the conduction band of the solid and the valence level of the ion, respectively, $\rho(\varepsilon)$ is the density of states of the conduction band, $f(\varepsilon)$ is the Fermi-Dirac distribution of electrons in the solid, $\tilde{T}^{(2)}$ is the time-evolution operator expressed in the interaction picture to second order, and the other quantities are explained in Figure 1. The second topic is resonance fluorescence of a two-level atom near a metal surface, where we have obtained the power spectrum for the case of a strong driving laser field by solving a set of surface-dressed optical Bloch equations which describe multiphoton effects of the surface-reflected field and the surface plasmon resonance.

In the above equation, $P_T(\infty)$ corresponds to the experimental observation of outgoing negative ions after the scattering event is complete, and calculations of $P_T(\infty)$ for $T = 0K$ are in good agreement with molecular beam experiments on the conversion of $H^+(D^+)$ to $H^-(D^-)$ by scattering from a cesiated W(100) surface. The calculations indicate that the correlation energy U plays an important role. At finite temperatures, the electrons in the solid lying within the range of k_BT below the Fermi level can be thermally activated. The thermal energy may then be used to overcome the extra energy barrier U for the second electron, provided $k_BT \geq U$, and thus enhance negative-ion formation, as shown by means of a model calculation in Figure 2. In regard to the study of resonance fluorescence of a two-level atom near a metal surface, for a sufficiently strong driving laser field of frequency ω_L, the emission spectrum exhibits three peaks: a central one at $\omega_0 = \omega_L$ (Rayleigh component), a left one at $\omega_- = 2\omega_L - \omega_{21} - \delta$ (three-photon component) and a right one at $\omega_+ = \omega_{21} + \delta$ (fluorescence component), where ω_{21} is the frequency difference between the adatomic levels and δ is the ac Stark shift. Results for the peak heights H_-, H_0 and H_+ are shown in Figure 3 for the case of a silver surface. The key feature, which is a unique behavior due to the surface, is that for certain adatom-surface distances H_- is larger than H_+, whereas in the pure gas-phase resonance fluorescence spectrum H_- is always less then H_+ (due to molecular collisions for positive detuning).

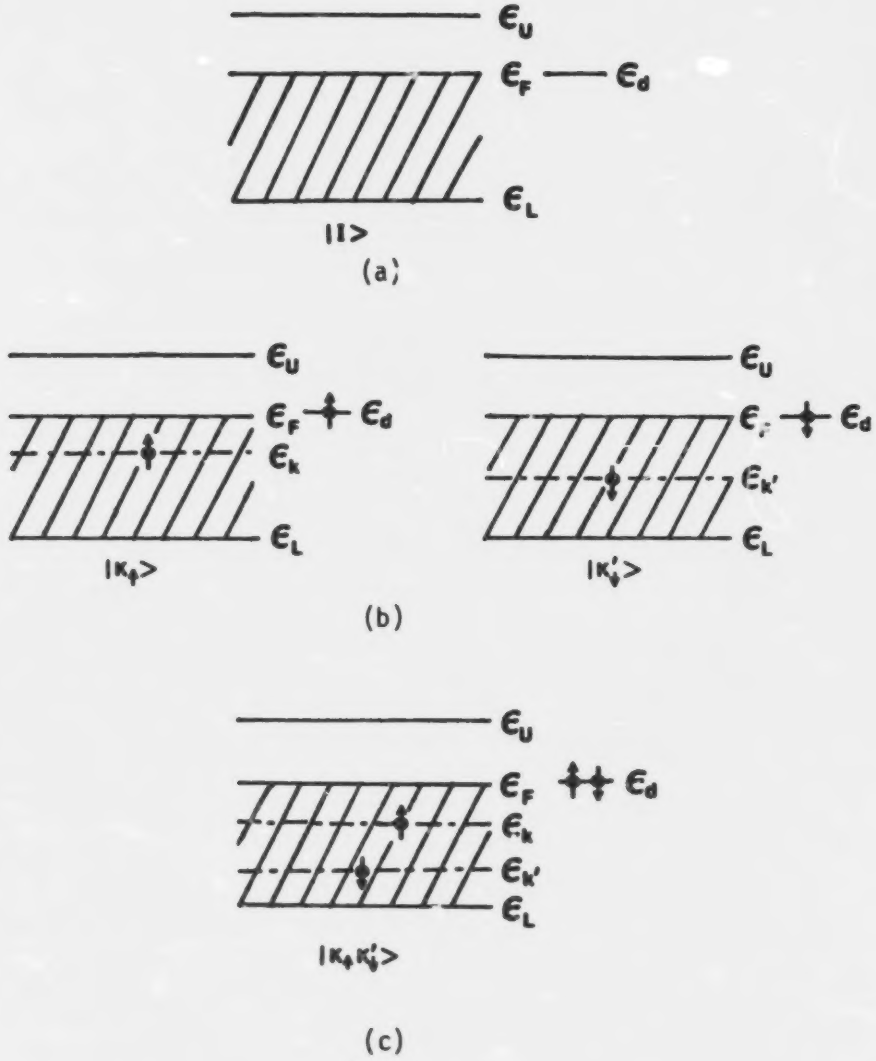
ϵ_U
ϵ_F
ϵ_d
ϵ_L
|I>
(a)
ϵ_U
ϵ_F
ϵ_d
ϵ_k
ϵ_L
$|k_\uparrow>$
ϵ_U
ϵ_F
ϵ_d
$\epsilon_{k'}$
ϵ_L
$|k'_\downarrow>$
(b)
ϵ_U
ϵ_F
ϵ_d
ϵ_k
$\epsilon_{k'}$
ϵ_L
$|k_\uparrow k'_\downarrow>$
(c)

Figure 1. Schematic diagram of electron transfer in negative-ion formation. ε_U is the upper and ε_L the lower edge of the band. (a) Initial state $|I>$: valence state ε_d empty, band filled up to the Fermi level ε_F. (b) Intermediate states $|k_\uparrow>$ and $|k'_\downarrow>$: states corresponding to the neutralized atom; one electron transferred from the ε_k or $\varepsilon_{k'}$ level to the ε_d level. The arrows denote the spin states of the electrons, and the solid and hollow circles represent electrons and holes, respectively. (c) Final states $|k_\uparrow k'_\downarrow>$: negative-ion states; two electrons transferred to the ε_d level.

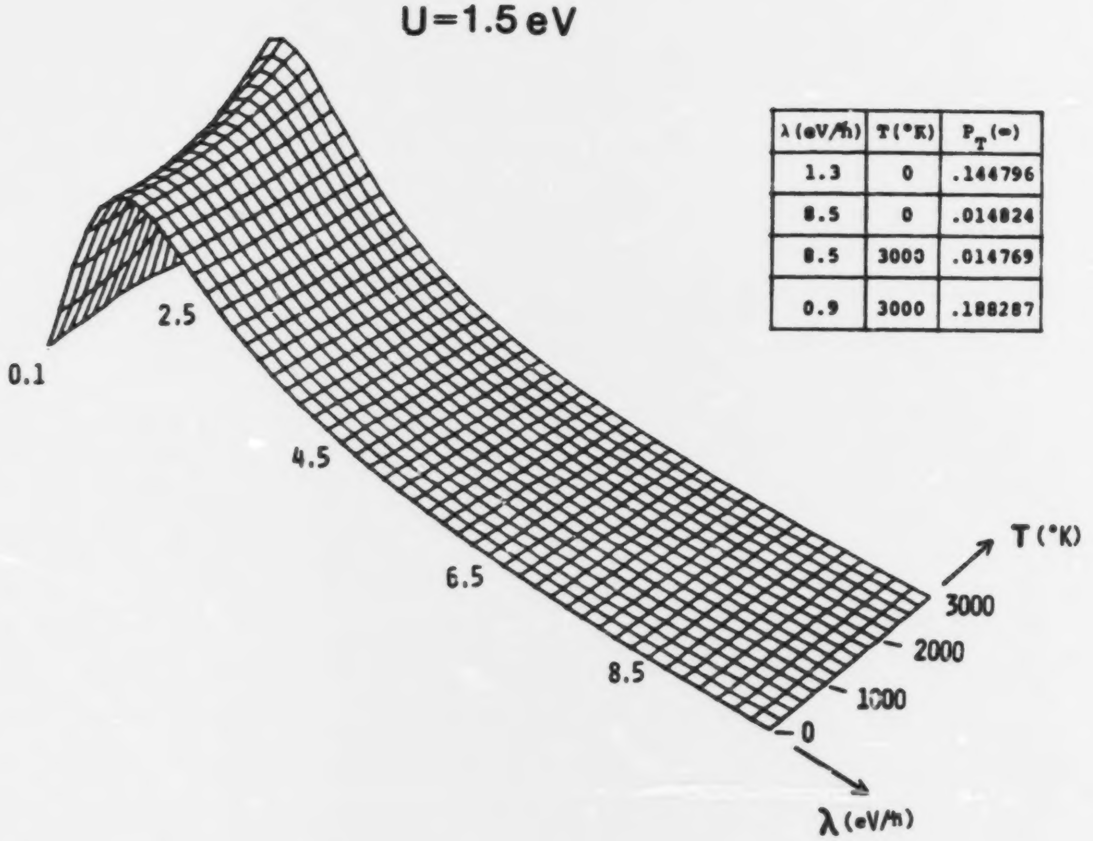

λ (eV/ħ)	T (°K)	$P_T(\infty)$
1.3	0	.144796
8.5	0	.014824
8.5	3000	.014769
0.9	3000	.188287

Figure 2. $P_T(\infty)$ vs λ and T for the following parameter values: $U = 1.5$ eV, $\varepsilon_L = -10$ eV, $\varepsilon_U = 5$ eV, $\varepsilon_F - \varepsilon_d = -0.06$ eV and $\rho V^2 = 0.43$ eV. The time-dependent interaction matrix element connecting the valence state of the impact ion with a conduction band state of the solid is given as $V\exp(-\lambda|t|)$, where λ is a measure of the inverse of the duration of this bound-continuum interaction.

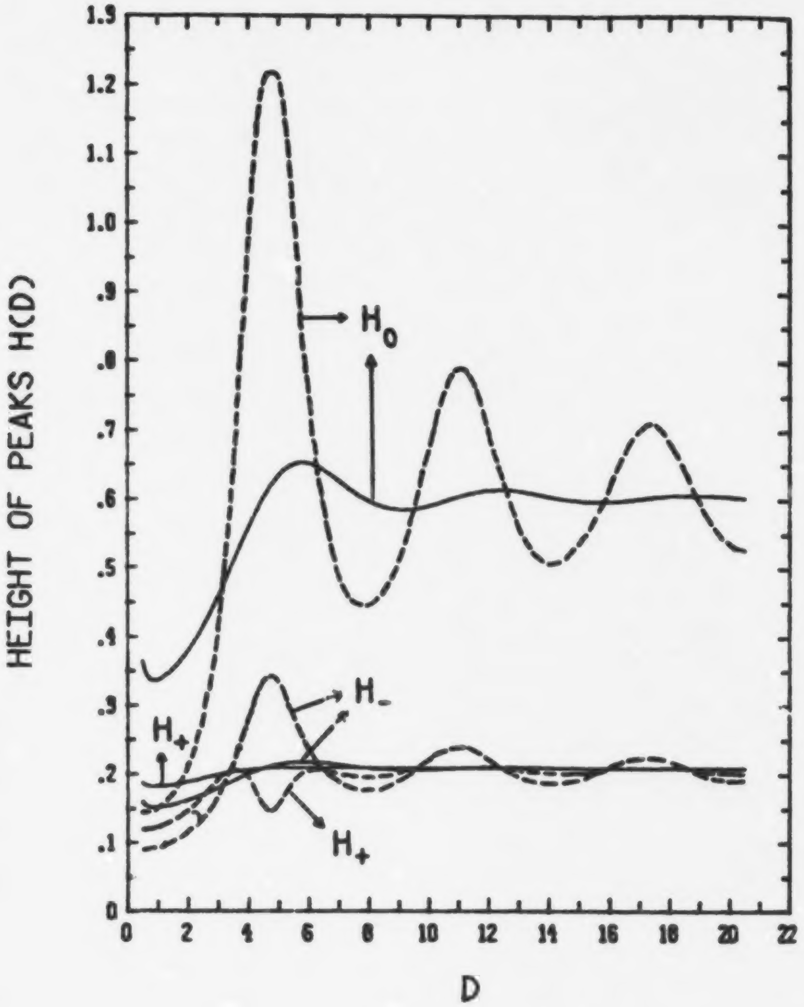

Figure 3. Adatom-surface distance dependence of the heights of the three peaks in the resonance fluorescence spectrum for the case of a silver surface, where H_-, H_0 and H_+ correspond to the peak heights (in arbitrary units) of the three-photon, incoherent Rayleigh and fluorescence components, respectively. D = 2kd is the reduced distance, where k is the wavenumber and d is the adatom-surface distance. The Drude model is used for the dielectric function of the metal, while the dielectric function of the gas medium is set equal to one. The detuning $\omega_{21} - \omega_L$ is 1 A and the Rabi frequency is 10 A, in the unit of Einstein's A coefficient. The solid curves are for the induced transition dipole of the adatom oriented perpendicular to the surface, and the dashed curves are for the parallel case.

BEST COPY AVAILABLE

THEORETICAL INVESTIGATIONS OF HOMOGENEOUS AND HETEROGENEOUS REACTIONS IN CHEMICAL VAPOR DEPOSITION OF SILICON FROM SILANE

L. M. Raff and D. L. Thompson
Department of Chemistry, Oklahoma State University
Stillwater, Oklahoma 74078

Because of its practical applications it is important that detailed mechanisms of chemical vapor deposition (CVD) be understood, particularly in the case of silicon. There are considerably experimental data that provide information about the process, but the exact mechanism is not known. We are carrying out theoretical studies in an effort to determine the relative importance of various elementary processes that may play a role in silicon CVD from silane. The processes being studied are illustrated in Fig. 1; they include: Unimolecular dissociation of SiH_4 and SiH_2, polymerization of SiH_2, nucleation of Si, gas/surface scattering, surface adatom migration, surface adsorption, and surface reactions.

The homogeneous unimolecular dissociation of SiH_4 (and CH_4) has been investigated using quasiclassical trajectories and Monte Carlo statistical theories. The trajectory results give linear decay curves (Fig. 2a), unimolecular falloff curves in agreement with experiment (Fig. 2b), and predict product translational energy distributions. The major SiH_4 decomposition channel leads to $SiH_2 + H_2$ products with a high-pressure limiting rate of $(1.085 \pm 0.02)\ \exp(-49{,}600\ \text{kcal/mole/RT})\text{s}^{-1}$. The statistical methods used to investigate the SiH_4 and CH_4 dissociation reactions include a Monte Carlo transition-state theory and a random walk procedure previously suggested by Doll. Microcanonical rate coefficients computed by these methods are found to be in excellent agreement with the corresponding trajectory results (Fig. 2c). In general, the statistical methods require an order of magnitude less computer time than do the trajectory calculations.

The unimolecular dissociation dynamics of SiH_2 are currently being computed by trajectory and statistical methods on a potential-energy surface obtained by combining the results of CI and SCF calculations with valence-bond procedures. This surface gives the correct reactant and product energies for all reaction channels. A small barrier to the back reaction $Si + H_2 \rightarrow SiH_2$ is predicted.

Surface adsorption and diffusion of Si atoms on Si(100) and Si(111) surfaces have been investigated using trajectory methods. The surfaces are modelled by explicit consideration of the first three atomic layers using a model developed by Keating to treat the elastic strain energy of tetrahedral crystals. The calculated sticking probabilities for Si atoms on a Si(100) surface are found to be near unity at all temperatures. Surface diffusion coefficients and activation energies for Si diffusion are computed from the time variation of the mean-square displacements, the velocity auto-correlation functions, Fig. 2d and 2e, respectively, and the jump frequencies of the adatom between adjacent adsorption sites. A new method to compute both upper and lower bounds for the diffusion coefficient has also been developed.

The recombination and desorption rates of H_2 on silicon surfaces are being computed using Doll's procedure modified by the incorporation of appropriate importance sampling methods. The potential surfaces are obtained by extension of the methods used in our studies of surface adsorption and diffusion.

Si Chemical Vapor Deposition

$SiH_4 \rightarrow SiH_3 + H$

$SiH_4 \rightarrow SiH_2 + H_2$

$SiH_2 \rightarrow Si_2H_4$

$SiH_2 \rightarrow SiH + H$

$SiH_2 \rightarrow Si + H_2$

$Si + Si + M \rightarrow Si_2 + M$

$Si_2 + Si + M \rightarrow Si_3 + M$

Gas-Phase Reactions

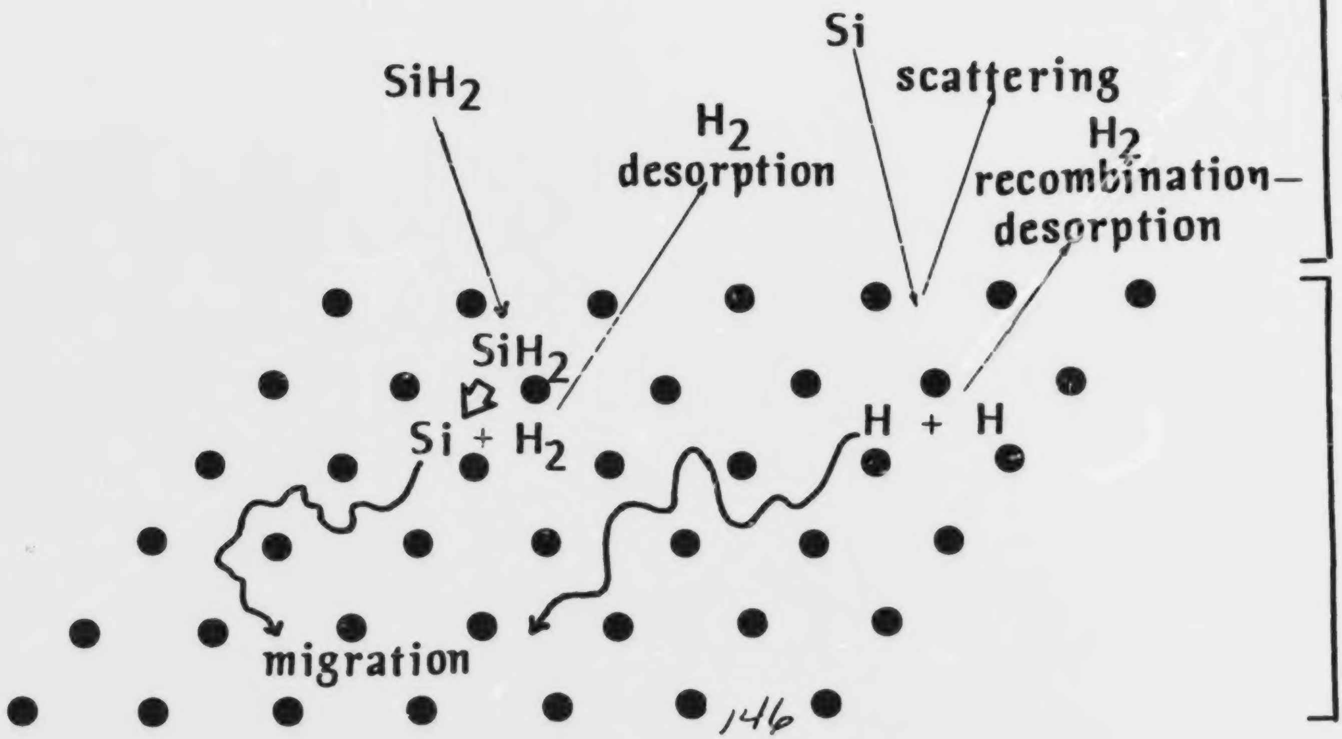

SiH₂
H₂ desorption
Si
scattering
H₂ recombination–desorption
SiH₂
Si + H₂
H + H
migration

Adsorption/ Desorption

Surface Processes

Fig. 1

FIGURE 2

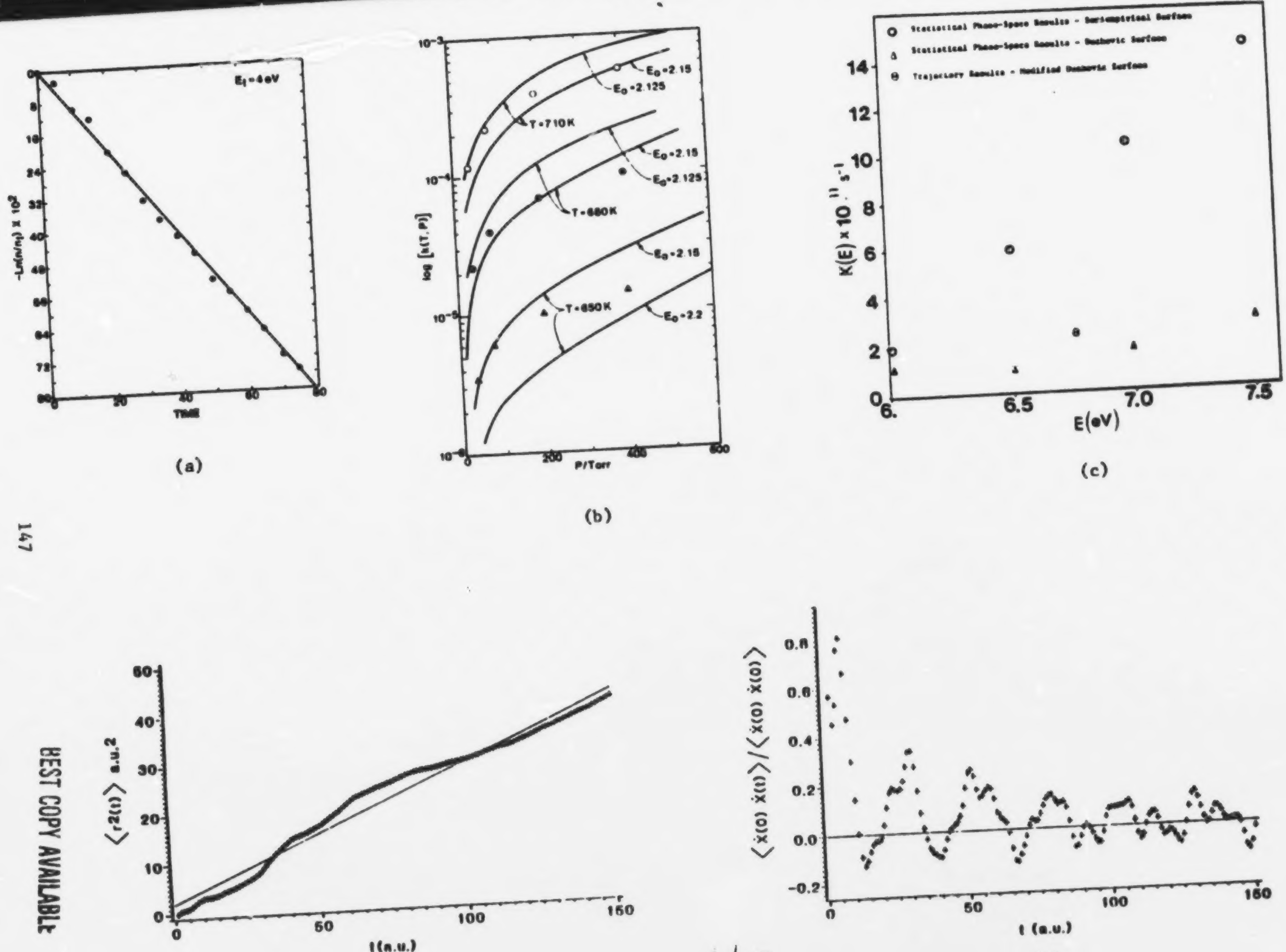

(a)

(b)

(c)

(d)

(e)

147

Dynamics of Gas-Surface Interactions

Steven J. Sibener

The James Franck Institute and
Department of Chemistry
The University of Chicago
5640 South Ellis Avenue
Chicago, IL 60637

This new research initiative deals with the scattering of atomic and molecular beams from well-characterized single crystal surfaces. These studies are motivated by a desire to understand and control catalytic surface chemistry, the technological need to characterize the physical properties of thin films and surfaces, and the desire to understand how energy and momentum are exchanged at the surface of a material when it is subjected to gas-surface collisions, optical illumination, or chemical reaction. Experiments aimed at determining the surface phonon dispersion relations for a variety of systems will play a central role in this program. Especial attention will be given to elucidating which surface vibrational modes actively participate in collision induced energy exchange, determining under which energy regimes single and multiphonon transitions dominate, and determining when electron-hole pair generation becomes a significant energy absorption mechanism.

The proposed scattering experiments will be carried out in a new ultra-high vacuum beam-surface scattering apparatus which is currently under construction. When completed, this instrument will be uniquely suited for studying inelastic scattering events as its design goals were to simultaneously achieve an extremely low helium background in its detector, high angular resolution (important for 2-dimensional melting dynamics and surface morphology investigations), and excellent time-of-flight energy resolution (< 200μeV). The instrument is shown schematically in Figure 1. The design stage for this instrument has been completed, with fabrication and assembly now taking place.

The actual surface phonon measurements will be accomplished utilizing angle and velocity resolved inelastic neutral particle scattering as the dynamical probe. These experiments can be visualized as being a direct two-dimensional, i.e., surface sensitive analog to inelastic neutron scattering. In our laboratory we have recently demonstrated the feasibility of using inelastic atom scattering for determining how the surface vibrational frequencies of evaporated thin films evolve on a layer-by-layer basis into those of thick crystals. Figure 2 shows a typical time-of-flight spectrum from that study. This spectrum was taken in our current apparatus using a prototype of the new machine's high Mach number cryogenic beam source.

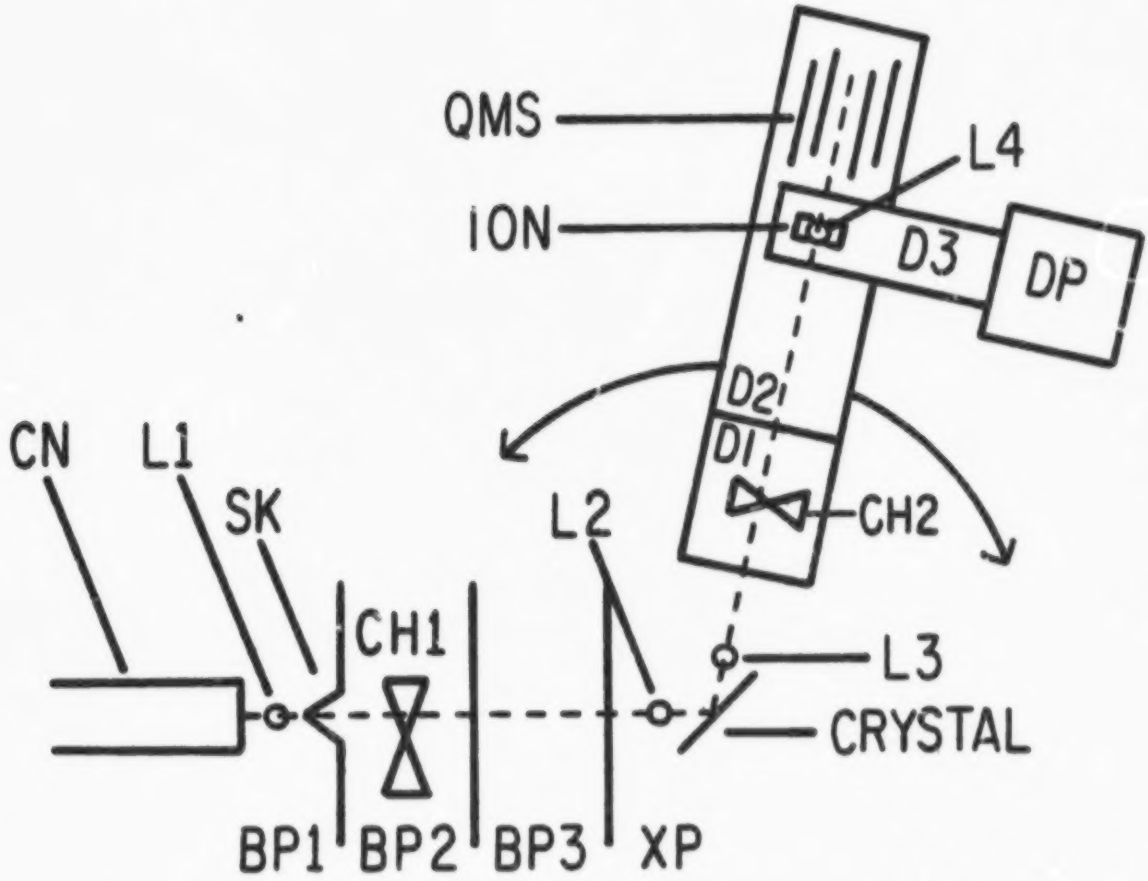

FIGURE 1

Schematic representation of the ultra-high vacuum scattering apparatus. BP1, BP2, and BP3 are the three beam pumping stages, XP is the crystal pumping region, while D1, D2, and D3 are the three stages of differential pumping in the detector. D3 is pumped by a turbomolecular pump which is in turn backed by a diffusion pump. CN: cryogenic nozzle, SK: skimmer, CH1: incident beam chopper, CH2: post-collision chopper, L1-L4: laser-molecular beam intersection zones, ION: electron bombardment ionizer, QMS: quadrupole mass spectrometer. The instrument supports two beam sources which can be connected at five positions. The crystal-to-ionizer distance can be easily varied between 45 and 100 cm. The crystal chamber is equipped with a variety of surface analysis instruments which are not portrayed in this figure.

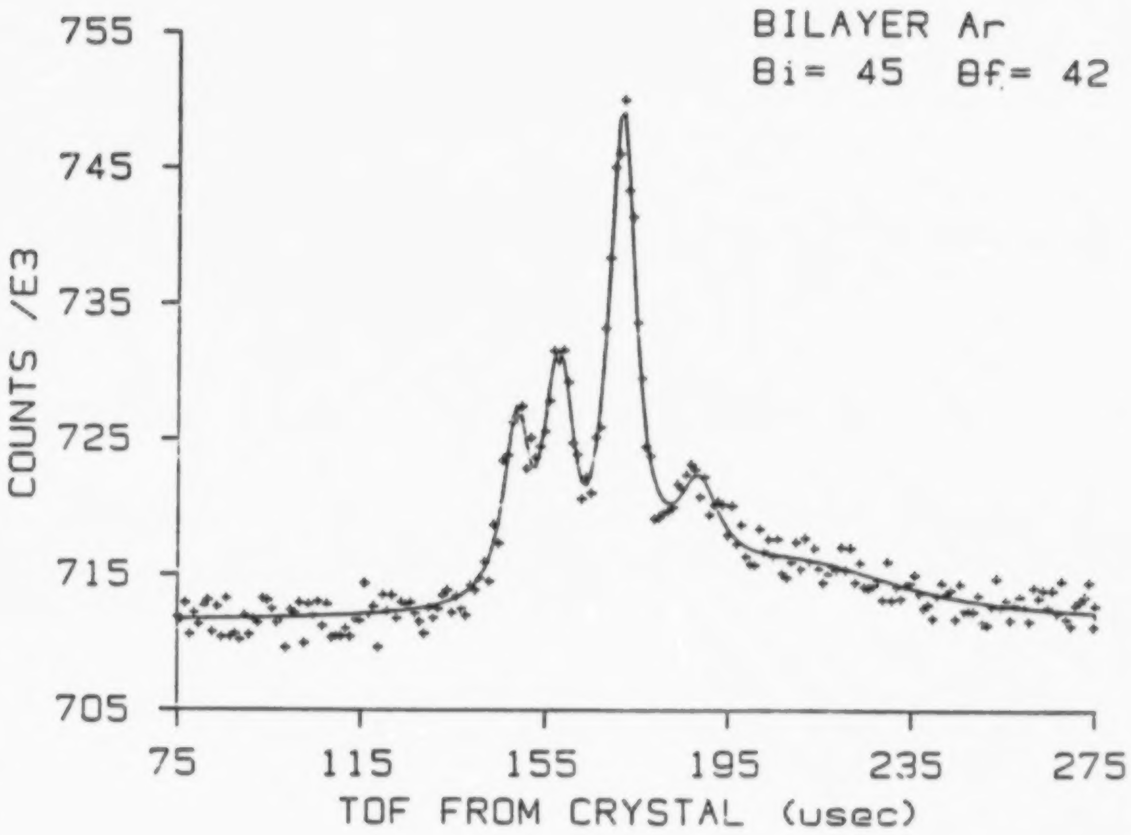

FIGURE 2

Time-of-flight spectrum of 18 meV He atoms reflecting from an Ar(111) bilayer physisorbed on Ag(111). Single phonon creation and annihilation peaks are clearly seen. The peak at ∿160μsec is the elastic peak.

SURFACE PRODUCTION AND LOSS OF EXCITED STATES OF O_2

TOM G. SLANGER
Chemical Physics Laboratory
SRI International
Menlo Park, CA 94025

The rationale of this research program is to develop an understanding of the factors that govern the efficiency of production of electronically excited O_2 molecules from surface recombination of oxygen atoms. An integral part of such a study is to evaluate the surface losses of these states.

During the last twelve months, we have concentrated on making measurements of the loss rates of $O_2(a^1\Delta_g)$ on a variety of surfaces, both metallic and organic, in order to develop a data base for making predictions of the efficiency of O_2(a) removal by different materials.

The apparatus is a discharge flow system in which, for this application, O_2(a) is generated by a microwave discharge in O_2/He. The resultant atoms are removed by passage of the gas stream over an HgO surface, and the discharge-produced O_2(a) is monitored downstream by vuv absorption at 1285 A. Samples mounted on an aluminum holder are lowered into the stream and their effect on the downstream O_2(a) concentration is observed. It has been established that aluminum itself does not discernibly quench O_2(a).

In Table 1 are shown the recent results, ordered by decreasing O_2(a) removal efficiency. By comparison of the loss ratios for a given sample size, it is apparent that the most effective metals are Cu, Ag, and Co, followed by Fe, Ni, Pd, and Pt. On a periodic table, these seven metals are contiguous, and what is particularly striking is that this group contains the metals - Ni, Pd, and Pt - which we have shown to be the most effective at generating the 4-5 eV O_2 from $O(^3P)$ surface recombination. Harteck and co-workers have also found Co and Fe to be effective in this respect, so that except for Cu and Ag. there is a qualitative equivalence between those metals generating the 4-5 eV O_2 states and those that destroy O_2(a). A realistic model must predict both of these effects, which are in a certain sense contradictory, as effective surface loss of O_2(a) suggests that there is good coupling between the O_2 and the surface phonons, whereas loss of surface-produced O_2^* without energy accomodation indicates the opposite.

The data in Table 1 also show that the O_2(a) destruction efficiency is independent of gross surface treatment, which implies that in all cases the surfaces seen by the O_2(a) are metallic oxides, a not unexpected conclusion. Of the substantial number of organic materials tested, all have activities comparable to those of the most inert metals.

TABLE 1

RELATIVE $O_2(a^1\Delta_g)$ SURFACE LOSS RATES

Surface	$[O_2(a)]_o/[O_2(a)]$	Sample Size
Cu	2.25±0.15	A
Cu(acid-cleaned)	4.77	B
Cu(oxidized)	4.52	B
Ag	2.00	A
Monel(Cu/Ni)	1.90	A
Co	1.90±0.05	A
Fe	1.50±0.05	A
Ni	1.50±0.05	A
Ni(uncleaned)	4.30	B
Ni(acid-cleaned)	4.00	B
Pb	1.34	A
Mn	1.25	A
Sn	1.22±0.02	A
Cr	1.19	A
Mo	1.17±0.03	A
Zn	1.17	A
Ta	1.12±0.03	A
Al	1.10±0.05	A
Hg	1.04	A
Cu	1.53	C
Ni	1.33	C
Pd	1.32±0.03	C
Pt	1.27	C
Rh	1.19±0.02	C
Ir	1.10±0.08	C
Sc	1.10±0.04	C
In	1.07±0.05	C
Au	1.06±0.03	C
W	1.05±0.02	C
Ti	1.05±0.03	C
Zr	1.05	C
Scotchguard	1.04	A
PVC	1.05	A
Graphite	1.28	1.4"x2"
Alumina	1.04	A

Sample Sizes		
	A	2"x2"
	B	cylindrical configuration
	C	1"x1"

AVAILABLE

INVESTIGATION OF COUPLED SURFACE AND BULK REACTION PHENOMENA USING COMBINED-BACKSCATTER-CONVERSION ELECTRON AND BACKSCATTER-PHOTON MÖSSBAUER SPECTROSCOPY (CEAPS)

Bruce J. Tatarchuk
Department of Chemical Engineering
Auburn University, Alabama 36849

Mössbauer spectroscopy performed in transmission geometry is a powerful physiochemical technique for obtaining information from the bulk. Relaxation, following a resonant nuclear absorption event, however, favors production of a conversion electron and subsequent Auger electrons and/or fluorescent x-rays rather than reemission of the resonant γ-ray. The goal of this recently initiated study, is to construct and utilize a new spectrometer to monitor the energy spectrum of backscattered-relaxation events in order to obtain depth-profiled information in a nondestructive fashion. By monitoring both backscattered-electrons and backscattered-photons, information from the topmost 1 nm to 20 μm will be obtained. This insight will be used to investigate: (i) the effects of submonolayer quantities of surface metals to assist/retard in the formation/discharge of surface metal hydrides, (ii) the ability and mechanisms by which ion implantation mixes layered-substrates at various depths, and (iii) the influences of ion implantation and surface chemical treatments to alter the depth-dependent transport of cations, anions and defects during oxidative treatments.

Figure 1 depicts the fashion in which backscatter-spectra are simultaneously obtained at: two different photon energies (i.e., energy windows) and seven or more electron energies. This is accomplished using a single germanium detector and seven different electron detectors to increase the effective solid angle of detection. Figure 2 illustrates the procedure in which backscattered-Mössbauer spectra, collected at various energies, are deconvoluted according to depth.

References

1. Tatarchuk, B. J. and Dumesic, J. A., "Backscatter-Mössbauer Spectroscopy: Applications to Surface and Catalytic Phenomena," in Chemistry and Physics of Solid Surfaces, Chapter 4, Volume 35, Springer-Verlag, in press.

2. Sawicki, J. A. and Sawicka, B. D., "Experimental Techniques for Conversion Electron Mössbauer Spectroscopy", in Hyperfine Interactions, 13, 199 (1983).

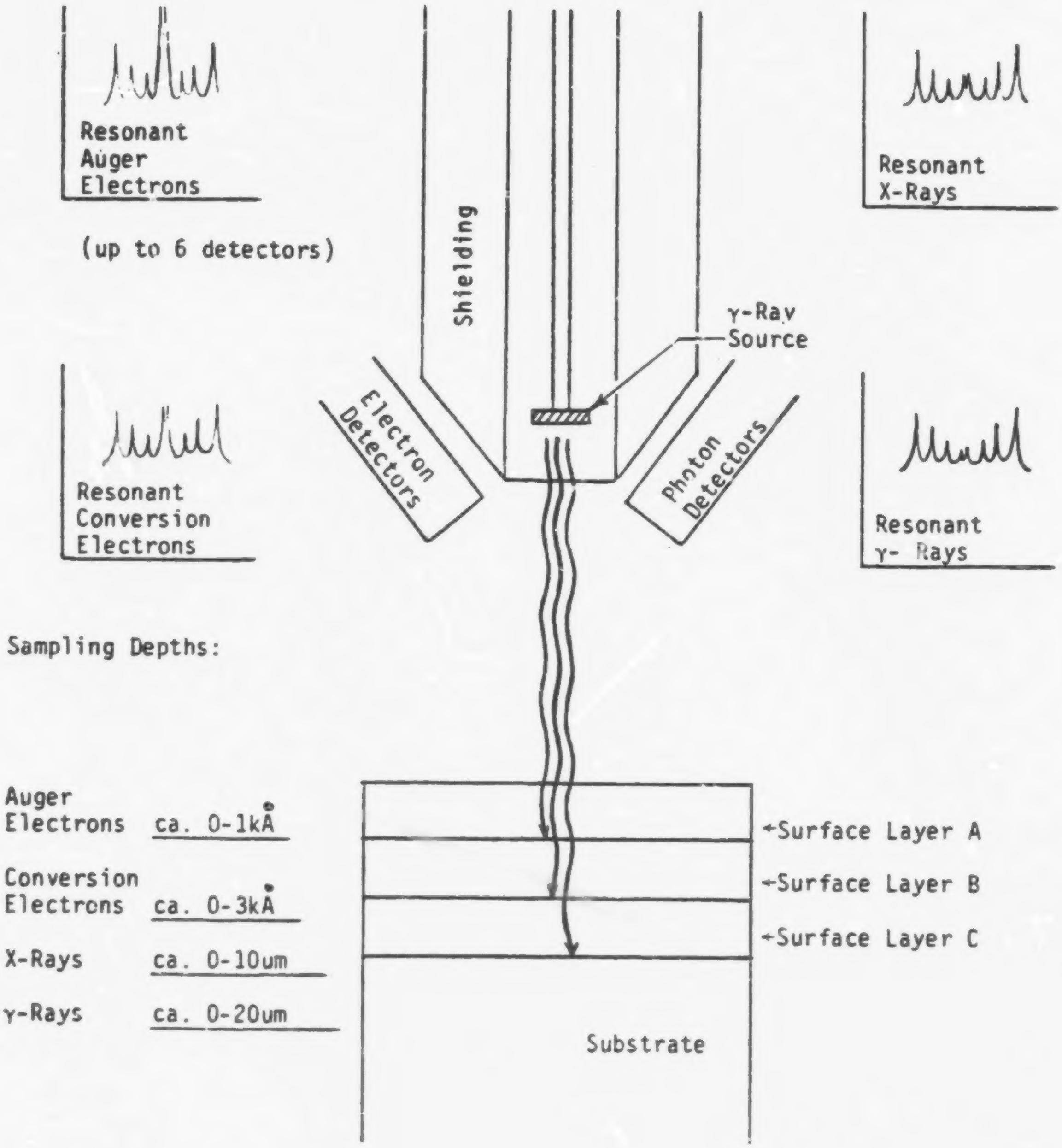
Resonant Auger Electrons
(up to 6 detectors)
Resonant Conversion Electrons
Shielding
γ-Ray Source
Electron Detectors
Photon Detectors
Resonant X-Rays
Resonant γ- Rays
Sampling Depths:
Auger Electrons ca. 0-1kÅ
Conversion Electrons ca. 0-3kÅ
X-Rays ca. 0-10um
γ-Rays ca. 0-20um
←Surface Layer A
←Surface Layer B
←Surface Layer C
Substrate

Figure 1. Schematic Diagram of Combined-Backscatter-Conversion Electron And Backscatter-Photon Mössbauer Spectroscopy (CEAPS). Spectra obtained at different electron or photon energies yield information from appropriate escape depths.

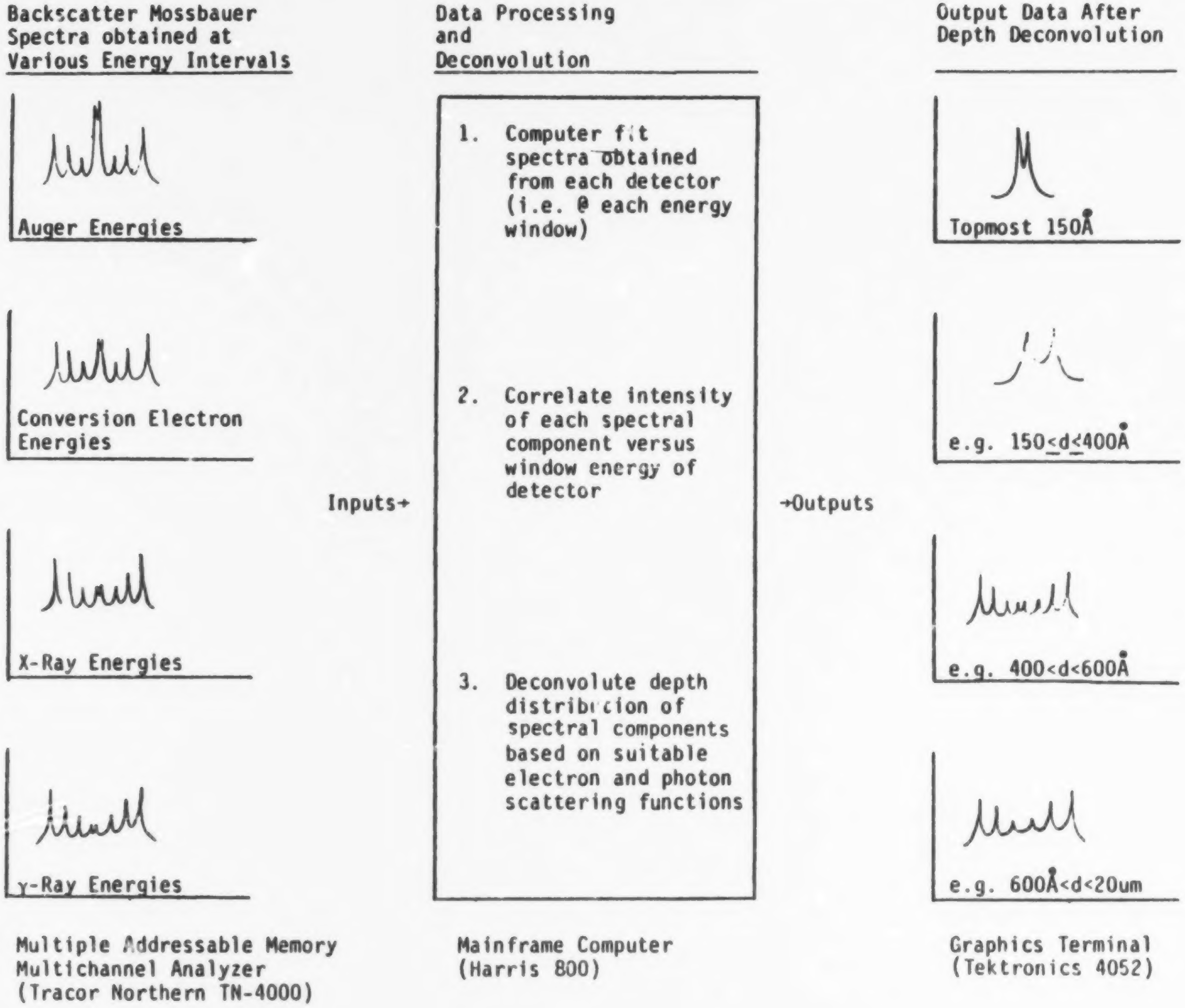
Backscatter Mossbauer Spectra obtained at Various Energy Intervals
Auger Energies
Conversion Electron Energies
X-Ray Energies
γ-Ray Energies
Multiple Addressable Memory Multichannel Analyzer (Tracor Northern TN-4000)
Inputs→
Data Processing and Deconvolution
Mainframe Computer (Harris 800)
→Outputs
Output Data After Depth Deconvolution
Topmost 150Å
e.g. 150≤d≤400Å
e.g. 400<d<600Å
e.g. 600Å<d<20um
Graphics Terminal (Tektronics 4052)

1. Computer fit spectra obtained from each detector (i.e. @ each energy window)
2. Correlate intensity of each spectral component versus window energy of detector
3. Deconvolute depth distribution of spectral components based on suitable electron and photon scattering functions

Figure 2. Procedural steps for obtaining nondestructive depth profiles using CEAPS.

STUDIES OF IONS AND NEUTRALS DESORBED FROM SOLID SURFACES BY ION AND ELECTRON BOMBARDMENT

Nicholas Winograd
The Pennsylvania State University
Department of Chemistry
152 Davey Laboratory
University Park, Pennsylvania 16802

The study of the interaction of energetic particle beams with solids is of interest to a number of technologically important fields including, for example, the processing of electronic materials, the analysis of plasma-wall interactions in Fusion reactors and in surface characterization. We have developed a theoretical approach to understanding this interaction which has been applied to the analysis of metal single crystals, surfaces with chemisorbed layers and selected molecular solids (1). It is possible to test this model by the analysis of the material desorbed from the solid by ion bombardment. Of interest is to measure the intensity of secondary particles as a function of their velocity and take-off angle (1). The experiments have so far been only performed on the surface-ionized particles since there has not been a sufficiently sensitive method to detect the neutrals.

We have designed an apparatus that operates in an ultra-high vacuum environment, on well characterized surfaces, with low total ion doses, and with mass, energy, and angular resolution for the desorbed neutrals. It is based on a time-of-flight measurement for the neutral energies, multiphoton resonant ionization (MPRI) for particle selectivity, a time-of-flight measurement of the ionized particles for additional mass selectivity, and multichannel position sensitive detection for the angular information. A schematic of the apparatus is shown in Figure 1. MPRI has been chosen because of its selectivity and high ionization efficiency. It is most efficiently applied to neutral atoms in cases where the sputtering process appreciably populates only a few discrete states. With sufficient laser power, 100% of the neutrals in the probed state can be ionized during the short laser pulse. The ionization scheme does not involve virtual transitions (and consequently tight focussing) so that a large region of space can be probed by an unfocussed laser beam.

Initial experiments have been performed on a Rh(001) crystal bombarded by 3 kV Ar^+ ions at an angle of incidence of 45°. The Rh yield as a function of polar angle is compared to classical dynamics calculations performed on the same system. The sensitivity of the results is 10^3 to 10^4 times higher than anything reported earlier. The results also indicate that this approach should allow for studies of the geometry of adsorbed atoms and molecules to determined, as has been previously demonstrated for the secondary ions (1).

1. Garrison, B., Winograd, N., Science, 216, 805 (1982).

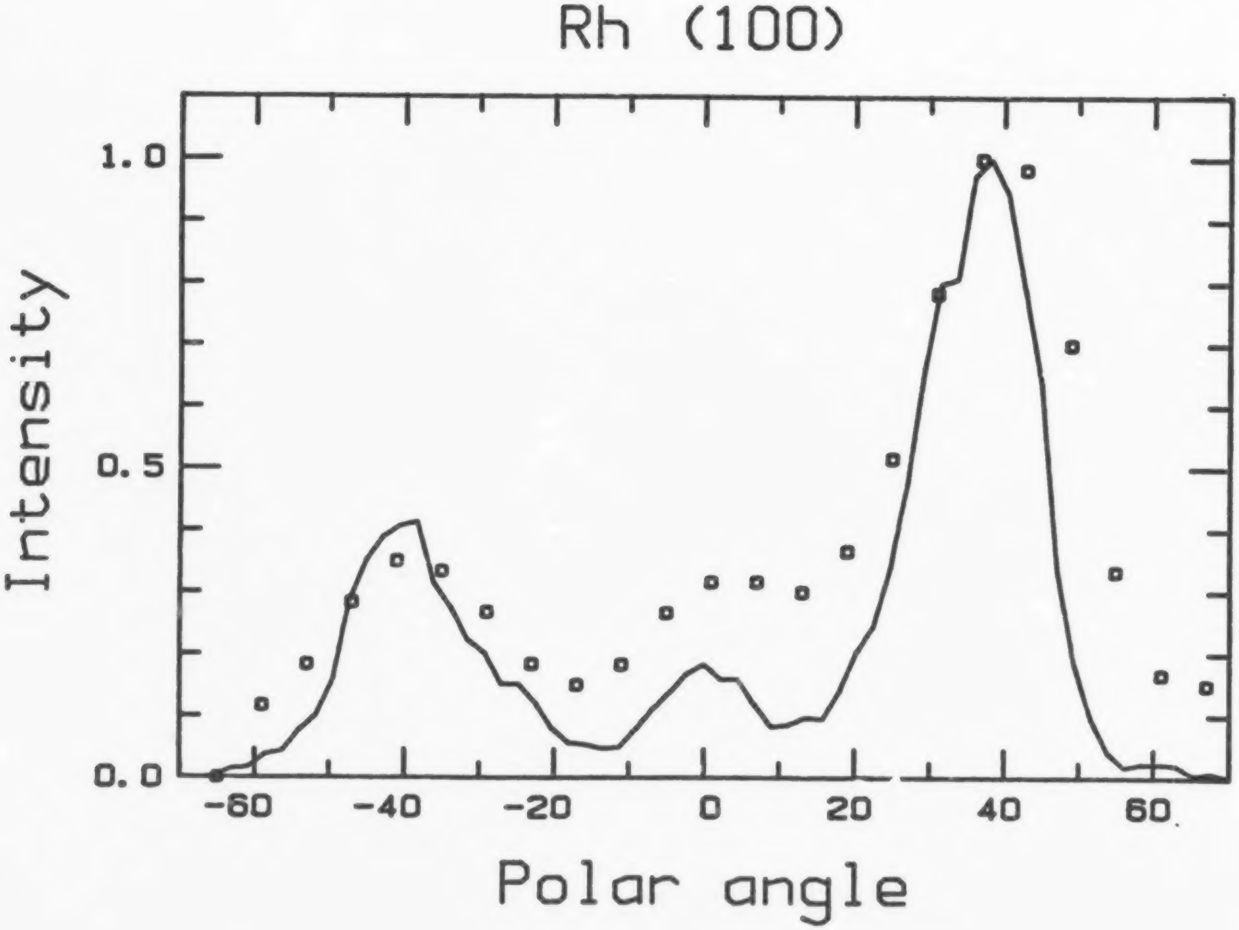

Figure 2. ________ Calculated
□□□□□ Experimental

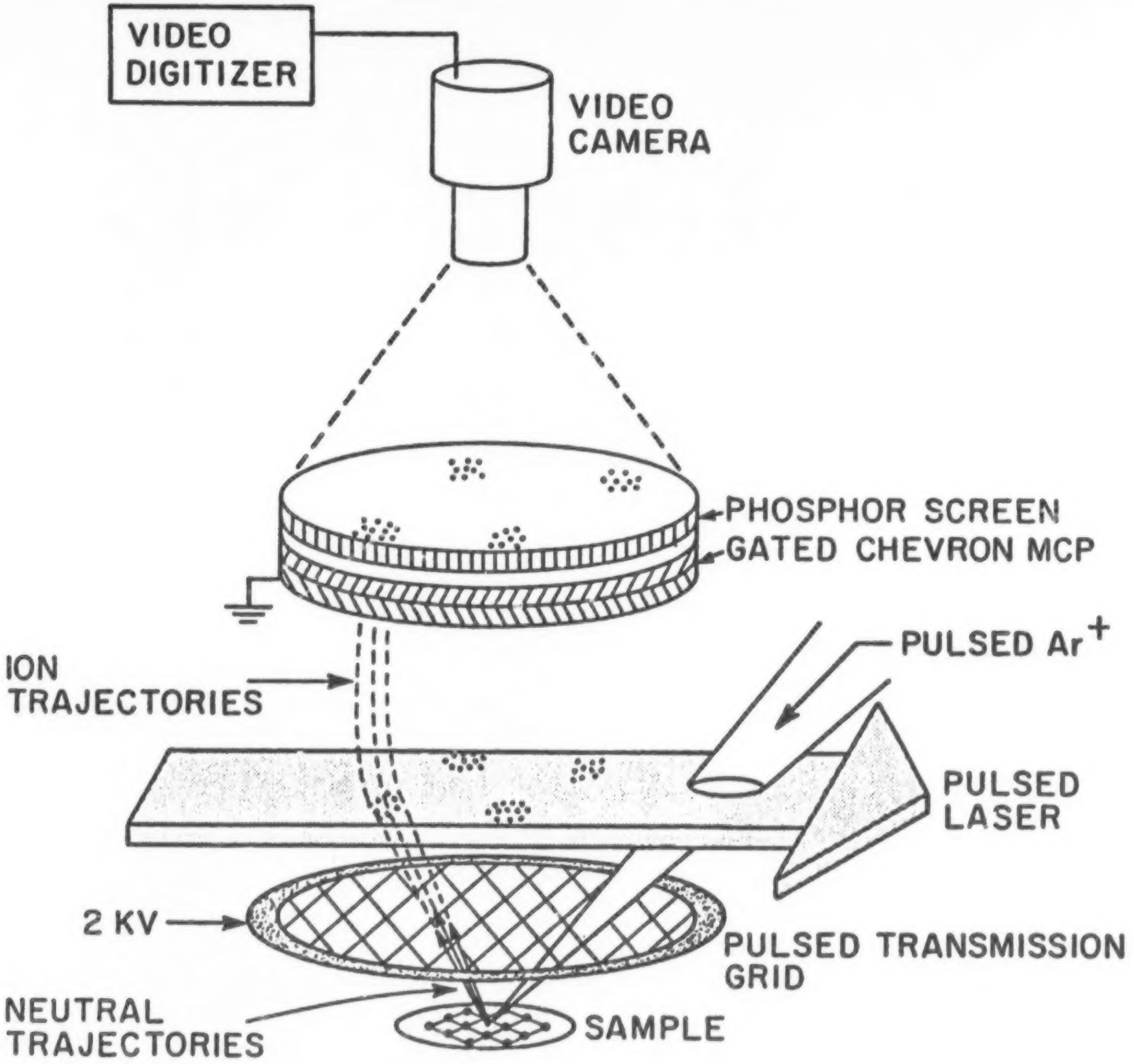
VIDEO DIGITIZER
VIDEO CAMERA
PHOSPHOR SCREEN
GATED CHEVRON MCP
PULSED Ar$^+$
ION TRAJECTORIES
PULSED LASER
2 KV
PULSED TRANSMISSION GRID
NEUTRAL TRAJECTORIES
SAMPLE

Figure 1.

CHEMISTRY OF NON-EQUILIBRIUM FILM DEPOSITION

FRANCIS J. WODARCZYK
Rockwell International Science Center
P.O. Box 1085
Thousand Oaks, CA 91360

There is much interest in laser interactions at and with surfaces, particularly with respect to the deposition of thin films for both electronic and optical applications. This current research program is directed toward understanding some of the fundamental mechanisms involved in laser interactions with surfaces in the course of photochemical thin film deposition. Studies include both desorption of species from surfaces and deposition of coatings onto various substrates, including both transparent and absorbing materials.

Fig. 1a shows a simple schematic drawing of the apparatus for studying laser desorption. Various laser sources can be focussed onto a substrate held in an ultra high vacuum (UHV) chamber. Signals from the desorbed species are detected using a quadrupole mass filter, signal averaged using a multi-channel scaler, and analyzed for both time and intensity information using a laboratory computer. Fig. 1b shows one cell used to study photochemical deposition of thin films. In these experiments a substrate is immersed in a reagent gas flow usually containing a metal organic (M.O.) plus oxidizer. High intensity radiation is focussed into the reaction cell either parallel or perpendicular to the substrate on which depositions are made. The resulting deposits are analyzed for chemical state information, stoichiometry, and morphology using surface analysis (XPS, AES, SIMS) and electron microscopies (SEM, TEM) in addition to analysis of physical film characteristics using standard optical, electrical, and mechanical techniques. The results can be used to obtain information about the fundamental photochemistry involved in the deposition process as well as to determine the optimum conditions for deposition of films with desirable properties. Both these studies uniquely combine UHV cleanliness, surface analysis, and standard chemical kinetics and allow us to answer fundamental questions about thin film desorption and deposition.

Some of our earlier results (Fig. 2a) had shown that desorption of organic contaminants from nonabsorbing substrates (e.g., quartz) using visible laser light proceed via a two-photon process. More recent experiments (Fig. 2b) indicate that only one photon of ultraviolet light (e.g., at 248 nm) is needed to desorb these contaminants, suggesting that absorption by the organics adsorbed on the surface and subsequent energy rearrangement results in the rupture of the surface bond. Analysis of data from the desorption of deliberately deposited organics indicates that photofragmentation is not part of the desorption process. Temperature dependence studies indicate physisorption of the adsorbed organics, while time-resolved studies show desorbed species with a cold Maxwell-Boltzmann distribution. These data are consistent with a picture of a non-equilibrium desorption process whereby absorbed energy is randomized in the surface species until just enough leaks into the bond to the surface to break it.

Our earlier studies of photochemical deposition of dielectric materials had shown that TiO_x ($1<x<2$) is formed by UV irradiation of a substrate immersed in $Ti(Oi\text{-}C_3H_7)_4$ vapor regardless of wavelength. Subsequent work shows that inclusion of a nonreactive oxidizer into the reagent gas mixture during photolysis yields more stoichiometric TiO_2 films without the carbonyl-containing contaminant present in earlier films. More recent experiments with tin alkyl compounts shows that Sn films for doping semiconductors can be deposited photochemically on various substrates, but they too contain hydrocarbon contaminants, indicating incomplete photolysis of the parent compound. Studies of the mechanism of photolysis of these metal organic reagents which would indicate why they almost universally show incorporation of carbon will be carried out in a UHV photolysis chamber currently under construction and shown schematically in Fig. 3. The chamber consists of a rotatable effusion source which produces a molecular beam of reagent molecules which are photolyzed by a laser. Subsequent analysis using a quadrupole mass filter will indicate the species present in the beam before and after photolysis. Of particular interest is the determination of conditions under which ionized and neutral clusters are formed, since these most likely are the nuclei on which the depositing films grow.

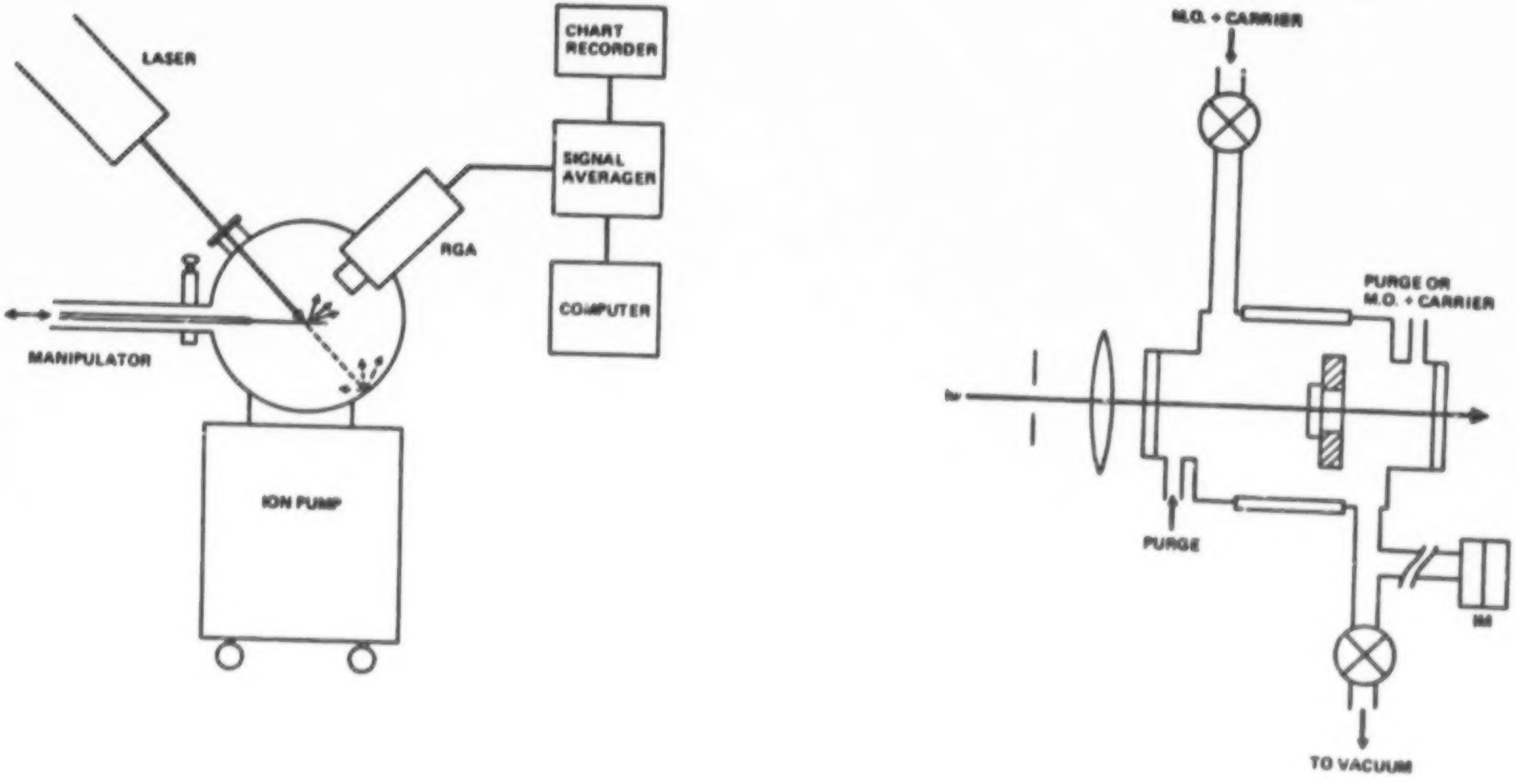
LASER
CHART RECORDER
SIGNAL AVERAGER
RGA
COMPUTER
MANIPULATOR
ION PUMP
M.O. + CARRIER
PURGE OR M.O. + CARRIER
hν
PURGE
IM
TO VACUUM

1a

1b

Fig. 1

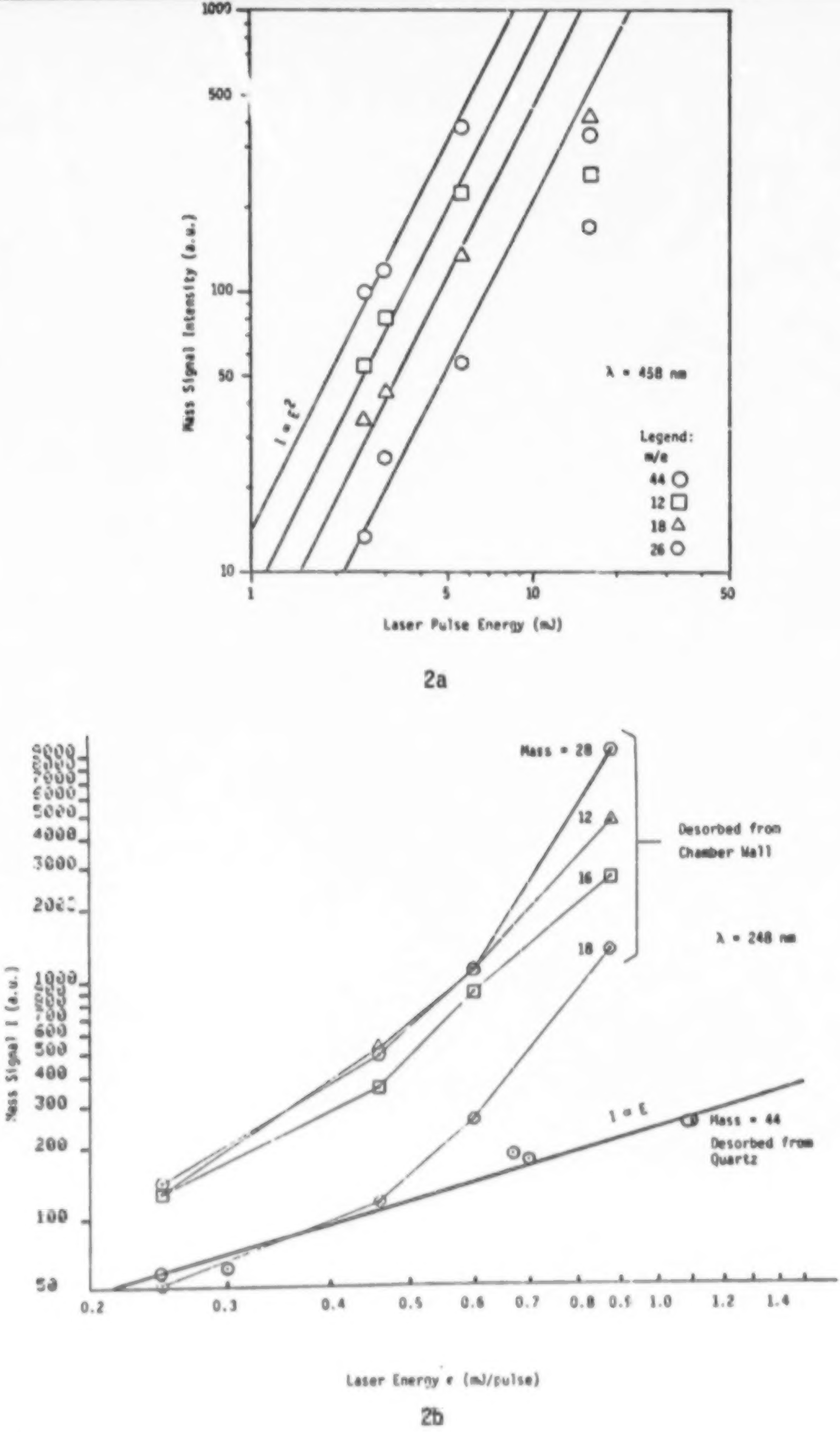
1000
500
100
50
10
1
5
10
50
Mass Signal Intensity (a.u.)
Laser Pulse Energy (mJ)
I = ε²
λ = 458 nm
Legend:
m/e
44 ○
12 □
18 △
26 ○
2a
9000
8000
7000
6000
5000
4000
3000
2000
1000
900
800
700
600
500
400
300
200
100
50
0.2
0.3
0.4
0.5
0.6
0.7
0.8
0.9
1.0
1.2
1.4
Mass Signal I (a.u.)
Laser Energy ε (mJ/pulse)
Mass = 28
12
16
18
Desorbed from Chamber Wall
λ = 248 nm
I = ε
Mass = 44
Desorbed from Quartz
2b

Fig. 2

MOLECULAR BEAM PHOTOLYSIS CONFIGURATION

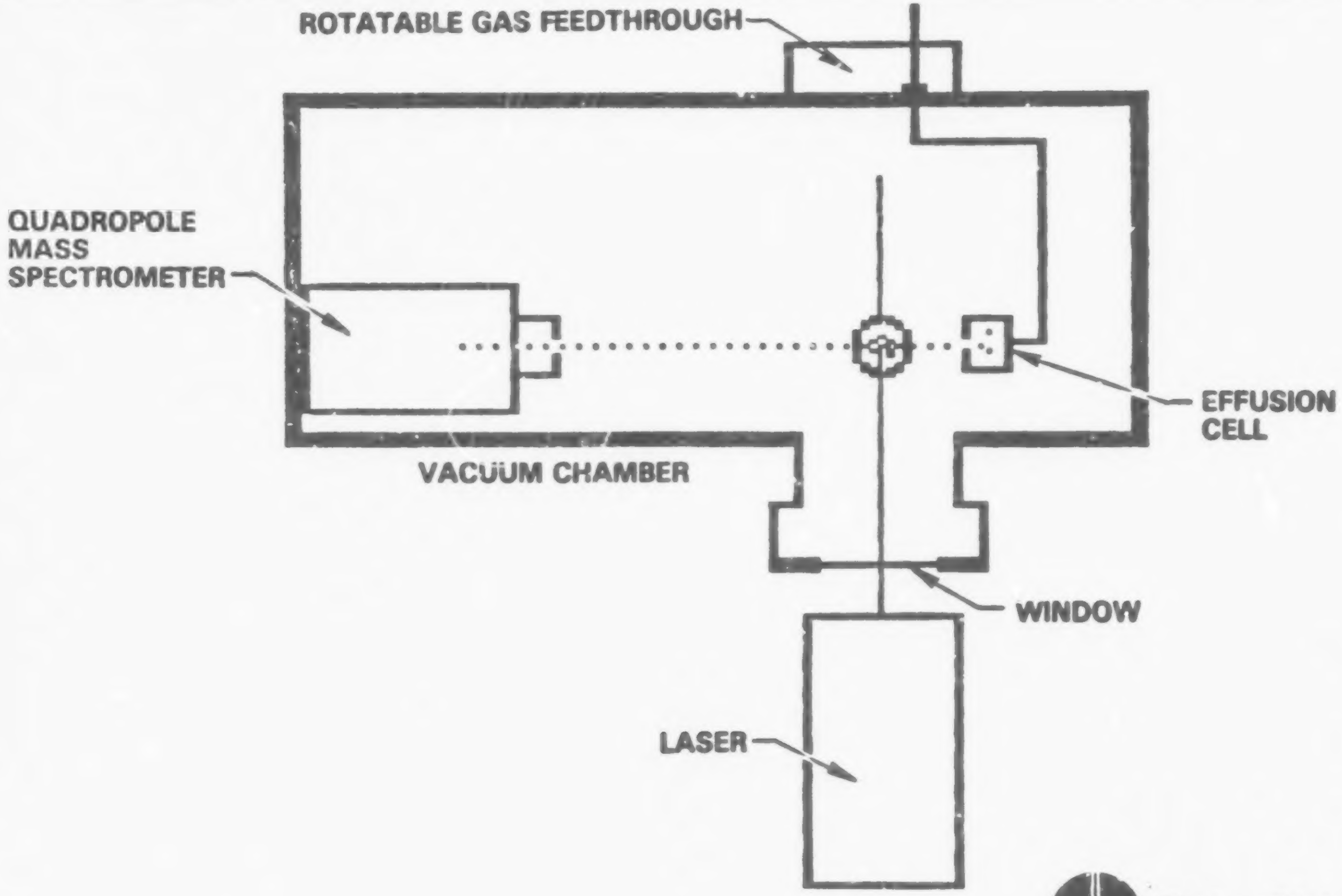
ROTATABLE GAS FEEDTHROUGH
QUADROPOLE MASS SPECTROMETER
EFFUSION CELL
VACUUM CHAMBER
WINDOW
LASER

Rockwell International
Science Center

Fig. 3

IMAGING MOLECULAR STRUCTURES ON SINGLE CRYSTAL SURFACES

Dr. John T. Yates, Jr.
Department of Chemistry, University of Pittsburgh

At the heart of the study of surface chemistry is the question of the structure of surface species. How do molecules and radical species bond to surfaces? What is their molecular orientation in the surface layer? Which adsorption sites are selected? What is the influence of interspecies interactions on the bonding character at the chemisorption sites?

These questions may be conveniently addressed by employing a novel technique - ESDIAD - (Electron Stimulated Desorption Ion Angular Distribution)(1). It has been demonstrated that when an array of oriented molecules on a surface is bombarded by electrons, positive ion fragments are liberated and escape in directions closely similar to the bond directions associated with the molecule (2). Thus by examining the shape and symmetry of the positive ion patterns produced by electron stimulated desorption one can often deduce the basic bonding geometry of the surface species being investigated.

The apparatus used for these studies is schematically illustrated in Fig. 1. An electron gun irradiates a 1/2mm spot on the single crystal containing an adsorbate. Positive ions, ejected in their natural directions from the oriented adsorbate species travel radially to a pair of hemispherical grids beyond which they are accelerated into a pair of micro channel amplifier plates: The electron signal generated is about 10^6 times the incident ion signal. The electrons are detected by a phosphor screen, and the pattern may be easily seen visually or photographed, yielding the basic ESDIAD pattern. By reversing potentials in the apparatus, it may be conveniently used as a LEED display apparatus, permitting the determination of crystallographic directions and ordered overlayer unit cell dimensions.

We have been able to determine a number of surface structures for 3 different adsorbate species on the Ni(110) plane using ESDIAD patterns of fragment ions. This plane is of particular interest because of its sutructure consisting of ridges and valleys. The results of these three studies are summarized in the attached series of photographs which are made using scale models of the oriented molecules. The crucial information about molecular location and orientation has been obtained by ESDIAD in each case.

Summary of Results

A. Ni(110) + NH_3

We have performed our studies on the Ni(110) single crystal plane shown in Fig. 2A. This plane is characterized by a ridge and valley structure. The NH_3 molecule is adsorbed non-dissociatively on Ni(110). The orientation of the C_{3v} axis is normal to the (110) plane and there is no preferential azimuthal orientation of the N-H bonds, as shown by the circularly symmetric H^+ ESDIAD ring pattern. Cooling to 29° K does not freeze out the motion responsible for the symmetric pattern, suggesting that any barrier on this site to rotation will be below about 1.5 Kcal $mole^{-1}$. Steric arguments exclude the valley site for NH_3 adsorption and suggest that the atop ridge sites are occupied as shown is Fig. 2B (3).

ESDIAD APPARATUS

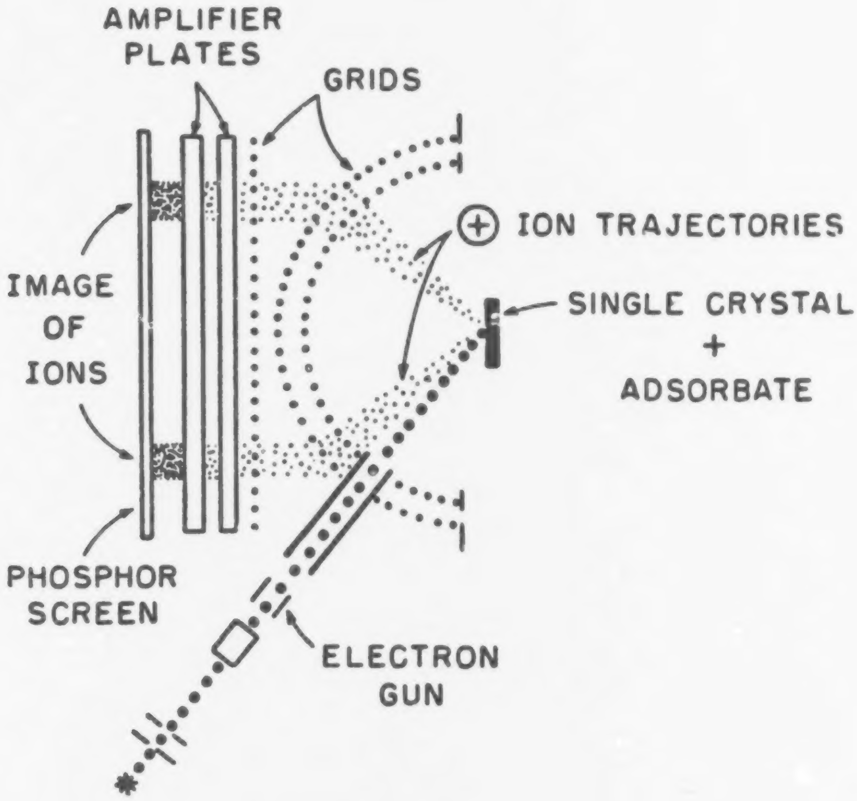
AMPLIFIER PLATES
GRIDS
ION TRAJECTORIES
SINGLE CRYSTAL + ADSORBATE
IMAGE OF IONS
PHOSPHOR SCREEN
ELECTRON GUN

Figure 1.

ESDIAD Apparatus for Imaging Molecular Structures on Single Crystal Surfaces (Schematic)

B. Ni(110) + NH_2

The adsorbed radical species, NH_2 (ads), may be quantitatively produced from NH_3 (ads) by electron bombardment. The ringed shape H^+ ESDIAD pattern of NH_3 (ads) converts to a two beam pattern with the beams being directed to the left and right hand sides of the channel-ridge direction. The location and structure of NH_2 (ads) is shown in Fig. 2C (4).

C. Ni(110) + CO

At low coverages below about 0.5 monolayer, CO exists primarily as terminal species bound to ridge Ni atoms which produce a normal beam of CO^+ ions. Above about 0.5 monolayer coverage, the CO^+ beam disappears as repulsive interactions between neighbor CO species cause a sharp reduction in the strength of the CO chemisorption bond as evidenced by the appearance of a new thermal desorption state at lower temperatures. It is believed that the CO axes tilt into a non-normal orientation as a result of intermolecular repulsion. Auxiliary information obtained from Penning ionization spectroscopy(5) and from EELS(6) is consistent with this interpretation. A molecular picture of these events is shown in Fig. 2D.

D. Summary of Results

The photographs of the molecular surface structures deduced from ESDIAD measurements succinctly summarize about 3 man-years of effort and 3 papers concerned with the systems chosen. The power of ESDIAD to give incisive information about surface structures may be employed to give similar bonding information about surface species of importance in catalysis, lubrication, adhesion, semiconductor technology and corrosion. But more importantly, this information is useful in developing a conceptual framework about surface bonding, currently an active theoretical area of research in the surface science field.

References

1. J. J. Czyzewski, T. E. Madey, and J. T. Yates, Jr., Phys. Rev. Letters, 32, (1974) 777; Surface Science, 49, (1975) 465.
2. T. E. Madey and J. T. Yates, Jr., Surface Science, 63, (1977) 203.
3. C. Klauber, M. D. Alvey, and J. T. Yates, Jr., Chem. Phys. Letters, 106, (1984) 477.
4. C. Klauber, M. D. Alvey, and J. T. Yates, Jr., submitted, Surface Science.
5. J. Lee, H. Metiu, R. Martin, J. Arias, C. Hanrahan, C. Klauber, M. D. Alvey and J. T. Yates, Jr., submitted, Phys. Rev. Letters.
6. W. Ho, private communication.

Structures of Surface Species Deduced from ESDIAD

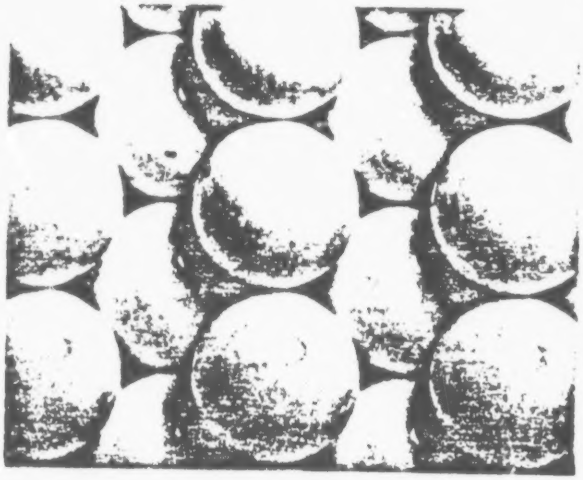

Figure 2A.

Ni(110) surface viewed from above.

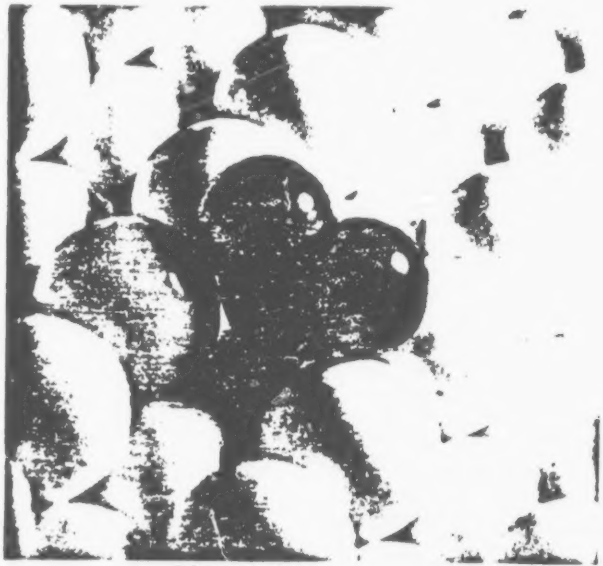

Figure 2C.

Ni(110) surface containing chemisorbed NH_2 species in valley site.

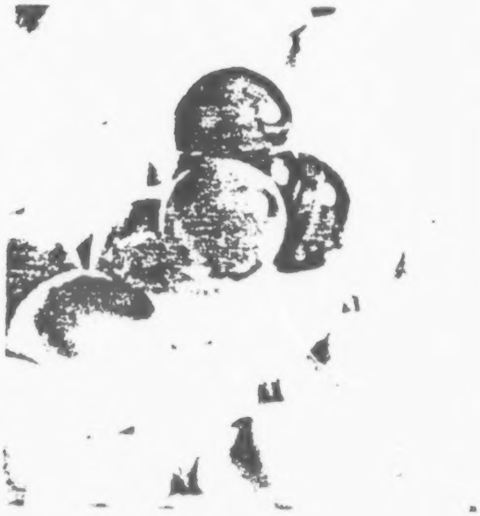

Figure 2B.

Ni(110) surface with chemisorbed NH_3 on atop-ridge site, viewed from an angle.

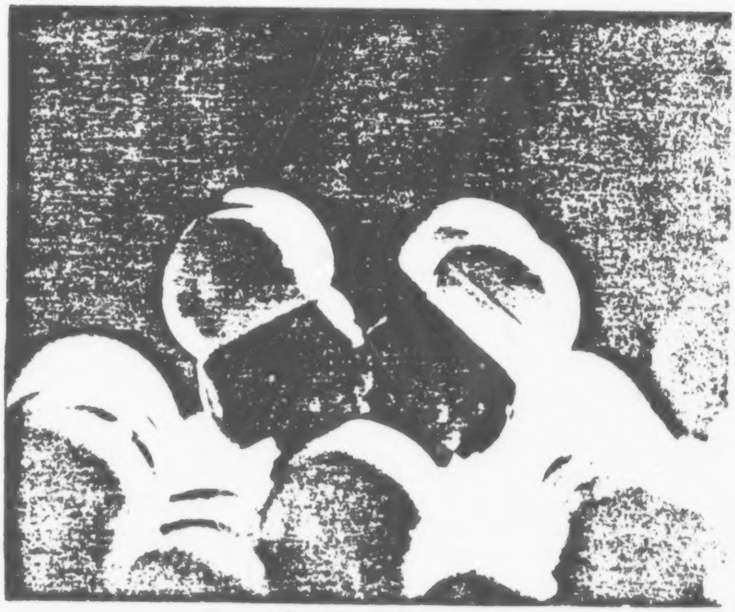

Figure 2D.

Ni(110) surface containing adjacent terminal CO molecules which repel each other resulting in non-normal alignment.